A Sensor for Three-Dimensional Limb-to-Prosthesis Interface Motion and Physiological Adaptations from Lower Extremity Prosthesis Use

Conor Lanahan

A dissertation
submitted in partial fulfillment of the
requirements for the degree of

Doctor of Philosophy

University of Washington
2024

Reading Committee:
Joan Sanders, Chair
Joseph Garbini
Janna Friedly

Program Authorized to Offer Degree:
Department of Bioengineering

University of Washington

Abstract

A Sensor for Three-Dimensional Limb-to-Prosthesis Interface Motion and Physiological Adaptations of the Lower Extremity from Prosthesis Use

Conor Lanahan

Chair of the Supervisory Committee:

Joan Sanders

Department of Bioengineering

Lower extremity prosthesis use following amputation introduces stark environmental changes to the skin and underlying tissue of the residual limb. As prosthesis socket fit is considered one of the most integral elements of increasing the likelihood a user adopts their artificial limb, it is crucial to understand how the limb interacts with the prosthesis at the contact interface. The individualized nature of socket fabrication means that a prosthesis can create unique fit conditions, presenting a challenge when observations from various users are compared. Furthermore, it has been known that even within a single prosthesis the pressure and shear forces are not uniform, meaning that different locations of the residual limb experience different magnitudes of stressors. It is thought that the skin of the residual limb adapts to the new stressors imposed by the socket, but the physiologic and biologic mechanisms are poorly understood in humans. Herein, a longitudinal study was conducted in attempts to directly compare the limb-socket interface mechanics and the physiology of adapted residual limb skin. An innovative sensing modality is presented that provides three-dimensional movements of the limb relative to the socket surface and is shown to have the sensitivity to detect clinically meaningful changes in socket fit. This sensor is one of few high-fidelity modalities that is cost-effective, unobtrusive to users, and easy to instrument, making limb-to-socket interface mechanisms feasible to measure in large cohorts and in everyday circumstances. Additionally, vascular adaptations were found in the residual limb using Optical Coherence Tomography Angiography imaging, and it is plausible that the adaptions can be correlated to the localized, repetitive, limb-socket interface motions found within the socket.

Table of Contents

List of Figures

List of Tables

List of Equations

Abbreviations

TTA – Transtibial Amputation
3D – Three-Dimensional
CAD/CAM – Computer Aided Design/Computer Aided Modeling
PTB – Patellar Tendon Bearing
TSB – Total Surface Bearing
LSM – Limb-Socket Motion
LCO – Inductor-Capacitor Oscillator
LC – Inductor-Capacitor
IRB – Internal Review board
OCT – Optical Coherence Tomography
INTRAY – Inductive Trilateration Array
TEWL – Transepidermal Water Loss
TcPO2 – Transcutaneous Oximetry
PORH – Post-occlusive Reactive Hyperemia
CSV – Comma Separated Values
EMF – Electromagnetic Field
SCS – Socket Comfort Score
STM – Sock Thickness Measurement

Chapter 1. Introduction

1.1 Background

1.1.1 Transtibial Prosthetics

Transtibial amputation (TTA) is a medical procedure in which the lower leg is removed below the knee joint, typically due to medical conditions like peripheral vascular diseases or diabetes and closely followed by traumatic injuries. Various surgical procedures can be implemented to perform a TTA, but the resulting appendage has typically been closed with sutures near the distal aspect of the limb (1). An emerging surgical intervention for transtibial amputations is to perform an osseointegration technique that leaves implanted hardware externally, but this is not a fully accepted procedure in the United States.

Transtibial prostheses are medical devices that are intended to be used by patients who have undergone TTA to regain functional mobility. A prosthesis consists of numerous components that can be interchanged to accommodate how a user may interact with their device. The most known element is the prosthetic socket, which is a carbon fiber and nylon laminated component that supports the residual limb. The socket shape is custom made for each patient and is fabricated to match the residual limb anatomy. Historically, negative plaster molds of the residual limb (taken directly on the patient's residual limb) are used to create positive molds of the residual limb that are used to shape the carbon fiber laminates. Modern efforts have been made to adapt digital technologies to this methodology and largely consist of residual limb scanning with white light cameras and creating a CAD/CAM object (2,3).

With a positive mold of the residual limb, prosthetic technicians can fabricate prosthetic sockets by standard operating protocols. A common fabrication technique is resin casting, where alternating layers of carbon fiber and nylon are positioned on the positive mold and resin is poured onto the layers while a vacuum is used to conform the layers to the inner shape of the positive mold. An alternative method is bubble forming, which is similar to vaccu-forming, and a current prospect in the field is to allow for three dimensional (3D) printing of sockets (4–6).

Prior to the lamination steps, prosthetists may modify the mold to better accommodate the fit of the resulting socket. It is known that some areas of the residual limb are more tolerant of socket stresses and prosthetists will modify the shape of the mold to apply more pressure to some regions of the limb while simultaneously creating reliefs in others to offload those regions of the limb. In general, the distal end of the tibia, the fibular head, the tibial crest and tuberosity, the medial and lateral femoral condyles, and regions with suture scars are pressure intolerant. Leaving the posterior midlimb, medial and lateral flares of the tibia, and patellar tendon as primary load tolerant zones (7). With this, clinicians commonly define sockets as Patellar Tendon Bearing (PTB) or Total Surface Bearing (TSB). Each socket shape design has benefits and contradictions depending on the limb anatomy, socket use cases, and financial limitations (8,9).

The next key component of a prosthesis is the prosthetic liner. A prosthetic liner is a, 2-9mm thick, protective barrier that is donned onto the residual limb prior to wearing a prosthetic socket. The liner is made of silicone or silicone-like material and is intended to dissipate the pressure and shear forces that

translate onto the skin from socket wear and use. The prosthetic liner is an essential element for each user and there are numerous styles of liner that are commercially available to accommodate different user tolerances and use cases. Furthermore, investigations have evaluated the mechanical characteristics of commercial liners and have shown significant differences between certain liner styles and materials, though this numerical evaluation is utilized by clinicians to inform liner selection for their patients (10–12).

Another major component of a transtibial prosthetic is the ankle and foot attachments. Like prosthetic liners, there are countless commercially available components that clinicians can source to customize a prosthesis for their patients. This part of the prosthesis can be simplified and considered in terms of energy storage and return to help make ambulation energetically efficient. For users who are muscular and have good coordination a softer-bending foot may provide more energy return to aid the toe off phase of the walking cadence (13). For those who do not ambulate as well, a more rigid foot can provide stability and confidence while walking. The influence of foot stiffness has been shown to have a multifaceted impact on prosthesis success (14) and clinicians thus resort to testing various componentry on patients to explore which option may best suit the users' needs (15).

In addition to socket shape, socket suspension is also considered during the fabrication step. Socket suspension is the mechanism that adheres the socket to the residual limb. Physically the socket adheres to the prosthetic liner, as users are highly recommended to always wear their prosthetic liner, so liner choice is also influenced by suspension type.

Two common suspension types are pin and pin-less suspension sockets. A pin-locking suspension type is one where a ratcheting mechanism in the bottom of the socket passively docks a locking-pin found on the bottom of the prosthetic liner. Prior to socket use the locking-pin is threaded onto the liner so that when the user dons the prosthesis, the limb, liner, and locking pin are driven into the bottom of the socket due to the users body weight. The ratcheting mechanism accepts the locking-pin and allows it to travel as deep as it needs so that the residual limb can fit within the socket shape, but when pulled against, the ratcheting mechanism prevents the locking pin from pulling out of the socket. Mechanically, this locks the liner within the socket and the friction between the liner and residual limb effectively couples the residual limb with the prosthesis.

On the other hand, a pin-less suspension socket uses negative pressure to adhere the socket to the residual limb. There are a variety of subtypes of pin-less sockets, but the simplistic design is known as a suction socket. During the fabrication process of a suction socket, a hole is drilled through the socket and plugged with an air-filter and one-way valve. Then as the user dons the socket and begins ambulating on the socket, the motion of the limb within the socket drives air through the one-way valve. The hole of the socket is typically drilled on the inferior surface of the socket so that any air trapped at the distal end of the socket can easily be pumped out. Additionally, a "suspension sleeve" is worn to seal the top of the prosthesis by creating an airtight barrier from the external surface of the socket to the upper residual limb.

Once the hardware and liner have been selected for a user, a prosthetist must fit the device to the patient. This process means that the clinician fits the height, angle, and offset of the hardware so that the participant can dynamically move with the prosthesis. This process tends to be matched with physiotherapy and it allows the participant to learn how to walk with a new prosthesis. For experienced prosthesis users, this

process can be easier because they can provide feedback to the clinician based on their prior experiences. If there is limited feedback from the patient, clinicians rely on visual clues about the participants gait to adjust the hardware alignment, and it can take years for clinicians to develop the skills to identify various visual gait cues.

Lastly, a common element of a prosthesis that allows the fit of the socket to be slightly modular, are prosthetics socks. A prosthetic sock is typically a synthetic-cloth or wool-based knitted sheath that is intended to be worn outside of the prosthetic liner. Socks come in various thickness denoted by "ply" where a larger ply sock is thicker than a smaller ply sock. Socks can be used to pad the residual limb or, in most cases, be used to accommodate daily and long term fit changes.

It has been studied that the fit of a prosthetic leg can significantly change over the course of the day and over time for varied reasons (16). At the diurnal level, it is thought that residual limb fluid volume fluctuations change the limb shape and size enough to cause the fit to deteriorate, while more gradual anatomical changes may drive long term socket fit issues (17).

Prosthetists can also address long term socket fit issues by making permanent and non-permanent alterations to the socket shape. If there is evidence that the socket is applying too much pressure in inappropriate locations, the socket can be ground down on the inside of the socket, creating a slight relief. This modification is limited by the thickness of the lamination layers of the socket because a hole in the socket would likely render the socket unsafe to wear. On the contrary, clinicians may adhere thin, foam pads on the inside of the socket to apply more pressure in specified areas on the limb.

Before insurance will fund a new socket fabrication process, clinicians must first try to accommodate the fit of the patients existing socket (18). Various components of the ankle and foot can be replaced, the alignment of the socket can be altered, and various modular changes to the socket shape can be explored. Thus the fit of a socket can take a long time and be a trial-and-error process that patients need to enduring.

Webster et al. prospectively studied the success of fitting a prosthetic socket to patients with vascular disease or diabetes and found that 65% of the transtibial amputee cohort had a fitting socket four months after initial socket fabrication and 93% had a fitting socket by twelve months. In addition to physical components needing to be modified during this period, a large element of creating a successful prosthesis revolved around socioeconomic and psychological factors (19).

1.1.2 Measurement Tools used in the Field to Investigate Socket Success

Excluding the various ways socioeconomic, psychological, and patient comorbidity factors can influence the adoption of a lower extremity prosthesis, it is thought that an improper socket fit is a driving factor for poor rehabilitation. The fit between a user's prosthesis and their residual limb is fundamental to socket comfort and residual limb health. Over the past half-century in the lower-limb prosthetics field, interface mechanics between the residual limb and the prosthetic socket has been of great interest and is thought to be a major source of residual limb injuries, of which hinder patient rehabilitation. It was found that preventing pressure ulcer formation was a significant factor in prosthesis adoption success (20,21).

Clinicians regularly evaluate the residual limb of a participant visually for indications of a poor socket. In addition to patient feedback, redness, callusing, or skin pallor are used a visual cues to determine if a socket is poorly fitting. Clinicians also refer to limb "pistoning" and "bell clapping" in a clinical sense as a method to evaluate a socket fit. Pistoning is the motion of the residual limb moving in and out of the socket during walking. Bell clapping is a motion where the distal end of the residual limb moves from one surface of the socket to the opposite with each step. Bell clapping is largely considered in the Sagittal Plane, where the distal limb hits the front and rear of the socket but can also happen in the Frontal Plane (medial and lateral motion). Larger amounts of pistoning and bell clapping are thought to be problematic and a result of a poorly fitting socket. Additionally, there is the "clay ball" method where a prosthetist places a small ball of clay a the bottom of the socket and asks the user to walk on the socket. If the ball is overly crushed after walking it is an indication of too much distal end bearing. Currently in clinical practice, socket fit evaluations are done by eye, and there are no readily available tools to objectively measure socket fit metrics (22).

Numerous studies have been conducted to explore the magnitude of limb-socket motion (LSM) and of the 16 publications reviewed by Baumann et al. (20) 13 used radiographic, optical motion capture, or photographic methods to collect LSM pistoning data. These imaging investigations have used a variety of landmarks to base the magnitude of pistoning off and have studied various socket suspension types to illustrate that the residual limb can piston between 2-40mm.

Beyond optical measurements that require laboratory-based equipment, few socket-embedded sensors have been developed to monitor residual limb motion in the socket remotely. Noll et al. presented a two-dimensional optical sensor that measured the texture of a prosthetic liner or sock to track transverse displacement of the limb (23). Henrickson et al. used an inductive sensor and liner-embedded iron-polymer target to measure one dimensional limb-socket separation values (24). Liu et al. used magnetic field intensity measurements from a liner-embedded magnet to measure proximal-distal (pistoning) movements (25). Wirta et al. used a plunger and potentiometer attached to suprapatellar strap suspension sockets to measure axial displacement (26). Ferguson et al. developed a diaphragm and pressure based tool to measure pistoning at the distal end of the socket (27,28).

In a different vein to limb-to-socket motion, within-socket pressure and shear measurement have been largely studied. Pressure being the force on the limb over a given area, and shear being a complex stress that originates from the residual limb's skin and liner compliance, pressure, friction, and LSM. From these investigations it is understood microenvironments of pressure and shear develop, likely due to the loading and unloading zones created during the socket shaping process. Furthermore, with dynamic ambulation the limb with move irregularly that can change the interface loading profile, changing the stresses the limb experiences. Ultimately, the pressure and shear waveforms are thought to be constrained by the model presented by Radcliffe (29).

In two separate studies conducted by Zhang et al. and Sanders et al. triaxial force sensors recorded limb-socket stresses across various sites on the socket, and it was found that areas designed to take load exhibited higher pressures but the pattern of loading for each prosthesis user was unique (30,31). Dumbleton et al. found that the pressure distribution in 48 transtibial prosthesis users was similar and corroborated the Radcliffe mechanistic model, but that the magnitudes of pressure between subjects was variable (32). In a

review published by Davenport et al. is was concluded that there was moderate confidence that rotational sagittal-plane alignment-modifications changed the proximal anterior and distal posterior pressures, but the data was highly participant specific and it was challenging to adequately compare across the cohort (33). In a case study with two participants, Sanders et al. found that weight loss had different effects on the limb-socket interface loading between participants, but generally there was increased distal end and patellar tendon loading and sock ply could not regain pre-weight loss loading profiles (34). Emerging from this research the pliance-RLS (novel.de, Munich, Germany) and the F-Socket System (Tekscan, Norwood, MA) became commercially available but have not been widely adapted in clinical practice.

It is believed that limb-socket movement, pressure, and shear can also directly impact residual limb health but seldom studies have directly compared the two. Common complications from lower extremity prosthesis use are bursitis, infection, neuromas, ulceration, and other dermatological issues that can be treated with conservative measures and prosthetic socket and liner modification but can frequently lead to surgical intervention. Furthermore, individualized amputee management plans amongst multidisciplinary medical teams is imperative for rehabilitation (35). Yet, nearly 75% of lower extremity amputee develop residual limb skin related problems (36). Visual inspection has remained the gold standard for prevention and diagnosis of these residual limb health issues.

Recently, investigations have explored numerous technological methods to evaluate skin health including Trans-epidermal Water Loss (TEWL), thermography, hyperspectral imaging, Transcutaneous Partial Oxygenation (TcPO2), sweat, Optical Coherence Tomography (OCT), Laser Doppler Flowmetry, ultrasound (37–39). One developed at the University of Washington used OCT angiography to visualize hemodynamic and structural blood vessel elements of the residual limb (40). In this investigation Swanson et al. stated that the methodology set forward could be effective at measuring vascular adaptations in the skin, as they saw some plausible adaptations, but a sample size of three was not powered to draw conclusions.

Optical Coherence Tomography is a known light-based medical imaging modality that works similar to, but has significantly improved resolution (axial and lateral resolution 1-10μm), to ultrasound. Various hardware can be implemented to conduct OCT imaging and in general the imaging is performed with a standard scanning pattern. In an A-Scan, light in the infrared spectrum (λ = 850-1050nm) is sent toward a semi-reflective mirror that splits the beam of light. Half of the beam is sent into the sample, while the other half is reflected off a reference mirror within the OCT hardware. Once each beam is reflected (by the reference mirror, or by a reflector in the sample) the ballistic light is returned to the semi-reflective mirror and focused on the photodetector. The signal of the two returning beams is an interferogram and that is mathematically resolved using the Fourier transform to produce reflectance data versus depth. A-scans are repeated along a single axis of the sample to create a B-scan, which is a cross section of the structural features in the sample. B-scans can then be repeated to construct a three-dimension structural image of the sample (41).

OCT angiography leverages OCT structural imaging and the flow of red blood cells within the vessels to articulate the vasculature systems. To acquire an OCT angiography image, A- or B-scans are repeated so that the reflective characteristics of the tissue in a given location can be averaged and a variance can be calculated. The theory assumes that as red blood cells flow through the lumen of the blood vessels, their

reflective properties will change, causing the variance in the voxel to increase. This imaging method is highly affected by sample motion, but post processing computations can rectify motion artifact. Choi et al. have describe high resolution computational methods that can produce clear microvasculature images (42).

1.2 Research Statement, Scope, and Limitations

Few tools currently used in reach today are easily translated into clinical practice. Here we propose a modification to an existing sensor (24) to provide accurate three-dimensional (3D) LSM information that is easy to instrument into lower-limb prostheses and can be worn passively by prosthesis users.

To date, the field has lacked direct comparison of LSM to objective measures of limb physiology, though there are logical hypotheses suggesting large magnitudes of LSM create residual limb injuries (20,43). Due to the proposed sensor's ease of use and sensitivity, we plan to compare localized LSM data collected from the sensor over specific anatomical locations to the physiological characteristics observed in the same anatomical locations. To do this we will collect LSM data from the sensors and obtain structural cutaneous angiography images by optical coherence tomography, and evaluate any changes or adaptations observed to the predicted heterogenous branching nature of the microvasculature (44). Beyond bridging the gap between LSM and residual limb physiology, data collected from the sensors will be compared to published literature and also be evaluated for its utility in tangential projects aimed at building futuristic auto-adjusting sockets that adapt to users' needs (45).

1.2.1 Aim 1: To validate an Inductive Trilateration Array Sensor

Preliminary evidence suggests that distance-sensing inductive antenna can be modified by using a small, 32mm diameter, ferromagnetic target about an array of three sensors to allow for detailed three-dimensional movement measurements using the mathematical method, trilateration.

Custom inductor-capacitor oscillator (LCO) antennae have been developed and shown to provide accurate one-dimensional distance measurements of a ferromagnetic target (45,46). In prior investigations, a sheet of ferromagnetic target, with a width much greater than the diameter of the LCO sensor, was used to saturate the electromagnetic field of the LCO (Figure 1a-b). A signal intensity versus distance regression was used to calibrate the raw LCO data and one-dimensional distance measurements could be made from the single LCO data (Figure 1c). This tool has been employed in transtibial prosthetics, with minimal burden to the user, and has provided stable distance measurements between the embedded ferromagnetic target within the prosthetic liner and LCO antenna in the wall of the prosthesis (45). Numerous experiments have been conducted to explore the clinical utility of these sensors for detection of socket fit, auto-adjusting sockets, and interface motion.

In this study, we introduce a novel technique to arrange three LCO antenna, paired with a small ferromagnetic target to provide three-dimensional (3D) location measurements. Pilot investigations have shown that modifying the size of the ferromagnetic sheet can elicit accurate radial distance measurements, in addition to the height measurements, from the LCO antenna. Accurately modeling the radial and height displacement of the ferromagnetic target relative to a single LCO sensor in 3D space allows the scalar distance value from the center of the sensor to the target in 3D space to be measured but is not enough information to determine the vector displacement quantity.

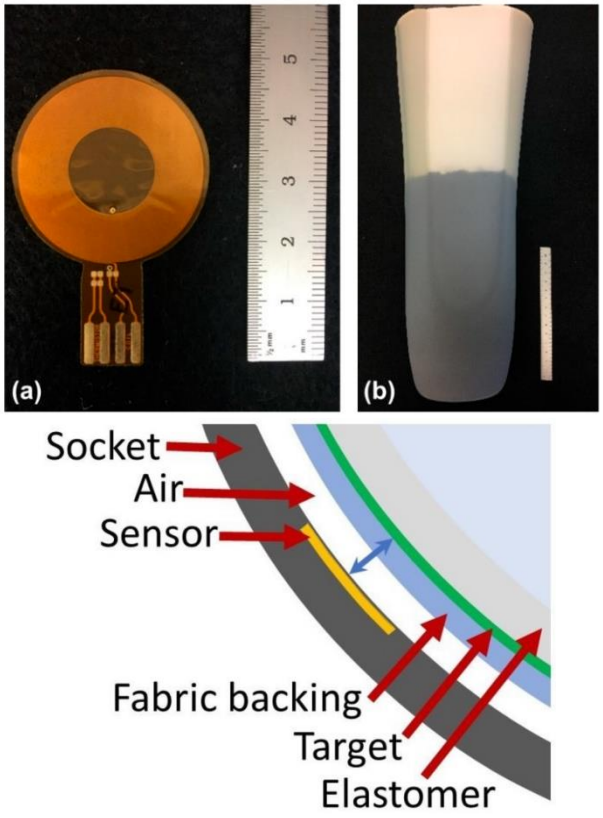

Figure 1: *(a) LCO antenna (b) sheet of ferromagnetic target embedded in prosthetic liner (c) cross sectional diagram of 1-dimensional distance measurement in transtibial prosthetics.*

Thus, instrumenting three LCO antenna into an array with specific coordinates provides three unique measurable signal intensities from each LCO sensors depending on where the ferromagnetic target is in proximity to the sensors. Using the mathematical method, trilateration, a system of equations can be solved using the three unique signal intensities, to find the vector displacement quantity of the target's location (47). As we have seen from the preliminary evidence, paraboloid surface functions can be used to model the Radial and Height displacement scalar values for a given signal intensity, and the system of equations solves for the point of intersection for the three paraboloid surfaces.

Aim 1.1: 3-axis Controller for Repeatable Experiments

In preliminary testing, calibration curves have been conducted by hand measurements and consequently precision has waned. In the first aim we propose to develop a custom 3-axis controller stage that can accurately and repeatably move the ferromagnetic target about a single- and three-sensor array. To do this a commercial three axis stage can be mounted on a custom designed frame to allow a proper range of motion for detection. A control software can be written in LabVIEW to allow the stage to be zeroed with reference to the sensor array and to execute predetermined flight paths for the target to be moved.

Magnetic and conductive materials will influence the signal obtained from the LCO sensors, and thus material choice in the design of the custom mounting hardware needs to be considered. Once the mounting hardware has been assembled testing can easily identify unintended effects of the stage on the LCO sensing capabilities and further design considerations can be made to reduce the magnitude of noise introduced by the stage. If materials need to be changed, rigidity and vibrational effects will need to be considered so that the 3-axis motorized sage does not deflect nor does vibrational motions affect the positioning reliability.

Aim 1.2: Sensor Modeling and Trilateration Solving

Following the development of the 3-axis motorized controller the first set of experiments will be centered on modeling the signal intensity surface heatmap of a flat LCO antenna with a 32mm diameter ferromagnetic target that is parallel to the sensor. This is an idealized case where both the target and sensor are flat and parallel to one another.

Validation of the inductive trilateration method will be conducted using the 32mm ferromagnetic target and 3-LCO sensor array. Initially the flat-parallel model will be tested as the ideal case for this method. Unique flight paths will be loaded into the 3-axis controller and position data from the Zaber 3-axis motorized stage will be recorded in the cartesian coordinate system relative to the sensor array. The recorded signal intensities from each LCO antenna will be used in the modeled signal intensity heatmap so that the trilateration mathematics can be used to solve for positional data of the target in the same cartesian coordinates relative to the sensor array. Accuracy will be measured as the variance from the known location of the target from the Zaber slide rail position data to the trilateration solved position.

Interpretation of Results.

Once construction of the 3-axis stage is complete, we will need to interpret the inductive interference introduced by the materials on the signal being recorded. To evaluate this, we will run a flight path above a LCO sensor with a target attached to the mounting plate of the stage and then rerun that same flightpath without a target mounted. To accept the stage design, we will need to observe near-zero signal from the flightpath run without a target.

While modeling the single sensor scalar distances, we will check for repeatability. The intention of this trial is to map different single-LCO heatmap model types and thus anticipate varying responses across different hardware, angle, and curvature builds. Thus, as we collect data and begin to build a base for the types of signals, we will rerun tests to confirm repeatability and accuracy.

While attempting to solve the 3-dimensional flightpaths, we will confirm that the proper models are being used and the flightpaths are being solved with acceptable accuracy. The programmable flightpath that controls the 3-axis stage will be used as the ground truth to which we can compare the accuracy of the solving algorithm. We expect that a Euclidean distance error (ground truth minus experimental solve coordinate positions) will suffice for reporting the accuracy of the models and algorithms used in the experiments. Additionally, we can investigate the accuracy of the solving algorithm at different regions within the detection location.

Beyond utilizing the quasi-static points programed into the flightpath to determine accuracy, we can investigate the accuracy of tracking a moving target based on the target's velocity. To do this we will time sync the 3-axis positional data with the solve data to see the accuracy of the solve.

Additionally, other solving algorithms may be tested during this investigation so that the absolute position solved by the algorithm provides the lowest positional error.

1.2.2 Aim 2: To develop a Sensor Platform for Limb to Prosthetic Socket Motion Measurement

We hypothesize that everyday activities will uniquely displace the user's residual limb within the socket and these events can be understood and predicted.

Translating the novel inductive trilateration sensing technique in lower limb prosthetics is crucial for limb-socket motion (LSM) tracking. In this aim we plan to explore fabricating the sensors into the socket, as well as the ferromagnetic target into the liner, and ensuring that users are unencumbered by the hardware. Furthermore, data collected from the sensors will be solved with the novel algorithms developed to identify LSM during laboratory-controlled and real-world ambulation and weight bearing. As the sensor technology can record data in real time, we will also begin to explore what common perturbations to transtibial prosthetic fits do to the observed LSM.

Tracking limb-socket motion (LSM) is a well explored field and various technologies have been developed to provide detailed LSM data (46,48). Technologies have ranged from radiographic (49–51), photographic (52), optical motion capture (53,54), and various sensory systems (23,25,45) measuring bouts of prothesis usage ranging from body weight bearing, level ground walking, and cycling. Though there have been numerous beneficial findings to these technologies, near all of them have been cost ineffective and relatively difficult to implement in real-life environments.

In this aim we focus on developing a method to fabricate an inductive trilateration sensor technology within a pin-locking, transtibial prosthetic socket so that LSM data can be captured in real-world environments. To embed the target in the socket, the ferromagnetic material will be incorporated in the prosthetic liner, while the LCO sensors will be embedded in the layers of carbon fiber and nyglass during the lay-up process similar to previously developed methods (46).

Once the fabrication is complete, LSM data will be collected in controlled laboratory and uncontrolled real-life environments. We anticipate that users will show similar characteristics in pistoning, anterior-posterior translation, and medial-lateral translation while ambulating in a controlled environment compared to the literature. Conversely, we expect that the LSM data will change slightly in amplitude once the user is wearing the socket in non-controlled environments because the user needs to adapt to the changing environment around them. As summarized by Bauman et al. (20), it is evident that LSM can be dependent on suspension type and the user of the prosthesis, so we anticipate a large variety of LSM measurements amongst our participant cohort though they will all have the same socket suspension.

Notably, during everyday use, the fit and function of the socket may change due to prophylactic or unintended fit events performed by the user, such as don and doffing socks, sweating, and limb fluid volume loss for example. We anticipate that there will be a region for the limb to be positioned in the socket so that the socket is of acceptable fit, but that some perturbations may cause the limb position to no longer be well supported in the prosthesis. These perturbations may cause drastic changes to the measurable LSM and that it is likely due to the complex redistribution of non-rigid elements within the socket.

The significance of this aim may be easy to compare to previous technologies that provide similar LSM data, but a novelty of this sensor technology is its ease of fabrication and detailed three dimensional LSM data. Prior inductive sensor technology is being pursued at a commercial level for central fabrication, illustrating the ability to translate this research into a clinically meaningful setting. Moreover, inductive sensing technology has been used in efforts to build auto-adapting sockets that conform to participants limbs undergoing a fit deterioration (45). Performing this Aim of research is a logical step in understanding the capabilities of inductive trilateration sensing, and ultimately it may provide unique information on how to design a future generation of auto-adaptable prosthetics.

Experimental Designs.

Aim 2.1: Socket and Liner Fabrication for Embedded Inductive Trilateration Measurements

This aim will be focused on optimizing the process of embedding the LCO sensor array in the pin locking suspension, carbon fiber prosthesis and the ferromagnetic target into the prosthetic liner. Preliminary efforts (Fig. 5) on this have been successful to collect reliable signal from the sensor array, but further work needs to be performed to optimize the performance of the sensor technology.

Potential Pitfalls and Alternative Approaches.

A major pitfall in fabricating the 32mm ferromagnetic targets into the prosthetic liner is deformation to the target. Current methods have taken punches from a commercially fabricated ferromagnetic polymeric laden liner and used a silicon epoxy to bind the punches to the existing liner. In this process, targets may become deformed and cause the target to not act like the modeling experiments conducted in Aim 1. Numerous avenues exist to work around this issue but the simplest method for testing this issue is to perform the fabrication step on a test liner and then use the fabricated ferromagnetic polymer in the 3-axis testing stage to test for repeatability.

A second pitfall is that the sensors do not conform to the inner shape of the prosthetic socket during fabrication and the curvature and angle of the sensors cannot be accurately approximated by the interior surface shape of the socket. If we find that the sensors do not perform as we anticipate based on our Aim 1 experiments, we may add fabrication steps to ensure that the sensors are flat so they can perform as anticipated.

Aim 2.2: Structured and Live-Environment Ambulation and Utilization

For each participant we want to confirm the LSM motion observed for the fabricated sockets are consistent with the published literature. To do this we will have participants walk through a laboratory-controlled body weight bearing and level ground walking protocols. This can then be compared to bouts of body weight bearing and walking in real-life environments when the user is expected to navigate varying terrain outside of the laboratory. By asking participants to use the fabricated sockets in real-life environments we can confirm the promising nature of translating this technology into clinically relevant conditions.

Aim 2.3: Socket Fit Perturbations

Fit perturbations are an everyday element of wearing a prosthetic device that can cause reduced function and ability to comfortably wear a prosthesis. To counteract a deteriorating fit users are generally provided techniques by their clinicians. In this aim we want to explore common fit perturbations and techniques used to counteract fit deterioration to understand how they effect LSM.

A largely accepted method for accommodating residual limb volume fluctuations that can cause an uncomfortable is to don or doff socks (55–57). Prosthetic socks are a layer of fabric that range in thickness depending on the sock's ply designation. In the pilot investigation, we have found that when adding layers of socks to the residual limb, the residual limb is restricted regionally, and we have hypothesized that sock ply addition may have predictable LSM outcomes. In a laboratory-controlled environment we explored the effects that sock ply will do to the magnitude of LSM.

Similarly, during the donning and doffing process it is easy to misalign the socket by rotating the limb with respect to the socket. When this is done, we will measure if there is increased LSM due to the socket being misaligned when donned poorly by the user. In the pilot investigation, the user's socket was able to realign itself during bouts of walking without input from the user.

The coefficient of friction for the liners we plan to use for these fabricated sockets have nearly no slip between the limb and the residual limb (12,50). Knowing that sweating within the liner is a clinically relevant issue and can cause a decrease in friction between the limb and liner, we want to explore how that can cause fit deterioration (58). Artificially allowing the limb to slip along the liner by putting petroleum jelly on the residual limb will allow investigation of a user's fit perturbation in a controlled environment. In the pilot investigation we've observed a dramatic increase in shear LSM when the limb is allowed to slip relative to the liner, but it is unknown how effective petroleum jelly was as a surrogate for limb hyperhidrosis (though many users had the sensation of having a too sweaty liner).

Potential Pitfalls and Alternative Approaches.

Notably we plan to fabricate pin locking and pinless suspension sockets. It has been well investigated that pin locking suspension create unique LSM data compared to vacuum and sleeve suspensions (20). The experiments and data will provide a platform to investigate various other suspension types. Ultimately the LSM measurements collected are variable due to the individualized fit of a socket in addition to the suspension type used. To complete an investigation comparing LSM between suspension type would require additional resources and time that are not feasible to complete in this proposal's timeline.

Interpretation of Results.

We anticipate there to be an LSM response similar to the published literature for pin locking transtibial sockets when walking and weight bearing in a controlled environment and slightly larger in magnitude when ambulating in a live environment. Solving the inductive trilateration data will provide us with the needed data along each shear and normal axis to compare our results against previous investigations. Ten

participants were consented with IRB approval and though a relatively small sample size, it was a feasible study to conduct.

Furthermore, we hope to investigate and better understand the implications of specified perturbations to socket fit. We appreciate that there is a complex response between the positions of the bone, soft tissue, linear, and target, all relative to the fixed LCO antenna array in the ridged socket wall with each of these socket fit perturbations, but we may find that there are common patterns that translate to the LSM data collected. The objective for this aim is to build the basis of knowledge for how the target moves in relation to the LCO sensor array with known perturbations.

1.2.3 Aim 3: To identify adaptations in the cutaneous microvascular structure using OCT.

We hypothesize that the everyday limb-socket motion will cause adaptive microvasculature remodeling that is controlled by the shear and normal stressors that the skin endures.

Limb-sock motion and residual limb health have seldom been studied for correlations in the prosthetic field. Data collected from the in-laboratory testing on LSM during common prosthesis usage will be obtained for specified anatomical locations along the residual limb and compared to structural angiography images captured with optical coherence tomography. Cutaneous microvasculature structural adaptations are hypothesized to be observed in regions of the limb that experience higher magnitudes of LSM, and lack of adaptations may be indicative of regions that are predisposed to skin breakdown injuries.

Immediately following major lower limb amputation, the tissue of the remaining limb is subjected to new daily stressors. Most notably, the skin and deeper tissues are subjected to full body load bearing as the prosthesis is used for ambulation. Normal and shear stresses from the socket have been well studied and have been shown to be large enough to occlude blood flow to regions of the residual limb, cause blistering and ulceration, and neuropathic pain (59,60). Socket fit issues causing skin breakdown and pain are leading causes of inability to wear a prosthesis which significantly impacts quality of life and function.

In recent investigations (40,61), optical coherence tomography (OCT) was used as a modality to measure post occlusive reactive hyperemia (PORH) and structural elements of the cutaneous microvasculature. It was thought that PORH and structural elements could be used as a physiological measure to predict residual limb skin health. To measure PORH in this experiment, the residual limb was cyclically loaded with an actuator and applicator tip, then serial images were captured with the OCT camera and analyzed for cutaneous microvasculature density within a constant region of interest on the limb. On a separate day, cutaneous microvasculature structure was imaged by slightly warming the skin to cause vasodilation and an OCT image was captured to map the patent vessels. These methods were shown to accurately capture the PORH response, and microvasculature structure. Ultimately, this technique was utilized on prosthesis users' residual limb and contralateral limb and it was found that two of the three subjects investigated showed a faster PORH response time and larger vessel density on the residual limb compared to the healthy contralateral limb, possibly showing an adaptive response in the cutaneous physiology.

These results were promising but there was a missing element to describe the adaptive changes observed at the locations tested with OCT - LSM interface stressors. Conceivably, the anatomical locations tested with

OCT did not see sufficient stressors to induce an adaptive response for some participants in the investigated location, yet for others, there was enough interface stress to create an adaptive response. Presumably these stresses need to be persistent and observable with each time the prosthesis user wears their prosthesis, and thus a sample of ambulation LSM data may provide insight on what the daily LSM stressor are for a given prosthesis user.

In this investigation we will measure interface motion and take structural cutaneous microvasculature images to observe any adaptations the physiology adopts to deal with the socket stresses. Furthermore, assuming that the limb has experienced similar LSM for prolonged period (as long as the user has worn this practitioner prescribed socket shape) at the measured location, we expect to observe fully adapted vasculature structure. From this analysis we anticipate observing well, and poorly adapted vasculature and we can begin to compare the likelihood of a skin injury based on a given regions structural components. Directly comparing LSM to limb health has yet to be done in the field and this investigation is the first, known, attempt to relate LSM and skin health in numerous regions on the residual limb.

Experimental Designs.

Aim 3.1: Structural Optical Coherence Tomography Imaging of Transtibial Prosthesis Users

Data collected from the embedded inductive trilateration sensors will be processed to gain insight on the interface movements for each participant recruited. Knowing that the investigational socket fabricated will be a duplication of the practitioner-prescribed socket worn by the user, we will assume that the interface motion observed within Aim 2 will be similar to what the limb experiences daily.

Prior to investigational socket fabrication, anatomical locations along the limb will be identified and the embedded trilateration sensors will be intended to track interface motion for the identified regions of the limb. These same four location will then be investigated with OCT imaging to develop structural microvasculature images for each participant.

The aforementioned method will be implemented where the participant's skin will be warmed with a custom warming ring, causing the microvasculature to become patent, allowing for clear speckle variance OCT imaging to be conducted. These images will be processed and *en face* projections of the vessels will be analyzed. Depth of vessels will be identified, and the vessel structure compared to the limb's motion during ambulation will be compared.

Interpretation of Results.

OCT microvasculature structure images will be obtained from a subset of the same participants in Aim 2 and will be oriented so that the inductive trilateration data are in the same cartesian coordinates. To do this the *en face* images will be aligned with the x- and y-axis of the inductive trilateration positional data, as they are in-plane when the socket is being worn.

From this experiment we can perform comparisons within each participant and comparisons amongst all participants. In preliminary experimental position data, it is clear that different regions of the limb

experience significantly different LSM. Knowing this, we can compare the four anatomical regions to each other within a single participant's data. We hypothesize that regions with greater interface motion will see greater structural adaptive changes because there is more motion to influence the blood being driven out of that region of the limb. Furthermore, we anticipate that the vessels may align with the longest motion of sheer stress.

Following this analysis, the same can be done when comparing one subject to the next. Some participants may be more capable of forming adaptations, but we hypothesize that it will be dependent on how well the socket is fitting in locations and the pattern of the LSM.

Ultimately, we expect to see that the heterogenous, fractal nature of microvascular structure (44) will be modified and aligned with large magnitudes of shear stress. Though if we do not observe structural adaptations in regions of high LSM for a given participant, we may further investigate the user's history of skin breakdown as evidence that physiological adaptations, or lack thereof, influence clinical outcome.

Potential Pitfall and Alternative Methods.

Difficulty with analysis may arise because of the difference in slippage between a user's practitioner prescribed liner and their limb compared to the experimental liner. Different coefficients of friction between the limb and the liner for the practitioner prescribed prosthesis may create a discrepancy in LSM that we do not capture with our investigation trilateration array socket and liner. If this is thought to be the case, the users' practitioner prescribed prostheses will be compared against the investigational sockets fabricated by various socket comparison and material testing methods.

Timeline.

This study should be completed within 2 years. All the Aims of this proposal can be completed simultaneously. Fabrication of the sensored sockets will be the most time-consuming aspect of study preparation, which will require 3-5 days of fabrication work per participant. While sockets are being fabricated the modeling work can be completed for Aim 1. Once a participant is fitted to the investigational socket and has completed the structured ambulation and fit perturbations in Aim 2, they will only need to return to the lab for one day of optical coherence tomography imaging.

Chapter 2. Inductive Trilateration Sensor Development

2.1 Theory and Rational

Trilateration is a known mathematic technique used to calculate a Point in three-dimensional space using three distance-sensing Anchors. With only the distance measurements from each Anchor to the Point and the relative position of the Anchors in three-dimensional space, the spatial coordinates of the Point can be determined.

In a simplified description of trilateration, Anchor distance is measured by the time an electromagnetic pulse is sent from the Anchor, reflected from the Point, and returned to the Anchor. Given the speed of light

constant, displacement the Point from the transducing Anchor can be calculated given Equation 1, where d is the displacement, r is the speed of light constant, t is the time that is recorded for the electromagnetic pulse to travel from the Anchor to the Point and back to the Anchor. In Equation 1, d is multiplied by two because the electromagnetic pulse travels twice the distance from the Anchor to the Point (there and back) in the time recorded from emission to reception.

$$2d = r \times \mathrm{t} \tag{1}$$

Further in this simplified model, it is assumed that the electromagnetic pulse radiates out in all directions and this allows the relationship of Anchor-Point displacement to be modeled as a sphere. Thus the Anchor-Point displacement (d) is known and is the radius of the sphere. The implication of this is that the location for the Point is constrained to the surface of the sphere, because any point of the surface of the sphere would satisfy the known Anchor-Point displacement. Lastly, to relate the possible locations of the Point to a location in 3D space, the location of the Anchor needs to be known so that there is a point of reference. For an anchor that is located at the origin of a Cartesian coordinate system and an Anchor-Point displacement, d_1, the model is described by Equation 2.

$$A_1(0,0,0) \rightarrow d_1^2 = (x-0)^2 + (y-0)^2 + (z-0)^2 \tag{2}$$

To resolve the Point's unknown location somewhere along the surface of the sphere, two additional Anchors are needed. The additional Anchors need to be in different locations compared to the others so that three unique models are created. For instance, Equation 3 depicts an Anchor that has been displaced along the x-axis (x_2) with a unique Anchor-Point displacement measurement (d_2), and Equation 4 depicts an Anchor that has been displaced in the x- and y-axis (x_3, y_3) with a unique Anchor-Point displacement measurement (d_3).

$$A_2(x_2,0,0) \rightarrow d_2^2 = (x-x_2)^2 + (y-0)^2 + (z-0)^2 \tag{3}$$

$$A_3(x_3,y_3,0) \rightarrow d_3^2 = (x-x_3)^2 + (y-y_3)^2 + (z-0)^2 \tag{4}$$

Conceptually, these three equations represent three spheres with unique radii, centered about the individual Anchors, and each sphere's surface describes a possible location of the Point. Assuming that the spheres overlap but are not tangential nor concentric, means that there will be at two locations of overlap (locations A and B in Figure 2). These two locations are locations in 3D space that satisfy the measurements and observations made by each individual Anchor.

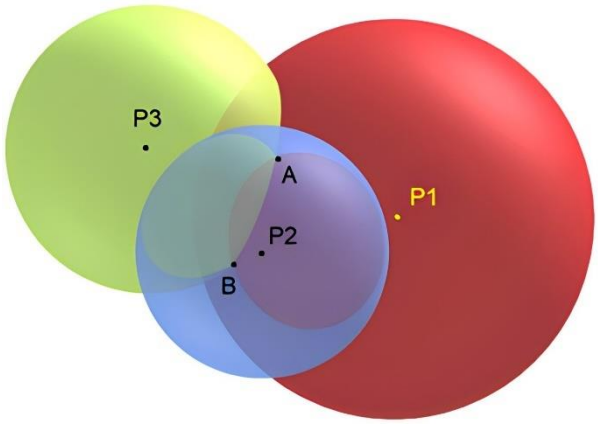

Figure 2: *Simplified trilateration conceptual model of three overlapping spheres (62)*

Mathematically, the overlap locations can be solved with a system of equations as described by Askari et al. (47) (Equations 5-7).

(5)

$$z = \pm \sqrt{d_1^2 - \left(\frac{d_1^2 - d_2^2 + x_2^2}{2x_2}\right)^2 - \left(\frac{d_1^2 - d_3^2 + x_3^2 + y_3^2 - \frac{x_3(d_1^2 - d_2^2 + x_2^2)}{x_2}}{2y_3}\right)^2}$$

(6)

$$x = \frac{(d_2^2 - x_2^2 - d_1^2)}{-2x_2}$$

(7)

$$y = \sqrt{d_1^2 - x^2 - z^2}$$

In this derivation the Anchors are along the xy-plane which causes the two solve positions of the point to be symmetric across the xy-plane. Depending on the application of the trilateration sensor, a fourth Anchor may be required to resolve the final position of the Point, or assumptions about the physical location of the target are used to discern between the positive and negative z-axis location of the Point. For example, if a trilateration algorithm is used in a Global Positioning System, it may be assumed that the Point is located near the surface of the Earth.

In lower limb prosthetics, the limb-to-socket interface is a field of significant interest. In 2018 Sanders et al. published a study describing a novel sensor that used inductive sensing to approximate socket usage (63). Later this technique was improved to measure the distance, normal to the internal socket surface, the limb was from the socket surface (24,64). The sensor technology was coined a Sock Thickness Measurement (STM) sensor because the sensors (aforementioned Anchors) were embedded in transtibial sockets, and the target (aforementioned Point) was embedded within a user's prosthetic liner. This technology allowed for single-axis distance measurements and in the following dissertation, the sensor technology was modified so the mathematical method of trilateration can be used to identify three-dimensional movements of a limb within a transtibial socket.

2.2 Three Axis Controller Jig for Positional Testing

2.2.1 Jig Design and Operation

In preparation for testing a sensor system that could track 3D positions a custom three-axis movement jig was designed to allow users to programmatically move an object relative to the base with high accuracy (Figure 3). The jig consists of 80-20 framing aluminum used to mount a fine-movement three-axis linear slide rail system with a two-phase stepper motor assembly, step size of 0.05µm, accuracy of 60 µm, and repeatability of <3 µm (Zaber Technologies Inc., X-XYZ-LSM200A-K0061-SQ3)(65).

Design considerations were made to ensure that the inductive sensor being tested would not be affected by the hardware used in the three-axis controller. Any magnetic or electrically conductive material (i.e. the framing and slide rails) was designed to be outside the region where an inductor-capacitor oscillation sensor would be placed. As such the framing dimensions of the jig was designed to be 30.5 by 61 by 61cm. Custom mounting parts that would be within range of the sensor and target were machined or printed with ABS, VeroClear, or Nylon so that the movement jig did not interfere with the inductive signals collected. A base plate to mount the sensors and a pylon for mounting the targets was developed.

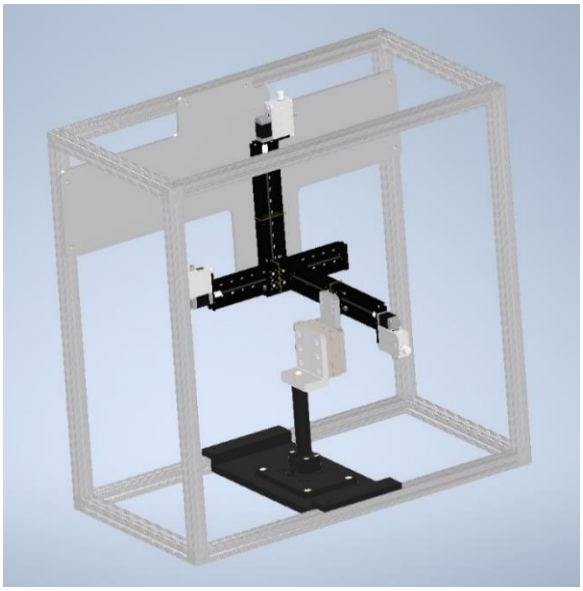

Figure 3: *Three axis controller jig CAD rendering. Parts include the thee-axis slide rail, custom plastic mounting pieces, collision reduction parts, and framing hardware.*

Software was developed to control the position of the target-mounting piece both globally and with respect to a locally defined reference frame (LabVIEW, National Instruments). To do this, the system was designed to handle manual positioning commands from an operator, move to coordinates defined either globally or locally, stream a predetermined path trajectory, and plan simple movement paths to avoid collisions between the pylon and hardware located within the travel volume of the system. By allowing positioning within a locally defined reference frame, this system is useful for a variety of applications such as inductive sensor calibration. The robotic control flow diagram can be seen in Appendix 1.

The operator-controlled manual positioning of the target-mounting piece was handled with an attached keyboard with both fine and coarse positioning states. User input directly moved the target-mounting piece to locations controlled by live input. Once the target-mounting piece was in a chosen location, the operator could mark the location as a reference position. Two additional reference locations were then marked (generally the center of the sensors, or anchors). With all three reference positions defined, a rotation matrix was established between the global coordinate system of the linear stages and the local coordinate system defined by the sensor locations. Local positioning coordinates were then translated into slide rail positioning commands using the rotation matrix to accurately situate the target-mounting piece with respect to the sensor locations.

Path-streaming was implemented by generating a queue of positioning commands read from an input CSV file containing hold times and Cartesian coordinates, defined locally. Once the queue was built, the system moved sequentially through each point, pausing at each coordinate for its specified hold time. Using this basic strategy, paths could be easily executed for performing inductive sensor calibrations or generating paths around obstacles.

2.2.2 Jig Validation

An initial experiment was run where three inductor-capacitor oscillation sensors were placed on the sensor mount plate and the three axis controller operated a randomized flightpath above the sensors without a target mounted to the jig. Immediately following the first flight path, a target was mounted and the same flight path was run with the target affixed to the jig. Data from the sensors were recorded, normalized to the baseline signal value, and evaluated for any signal changes from the sensors that could be related to the controller jig. Figure 4 shows the signal intensities recorded during both flight paths, where a target was added to the jig at Time = 1.14×10^5. Maximal signal changes observed from the target-less flight path was +1344 arb. unit, while maximal signal changes observed from the target flightpath was -739359 arb. unit. This suggests that the three axis control jig may introduce noise to the sensor that is <0.2% of the range of the sensor interacting with the target. This noise was considered negligible for further testing and no other design modifications were made to the jig.

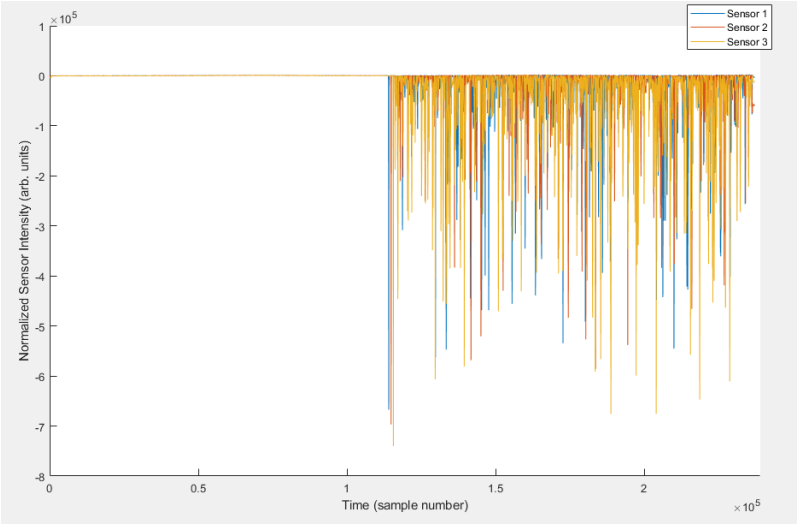

Figure 4: *Sample sensor data exemplifying that the three-axis jig does not introduce inductive noise to the sensor as the target-mounting piece is moved above the sensor.*

2.3 Modeling the Sensing Region of an Individual Sensor with Modified Target

In prior investigations by Sanders et al. the sensors were paired with targets that were of infinite surface area relative to the individual sensor. This was done because it was found that when a sensor was off center from a smaller target, the signal observed would decay[3]. By creating an 'infinite' sheet of target relative to the sensor, there was confidence that the signal observed was due to the target moving in the perpendicular axis to the sensor in one-dimension (the separation axis). This also assumed that if the target drifted in the

plane of the sensor, there was no signal change because the target was still able to saturate the sensor's signal. This was the theory that allowed for stable distance calculations presented in preceding studies.

In this dissertation, signal decay due to target-sensor misalignment was leveraged to perform multidirectional distance detection. Early observations while working with the sensors revealed that altering the size and shape of the target could allow for predictable signal decay.

To model the interaction of the sensor and target, first a single 32mm diameter (0.15mm thick) inductor-capacitor (LC) oscillation sensor was fabricated with 40 coils, a 220pF capacitor, 10kΩ thermistor, and 30AWG twisted copper wire. Flexible ferrite (0.30mm thick) was added to the back of the sensor to shield the magnetic field created by the LC sensors from erroneous noise. The LC oscillation sensor was mounted to the base of the three-axis controller and connected to a custom data collection board that measured the signal at 32Hz using as inductance to digital converter chip (LDC1614, Texas Instruments).

Secondly, the custom ferromagnetic polymer target was manufactured and embedded in a commercially available prosthetic liner (Alpha Silicone, WillowWood Global LLC). A 32mm diameter hollow punch was taken from the liner and mounted to the target-mounting piece of the three-axis controller.

A coordinate system was defined in the 3-axis controller software relative to the single sensor mounted on the base. The z-axis was defined as being perpendicular to the center of the sensor, defining the height above the sensor. Meanwhile the x- and y-axes were orthogonal to each other and the z-axis but due to the symmetry of the circular sensor, were not aligned with any physical element of the sensor. Additionally, the origin of the coordinate system was centered in the circular sensor in the xy-plane and on the surface of the sensor construct (height of construct was 0.45mm) in the z-axis.

A flightpath was run above the sensor in five planar movements that sprawled in a radial fashion from the center of the sensor with angles at 80^{o} and the final at 40^{o}. The target was moved in 1mm steps from 0-15mm along the z-axis and in 5mm steps from 0-45mm along the radial axis from the center of the sensor, creating 160 points per plane. The sensor's signal intensities were recorded continuously at 32Hz as the target was moved, but only values at the programmed flight path positions were recorded and analyzed. Figure 5 represents the five radially sprawling flight paths tested.

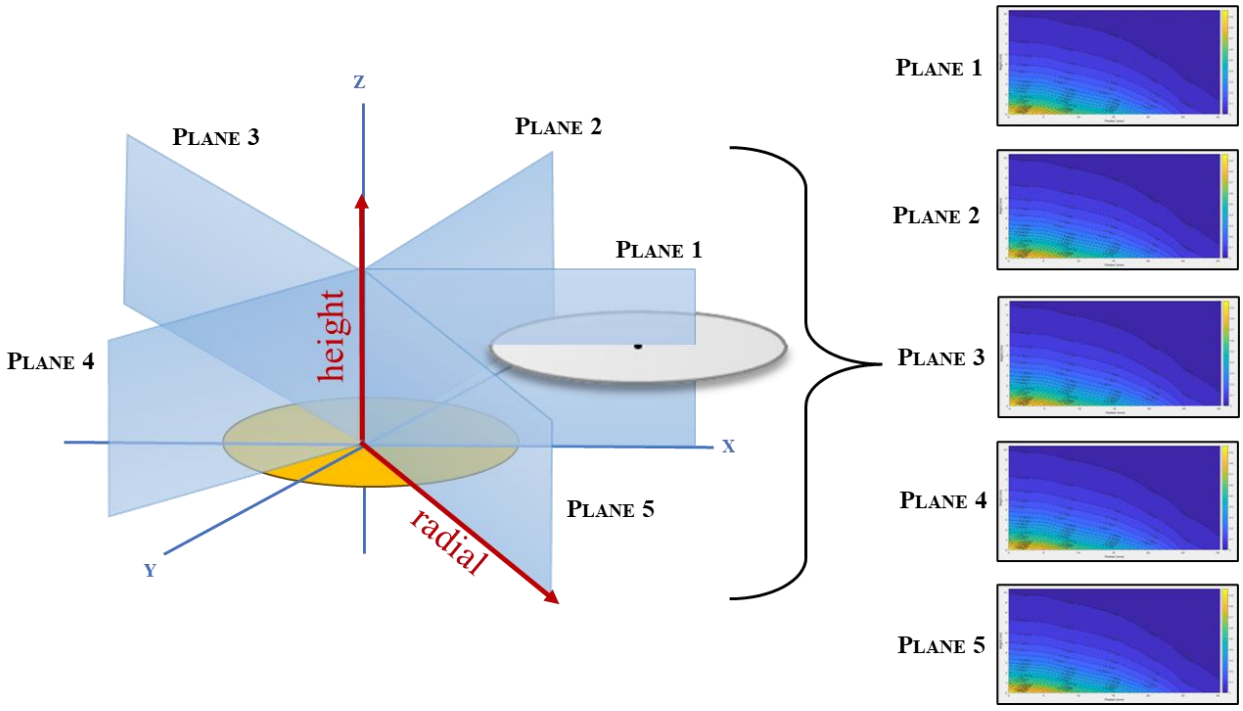

Figure 5: *Sensor-target displacement mapping schematic with a 32mm diameter target. Gold disc represents the sensor, grey disc represents the target, and the blue planes are the programmed flightpath positions.*

From the five planes of data collected a mean and standard deviation (Table 1 and 2, respectively) of positional signal values was calculated (all data can be found in Appendix 2). The largest signal reading (numerically the smallest when looking at the raw signal in arb. units) was when the target was moved to the origin, or directly on top of the sensor. Conversely the lowest signal reading was the baseline reading from the sensor, and that was observed when the ferrous polymer target was sufficiently far away from the sensor. Discernable signal could be observed 15mm from the surface of the target and 35mm radially away from the target. This range can be seen in Table 1, where the largest signal reading is 6175886.2 and the lowest signal reading was 6830830.6. Each plane showed similar signal characteristics, which is supported by the low standard deviation relative to signal change observed from the largest and lowest signal observed with a target introduced. The most variant signal was recorded at height 0mm, and radius 15mm, where it exhibited a standard deviation that was 2.6% of the range of signal intensities observed in the positional heatmap in Table 1.

Table 1: *Five-plane Mean for Positional Signal reported in raw counts (arb. unit)*

Mean Signal Value (arb. Unit)		Radial (mm)									
		0	5	10	15	20	25	30	35	40	45
Height (mm)	15	6825015.8	6825260.6	6825975.4	6826946.8	6828121.0	6829289.2	6830137.4	6830563.2	6830741.2	6830808.4
	14	6823329.0	6823700.0	6824648.8	6825942.2	6827458.2	6828933.2	6830026.0	6830518.8	6830730.2	6830808.2
	13	6821108.6	6821580.0	6822873.6	6824615.4	6826624.2	6828555.2	6829868.0	6830496.4	6830719.2	6830830.6
	12	6818099.6	6818777.4	6820553.2	6822873.4	6825534.4	6828043.2	6829745.4	6830485.4	6830730.2	6830808.4
	11	6814037.2	6814989.6	6817440.4	6820586.6	6824126.4	6827447.0	6829556.2	6830474.2	6830730.2	6830830.6
	10	6808516.2	6809907.6	6813284.6	6817536.2	6822306.6	6826668.6	6829411.8	6830429.8	6830730.2	6830830.2
	9	6800927.6	6802904.0	6807630.6	6813433.6	6819853.4	6825682.6	6829189.2	6830396.6	6830730.0	6830819.4
	8	6790392.2	6793265.6	6799936.8	6807841.4	6816550.4	6824437.4	6828955.6	6830396.4	6830752.6	6830819.4
	7	6775778.8	6780000.6	6789318.0	6800319.0	6812117.2	6822773.4	6828699.2	6830396.4	6830730.2	6830797.0
	6	6754985.8	6761123.4	6774536.0	6789733.0	6805898.6	6820568.2	6828373.4	6830374.4	6830730.2	6830797.2
	5	6725612.4	6734687.4	6753948.6	6774999.6	6797268.0	6817573.4	6828084.2	6830385.2	6830719.0	6830797.0
	4	6683396.0	6697066.4	6724671.4	6754257.2	6784933.0	6813393.4	6827724.8	6830385.2	6830708.0	6830774.6
	3	6621101.8	6641719.8	6682294.4	6723907.2	6766589.4	6807316.8	6827258.2	6830396.4	6830697.0	6830763.6
	2	6529380.0	6561285.0	6620702.4	6679459.4	6739163.4	6798104.4	6826698.4	6830374.0	6830697.0	6830741.4
	1	6389060.2	6439064.2	6527342.6	6610974.8	6695306.8	6783437.8	6825790.2	6830270.6	6830607.8	6830674.6
	0	6175886.2	6255287.8	6389329.4	6509854.2	6630380.4	6762174.2	6824537.4	6830045.0	6830693.4	6830574.4

Table 2: *Five-plane Standard Deviation for Positional Signal reported as a percentage of the range between target and sensor*

St. Deviation of Signal Value (% of Range)		Radial (mm)									
		0	5	10	15	20	25	30	35	40	45
Height (mm)	15	0.0	0.0	0.0	0.0	0.0	0.0	0.0	0.0	0.0	0.0
	14	0.0	0.0	0.0	0.0	0.0	0.0	0.0	0.0	0.0	0.0
	13	0.0	0.0	0.0	0.0	0.0	0.0	0.0	0.0	0.0	0.0
	12	0.0	0.0	0.1	0.1	0.0	0.0	0.0	0.0	0.0	0.0
	11	0.0	0.1	0.1	0.1	0.0	0.0	0.0	0.0	0.0	0.0
	10	0.0	0.1	0.1	0.1	0.0	0.0	0.0	0.0	0.0	0.0
	9	0.0	0.1	0.1	0.1	0.0	0.0	0.0	0.0	0.0	0.0
	8	0.0	0.1	0.2	0.2	0.1	0.0	0.0	0.0	0.0	0.0
	7	0.0	0.2	0.2	0.2	0.1	0.1	0.0	0.0	0.0	0.0
	6	0.0	0.2	0.3	0.3	0.1	0.1	0.0	0.0	0.0	0.0
	5	0.0	0.3	0.5	0.4	0.2	0.1	0.1	0.0	0.0	0.0
	4	0.0	0.4	0.6	0.5	0.3	0.2	0.1	0.0	0.0	0.0
	3	0.1	0.6	0.9	0.8	0.5	0.3	0.1	0.0	0.0	0.0
	2	0.1	0.7	1.2	1.1	0.7	0.4	0.1	0.0	0.0	0.0
	1	0.1	1.0	1.7	1.8	1.3	0.7	0.2	0.0	0.0	0.0
	0	0.9	1.6	2.4	2.6	2.4	1.3	0.4	0.1	0.1	0.0

The standard deviation data suggests that the mean signal value heatmap is symmetric about the height-axis. Furthermore, to map the entire target-sensor interaction in 3D space, the mean signal value heatmap can simply be revolved around the height-axis. Figure 6 is a depiction of the mean signal value heatmap in the height-radial plane revolved around the heigh-axis and put in relation to the standard x-, y-, and z-axis coordinate system.

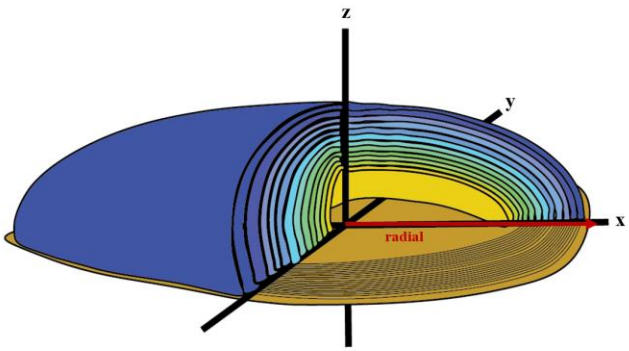

Figure 6: *Artistic depiction of the target-sensor interaction. Colored shells represent the signal intensity values and can be considered proportional to the colors in Table 1 (yellow is a stronger signal and blue is a weaker signal).*

A recurring source of error in this experiment was defining the coordinate system relative to the sensor by eye. The software of the 3-axis controller was designed to allow the user to identify the origin using keyboard presses, controlling where the target-mounting piece traveled. This meant that the operator was required to precisely align the head of the target-mounting piece and the center of the sensor to ensure that all of the movement of the flightpath was in correct reference to where the sensor was mounted. Human error of this sort was around 1mm.

Additionally, the liner-embedded ferrous-polymer target punch was collected from a commercially fabricated tapered liner, which when mounted to the 3-axis controller, caused the layer of ferrous-polymer to be at a slight angle to the plane of the mounted sensor. Measurements from the liner yield a target angle of about 2 degrees relative to the surface of the sensor. The height discrepancies were small (~1mm) but may be responsible for some of the variance seen amongst the different plans of positional signal values.

There was also visual evidence that the ferrous-polymer layer might have variability in the thickness. Formal quantification was not conducted for this variability as it was thought that the commercial fabrication quality could not improve to maintain a uniform layer. If the thickness of the iron target was variable, this was considered to also introduce variability into target-sensor interaction measurement.

The standard deviation heatmap seemed to show a pattern where the most variable signal intensities were found along the sensor surface and offset radially, by 15mm. This distance is curiously close to the radius of both the target and sensor, which at this position, half of the sensor is being occluded by the target. The orientation of the target was held constant which means that different portions of the target material were covering the sensor as the flight path revolved around the height-axis. So, if there was a slight angle in the iron sheet, some ferrous-polymer would be slightly closer to the target proving a higher signal compared to when the target was interacting with the ‘higher’ edge, providing a lower signal intensity (thus a larger variance in signal). Similarly, if the thickness of ferrous-polymer was not consistent, we would observe a similar phenomenon.

Another plausible explanation for this high variance is that at this location is the human factor of aligning the sensor and flightpath in the three axis control jig. The target-sensor signal seems to be changing at the

fastest rate around the locations of where the standard deviation data is largest. So, if there was human error in aligning the center of the target with the center of the coordinate system, then the signal measurements could have been taken at different target-sensor displacements due to the coordinate system alignment error. Since the observed signal intensities were changing fastest in these locations, the standard deviation between measurements would thus be higher.

All considered, the error in these measurements were considered small enough to continue with the development of the inductive trilateration method, and further efforts to reduce the noise in this experiment was not pursued.

2.4 Inductive Trilateration Method

2.4.1 Model Choice

Similar to how electromagnetic pulses can be used to measure distance in the simplified trilateration method described before, the experimental data collected indicates that the distance of a target from the sensor can be determined based on the observed signal intensity. For instance, in Table 1, if a signal intensity of approximately 6.80×10^6 is detected, the target could be located at any of the following positions: (0,9), (5,9), (10,8), (15,8), (15,9), (20,6), (20,5), (25,3), or (25,2). This is a crude approximation but also demonstrates that the signal observed does not yield a uniform distance measurement. The plausible distances for the observed signal 6.80×10^6, are 9.0, 10.3, 12.3, 17.0, 17.4, 20.8, 20.6, 25.2, 25.0mm for the given coordinates, respectively.

The depiction in Figure 6 illustrates that the target interacts with a single sensor in a rounded nature, but it is not perfectly spherical. As a result, the spherical model presented in the simplified trilateration description cannot accurately describe the relationship between signal intensity and target location. Instead, the mean positional signal intensity data was linearly interpolated, and a contour plot was created along the two-dimensional plane so that an alternative model could be fit to the data.

The chosen fit was a parabola in which both the height and radial intercepts could be controlled by variables h and r respectively (Equation 8). The control of the intercepts is important because the dome-like relationship between position and signal is wider than it is taller.

(8)

$$\mathrm{h}\left(1-\frac{x^2}{r^2}\right)=z$$

For comparison a second model fit was evaluated. This fit was a circular fit in which both the height and radial intercepts could be controlled by variables h and r respectively (Equation 9). Since r was always greater than h, this equation defines an oblong circle centered on the origin.

(9)

$$\frac{x^2}{r^2}+\frac{z^2}{h^2}=1$$

Multiple signal intensities were tested and visually inspected for best fit. Figure 7 displays the experimental mean positional data and the curve fits with give x-intercept (r) and z-intercept (h) values for four signal intensities. Visually the parabolic function fit the experimental data better than the oblate spherical function, and subsequently, the parabolic model was chosen for further modeling.

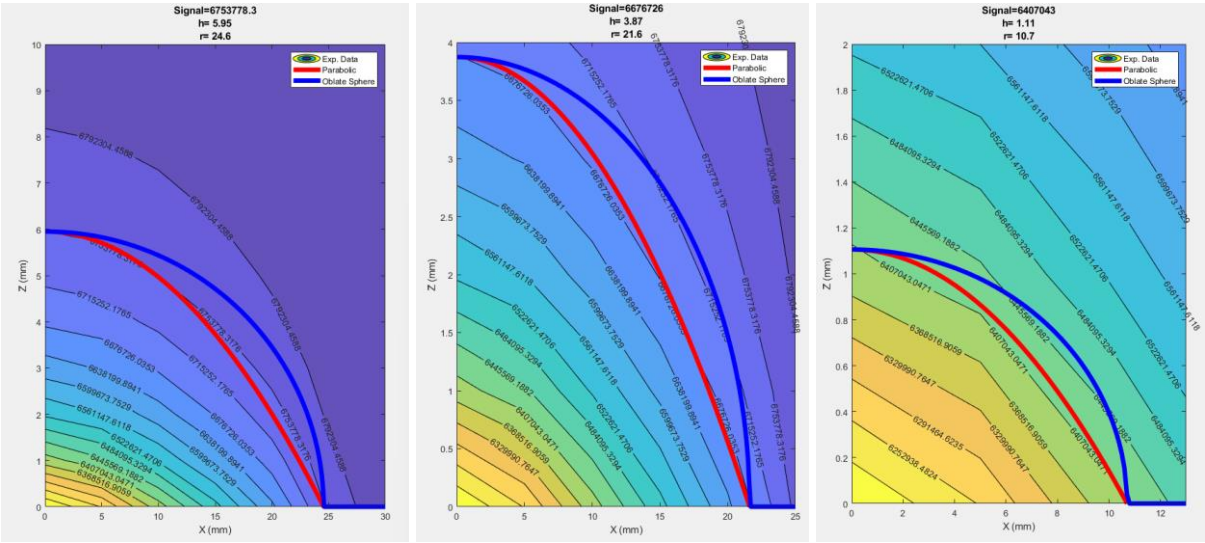

Figure 7: *Signal intensity heatmap and model fitting lines for various signal observations*

As an aside, this thesis was not focused on model fitting, but rather on the proof of concept for this technique. Admittedly, the parabolic model does not fit the experimental data perfectly but was sufficient for the application of the sensor. If time were taken to build a correct arithmetic model of this technique, the sensing region would need to be sampled more densely compared to what has been presented here. As can be seen in the rightmost panel of Figure 7, the contour plot has performed a linear interpolation between the sampled points, which were at 5mm spacing along the x axis. This exemplifies that much of the shape of the sensor-target interaction has been interpolated and would be a source of error for a more exact model. Moreover, the parabolic equations used in this dissertation roughly fit the experimental data but would benefit from more complex equations used to fit at the various levels of signal intensity. Attempts at this should be completed when final sensor and target hardware designs are validated (discussed more in Chapter 3.1.3).

With an appropriate two-dimensional equation identified, the three-dimensional equation was derived. As discussed previously in section 3.4 the experimental signal presented as symmetric about the z-axis and thus the equation could be minimally modified to represent the interaction between the target and sensor in 3D space. The equation for the paraboloid is shown in Equation 10.

$$\mathrm{h}\left(1-\frac{x^2+y^2}{r^2}\right)=z \tag{10}$$

Similar to the two-dimensional equation, the size of the "dome" defined by Equation 10 is controlled by the variables h and r, where h describes the z-intercept and r describes the radial intercept. This means that h and r are inherently a result of the strength of the signal observed. For example, a weaker signal, because

the target is far away from the sensor, creates larger radial and z-intercepts (left pane of Figure 7), producing a larger "dome". Whereas a stronger signal, because the target is close to the sensor, creates smaller radial and z-intercepts, producing a smaller "dome".

To create a continuous model with paraboloids of varying sizes, signal intensity was related to the variables that described the size of the paraboloid, r and h. To do this, intercept distances (radial and z) were plotted against signal intensity and interpolant equations were fit to these relationships (Figure 8). The result from this was two equations that took signal intensity as an argument and returned the radial- and z-intercepts for a given signal intensity observation. Subsequently, Equations 11 and 12 could be substituted into Equation 10 to develop an equation that takes signal intensity as an argument to describe the possible locations that the target could be from the sensor (the surface of the paraboloid described by the equation).

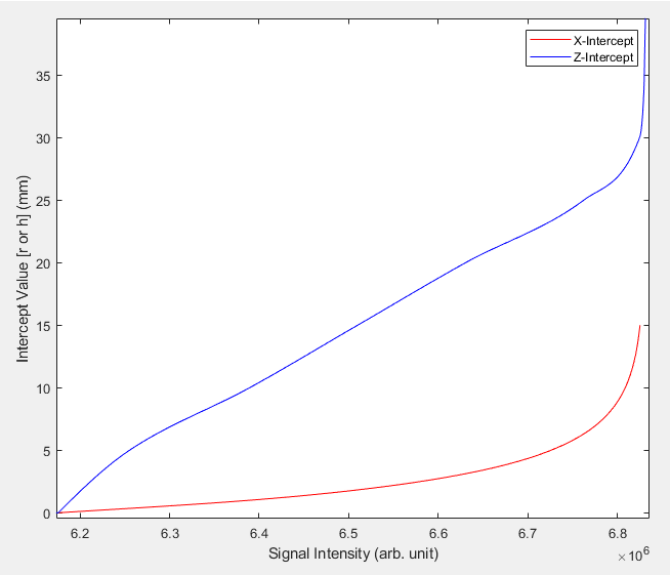

Figure 8: *Radial and height intercepts as a function of signal intensity observed*

$$r = X_{interpolant}(signal\ intensity) \tag{11}$$

$$h = Z_{interpolant}(signal\ intensity) \tag{12}$$

$$Z_{interpolant}(signal\ intensity)\left(1 - \frac{x^2 + y^2}{X_{interpolant}(signal\ intensity)^2}\right) = z \tag{13}$$

2.4.2 Trilateration Array Design

It was discovered that with the chosen target size of 32mm, the observed signal intensity waned when the target was displaced 32mm radially. This suggested that there is limited to no sensing capability when the target was moved so that the edge no longer overlapped with the edge of the sensor, and this was attributable to the target size, the sensor size, and the sensing region of the sensor. Knowing that the trilateration method

requires three unique measurements of distance to succeed, it was decided that three sensors be placed as close to one another so that the observed signals from each of the sensors were as large as possible. Accordingly, a standard inductive trilateration array (INTRAY) arrangement was developed.

The INTRAY arrangement is best described in a cartesian coordinate system, which ultimately provides a reference for where the sensors and target are in 3D space relative to one another. The coordinate system axes are referenced in millimeters. The first sensor is centered at the origin, (0, 0, 0), the second sensor is located along the x-axis such that the edges of the first and second sensor are tangential, (32, 0, 0), while the third sensor is located in the fourth quadrant such that it's edge is tangential to both the first and second sensor, (16, -27.7, 0). All the sensors are assumed to be placed along the xy-plane and are tangential to each other in the shape of an equilateral triangle (Figure 46).

Defining a standard for positioning the sensors within the INTRAY also defined the three equations to be used when solving for the position of the target. Equation 10 was used to describe the target-sensor interaction of each of the three sensors and it was assumed that each inductive sensor will function identically to the empirical model developed from the single sensor testing. Equations 14 to 16 were used to describe sensors one to three, respectively.

(14)
$$z = h_1\left(1 - \frac{x^2 + y^2}{r_1^2}\right)$$

(15)
$$z = h_2(1 - \frac{(x - 32)^2 + y^2}{r_2^2})$$

(16)
$$z = h_3(1 - \frac{(x - 16)^2 + (y + \sqrt{32^2 - 16^2})^2}{r_3^2})$$

Where h_1, h_2, h_3, r_1, r_2, r_3 are the z- and x-intercepts, respectively, for sensors one through three given the observed signal intensity from that sensor. Likewise, the operators modifying x and y are defined by the physical positions of the sensors in the standard INTRAY.

Equations 14 to 16 are the recapitulation of Equations 2 to 4 for the application of this dissertation. Equations 14 to 16 are the non-spherical model of the target-sensor interaction that is defined based on the signal intensity observed by the sensor, and unlike the simplified trilateration description, reducing the system of equations is more complex. For a given observation, one set of signal intensities is observed for the three sensors, meaning that h_1, h_2, h_3, r_1, r_2, r_3 would remain constant for that solve location. Because of this, those variables were left as constants in the system of equations, so that the positional solve equations (for X, Y, and Z) would be a function of the signal intensity observed. Anecdotally the solved equations are similar to Equation 5 through 7 but have a large number of terms and it is not useful to display the final equations.

Notably, the solved Z component of this equation does not contain two solutions as it does in the simplified description. This is because the model equations used are not spheres, they are paraboloids. Three paraboloids overlap in exactly one location and thus only one three-dimensional location can satisfy the

signal observed by the sensors. Additionally, in the physical arrangement of the INTRAY the sensor, the target cannot go in the negative Z space due to the surface of the sensors. The surface of the sensors are in the xy-plane with a height of zero and in the presented application, the target cannot go on the other side of the sensors.

2.4.3 Considerations for Inductive Trilateration Method

An alternative strategy considered for the trilateration solving methodology was a lookup table. Though not used, this method may provide a better representation of the experimentally collected data. To do this, each target position sampled would be mapped to the signal intensity observed. This table would be used so that an incoming signal intensity observation from each of the sensors creates a list of possible locations that closely matched the signal intensity observed. After offsetting for the location of the individual sensors, the common position of the three lists would be the point that satisfies all the observed data and would be the location of the target. A limitation to this methodology is that to have fine resolution in the solve data, the experimental data needs to be thoroughly sampled. This could increase the size of the lookup table, making the computation programmatically more expensive.

A limitation of the experimental data is that it was collected in an ideal environment, specifically, a flat environment. The INTRAY sensors will be mounted in curved sockets both with spherical and cylindrical curvatures. Attempts were made to sample the target-sensor interactions in curved environments but were constrained by the limited degrees of freedom of the three-axis controller. The target-mounting piece did not have degrees of freedom to rotate relative to the curvature. Instead, attempts were made to align the angle of target to match the curvature of the sensor mount but was challenging. Furthermore, this could only be done with cylindrically curved surfaces, while spherically curved surfaces were prohibitively difficult to align the target and sensor. To accurately quantify the differences between the idealize flat interaction versus a curved surface, a custom three degree of freedom target-mounting head needs to be deigned of non-interactive material and controlled to align the target and sensor appropriately.

The inductance to digital converting chip used on the data collection board in this dissertation has a maximal sampling rate of 32Hz for the eight individual sensors. This means that an individual sensor is being sampled within 3.9 milliseconds, and all eight sensors are sampled sequentially. In the model described, it is inherently assumed that the target can only be in one location and that the observations are made simultaneously. In reality, there is a timing delay between the three observations made per INTRAY (7.8 milliseconds from sensor one to sensor three) and in that time the target could move, invalidating our assumption. As it happens, though the target may move from one sample to the other, the system of equation solve still converges and we can approximate the 3D position of the target. Though this phenomenon was not investigated, it is thought that this may introduce a small amount of error compared to other aspects of this method.

A unique feature of the experimental data collected was that there was only one point that had the highest signal intensity, and this is important because if the target were to saturate the signal at a location away from the origin, the system of equations could break down. The data collected suggest that for a given signal intensity, the target could be located on a continuous *surface* that could be easily modeled. If, on the other hand, it was observed that the target saturated the signal away from the origin and maintained that signal

intensity up to the origin, then the signal intensity would describe a *volume* of locations describing where the target was. If this were true, there would be cases where for a given target location the signal from one sensor would saturate, needing a *volumetric* equation to describe the possible locations, while the other two sensors (because it is farther away from the other two sensors) would have *surface* functions describing the possible location of the target. Thus, instead of a single point of intersection between the three "domes", there would be two domes overlapping in a volume, meaning that the possible locations of the target would be described by a line. This would mean that the function would not converge on a single point, and thus the model would break down.

Though this could detrimentally affect the solving capability of the model, this same consideration could be leveraged to improve signal to noise. For example, if in the application the sensor is used, it was known that the target would not reach the center portions of the sensors, then the target could saturate the signal in locations the target would not reach, and that would subsequently create stronger signal in the areas the target would reach. Target size is explored in a later chapter as it was needed to improve signal to noise ratios. Additionally, sensor size and coil number could be altered to affect the target-sensor interaction signal, but this was not explored in this dissertation.

2.5 Proof of Concept

With the trilateration model established, proof of concept experiments were performed. One of numerous similar proof of concept experiments is presented here to illustrate the test performed to compare the known target movement and trilateration solve positions. To perform the experiments, an INTRAY sensor was fabricated, as described earlier, and mounted to the base mounting plate of the three-axis controller. A 32mm diameter ferromagnetic target was taken from a commercially fabricated liner and mounted to the target-mounting piece. The three-axis controller was calibrated by eye so that the INTRAY coordinate system defined the local coordinate system and a predetermined flight path was used to move the target above the INTRAY sensor.

2.5.1 Signal Calibration

Slight variations in hardware are inevitable when manufacturing individual inductive sensors, the data collection board, and ferromagnetic targets. These slight variations have been observed to influence the raw signal intensities collected from the inductive sensors. Most commonly, it was seen that the baseline signal and range of signal intensity collected as the output signal from the sensors varies. Figure 9 shows continuous signals, sampled at 32Hz, from three sensors while a ferromagnetic target was moved above the INTRAY in the predetermined flight path.

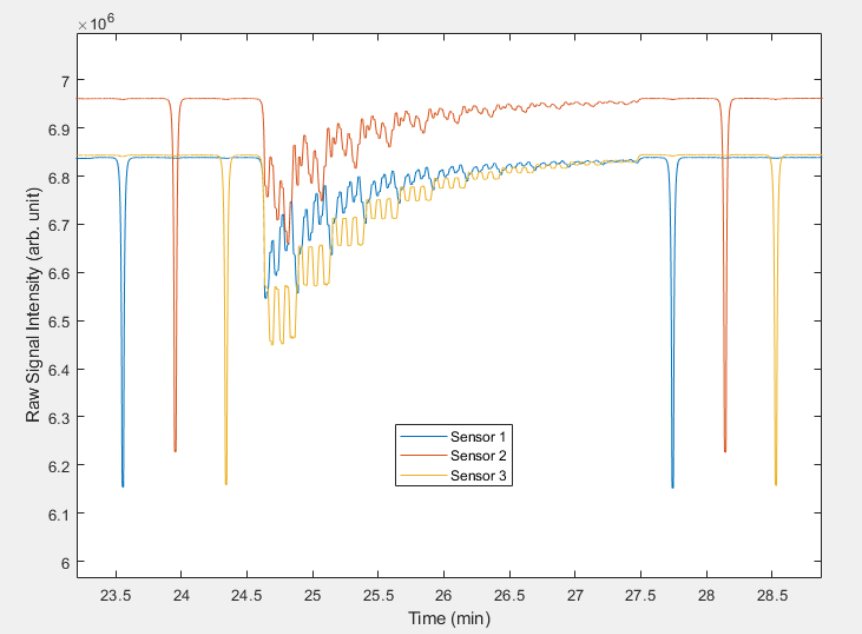

Figure 9: *Raw signal intensities observed from a patterned test flightpath. Spikes at the beginning and end of the flightpath correspond to the target eclipsing the given individual sensor.*

In Figure 9 there are three obvious spikes at the beginning and end of the flightpath shown. This is when the target was brought directly to the surface of the individual sensor. The apex of that spike is the maximal signal intensity observed from that sensor and the flat region around the spike is when the target was not near the sensor (in between the spikes is an arbitrary flightpath where the target interacts with all of the sensors). Notably we can see that Sensor 2 (orange) has an offset in the baseline reading, but visually there is not as drastic of a change to the range of the sensor.

An intermediary step was subsequently developed to calibrate raw signal intensity into a normalized signal intensity to manage the variation in baseline signal readings due to hardware differences. Raw signal intensity was normalized to a variable coined as the percent signal intensity. To perform this calculation, the strongest and weakest signal values from an individual sensor are used to define the range and offset the sensor. The weakest signal intensity value is recorded when there was no ferromagnetic target close to the induced electromagnetic field (which, numerically, is the maximal value observed), while the strongest signal intensity is recorded when the ferromagnetic target is on the surface of the sensor and completely occluding the sensor (which, numerically, is the minimal value observed).

In the case of Figure 9, Sensor 1 had a range from 6142703 to 6838670, Sensor 2 had a range from 6227220 to 6961330, and Sensor 3 had a range from 6142953 to 6844500. Once the strongest and weakest signal values were determined for each sensor in the INTRAY, the raw data could be converted into percent signal intensity for the given individual sensor with Equation 17. Results from converting the raw data stream in Figure 9 are displayed in Figure 10.

(17)

$$Signal_{\%} = \frac{Signal_{raw} - weakest}{\text{strongest} - \text{weakest}}$$

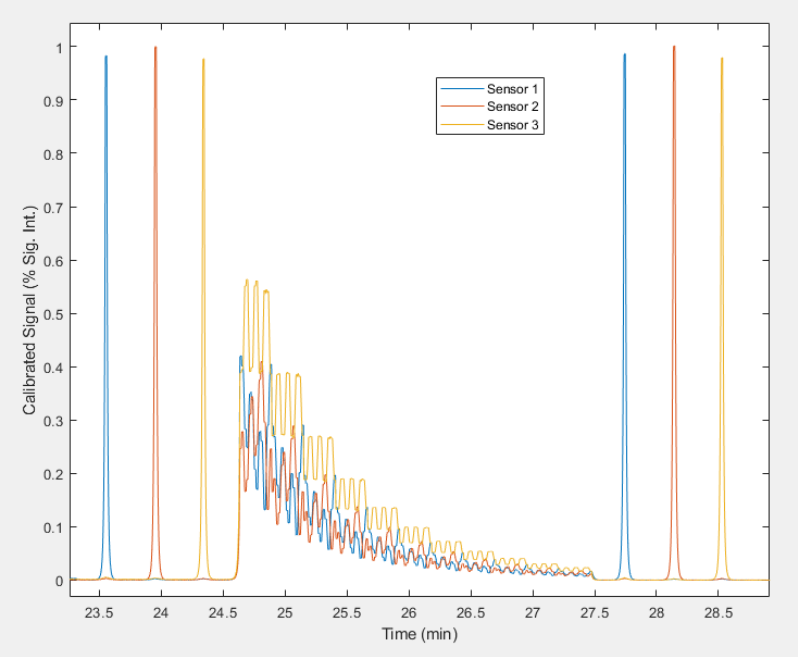

Figure 10: *Signal intensity data from Figure 9 converted to Percent Signal Intensity*

Next, data from the empirical model was converted into percent signal intensity using the same formula (Figure 11a). This also necessitated that Equations 11 and 12 be refitted to take percent signal intensity as arguments instead of raw signal intensity (Figure 11b). This intermediary step worked well to account for hardware differences and required a minimal amount of data for calibration.

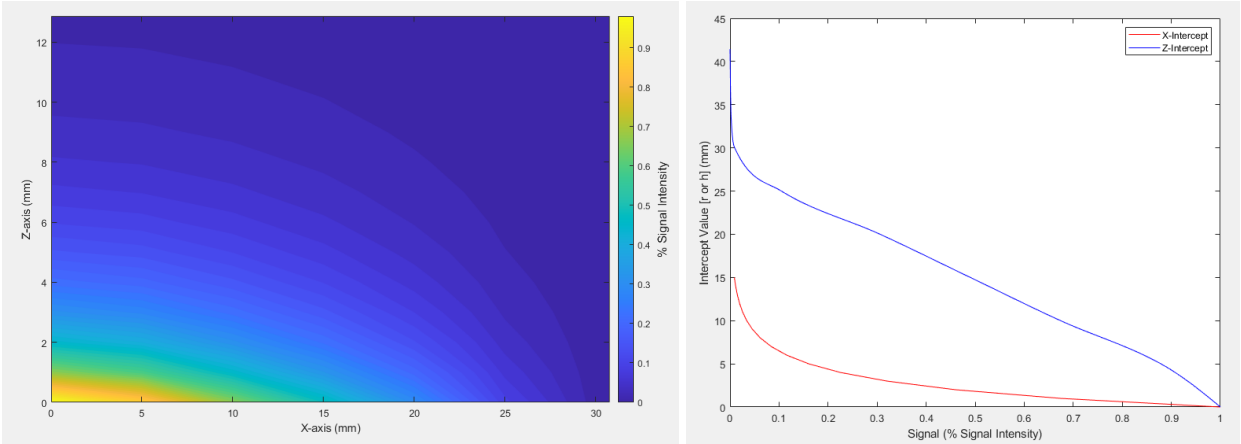

Figure 11: *(a) Data from Table 1 converted to Percent Signal Intensity and interpolated for sensor-target spatial interaction. (b) Data from Figure 8 showing radial and height intercepts as a function of Percent signal Intensity.*

2.5.2 Solve

The data presented in Figure 9 (between the first and last three spikes) was collected from a patterned flight path that was easy to compare against the INTRAY solving. The raw signal was calibrated into percent signal intensity and used in the functions described by the INTRAY solving methodology to generate three-

dimensional positions of the target. This data was plotted and visually compared to the known, programmed, position of the target taken from the flightpath data. Two plots were used to quickly evaluate the plausibility of the solved position data. The first plot (Figure 12) is the time versus directional component which is helpful for comparing specific differences between the known and solved position. The second (Figure 13) is a 3-dimensional plot, showing the spatial relationship of all the positions the target went to. Visual inspection suggested that this methodology may be a method to track the 3-dimensional position of a 32mm diameter ferromagnetic target.

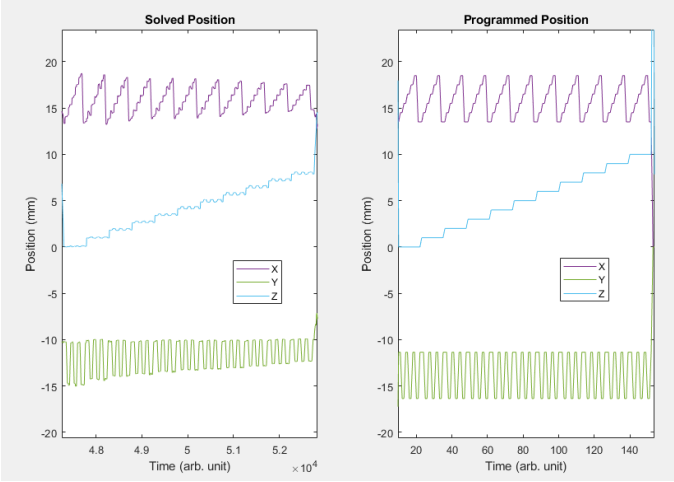

Figure 12: *(a) Inductive trilateration method for target position solve data versus (b) the known position of the target.*

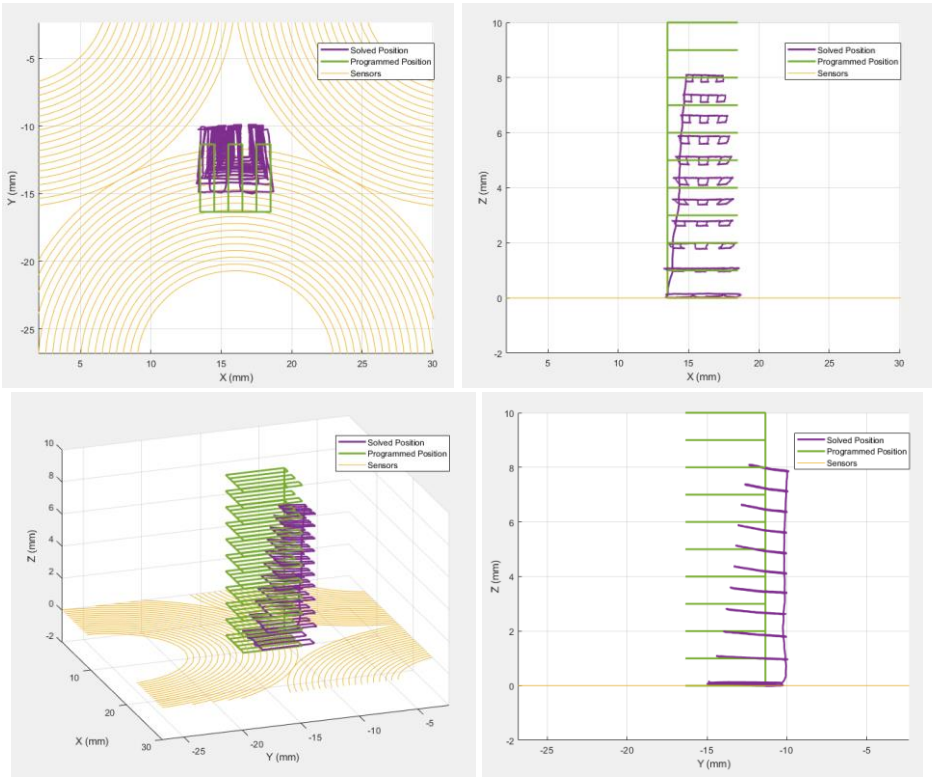

Figure 13: *Solved positional data plotted versus known positional data*

2.6 Inductive Trilateration with Ferrous Polymer Target Error

Ultimately a test was performed to evaluate the accuracy of the sensor's three-dimensional solving. The same sensors and target from the proof-of-concept tests were used in this experiment but a new programmed flight path was run. This flightpath consisted of 1000 randomly generated points within the bounds along the x-axis, -15 to 46mm, within the y-axis, -45 to 13mm, and within the z-axis, 0-15mm. The randomly distributed points of the flight path are shown in Figure 14, with the travel path between points being a line connecting the two points. The width of the bounds for the randomly generated positions was selected based on the size of the INTRAY and what was thought to be close to the sensing region between the target and sensors in the INTRAY. With the INTRAY and target mounted, the three-axis controller was calibrated by eye again so that the INTRAY coordinate system defined the local coordinate system and a predetermined flight path was used to move the target above the INTRAY sensor.

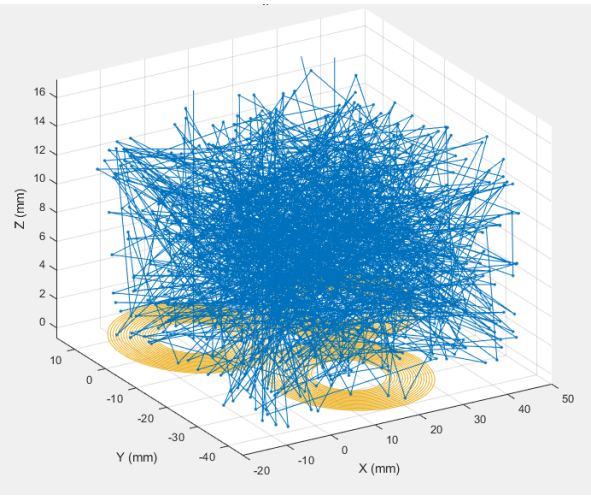

Figure 14:*Randomized flightpath for accuracy and sensitivity testing. Each node is a quasistatic hold position and the edges connecting the node is the direction of the flightpath. Gold rings represent the INTRAY sensor.*

Data was recorded at 32Hz and thus all programmed points and the movement from point to point were recorded. The flightpath took 92.7 minutes to run, and 178,000 signal intensity samples were collected. Raw signal intensities were calibrated, and then solved in the system of equations to produce the coordinate positions of the target respective to time.

Two calculations were conducted to evaluate for error, the first being an absolute position error, which was defined simply as the Euclidian distance from the known position to the solved position. The second error calculation had an algorithm that was more involved because it tested the error in displacement of target as it traveled between two points. To start, a single point of the 178,000 solved locations was used to mark the center of the test. A region with a radius of 3mm was drawn around that central location and all solved points that were within the 3mm radius were kept for comparison. A vector was calculated from the center point to each of the other points in the inclusion zone, where the magnitude of displacement and the angle offset was compared from the solved location to the known position. A difference between the magnitude of displacement and angle of displacement between the known and solved position was calculated and

referred to as the motion tracking error. This process was then repeated for each of the 178,000 solve locations in the flightpath.

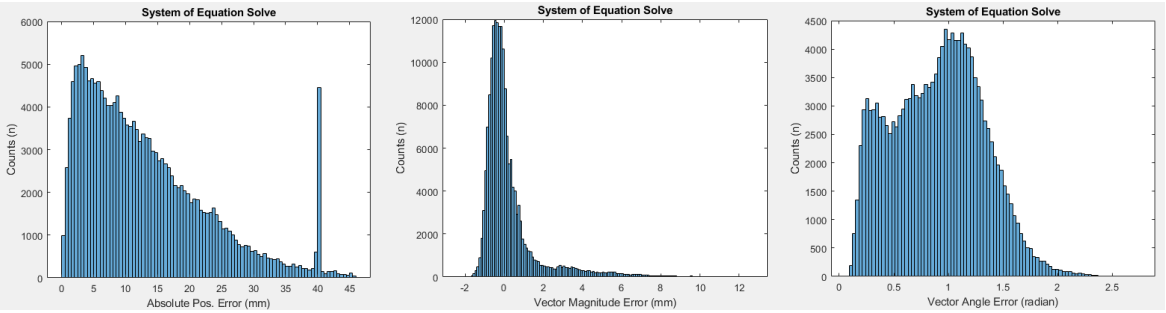

Figure 15: *(a) Absolute position error histogram as a proxy for accuracy, (b) Vector magnitude error histogram as a proxy for sensitivity, and (c) Angular error histogram within the sensitivity measurement.*

Figure 15 displays the histogram of errors in the entire tested region. The median error for absolute potion was 10.8mm (0.0 to 45.6mm), for magnitude of displacement was -0.2mm (-2.3 to 12.7mm), and angle of displacement was 0.9radian (0.1 to 2.7radian). Figure 16 shows the distributions of the error calculations for all positions tested in the flightpath.

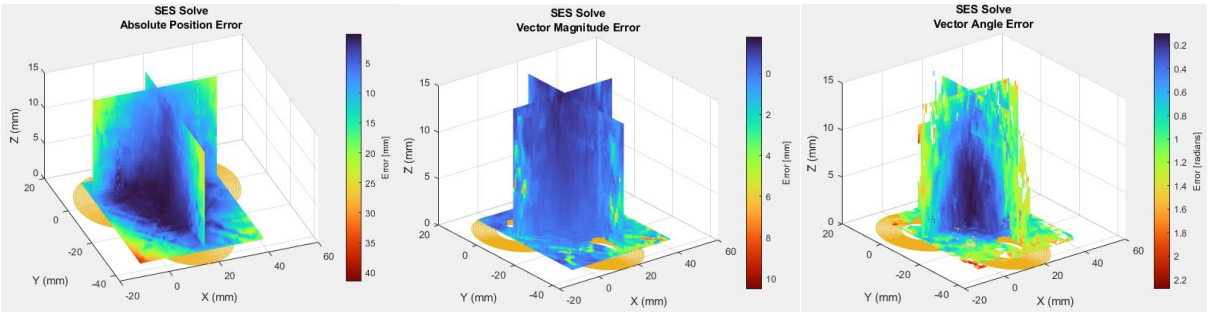

Figure 16: *(a) Absolute position error, (b) vector magnitude error, and (c) angular error plotted based on the location of the target relative to the INTRAY. Different locations above the sensor array have varying levels of accuracy and sensitivity.*

It was evident that there was a clustering of low error centered on the surface of the INTRAY (Figure 16), and it was considered that by limiting the solve space to this region the overall sensor error could significantly improve. Furthermore, the low error shape was discovered to be a result of the model shape of the INTRAY, rather than an arbitrary region. For example, if the target were at a point farthest away from the sensors that was minimally detected, all three sensors in the INTRAY would yield a large “dome” shape based on the modeling discussed earlier. The overlap of these three “domes” would create a surface of the minimum detectable region, because any target position closer than that would create a stronger signal and the sensor would be able to detect the target’s position. This means that the sensing region of the INTRAY is defined by the model based on a low signal intensity. As a result, a signal observation of 1.5% was used as a cutoff for the minimal detectable signal, and points with a signal less than 1.5% were excluded.

Thus, the error calculation was repeated where the 178,000 solved positions was filtered by the signal intensity observed and resampled our error. Solve positions that had at least one sensor’s signal observation lower than 1.5% was removed and 18,911 remained.

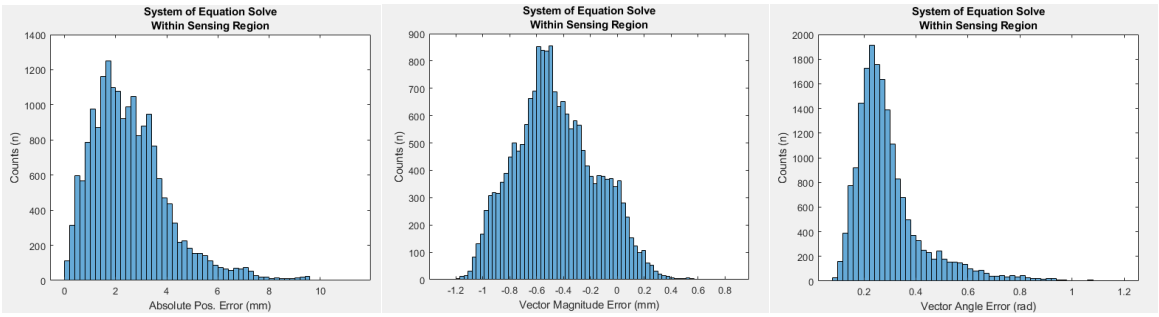

Figure 17: *(a) Absolute position error, (b) vector magnitude error, and (c) angular error after signal intensity thresholding.*

Figure 17 displays the histogram of errors in the threshold-defined region. The median error for absolute position was 2.3mm (0.0 to 11.3mm), vector magnitude was -0.5mm (-1.2 to 0.8mm), and vector angle was 0.3radian (0.1 to 1.2radian). Figure 18 shows the distribution of error measurements reported and Figure 17 illustrates the error based on location above the INTRAY. Given this signal filtering, the sensing region volume was approximated by the equation for a Reulaux tetrahedron, which revealed a sensing volume of 9.3cm^3. These results suggest that the sensor has higher precision than it does accuracy.

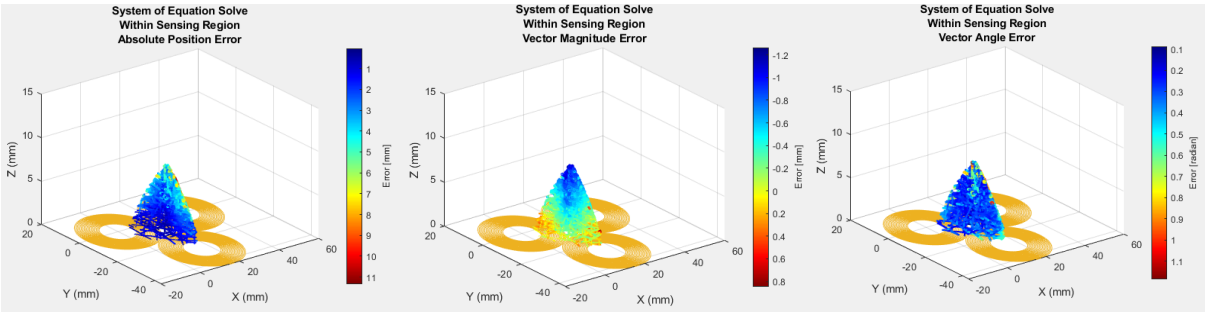

Figure 18: *(a) Absolute position error, (b) vector magnitude error, and (c) angular error after signal intensity thresholding, plotted by location relative to the INTRAY.*

Chapter 3. Inductive Trilateration in Prosthetic Sockets

3.1 Socket, Liner, and Target Fabrication

3.1.1 Socket Fabrication

Embedding the INTRAY sensors within the layers of the prosthesis during fabrication closely followed the published methods for sensor embedding (66). For both pin-locking suspension and pin-less suspension sockets an INTRAY stencil was used to draw on the locations of the sensor placement. Areas of relatively low curvature were preferred to try and create an ideal sensor target interaction as studied in the benchtop experiments. Three common locations, anterior distal, posterior midlimb, and fibular head relief, were identified and used as locations to mount the INTRAY sensors in almost all investigational sockets fabricated. The anterior distal site was identified as the point most distal along the anterior aspect before the socket began to curve into the inferior aspect. Inevitably the distal sensor of the INTRAY would be curved due to the shape of the socket but the two proximal sensors, that flanked the anterior crest, had low

curvature. To address the excess curvature, the center of the distal sensor was removed so that the sensor could flex easier and contour to the socket curvature. The posterior midlimb site was identified by eye as the central part of the posterior part of the socket, and the fibular head relief was identified by eye as the fibular head relief prominence.

For pin suspension sockets, an "anatomical point of interest" was chosen as the fourth INTRAY site. This was chosen by the research prosthetists based on the clinical judgment of how the limb interacted with the socket. For pinless suspension, instead of an anatomical point of interest, a common INTRAY placement was on the Inferior edge of the socket. As most participants wore a suction socket, and expulsion value was instrumented in the center on the INTRAY sensor. No magnetic or conductive material was added or removed near the INTRAY sensor, and this fabrication technique was thought to not interfere with the signal values recorded.

The orientation and order of the individual sensors in the INTRAY required specific considerations. These considerations attempted to maintain the cartesian coordinate system developed in the previous section and to align the axes with common anatomical axes, meaning that the INTRAY sensor was rotated to align with the socket anatomy. Each INTRAY's axes were aligned so that the X-axis was the socket's circumferential axis, the Y-axis was the socket's longitudinal axis, and the Z-axis was the distance between the surface of the INTRAY and the target. The Z-axis was restricted so that a negative Z position could not be a realistic solve position because that would mean the target would be on the outside of the socket. Furthermore, a positive movement in the sensor's X-axis means that the target would be rotating clockwise within the socket (negative is moving counter-clockwise), and a positive movement in the Y-axis means that the target would be moving in the proximal direction (negative is moving distal).

The order of the wiring for each sensor within the INTRAY also needed to be well tracked to use the collected data with the system of equations seen in the previous section. When fabricating the socket, the order of the sensors within the INTRAY is reflected because the socket is being fabricated from the inner surface, outward. As seen in Figure 19 the white inner layer of the socket shape is used to mount each of the targets, meaning that the inner surface of the socket, from the point of view of the target, is reflected from the perspective of the fabricator. Though not difficult, care is needed to efficiently wire the sensors in the proper order to work with the standardized equations.

Figure 19: *INTRAY sensor placement and wiring during the socket fabrication process for Participant One. Two arrays were wired into a single data collection board.*

It should be noted that in the early iterations of the socket fabrication, sensor placements were performed with a complex methodology that was discontinued and simplified to the above description. At the outset,

participants were asked to don an investigational liner, the anterior distal, posterior midlimb, and fibular head locations were identified by palpation along the liner, and a mark was made on the liner where the target should be placed. The INTRAY sensor placement, during socket fabrication, was then transcribed from the marks made on the investigational liner. Once the fabrication was completed, generally the targets did not align with the sensing region and the target would need to be shifted on the liner to align with the INTRAY. The low rate of success with aligning the target and sensor required the fabrication methodology to be improved.

3.1.2 Liner Fabrication

Ideal liner-target fabrication has yet to be completed. The two methods used in this project have laid the foundation for target-liner fabrication but the technique has not been perfected. Initially a punch-based method was used to convert an off-the-shelf liner to an investigational liner (Figure 20). In this technique, a 32mm punch was taken from an iron laden liner (commercially fabricated Alpha Silicone Liner, WillowWood) at the same location on the liner as it was being mounted. Then a 32mm punch was also removed from the off-the-shelf liner and the iron laden punch was then glued, with silicone glue (Silpoxy, SmoothOn), into the hole created in the off-the-shelf liner.

Issues with this fabrication process arose because the junction between the target and the liner created stress concentrations directly onto the residual limb. Figure 21 depicts a target glued to the inferior aspect of a liner for a pin-less suspension user. On the bottom of the target shown, there is a sizeable (~1-2mm) difference between the target and liner which rendered the liner not safe for the user to wear (this liner was used in an in lab session, and the session was shortened due to this liner defect).

Figure 20: *(a-c) The outside of an investigation liner fabricated using the punch method. (d) The inside of an investigation liner fabricated using the punch method. (e) A ferromagnetic-target liner punch compared to a single sensor from an INTARY, both having a diameter of 32mm.*

To address this issue, a second fabrication method was developed. In this method, a thin iron-polymer target is simply glued to the outside of the liner, leaving the inner surface of the off-the-shelf liner unaltered. Using materials previously shown to fabricate stable liners (67), a target <1mm thick, and robust enough to withstand the testing performed in the lab was created. These targets were then affixed to the liner with Silpoxy (SmoothOn) in locations that overlapped with the INTRAY sensors (Figure 22).

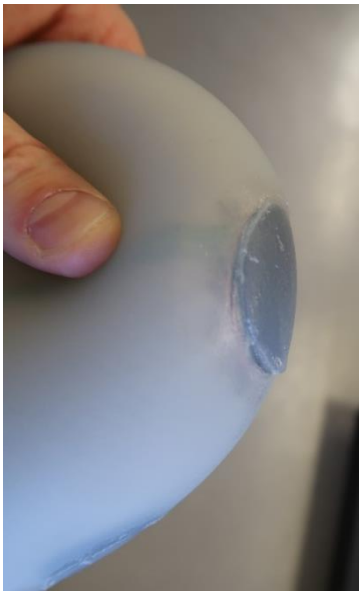

Figure 21: *An example of Participant Seven's poorly fabricated punch method liner. The edge created toward the bottom junction of the target and liner created stress concentrations on the skin that required the protocol to be adapted.*

Both investigational liner fabrication techniques had limited integrity testing, but were able to withstand a two hour in laboratory testing session. At times, the pink fabric backing on the thin iron-polymer targets would peel, but that did not cause concern for participants, nor did it affect the data collected.

The most difficult aspect of liner fabrication was aligning the targets with the INTRAY sensors. As mentioned in the socket fabrication section, the INTRAY sensors were placed based on physical landmarks of the socket, which required the liner fabrication to match the location of those sensor placements. As a result, liner fabrication could only happen after a socket was fully fabricated so that the sensor locations could be translated onto the liner. To transfer the location of the sensors to the liner a technique was borrowed from the clinic, the "lip stick" method. To do this, cheap, colored lipstick was used to mark the center of the INTRAY on the inner surface of the socket and the liner was then slid into the socket and hand-pressed firmly onto the inner surface of the socket. The waxy nature of the lipstick meant that the color would not easily transfer onto the liner as it was slid into the socket but would quickly transfer with pressure added.

With colored marks identifying the center of the INTRAY on the liner, target locations were identified, and liner fabrication could ensue. Though this worked on a small scale, this technique required care to do correctly. After each target was put onto the liner, data was collected from the liner-sensor interactions to check if the target aligned with the sensor. Generally, the targets would align well, but there were instances when the target would need to be moved so that it aligned better. Even then, there were sessions that users' limbs stretched and distorted the liner so that the target would not interact with the sensors.

Figure 22: *Participant Eight's glue-on liner fabrication method. Pink fabric was used to support and protect the ferrous-polymer material that composed the target.*

3.1.3 Target Fabrication

Prior experiments studied the optimal iron-polymer formula for a single inductive sensor system. Of which, a sheet with thickness 0.75mm, and 85% iron by weight density was chosen to maximize signal intensity and decrease bulk when added to the prosthetic liner (46). The trilateration method required the previously reported target to be changed and it was evident that the thin universal layer of iron could be modified to strengthen the signal observed by the INTRAY sensors (64).

Described in the prior section, trilateration targets were initially taken from the commercially fabricated liners. This meant that the iron polymer target used was 0.75mm thick, 85% iron by weight, and 32mm in diameter. This was done because the materials to do that were on hand and did not require any additional fabrication. Later, when iron-polymer targets were needed in the second liner fabrication technique, optimized target specifications were explored.

Using previously defined methods, custom iron-polymer trilateration targets were fabricated (67). Four samples were made at 85% iron by weight, 1) 0.75mm thick, 32mm diameter, 2) 0.75mm thick, 48mm diameter, 3)1.125mm thick, 32mm diameter, and 4) 1.125mm thick, 48mm diameter. The targets were mounted to the three-axis controller and aligned so that the local coordinate system was defined from the center of the sensor. A planar flight path (similar to what was described in Section 3.4, but with 1mm resolution in each direction), was repeated for all target samples and the sensor signal intensities were recorded. Spatial signal intensity heatmaps were created to compare the interactions between each of the targets and the sensor (Grayscale plots in Figure 23). While the differences were plotted to more clearly observe how different target sizes and shapes altered the sensor-target interaction heatmap (Rainbow-colored plots in Figure 23).

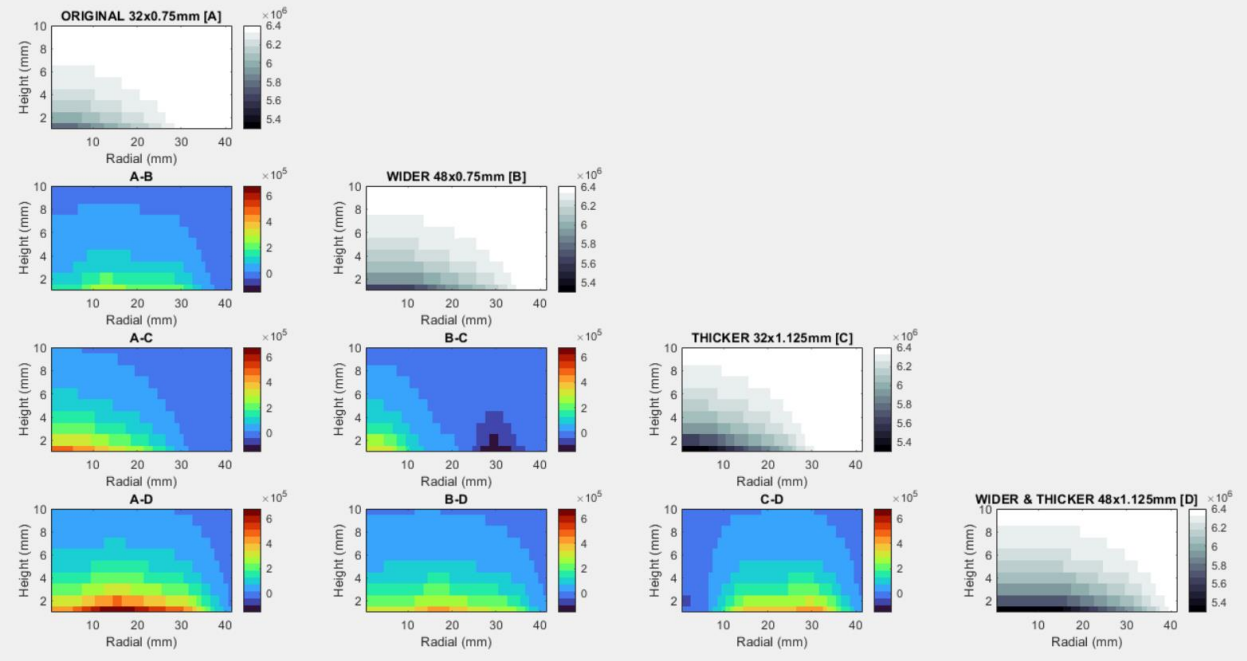

Figure 23: *Comparison of raw signal intensity values recorded from target types that were of original size, wider, thicker, and wider & thicker. The grayscale images show the raw counts. The color heatmaps illustrate the difference in raw values between two various target types labeled by each frame's title.*

As anticipated, the signal intensity waned as the targets were moved further from the sensor. It was observed that the targets with additional iron compared to the original size (wider, thicker, and wider and thicker) had more interaction with the sensor from further away. The wider target had the most signal improvement as it was moved radially off of the sensor, while the thicker has the most signal improvement as it was lifted off the surface of the sensor, and finally, the thicker and wider sample improved signal in both the radial and height (Grayscale plots in Figure 23).

To better visualize the effect that the target sizes had on the signal, plots were created specifically comparing two target types (Rainbow-colored plots in Figure 23). In the first column of the comparative plots, all targets that contained more iron (thicker, wider, and wider and thicker) increased signal intensity significantly. In the comparative plot between the wider versus thicker, the signal observed decreased when the target was radially displaced but strengthened directly over the top of the sensor.

These results help to confirm the general trend that the sensor interacts with the iron target that is directly above the column of the sensor. The thicker target has more iron stacked vertically, while the wider target has more iron spread out laterally. The wider target can interact with the sensor from further away, because more iron remains above the column of the sensor. Yet the thicker iron target has more cumulative interaction with the sensor directly over the top of the sensor, because it has all of the iron contained directly above the sensor.

Next, the spatial signal heat maps were converted to percent signal intensity (grayscale plots in Figure 24) to show that the modeling equations presented in Chapter 2 are directly impacted by the target shape.

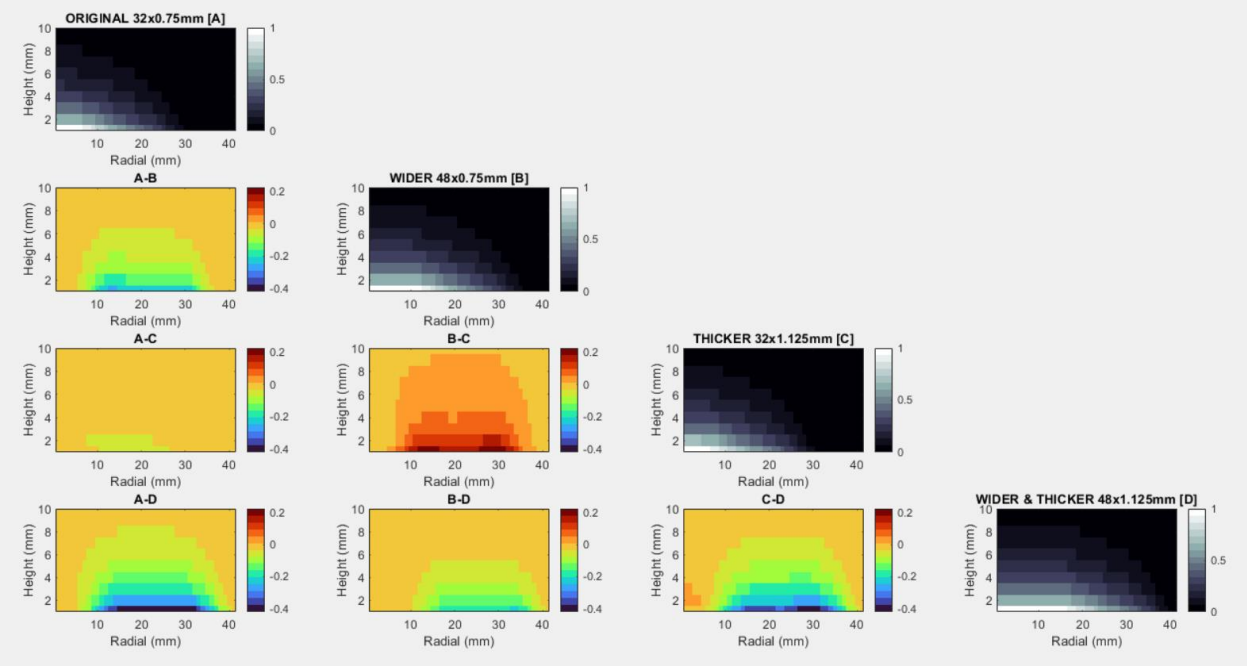

Figure 24: *Comparison of percent signal intensity values recorded from target types that were of original size, wider, thicker, and wider+thicker. The grayscale images show percent signal intensity target-sensor proximity plots. The color heatmaps illustrate the difference in percent signal intensity values between two various target types labeled by each frame's title.*

In the comparative plots (rainbow-colored plots in Figure 24), we see how the empirical heat maps vary with different target types. One exception is the thicker target. The thicker target increases signal intensity (Figure 23), yet the rate of signal intensity degradation as the target is moved away from the sensor remains similar to the original sized target. This means that the thicker target causes the range of signal observed to be larger, but the signal decay as the target is moved off of the sensor remains very similar to the standard target size (<4% difference). It is plausible that the current paraboloid model equations could be used in conjunction with the thicker target, but additional studies are needed to confirm this.

This data supports why efforts to improve the modeling equations in this thesis were not pursued. A study should be conducted to optimize the target size for this application, and then the modeling equations can be improved. In addition to changing overall signal intensity observations, target size may affect the comfort of the liner for a participant or even change the integrity of the liner fabrication process. If the wider targets are to be used in future liner fabrication, new empirical paraboloid equations would need to be developed to model the sensor-target interaction. This experiment was intended to be preliminary and further investigation is needed to validate the development of an optimized target size.

3.2 Balloon and Thermal Calibration

3.2.1 Balloon Calibration

An integral step in the trilateration solve calculation is converting raw signal to percent signal intensities as described in Section 3.6.1. The sensors embedded within the wall of the prosthetic socket exhibit the same

baseline raw signal variability that was observed in the bench top experiments and thus individualized calibration values were required and a repeatable process was developed. Initially, an investigation was conducted to understand the difference in maximal signal intensity output from a single sensor using the 32mm diameter ferromagnetic target compared to an infinitely large, uniform layer of ferromagnetic target.

To start, a single 32mm target was placed along the inner surface of the socket and light pressure was applied by hand to cause the target to contact the inner surface of the socket, but not so much pressure that the target deformed. Care was taken to move the target above each sensor so that the target completely occluded the sensor, creating the maximal signal intensity observed by the sensor. This was considered to be similar to the benchtop experiment where the target was placed, centered, on the surface of the sensor.

Following the “hand calibration”, a custom silicon “balloon” was placed inside of a pin-locking liner containing an infinitely large, uniform layer of ferromagnetic target. The silicon balloon was in the rough shape of the inner surface of a socket, and because of the friction between the balloon and liner, the liner was rather rolled onto the balloon. The balloon was fitted with a pressure gauge and one way valve for inflation. Next, the transtibial socket, instrumented with INTRAY sensors, was anchored onto a base and a data collection board was connected to the socket and data was recorded at 32Hz. The balloon-liner element was placed into the socket and seated so that the pin was as deep in the shuttle lock as possible. A “restraining parachute” was placed over the top of the socket and balloon-liner configuration to provide a normal force on the balloon as it was pressurized, so that balloon-liner element was contained within the socket. Finally, the balloon was inflated to 5psi, held for 10 seconds, and then depressurized. This process was repeated three times.

Data from this experiment were processed and revealed that the maximal signal intensities observed during the balloon inflation were similar to the maximal signal intensity observed during the hand pressed 32mm target for four of the six sensors (Figure 25). The two sensors that showed lower signal intensity changes during the hand calibration were both from the anterior distal site, which it may have been difficult to fully align the 32mm target with the sensor possibly leading to a smaller intensity change. It was challenging to consistently do a hand calibration that reliably obtains the maximal signal intensity, while the balloon calibration has a very large area of target and consistent pressure making the measurement more standard across all the sensors and sockets fabricated.

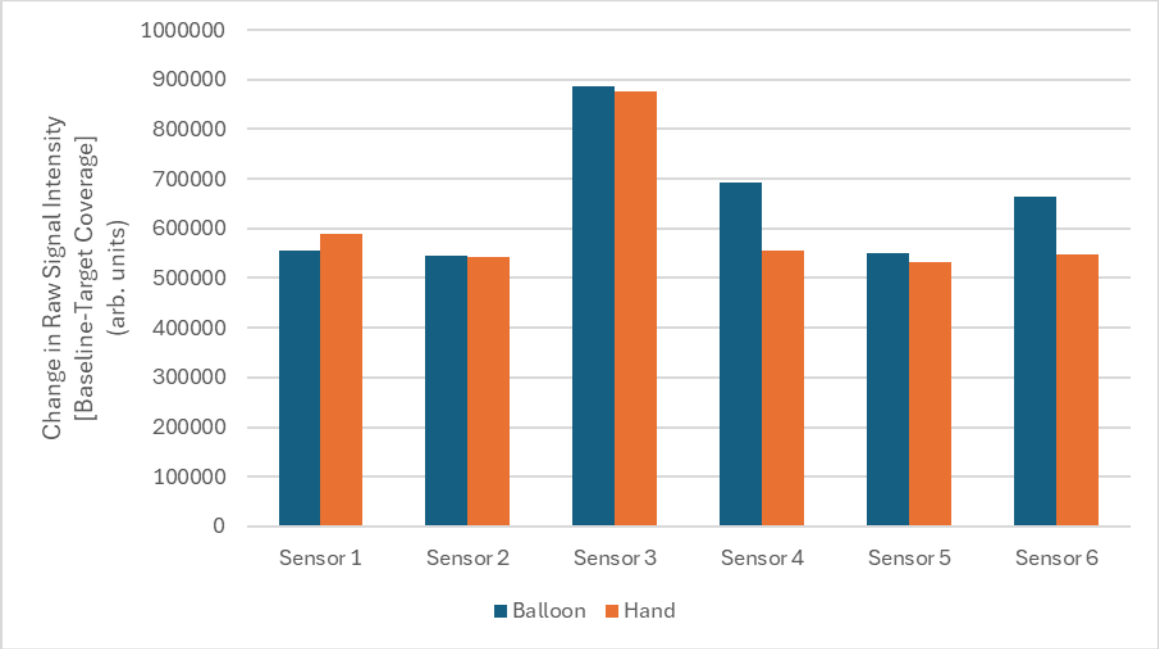

Figure 25: *Maximal signal intensity counts observed during the balloon and hand calibration experiments. Raw counts are displayed to show the difference between the two methods, and also exemplify how different sensors have different intensity ranges.*

It is known that putting pressure on the sensors can affect the signal observed (further discussion in Chapter 3.4), so a similar maximal signal was deemed sufficient in this experiment. Additionally, the general trend that the sensor only interacts with target that is in the cylinder directly over the sensor reemerges, supporting this methodology. The infinite iron sheet did not result in more signal intensity to be observed, which implies that the iron to the sides of the sensor did not influence the signal value observed. If it did, larger signals would have been expected compared to the hand calibration technique, like what was presented in the target fabrication experiments (Chapter 3.1.3).

The maximal signal intensity data obtained from this experiment was used to calculate the range of signal each individual sensor records. Intuitively the values reported describe the entire signal intensity range of each sensor, but with a caveat. The maximal signal intensity observed is not 100 percent as defined by the empirical model in Chapter 2.3 because the sensor is embedded in the socket. The target remains separated from the sensor by the thickness of the nyglass inner layer, which is approximated by 0.5mm. Rather than the range being a measure of zero to 100 percent, the maximal signal observed in this experiment is around 80% signal intensity given the model in Figure 11a. This is accounted for in the calibration equation, which is adapted from Equation 17.

The goal of the balloon calibration is to convert raw data to percent signal intensity given the range of the sensor and its baseline. The balloon calibration experiment was conducted prior to any session data being collected and yielded the range of signal intensities possibly observed by each sensor. The baseline of the sensor was allowed to be chosen based on the file being calibrated. To do this the user was asked to identify the baseline reading from the sensor prior to a liner or target being introduced into the socket. Equation 18 shows the relationship between the balloon calibration, baseline reading, and raw signal accounting for the nyglass thickness.

$$Signal_{\%} = 0.8 \times \frac{Signal_{raw} - signal_{baseline}}{range_{balloon\ cal.}} \quad (18)$$

3.2.2 Thermal Calibration

In prior work with the inductive sensors used in this dissertation, it was found that the signal is linearly correlated with the temperature of the sensor. Data collected from the INTRAY sensors showed the same fate. As a result, thermal compensation was required to accommodate the thermal noise being introduced into the signal intensities observed and a thermal calibration method was developed. In session data collected it was apparent that socket use created large temperature changes (Figure 26).

In the fabrication process, one 10kΩ thermistor was soldered onto one of the inductive sensors in the INTRAY. Then while orienting the individual inductive sensors during the socket fabrication process, the thermistor was placed as close to the center of the INTRAY with the aim that the one thermistor would be an apt temperature reading for all three sensors in the INTRAY. The data from the one thermistor was used to calibrate all three sensors. The sensor to thermistor ratio, 3:1, was a result of the channel limitations on the data collection board. The board was designed to accept eight inductive sensor channels and only four thermistor channels. In an ideal case, the board may be redesigned so that the sensor to thermistor ratio is 1:1 so thermal calibration is specific to each individual sensor.

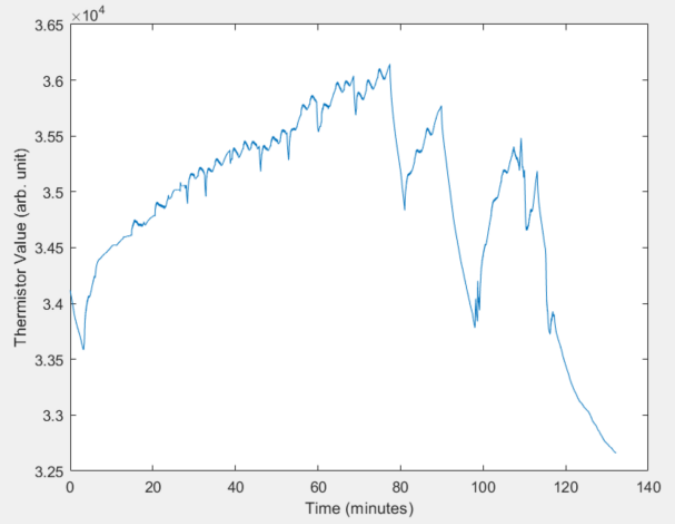

Figure 26: *Typical thermal fluctuations during an in-laboratory controlled session. Doffing causes large cooling to be observed in the socket while prolonged socket wear increases socket temperatures. The values displayed are in arbitrary signal units.*

The thermal calibration experiment was conducted prior to any session data being collected. To start, a microbiology incubator oven (Imperial III, Lab Line) was turned on and set to 40ºC and given enough time to reach a stable temperature. While the oven warmed, the data collection board was initiated, and data was collected at 32Hz from a typical data collection board from the six individual sensors and two thermistors. With the board running, the socket and data collection board assembly were placed into the oven and allowed to warm for 40 minutes. After 40 minutes, the socket was removed from the oven (the oven was turned off) and the socket was allowed to cool at room temperature for at least 40 minutes.

Data collected from the calibration experiment was truncated to only the warming and cooling time period, the sensor and associated thermistor values were plotted against each other, and a linear fit was determined for each sensor (Figure 27). Each sensor-thermistor combination showed a negative correlation, meaning that as temperature increased, signal intensity increased (a negative offset in raw sensor values observed is

an increase in signal intensity). Additionally, each sensor-thermistor combination displayed slight hysteresis as the socket transitioned from warming to cooling but was not addressed because it was thought that the linear regression sufficiently calibrated the thermal noise.

The crucial element from the linear regression was the slope. This value reflected the change in sensor signal observed, in raw counts, due to the change in temperature observed by the thermistor. The slope determined from the calibration experiment was then used on experimental data.

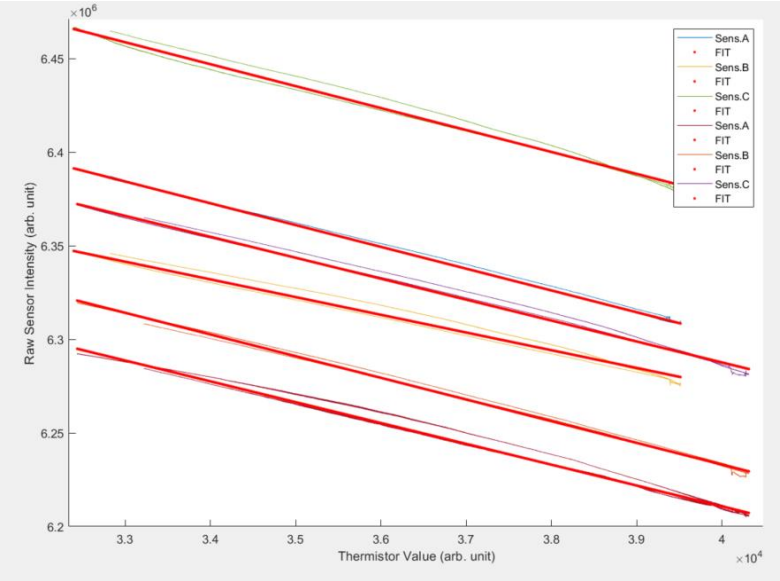

Figure 27: *Linear regression fitting lines for the six individual sensors in an INTRAY sensor. Warming-to-cooling hysteresis can be observed around the linear fit line.*

To calibrate experimental data, first the thermal data was offset to the first period identified that did not have target interaction with the sensors (previously referred to as the baseline). This then provided a change in temperature throughout the session relative to the starting temperature of the socket. This data was then multiplied by the slope, creating a dataset that was the sensor signal intensity offset due to changes in the thermistor counts observed, and then added to the observed signal from the sensor (Equation 19). Figure 28 illustrates the affect thermal calibration had on the output data.

$$Signal_{\text{thermal cal.}} = Signal_{raw} + (\Delta\text{Thermal} \times m_{thermal}) \tag{19}$$

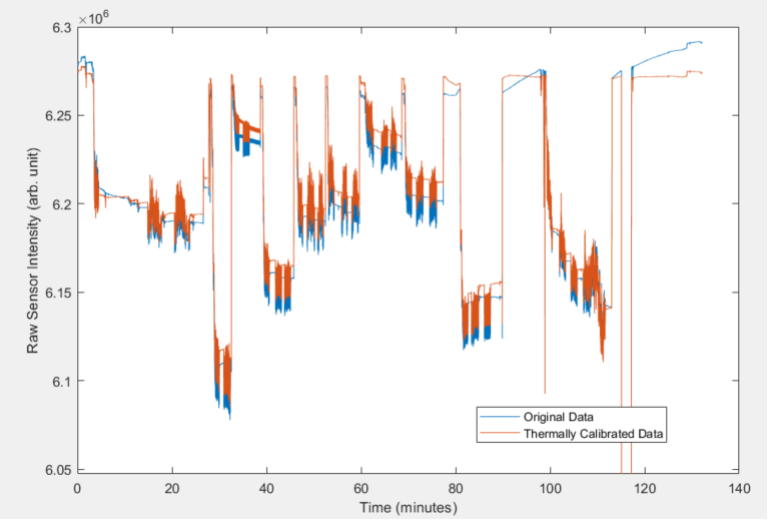

Figure 28: *Thermally compensated signal intensity values from an example in-laboratory session. Most evidently, signal stability in the calibrated data can be seen at times of socket doffing, while for the original data, signal drift can be observed*

3.3 Processing Algorithm

An algorithm was written to succinctly process the data and the flow diagram is shown in Figure 29. Due to the limited number of individual sensors the data collection board could record, two data collection boards were used. Each board record six individual sensors and two thermistors (from two INTRAY sensors). Crosstalk between the EMF or targets from the separated INTRAY sensors may have been possible because the two boards meant that the sensors sampling of two nearby individual sensors could happen at the same time. This noise would have been introduced randomly based on how the boards were initiated and it was deemed that the sensors were adequately far apart to not interfere with each other. In future iterations, if all sensors were recorded on one board, cross talk would not be an issue.

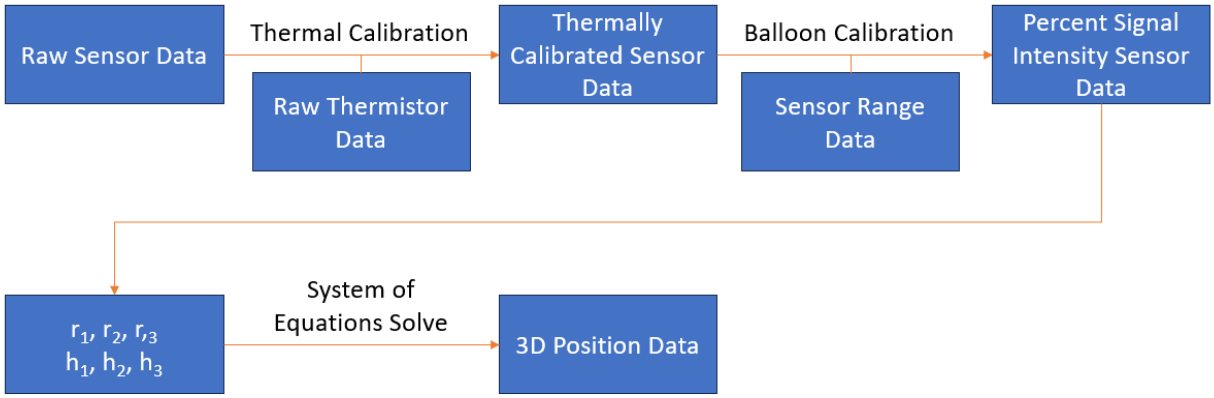

Figure 29: *Workflow for converting raw signal observations to three-dimensional position data. Calibration file data is required in addition to session data for successful calculations.*

3.4 Sources of Sensor Noise while the Socket is Worn

Thermal noise has been well understood and the compensation required could be improved but works sufficiently well. Four additional types of noise were observed when taking measurements within the sockets. These sources of noise are from a lack of electrical insulation, electromagnetic shielding, changes in pressure, and socket flexing.

An immediately apparent form of noise, that renders sensors unusable, is poor insulation around the electrical components during fabrication. Sensors that do not have sufficient electrical insulation will exhibit a raw signal output that offsets drastically and unpredictably when the socket is handled. In this thesis work insulation errors like this were of low likelihood, and care was taken during the fabrication process to prevent this from happening. One socket succumbed to this, and it was remade before testing.

The inductive sensors used for the INTRAY work by producing an electromagnetic field (EMF) and allowing the iron-polymer target to interact with that EMF. The sensors are thus disposed to interact with erroneous EMF noise. To reduce this noise, semi-flexible ferrite sheets were cut to size to match the diameter of the coil and placed on the back (external side) of the socket. The ferrite “backing” sufficiently

shielded the sensor from EMF noise being produced external to the prosthesis. Consequently, the ferrite backing on the sensors influenced the EMF produced by the coil and thus the sensor used during the modeling in Chapter 2.3 had ferrite backing, though it was known EMF noise had already been contained.

Pressure and flexing signal noises were challenging to tease apart from socket use data, so remained under the same umbrella. Experimentally, pressure and sensor flexing were easy to isolate and preliminary studies were done to quantify the noise introduced by each.

A benchtop, back-of-the-envelope, experiment was conducted where a sensor (without ferrite backing) was flexed by hand while signals were recorded. As expected, with a small amount of curvature, the signal intensities changed dramatically. The direction of signal intensity offset was determined by whether the sensor was curved in a concave versus convex nature. Concave flexing made signal intensities from the sensor increase and convex flexing made the signal intensities decrease. For the same limitations described in Chapter 2.4.1, the relationship of sensor flex and signal observation was not pursued further, and instead earmarked for further studies.

Next, pressure-sensor effects were investigated. Initially a benchtop, back-of-the-envelope, experiment was conducted where a sensor (with ferrite backing) was mounted in the three-axis controller. The baseline and 100 percent signal intensity values were obtained by attaching a target to the target-mounting piece and lowering the target to the surface of a single sensor. Care was taken to bring the target to the surface of the sensor without adding pressure. Next the three-axis controller was moved downward in increments of 0.5mm, applying pressure on the sensor. The three-axis controller had a spring element to protect against bashing the target into the surface, so the sensor was progressively loaded proportionally to the spring constant in the bash-protection element of the three-axis controller. Once the spring was stretched sufficiently, a maximal pressure, 137kPa, was applied to the sensor by resting a 11.3kg mass above the target-mounting piece. Once the iron-polymer target was tested a liner piece without the iron polymer (nude liner) was repeated through the same procedure. The signal range observed while under pressure versus unpressured was compared in Figure 30. As we would expect, there is almost no signal change when the nude liner was moved closer to the target, while for iron-polymer target created a large amount of signal change (blue portion of Figure 30). Interestingly, for both the iron and nude liner sample, once pressure was applied from the liner sample to the sensor, the signal observed by the sensor increased (orange portion of Figure 30). The nude liner created a signal intensity change of about 21% the magnitude of the iron-polymer target while under pressure.

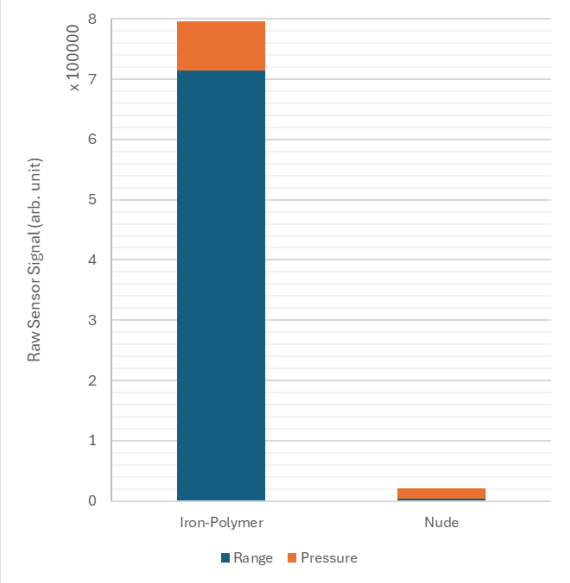

Figure 30: *Magnitude of signal intensity change due to pressure. A traditional ferrous-polymer target was used and compared to a nude sample of the same liner.*

Studies previously showed that putting an infinitely large iron-polymer target under cyclic pressure above an isobaric sensor did not significantly alter the distance measurement obtained from the sensor (46). This suggests that as the target is compressed, the space between the target and sensor (fabric backing and iron-less polymer) reduced negligibly. We would expect this phenomenon (liner distortion not affecting signal strength) to occur in the present experiment, but there are other limitations. In our experiment a finite-sized target was used and aligned with the sensor by eye. The target may have been slightly misaligned with the sensor and while under compression the iron polymer may have flowed laterally, moving iron closer to the target, increasing signal. Among many other confounding factors behind this experiment, it was surmised that putting the sensor under pressure may cause signal intensities to increase. Further, more rigorous studies are needed to support this claim.

In leu of performing better flexing and pressure experiments on the bench, the overall noise of this effect was quantified by a participant walking on the socket without iron targets fabricated in the prosthetic liner. An important feature of this experiment was that the sensors were embedded in the carbon fiber layup, which were hypothesized to help prevent flexing and dissipate pressure directly imparted on the sensor.

Following an in-lab session, one participant walked on an investigational prosthesis using an off-the-shelf liner. The liner did not contain iron targets, and it was an identical make and model of the investigation liner fabricated with iron targets. The liner model was constrained so that any slight interactions between the liner material and the sensors could be controlled. This, in effect was a repeat of the benchtop experiment described, the walking bout was a nude liner compared to the balloon calibration data. Furthermore, this was testing the combination of pressure and flexing inside the socket because if there was any flexure in the socket (in addition to pressure) due to walking, it would be captured.

Raw signal data was collected at 32Hz, calibrated to percent signal intensity with standard procedures, and plotted versus time. Figure 31a shows three bouts of one-minute walks with the investigational, iron liner, while Figure 31b shows four bouts of one-minute walks with the nude liner. Chronologically, the walks had 5-ply, 4-ply, 6-ply, and 5-ply socks donned during the walking bouts. The horizonal data connecting the oscillatory walking waveforms are bouts of sitting and the socket was doffed to make the changes in sock ply.

The nude liner created a signal that mimics a walking waveform, but the magnitude of signal is significantly smaller than with the iron liner. Nearly all signal created with the nude liner was less than 2.5 percent signal intensity, while the iron liner creates signal greater than five percent. The peak to valley in the walking oscillations in the nude liner was generally less than one percent signal intensity, while the peak to valley in the iron liner was generally greater than 1.5 percent signal intensity. These results suggest some of the signal observed from the sensors can be attributed to pressure and/or flexure, but that the magnitude of noise is less than the total observed signal.

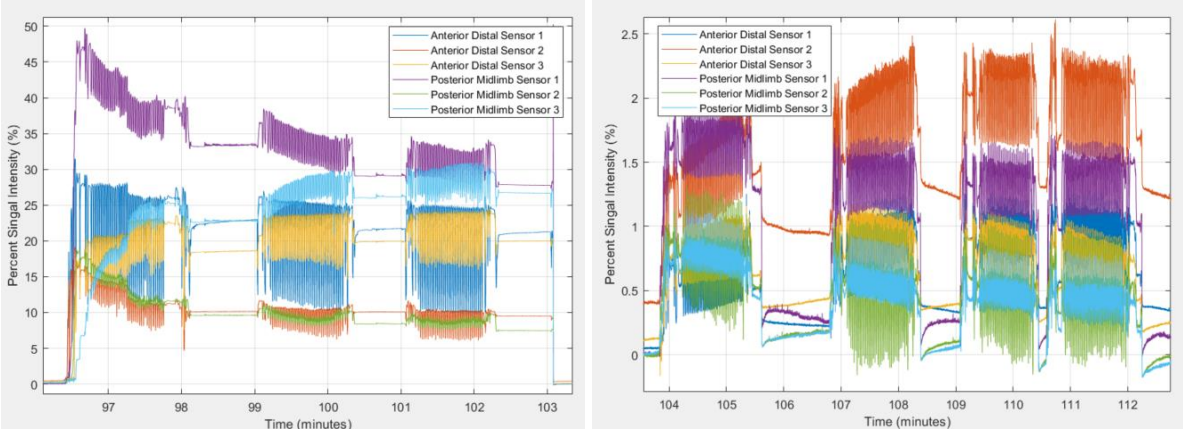

Figure 31: *(a) Percent signal intensity observed during experimental walks from six individual sensors while a glue-on liner was worn by Participant Seven. This data was sampled when there was evident overlap from the ferrous-polymer target and all individual sensors during three identical one-minute walking bouts. (b) Percent signal intensity when Participant Seven walked on the same socket immediately following the data in panel (a). The liner was the same make and model as the investigational liner but did not contain ferrous-polymer target (thus no iron was near the sensor). Various sock ply changes were made across each of the four unique one-minute walking bouts.*

Interestingly, the Posterior Midlimb Sensor 2, during the second bout of nude walking (Figure 31b), shows signal intensity to go into the negative values. This may be evidence of flexure. From our benchtop experiments, increased pressure showed increased signal intensity. In the walking waveform, when a participant wights the socket, they inevitably increase pressure within the socket. This means that the peaks in the oscillatory walking waveform happen during the "stance phase" of walking when pressures are expected to be greatest. Then as the socket is unweighted during the "swing phase" of walking we would expect pressure, and thus signal intensity, to return to a baseline state. The data shows that the signal from the sensor goes beyond the baseline and records slightly negative values. From the benchtop experiments, the only known factor to create signal intensity noise in this direction is convex flexure of the sensor.

In this experiment different sock ply were worn in an A-B-C-A style study design. The participant wore a 5ply, 4ply, 6ply, and 5ply sock respectively. The calibrated signal intensity did not obviously change with the sock ply being worn in the walking bout, and furthermore, the repeatability of the 5ply walks was not conclusive. The importance of this results suggests that the liner does not have a strong enough innate signal interaction with the INTRAY embedded in the socket wall. If the liner had a baseline signal intensity reading with the sensors then we would expect to see that the calibrated signal intensity trended with sock ply (or distance of target-sensor separation). This was not the case, and thus we expect that there is additional noise being introduced.

The environment found within the socket is highly complex and the data presented in this section was intended to frame the challenge of quantifying the observed sensor noise. The participant experiment can be used as a benchmark to understand the extent of all possible sources of noise because the iron target was removed, and non-zero signal observations were still seen. Furthermore, the noise oscillated similar to the walking waveform oscillations leading to the hypothesis about pressure and flexure. Admittedly, there may be other sources of noise not discussed here and more rigorous experiments are needed to better understand the origin of the noise. Ultimately, the noise introduced in the sensors when a participant is wearing the socket is less than 2.5% of the total signal observable.

Two avenues forward to reduce the effect this type of noise had on the output trilateration solve point were discussed. The first being a better definition of the noise observed in this experiment so as to reduce the noise in further collections. The second being an improved signal to noise ratio by improving the signal strength coming from the target. As is the, noise from this signal is within the threshold for solving the data as described in the first chapter. This also introduces the error that this signal could simply be from walking on the socket with poor liner-socket alignment. Notably we can also see that all of the peaks and minimum align temporally, but the magnitudes are different even amongst the sensors within the same array. The signal observed during this noise experiment is large enough to provide solve data and that solve data is of the same magnitude of movement as the ferrous polymer data. The absolute position of the solve data is near the center of the array with a large amount of separation but the magnitude of movement is about half to that observed with the polymer. This introduces the question of what is the reliability of the movement data.

3.5 Data Aggregation Algorithms

The walking waveform, briefly introduced in Chapter 3.4, has various landmarks that can be used to better understand how a lower extremity amputee interacts with their prosthesis. From a kinematics perspective there are two main components of walking for a single leg, the “stance phase” and “swing phase” of the gait. The stance phase of walking is when the ipsilateral foot is in contact with the ground and swing phase is when the ipsilateral foot is in the air traveling between steps. For a brief moment at the end of swing phase for one leg and at the end of stance phase for the contralateral leg, the body is supported by both limbs. In healthy, ambulating people, swing phase and stance phase are about equal durations and take about one second to complete. Gait abnormalities may affect this generalization, such as a limp that may mean a stance phase is shorter than a swing phased for one limb and the opposite for the contralateral.

Within stance phase there are three sequential landmarks, heel loading, midstance, and terminal stance. Heel loading encompasses heel strike and weight loading onto the limb, midstance encompasses weight distribution onto the sole of the foot, and terminal stance encompasses toe loading and the pre-swing, bilateral body support. Following stance phase, swing phase has three sequential landmarks, toe off, mid-swing, and terminal swing. Toe off is the time when the limb is driven off the ground and loses contact with the ground, mid-swing is the time when the limb is swung through the person’s gait, and terminal swing phase is when the limb prepares to contact the ground.

In this dissertation the walking waveform was used to perform the limb-to-socket motion analysis because it was thought to be the most consistent limb-to-socket contact environment. This is because the participants’ gait is maintained step-to-step in order to walk at a constant pace on a treadmill. Sitting and standing were not used because bodily postures can create variation in where the limb is positioned within the socket. Furthermore, walking and standing (equal weight bearing) do not impart the maximal forces on the limb compared to walking. Ultimately, aim three was focused on exploring how limb-to-socket motion may influence limb physiology and it was hypothesized that walking on the socket would create stresses that could cause adaption.

Future efforts are needed to evaluate sitting and standing weight shifting interactions between the limb and the socket. In the protocol presented in Chapter 4, postural data was collected but limited analysis was conducted at the time of this dissertation.

3.5.1 Heel-contact and Toe-off Identification Algorithm

As seen in Figure 32, walking data collected by the sensors were cyclical at about 1Hz, which is common for an average walking cadence. The sampling rate of the sensors, 32Hz, provided a resolution that could be used to clearly define the different elements of the kinematic walking gait. Visual inspection of the 3-dimensional solved data, collected from study participants wearing a transtibial socket with INTRAYs, found that the phase-of-step-identification could occur in the Z-axis of motion, or the separation away from the socket wall axis. Instinctively this is because as the user walks and transfers their body weight onto the socket during "stance-phase", the socket needs to provide a normal force to support the residual limb within the socket which is seen by the displacement of the limb toward the socket wall. Afterward, as the user unweights the prosthesis during "swing-phase" the limb is released from the maximal normal pressure from the socket wall and there is slight separation from the target and the socket wall. Furthermore, the noise introduced to the signal from pressure and flexure may influence the Z-axis motion, but this is conjecture.

Numerous force-based-measurement investigations support this theory. More granular to stance phase and swing phase, these studies suggest that pressure exhibits a dual-maxima characteristic, once during the instance of heel-contact and toe-off. This double-peak characteristic was also visually identifiable in the INTRAY Z-axis data (Figure 32), and a data reduction algorithm was used to accurately identify the moment of heel-contact and toe-off. Once these two landmarks were accurately identified in the Z-axis, the step-to-step timing could be used to bin the X- and Y-axis movements as well. The X- and Y- axis movements were more variable amongst participants and did not show as obvious kinematic landmarks to identify steps (Figure 33).

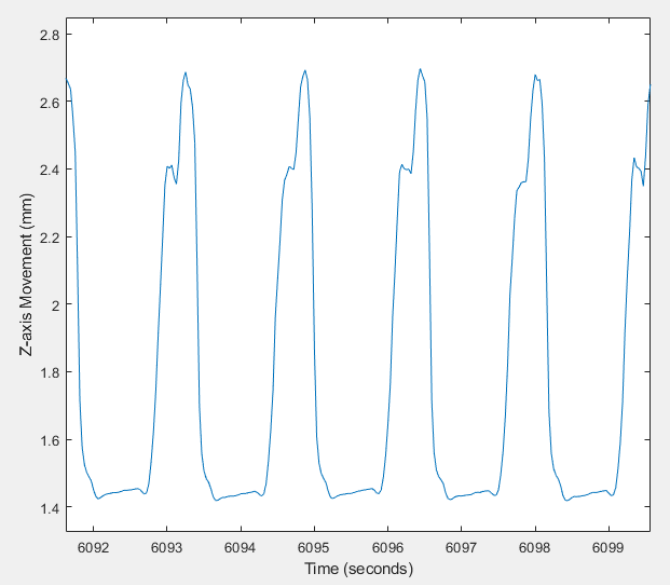

Figure 32: *Sample Z-axis position data during walking. The walking cadence is near 1Hz as the limb gets close to the socket wall during stance-phase of walking and further from the socket wall during swing-phase.*

Briefly, the algorithm used in this data reduction required an engineer to visually identify a single step for a given sensor in the Z-axis. This template-step waveform was used in a sliding window across the full data stream to calculate a difference in waveform shape between the template-step and data within the window. Local minima were then identified and defined as a step. Within each step the double-valley characteristic was identified, and heel-loading and toe-off time points were stored. Though time was not a crucial factor for postprocessing the code ran in O(2n). Alternative coding solutions will need to be explored if this is to be implemented in real time, but the methodology could be leveraged.

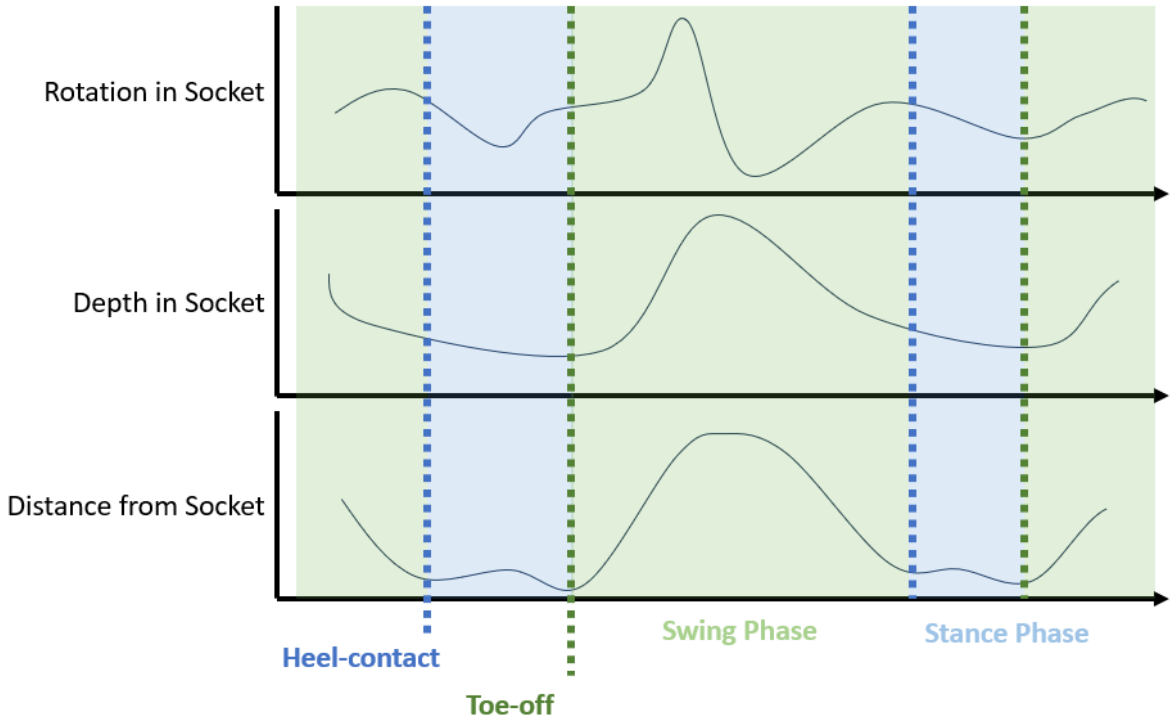

Figure 33: *Example of the time-binning identification of heel-contact peak and toe-off peak. The Distance from Socket wall axis (Z-axis) reliably exhibits the double peak nature of stance-phase walking and can be used to bin the stance- and swing-phase movements in the Rotation and Depth in Socket axes (X- and Y-axes).*

3.5.2 Stance-phase Timing, Swing-Phase Timing, and Cadence

The first metrics calculated were the time elapsed during heel-loading to toe-off (stance phase) and from toe-off to the next step's heel-contact (swing phase). "Cadence" was calculated by the percentage of time the limb was in swing phase during the step. Time was determined by the binning of heel-contact and toe-off to the following heel-contact. Data was always collected at 32Hz so the step size between data points was 0.03 seconds and could easily be converted from sample to time.

The hypothesized utility behind this metric was to evaluate the consistency of walking cadence. Together, these metrics can identify a user's step rate and how user's cadence may change. For instance, if we see that the step rate is maintained but the cadence percentage shifts, it may be indicative of a change in walking gait – primarily the focus of this metric was to identify limping and or compensatory gait changes in users.

3.5.3 Relative Global Limb-Socket Rotation, Depth, and Separation

This metric was calculated to identify the location of the limb position in the socket over time. From the benchtop experiments, the absolute positioning reported by the sensor had 2.3mm of error, while the relative displacement error was 0.5mm. Because of this error, global limb-socket rotation, depth, and separation were calculated as a relative displacement from an observed starting location.

The observed starting location was calculated as the median X-, Y-, and Z-axis positions sampled during heel-contact and toe-off throughout an entire session. In lay terms, this was the most common location of the limb while the peak stresses (heel-loading and toe-off) occurred. This position was subtracted from the solved positional data stream, creating values that were a relative global position from the median position of the limb during stance phase. Mathematically, this changed the reference location of the solved data from the INTRAY's coordinate system, to a relative coordinate system based on the data collect (the same was done to reduce the movement magnitude error to 0.5mm).

Other electable timepoints could conceivably be used to create the data's relative coordinates depending on how the data needs to be interpreted. For instance, if the data was assessed to detect how much a participant moved over the course of a day, walking bouts at the beginning of the day should be used to provide the relative starting location of the limb. In the sessions described in Chapter 4.1, there were numerous control walks that were considered to drive the median value of the global position. As a result, the global socket position metrics reported are normalized to the limb's "neutral" position within the socket, which was approximated by the median of the entire session's data.

This metric can succumb to a confounding variable though. If the liner is doffed and donned again with some degree of misalignment, the position of the limb can appear to change though it is in the same location. This is because the liner can been rotated with 3 degrees of freedom (roll, pitch, and yaw) on the limb. So, if the limb is in the same location, but the targets rotate around the shape, the sensors will show that the relative position of the targets has shifted, though the position of the limb is the same. Furthermore, there are varying degrees of precision at different positions in the solving space above the sensor array. If the target shifts drastically in global position the relative change in location may have less or more precision compared to the data collected when the target was in a different location relative to the sensors.

To reduce this compounding error, the solution would be to better model the system of equations solution so that the error is more consistent and reduced within the entire sensing region. Also, it may be possible to filter out this error given a shift in all of the sensors. If the data suggests that there was a large shift in the same direction in each of the INTRAYs in the socket, we may assume that it is due to the liner being shifted along the limb as opposed to the limb physically moving within the socket. If this were to occur, the data would show how much the targets translated and that could be compensated for. Furthermore, we would expect this to happen only at a time directly following the socket being donned, because the socket would need to be doffed for the liner to be taken off and realigned. There may be additional clues that could indicate when a liner was doffed, but this was not explored in this thesis. Rather, the data collected where a liner doff was known to have happened were analyzed with additional metrics that were not affected by this error.

3.5.4 Pistoning, Slippage, and Swing Phase Control

The third type of metric explored was relative motion within each step, whereas the prior metrics explored the position of the limb and timing of heel-contact and toe-off.

Pistoning, a term commonly used by clinicians, is the amount of movement in the axial direction of the limb and socket and increased up and down motion is generally considered to be due to a poor suspension and fit between the residual limb and the socket. To calculate pistoning, the minimum and maximum Y-axis positions were identified from an entire step. The minimum was subtracted from the maximum position and a pistoning "height" was reported in millimeters.

Slippage was chosen to describe the amount of motion in the shearing directions during stance-phase. Slippage was determined by calculating the cumulative resultant displacement from heel-contact to toe-off using the Pythagorean theorem along the X- and Y-axes.

Swing Phase Control was complimentary to Slippage, as it described the amount of motion in all axes during the swing phase of walking. It was determined by calculating the total resultant displacement from toe-off to the subsequent heel-contact using the Pythagorean theorem along the X-, Y-, and Z-axes.

Many other investigations (48) have quantified 'pistoning' and there is thought that field could greatly benefit from a technology that could reliably report pistoning to clinicians as a method to improve the fit of a socket. The data collected from the sensors was used to directly calculate the displacement in a manner that was consistent with prior studies.

An additional sub-topic of research in lower limb prosthetics has investigated the forces between the limb and the socket. These studies found that the limb is minimally stressed when a socket is donned, which is known a pre-stress. Maximal forces, rather, were observed when the socket was used to ambulate and the residual limb side was unilaterally supporting the body weight of the user. The force waveforms created during stance phase have been heavily studied and shear forces have been clearly observed in addition to pressure. It is debated if slippage between the socket-to-liner or limb-to-liner occurs, but various models have been used to try to predict this phenomenon. The metric calculated in this dissertation was aimed at better understanding the interface mechanics, and because the sensor presented here measures position, the data was aimed at observing socket-to-liner movement. Though as alluded to, pressure may be a confounding variable with this measurement. Chapter 3.4 discusses that pressure may be a source of signal intensity noise, and the empirical data collected in the force measurement investigations, suggests that there is dynamically changing pressure in the socket that could create a large enough signal to show movement, or slippage.

Furthermore, force data that has been collected presents limited information during swing phase because the change in forces were relatively small. Thus, we present the Swing Phase Control metric, which was calculated to gain better understanding of the limb to the socket during swing phase. The metric was termed Swing Phase Control due to one of the participant's feedback while wearing the investigational socket. The participant felt that the socket was, at times, being thrown off their limb during mid- and terminal swing

phase, hindering their confidence in limb position during heel strike. They felt a loss of 'control' of the residual limb, and this metric was used to explore the feedback from the participants on study.

3.5.5 Alternative Metrics

The data collected from the INTRAY sensors is exceptionally granular. Above, nine metrics are calculated, and it is believed that numerous additional metrics could be explored. A considerable amount of effort may be needed to explore the utility of various exploratory metrics, which as an example, not every metric above was reported in a final analysis.

One logical step for another metric would be to calculate the limb angulation, or as clinicians refer to "bell clapping", in the sagittal (Anterior-Posterior) and frontal (Medial-Lateral) planes. At a minimum, this requires combining the data collected from two, time-synced, sensors and measuring how the limb is moving amongst the two sensors. Using this as a benchmark, numerous sensors could be time-registered and more complex 3D movement calculations could also be performed.

Another compelling step would be to take the derivative of position versus time during the step waveform. This would result in liner-to-socket velocity, acceleration, and jerk metrics. Many times in the study presented here, participants could pinpoint very specific moments during the walking cadence that were problematic. Participants were referring to a repetitive movement that occurred within a fraction of a second, and they could identify it by quickly verbalizing "now" at the instant the socket was causing them discomfort. Furthermore, some participants referred to the issue as it felt like the socket was "jerking", which could be physically measured with the data collected from the INTRAY sensors. To improve a metric of this sort, the sampling rate may be increased so that the derived jerk-data is smoother and subject to less variability in magnitude.

Chapter 4. Participant Testing

4.1 Controlled Laboratory Protocol

Three primary hypotheses were tested in a single, two-hour, laboratory experiment. Following fabrication of the investigational prostheses, a certified prosthetist fit each socket to the participant. Participants were asked to complete a sequential series of walks, sits, and stands to evaluate the limb-socket interface after 1) rotational donning of the socket, 2) change of sock ply within the socket, and 3) the use of petroleum jelly between the limb and liner. The specific hypotheses for each condition, were as follows:

1. Rotationally donning the prosthesis will exhibit a change in X-axis INTRAY sensor data compared to a Neutral fit because the limb will be rotated within the socket.

2. Changing sock ply will exhibit a change in Z-axis INTRAY sensor data compared to a Neutral fit because the additional sock ply offsets the limb further from the socket wall, and the opposite with sock ply reduction.

3. The addition of petroleum jelly, directly to the limb, compared to a Neutral fit will cause there to be less observed motion in the INTRAY data because the reduced friction within the liner will allow displacement between the limb and liner and not show as much slippage between the liner and socket displacement.

For each experimental condition the participant completed Neutral walking bouts prior to completing the given experimental walking bouts. The Neutral walking bouts were conducted to control for diurnal residual limb changes. It has been well documented that the residual limb can change size (17) over the course of the day, and users may find that volume accommodation is needed to maintain a comfortable fit. The multiple Neutral walking bouts allowed for users to maintain a comfortable fitting socket so that they could complete the entire protocol. Thus, a unique Neutral fit condition was recorded immediately prior to each experimental condition so that the two conditions could be compared (Figure 34 is a graphic of the detailed experimental protocol).

At the start of the session the investigational liner was donned and not removed until the petroleum jelly was added to and cleaned from the residual limb. During the petroleum jelly experimental condition, the liner was removed, and the middle portion of the residual limb was covered in petroleum jelly so that it was on the aspects of the limb that were contained within the socket (the inferior edge of the limb was not covered with petroleum jelly, and the petroleum jelly was kept below knee height).

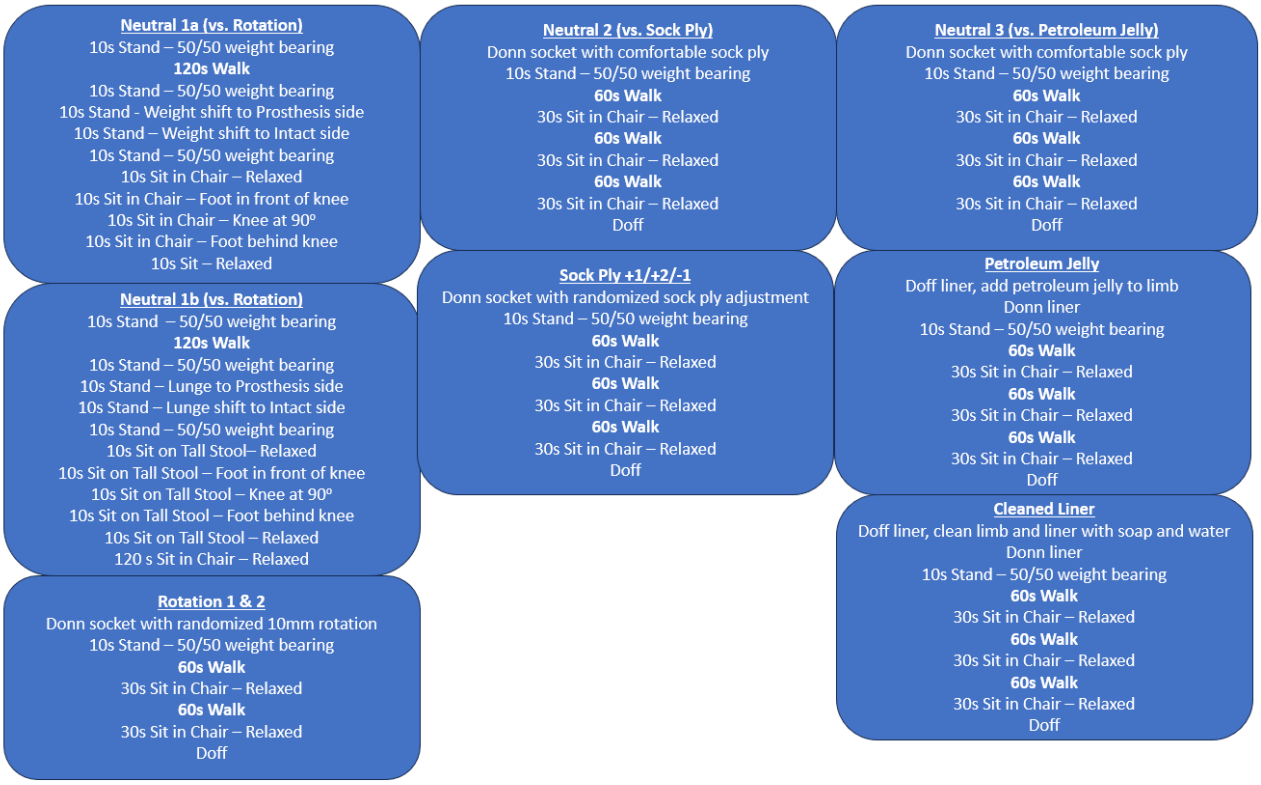

Figure 34: *Detailed in-laboratory controlled protocol. Walking bouts are identified because they were used as the primary points to calculate socket fit metrics. Rotational conditions, and sock ply were in randomized order and the displayed activity blocks were repeated until all conditions were completed. Petroleum jelly and Cleaned Liner order were not randomized due to the a priori determination that the Neutral and Clean*

condition were thought to be the same. Hindsight suggests that the protocol design could have benefitted from this order also being randomized.

In the following sections (4.1.1 through 4.1.10), the data collection process, initial results, and discussion for each participant are presented. Noticeably, the sections have a range of what was remarkable, and ultimately what we learned drove the cumulative analysis performed in Chapter 4.2.

4.1.1 Participant One

Participant One is a right legged prosthesis user, female, Medicare Functional Classification Level K4, locking pin suspension, 3ply Neutral sock usage, 74.4kg, 157cm tall, 40y of age, 17y and 7mo since amputation, 18hrs/day usage, PTB socket design, 11cm residual limb, and lost their limb to trauma. Their limb shape can be seen in Figure 35.

Figure 35: *Participant One's residual limb*

The investigational socket was fabricated to have an Anterior Distal, Posterior Midlimb, Medial Brimline, and Lateral Brimline INTRAY. A liner was fabricated using the punch method. Balloon calibration, thermal calibration, socket fabrication, liner fabrication, data collection, and data processing were all conducted as described in Chapter 3.

Bioimpedance data was collected during this experiment. The electrical currents used in Bioimpedance were so small that they were not expected to interfere with the inductive signals collected by the INTRAY sensors, as suggested by prior experiments (68–70).

The rotational data suggested that the limb was rotated globally within the socket. Figure 36 illustrates the two rotational walks, but does not show the corresponding Neutral walks. The first bout of walking shows an X-axis displacement, in all INTRAY locations, of nearly -5mm from the Neutral position (Figure 36a-d). The signage of the X-axis displacement suggests that the limb is rotating counterclockwise in the socket, and that for a right-sided prosthesis, this is a "toe-out" limb-socket rotation. Furthermore, it takes about 25 steps for the limb to fully regain the Neutral position and once at the Neutral position the limb remains there for the subsequent walk.

During the third bout of walking, the X-axis data was observed to have an equal and opposite global (all INTRAY sensors recording the same direction of displacement) rotation of the limb and liner to +6mm from the Neutral position. The signage, being inverted from the previous rotation suggests that the limb is rotating clockwise in the socket, which is a "toe-in" alignment for a right legged amputee. After nearly 30 steps, the limb-liner regains the Neutral position and maintains that position through the end of the fourth walk.

As designed, the X-axis is aligned with the Circumferential axis of the socket so that the X-axis data may reflect rotation within the socket. Furthermore, all INTRAY sensors are aligned so that a positive displacement from Neutral represents the limb rotating clockwise and a negative displacement from neutral represents the limb rotation counterclockwise in the socket. In both rotational dons presented, all INTRAY sensors within the socket reported the same signage of rotation. The signage recapitulated the experimental condition performed, and suggested that the entire limb was rotationally mis-aligned (compared to Neutral) within the socket.

Additionally, it seems that this participant was able to return the Neutral position without any external aid – simply walking on the socket quickly corrected the rotational misalignment. Stance phase and swing phase data were both rotated suggesting that the socket was entirely shifted in the given direction and when the socket naturally realigned, the envelope of stance and swing phases shifted. Observational notes from the research engineer implementing this protocol noticed that, visually, the socket seemed to be properly aligned after the first walk with the toe-out rotation. Though it was not explored, this data could be used to better understand which phase of walking was most associated with the prosthesis realigning.

No obvious trends in the alternative anatomical axes (Y- and Z-) were visually apparent from this experimental condition.

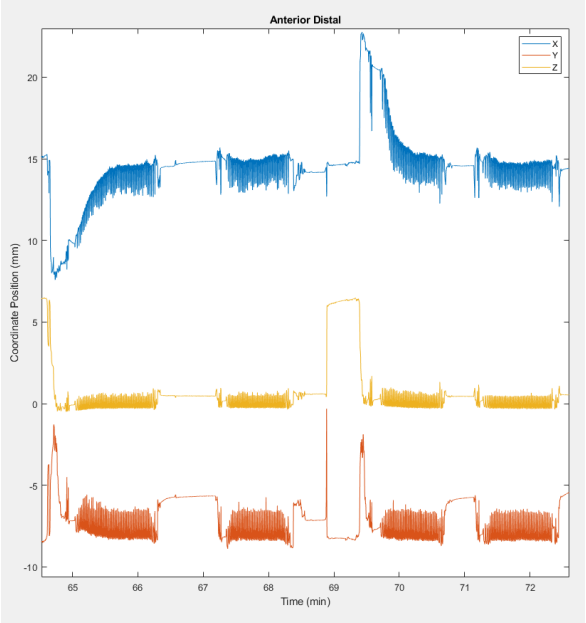

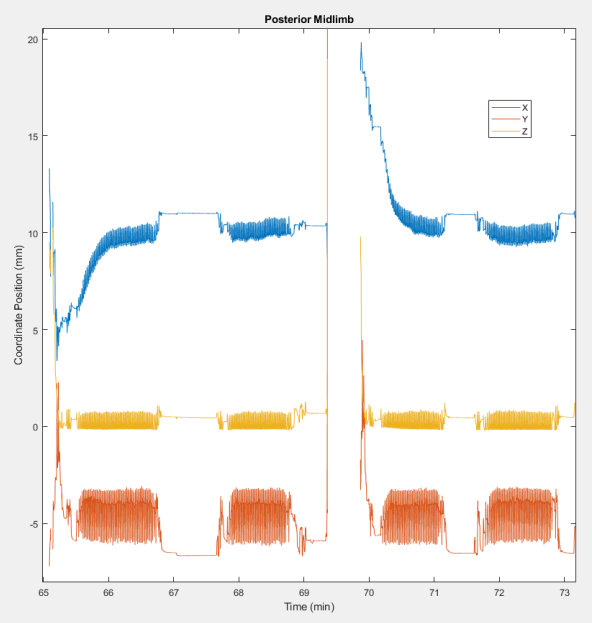

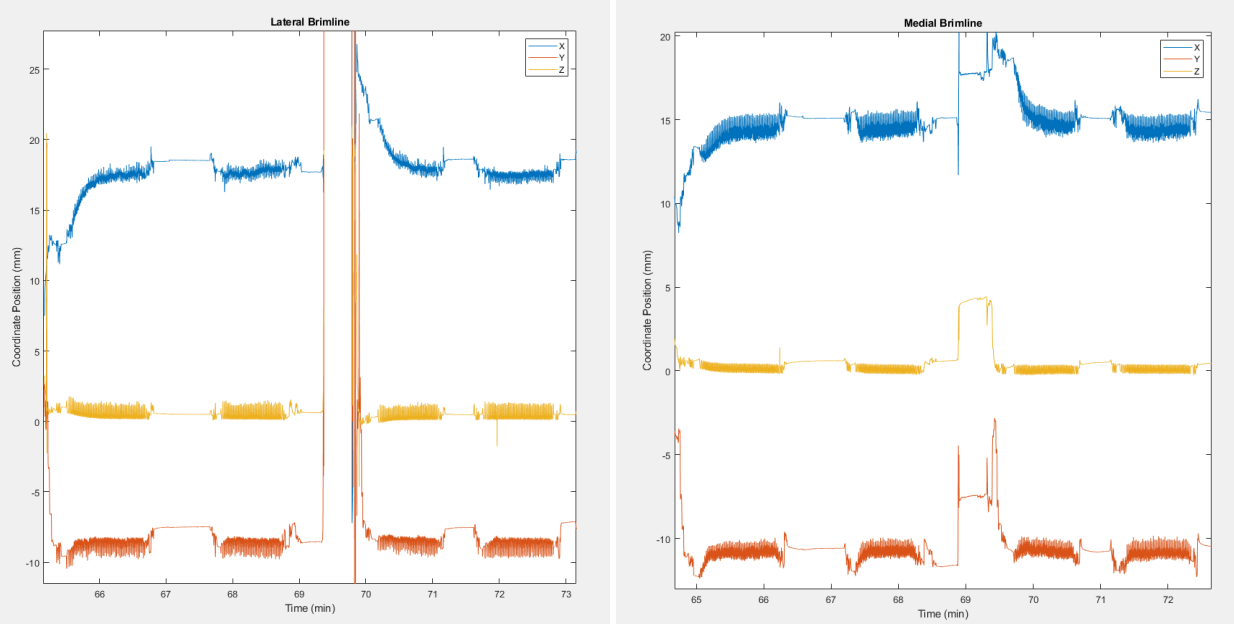

Figure 36: *Rotational experimental conditions for Participant One. Walk bouts one and two are toe-out, and walk bouts three and four are toe-in rotation. INTRAY sensors are (a) anterior distal, (b) posterior midlimb, (c) lateral brimline, and (d) medial brimline.*

Following the rotational don experiment the participant was asked to vary the sock ply they were wearing. Three experimental conditions and two baseline conditions were conducted, which in chronological order were Neutral (no socks), 2-ply, 2-ply, Neutral (no socks), and 1-ply (Figure 37). The order of the experimental conditions differs from the protocol presented in the introduction above because the 2-ply sock was mislabeled and mistakenly tested twice. At this point the socket was well fitting with 0ply of socks and the addition of 2-ply was not needed to maintain the comfort of the socket.

In the data, it can be observed that for all sets of walking bouts the majority of limb-socket motion occured during swing phase. Generally, in the Anterior Distal site for instance, the limb moves closer to the socket wall, deeper into the bottom of the socket, and rotates clockwise during heel contact of each step, and it holds relatively still until it is released during the start of swing phase. The limb regularly oscillated between similar locations in the socket (depending on the sock ply worn), and the magnitude of movement is about 1-2mm in each of the directions for that site.

Along the Z-axis channel, data shows an increase in separation distance between the liner and socket when more sock ply are added. This measurement can be observed in both stance phase and swing phase portion of walking. Intuitively, as more socks are added to the limb there will be more separation between the socket wall and the liner, globally. The data captured reflects that.

The Y-axis channel identifies the amount of pistoning the limb is experiencing. In general, for stance phase minima, all four sensors suggest that the limb reaches more distally in the socket when fewer sock ply was worn. Conversely, when more sock ply was worn, the minima did not reach as deep into the socket. On the other hand, when the limb pulls out of the socket during swing phase (maxima), we see that the 0-ply condition allows the limb to pull out the furthest, while more ply socks restricted the upward motion of the limb in the socket (the Brimline sensors were an exception because the target was severely shifted).

While the X-axis showed a more unpredictable pattern, it is plausible that fewer socks allowed more minimum-to-maximum rotation compared to conditions with more sock ply.

These observations likely describe a moderately complex limb-socket interaction. In lay terms the concept is that by adding unnecessary sock ply, the limb became wedged within the socket. The data presented in the Z-axis suggests that additional socks move the limb further away from the socket wall, supporting that the addition of socks adds more volume between the liner and socket. The minima in the Y-axis suggest that the limb with additional socks did not sit as distally in the socket compared to with the appropriate sock ply. Lastly the minima-to-maxima in the X- and Y-axes may suggest that the motion of the limb from stance phase to swing phase is reduced with additional sock ply. Each of these pieces of evidence help to suggest that the limb may be wedged in the socket and cannot move as freely as in the Neutral condition.

Repeating the Neutral and 2-ply walking conditions also suggested that this effect occurred instantaneously once a sock was added or removed, and that the fit response was repeatable between different sets of walking bouts. This was different compared to the rotational experimental conditions where the limb was able to settle into the socket fit over a number of steps.

Of note, during the third bout of the first set of walking (0-ply walk) the participant voiced that their limb was feeling loose in the socket, and they could walk for a little while longer but may need to add 1-ply of sock. The bioimpedance data collected indicates that there was no reduction in residual limb fluid volume, but prior literature suggests that it is common for prothesis users to lose limb fluid volume while using their prosthesis.

The participant voiced that her limb was “inch worming” during the first bout of the third set of walking (2-ply walk). She further clarified that the residual limb pistoning felt slower than it was before. We observed that there was reduced pistoning, which if we assume the cadence and timing of her toe-off to swing phase was consistent, the speed of pistoning would be slower due to the less distance of positioning observed in the data.

It was noticed that the participant began dragging the heel of their foot during the second bout of the third set of walking (2-ply walk), which when asked, the participant said the limb did not “feel longer”. In the INTRAY data we see that the limb was forced to be in a position that was more proximal compared to the Neutral walking condition. This means that the total length of the limb was likely longer, because the prosthetic device was interfacing with the residual limb further down. As a result during swing phase, the limb may have been long enough to slightly drag on the treadmill and the gait accommodation was small enough that the user didn’t feel a drastic affect.

Figure 37: *Sock ply experimental conditions for Participant One. Walk bouts are in sets of three and correspond to 0-ply, 2-ply, 2-ply, 0-ply, and 1-ply, respectively. INTRAY sensors are (a) anterior distal, (b) posterior midlimb, (c) lateral brimline, and (d) medial brimline.*

In the final experimental condition, the socket fit was tested when petroleum jelly was added to the limb and then again after the limb was cleaned with soap and water. Figure 38 plots these two sets walking bouts with the preceding Neutral walking bout. 2.1g of petroleum jelly was applied directly to the residual limb, and the liner was rolled on atop of the jelly. Notably, at this point in the protocol the participant needed 1-ply of socks to maintain a comfortable fit, so the two sets of experimental bouts of walking were done with 1-ply of sock being worn and compared against the Neutral 1-ply walk.

Observationally, the participant had a Socket Comfort Score (SCS) of 8 during both the Neutral and Cleaned sets of walking, but the SCS dropped to a 4 when walking with petroleum jelly on the limb. During the

petroleum jelly set of walking the participant was asked to verbalize their experience walking on the petroleum jelly. They were recorded saying:

- *"My leg is hitting a new part of the socket that it wasn't before [in this session]."*
- *"It felt like mile 5/6 when I used to be able to run that much [it felt sweaty]."*
- *"The majority of the pressure was around the sides/edges of the tibia/fibula, and under/on the sides of my knee where it rests inside the top of the socket."*

Before delving into the INTRAY data, it is crucial to notice that both the socket and the liner were doffed to add the petroleum jelly to the limb, and then again, to clean the limb. When the liner is doffed and redonned, we introduce a confounding variable, as described in Chapter 3.5.3. The targets may not be aligned with the residual limb as they were before, leading the INTRAY sensors to incorrectly indicate that the limb has repositioned within the socket. Though a global shift in the data may be seen, that does not necessarily mean that the limb has changed position within the socket, rather it could be a measure of the rotation of the targets along the limb, or combination of the limb shifting in the socket and a measure of the liner rotation along the limb.

In the data collected, there was no glaring global change in INTRAY target position, which suggests that Participant One did a sufficient job putting the liner on with similar alignment to their limb. The most obvious global change in limb position can be seen in the Y-axis. The petroleum jelly walk data suggests that all of the targets are slightly deeper in the socket. It is logical the data reflects that the limb in deeper in the socket, but the data may also describe a situation where the liner is pulled off the limb distally. Though this alternative description could be plausible it is unlikely because the participant was wearing a pin locking suspension socket, that may prevent the liner from moving deeper in the socket. Data from a pin sensing device may be able to corroborate this explanation.

If the user were to have rolled the liner on with a different orientation to the limb, we may expect a different pattern to occur in the data. Consider the liner to have three degrees of rotational freedom about the limb (pitch, yaw, and roll). If the liner were to be put on with more pitch (rotation in the Sagittal plane) so that the anterior target was lower on the limb and the posterior target higher, we would expect the sensing data to reflect that position. Again, this type of pattern was not observed in this data, so it is apt to suggest the participant donned the liner similarly between each of the experimental conditions.

Additionally, the verbal ques provided by the participant further support the downward limb displacement theory. Her limb felt as if it was in a "new part of the socket", and "added pressure under the knee where it sits in the socket" suggest that the participant may have felt the limb go deeper in the socket though the data could not directly show what the participant felt along her femoral condyles because there were no sensors in that location.

Besides the global downward limb displacement, it was evident that most sites experienced far more circumferential and pistoning movement during walking. The peak to valley movement along the X- and Y-axis with petroleum jelly on the limb were larger than when compared to a Neutral or Clean liner. A metric like pistoning, that uses a measurement within each step, is inherently less affected by the target-misalignment variable. This is because the measurement is relative to the starting position of the step and

how much it moves from that point, all while the target is aligned in the same location on the limb. The error that this measurement is subjected to though, is the variability is measurement error depending on where the target is above the sensor. Figure 18 exemplifies that different zones in the sensing region have different measurements error but are relatively small compared to the amount of movement observed while the socket is being worn.

Another notable feature of this data is the increase in maxima-to-minima in the Anterior Distal X-axis. This site had the largest change in movement across the Neutral and petroleum jelly condition and may represent evidence of the new “pressure” the participant was feeling at the edges of her tibia and fibula.

Interestingly, the data presented does not agree with our original hypothesis, that petroleum jelly reduces liner-to-socket motion. We thought that the petroleum jelly would allow the limb to slide within the liner and as a result the liner would be more stationary against the socket wall compared to Neutral. In turn the opposite occurred, and there was more motion between the liner and socket (occurring primarily during swing phase). With the data collected from the first participant, a new hypothesis was necessary to describe the limb-socket interface mechanics. Moreover, the subject’s feedback gave more direction to the petroleum jelly experiment and thus the experiment was framed in perspective of a common prosthesis user problem, sweating in the liner.

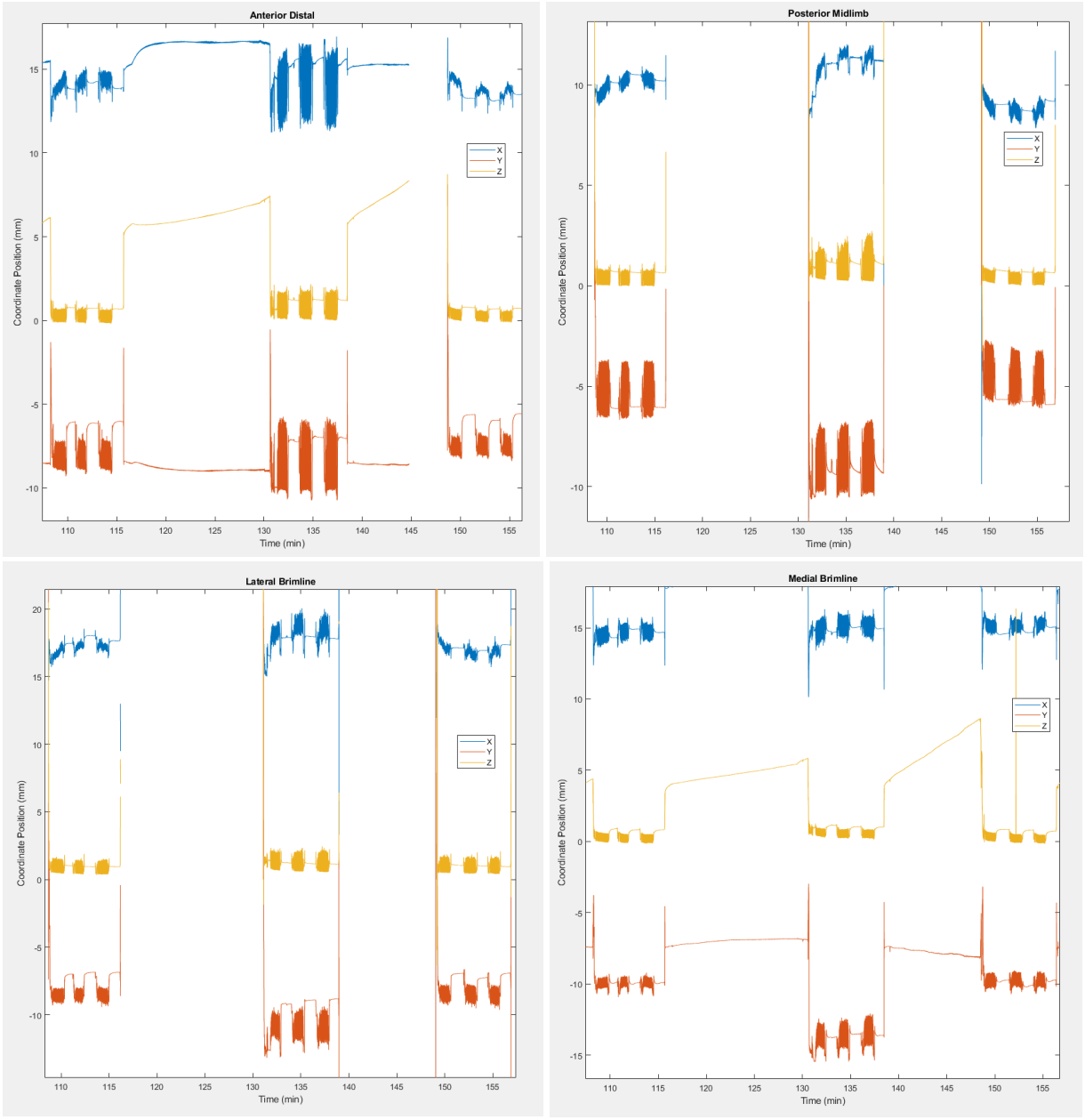

Figure 38: *Petroleum jelly and Cleaned experimental conditions for Participant One. Walk bouts are in sets of three and correspond to Neutral 3, petroleum jelly, and Cleaned, respectively. INTRAY sensors are (a) anterior distal, (b) posterior midlimb, (c) lateral brimline, and (d) medial brimline*

4.1.2 Participant Two

Participant Two is a right legged prosthesis user, male, Medicare Functional Classification Level K3, locking pin suspension, 0ply Neutral sock usage, 82.4kg, 188cm tall, 62y of age, 38y and 11mo since amputation, 16hrs/day usage, PTB socket design, 16.5cm residual limb, and lost their limb to trauma. Their limb shape can be seen in Figure 39.

Figure 39: *Participant Two's residual limb*

The investigational socket was fabricated to have an Anterior Distal, Posterior Midlimb, Medial Brimline, and Lateral Brimline INTRAY. A liner was fabricated using the punch method. Balloon calibration, thermal calibration, data collection, and data processing were all conducted as described in Chapter 3.

Considering the data recorded during the first session, the Anterior Distal and Posterior Midlimb sensors were wired into one board, while the Brimline sensors were put onto the other data collection board. This was done so that the data from the Anterior and Posterior channels were synchronized, and movement could be easily compared globally. Though it was thought that the data could easily time synced after the session, we found that making standardized plugs during the fabrication process would be easiest for intra-sensor comparison.

Different than the investigation prosthesis fabrication presented in Chapter 3.1, Participant Two's fabrication was done in reverse order. To start the investigational liner was donned and anatomical points of interest were located. The distal end of the tibia, the posterior midlimb, and the medial and lateral tibial plateau were palpated though the liner and dots were drawn to mark their location on the liner. These locations were translated to the inner socket shape using historical distal suspension data to account for the limb height offset while the socket was worn. Measurements made from the inferior aspect of the liner to the centers of the target were added to the historical suspension height, and these locations were translated onto the socket and INTRAY sensors were installed.

After fabrication, it was noticed that some of the targets did not match with the positions of the INTRAY sensors. As a result, corrections were made to the liner so that the target and sensors would overlap (Figure 40). This fabrication experience is what led to the current socket and liner fabrication method described earlier. It was clear that anatomical points of interest could be estimated from the internal socket shape and that it was easier and more reliable to translate the sensor locations onto the liner once fabrication was completed.

Figure 40: *Participant Two's investigational liner fabricated with the punch method. The Anterior Distal and Fibular head sites required re-working so that the targets overlapped with the INTRAY sensors.*

Soon after the start of the laboratory session started, four of the six sensors of the Brimline INTRAYs were affected by signal loss and it was unclear why the data was not collected properly. The data collection issue was not repeatable and was thought to be due to a data collection board initialization error. Both the thermistors and two of the individual sensors recorded data correctly, but with the loss of signal from four sensors, the target position could not be solved for and thus there was no Brimline data collected from this session.

The toe-out and toe-in rotational don test yielded similar results that were observed in Participant One's data. A global rotation of the liner relative to the socket was seen. For the toe-out rotation, the data showed a negative offset in the X-axis channel, while the toe-in rotation showed a positive offset. It was also observed that the socket realigned to the Neutral position without any external aid. A difference between Participant One's and Participant Two's data in this analysis is the amplitude of offset. For Participant Two the toe-out rotation was not as large as it was for Participant One. This could be due to the prominence of

this participant's tibial plateau and its inability to fit into the proximal edge of the socket with misalignment, though there was no qualitative evidence of this.

Participant Two conducted the sock ply experimental conditions wearing 0-ply (Neutral), 2-ply, 1-ply, and 0-ply (Neutral). Throughout this experiment the participant maintained a stable Socket Comfort Score of 9, but the participant was recorded as saying that he could walk on the socket for a little while before needing to make a change because the "[socket] was feeling full".

Though using different vernacular, both Participant One and Participant Two described the same sensation, where additional ply socks caused the limb to be wedged in the socket, making the socket feel too small. Likely because of this, the INTRAY data showed the same complex limb-socket interaction. It was observed that there was less pistoning and further separation from the socket wall when more sock plies were worn.

Unique to Participant Two, the posterior midlimb sensor shows that after donning the 2-ply and 1-ply socks, the limb takes a few steps for the limb to sink distally to a comfortable position (Figure 41). This was termed a "settling" period when socket use allowed the limb to gradually reach a stable location in the socket. The distal settling observed for Participant Two took about 15, 5, and 1 steps for the 2-ply, 1-ply, and 0-ply walking conditions, respectively. This concept supports the sensation that the users felt that the limb was being wedged in the socket. With each step, the limb was driven deeper in the socket and the limb maintained that position either due to frictional forces inside of the socket or the pin locking suspension not allowing the limb to release proximally.

Distal settling was not seen in at the Anterior Distal site for any sock ply condition. This is perplexing because this suggests that the participant was able to don the socket, and the distal part of the limb was able to reach its stable position immediately. One plausible explanation is that the limb is a nonrigid body, where the limb and liner are able to stretch and squish, so that the distal end of the limb reaches its stable position while the upper portion of the limb is "hung up". This would allow the distal end of the limb to reach the end of the socket, while the more proximal part of the limb is wedged in the socket, suspending the proximal parts of the limb more proximally. Data from Participant One corroborates this hypothesis, as the Brimline sensors during the 2-ply sock conditions were significantly offset proximally compared to the Neutral condition. Data collected from these experiments are preliminary evidence of this and more sensors, throughout the entire height of the socket, would be needed to confirm this theory. Limb shape and soft tissue characteristics would also need to be evaluated to better explore this.

During the sock ply conditions, the X-axis channel showed some global rotational settling depending on the participants ability to align the socket during the first don. It was thought that this had minimal effect on the fit of the socket compared to the other phenomenon observed.

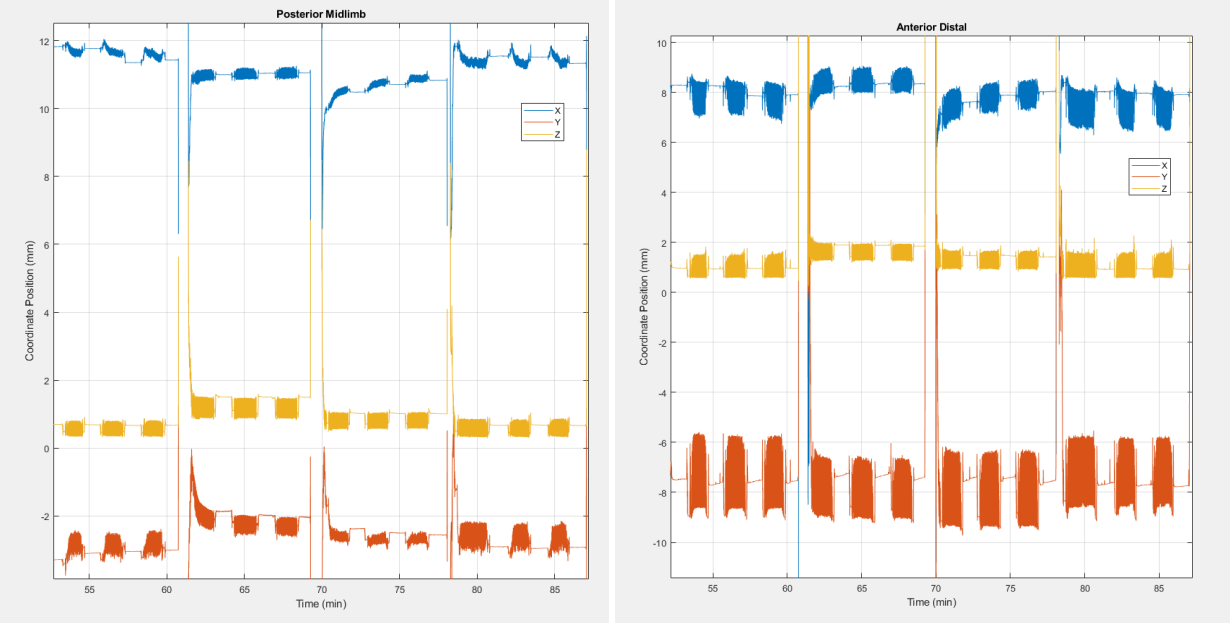

Figure 41: *Sock ply experimental conditions for Participant Two. Walk bouts are in sets of three and correspond to 0-ply, 2-ply, 1-ply, and 0-ply, respectively. INTRAY sensors are (a) Posterior Midlimb, and (b) Anterior Distal.*

1.2g of petroleum jelly was added directly to the residual limb in the same fashion as Participant One. Participant Two though, was wearing a silicon cup on the distal end of their limb, under the liner. Petroleum jelly was applied directly to the skin, the distal cup was donned after petroleum jelly application, and then the investigational liner was donned. The participant reported that their Socket Comfort Score decreased to a minimum of 7 while walking with petroleum jelly, and they as voiced that each subsequent walk with petroleum jelly felt increasingly better.

Data from this participant illustrated the target misalignment error discussed previously, and it can be seen in the positional data along the X- and Y-axes (Figure 42). Between each experimental condition (set of three walks) the liner is doffed from the limb and then re-donned. The first clue of the liner misalignment is in the X-axes, where the data is showing a global offset in the positive direction, as if the limb was rotating clockwise in the socket. The magnitude of this rotation was of similar magnitude to the rotation observed when the user was asked to purposefully misalign the socket on their limb. It is unlikely that the participant gravely misaligned their socket while donning, because in all other dons (besides the experimental rotational dons) the user was able to well align the rotation of their socket. The second clue is in the Y-axes. The Posterior Midlimb and Anterior Distal sensor sites seem to have equal and opposite relative global position offsets, meaning that the Posterior sensor offsets by 2mm proximally while the Anterior sensor offsets by 2mm distally. It is unlikely that the limb was able to rotate in such a drastic way due to the constraints of the rigid socket.

Instead, this data supports that the liner was rolled on with misalignment in 2 degrees of rotation. The X-axis data suggests that the liner was rotated with some rotation in yaw because there was a constant global rotation of the targets along the INTRAY sensors. Rather than the limb rotating in the socket, the liner was rotated along the limb and the limb likely remained in the same position, producing the data observed. In the Y-axis, data suggests that the liner was rotated with some rotation in pitch because the Anterior target

moved distally in the socket, while the Posterior moved proximally. The liner, though flexible, is rigid enough to maintain its shape, and instead of the limb angling inside the socket, it is more likely that the liner was donned so that the front of the liner was lower, pushing the back of the liner higher. Liner misalignment with respect to roll cannot be observed because there would need to be sensors on opposite sides of the socket along the Medial-Lateral axis to see how the targets interacted.

This understanding may provide an avenue to study how to compensate for liner doff/don misalignment but was not explored in this dissertation. It is common for users to misalign their liner when putting it on outside of the laboratory, so efforts may be placed on quantifying this phenomenon. Furthermore, many commercially manufactured liners are not uniform in shape and thickness. A future endeavor may evaluate how liner misalignment along the residual limb can change the limb-socket interface mechanics due to a change in limb-liner shape.

Ultimately the data was evaluated based on the relative movement found within each step, and it was observed that there was more pistoning with petroleum jelly on the limb compared to Neutral and Cleaned. Interestingly, after cleaning the limb there seemed to be less poisoning compared to Neutral.

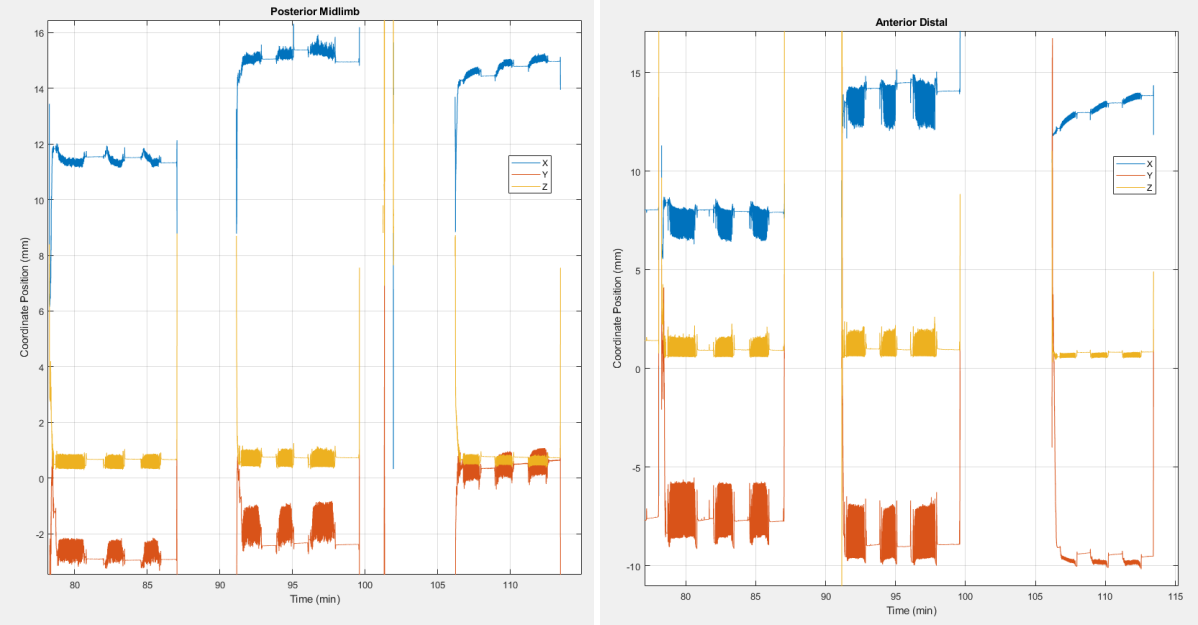

Figure 42: *Petroleum jelly and Cleaned experimental conditions for Participant Two. Walk bouts are in sets of three and correspond to Neutral 3, petroleum jelly, and Cleaned, respectively. INTRAY sensors are (a) Posterior Midlimb, and (b) Anterior Distal.*

4.1.3 Participant Three

Participant Three is a left legged prosthesis user, male, Medicare Functional Classification Level K3, locking pin suspension, 5ply Neutral sock usage, 106.0kg, 183cm tall, 59y of age, 33y and 4mo since amputation, 15hrs/day usage, PTB socket design, 13cm residual limb, and lost their limb to trauma. Their limb shape can be seen in Figure 43.

Figure 43: *Participant Three's residual limb*

The investigational socket was fabricated to have an Anterior Distal, Posterior Midlimb, Fibular Head, and Anatomical Point of Interest, which was in the Distal Lateral site, INTRAY. A liner was fabricated using the punch method. Balloon calibration, thermal calibration, socket fabrication, liner fabrication, data collection, and data processing were all conducted as described in Chapter 3. The Anterior Distal and Posterior Midlimb sensors were wired into one board, while the Fibular Head and Distal Lateral sensors were put onto the other board. This was done so that the data from the Anterior and Posterior channels were synchronized, and movement could be easily compared globally. Similarly, we wanted to synchronize the Fibular Head and Distal Lateral sensors, which were stacked along the same Y-axis, so that the global interaction of sensors could be explored more. A pin sensing device was also instrumented below the lock body to measure the depth of the locking pin in the socket (71).

The investigational liner was fabricated to match the locations of the sensors that were placed inside of the socket. As done for Participant Two, historical data about distal suspension for this participant was used to offset the location of the target to the sensor so that it was well aligned when the prosthesis was worn. Prior to the session, the liner was tested within the socket and there was no evidence of poor alignment between the targets and the TRAY sensors.

When the socket was worn during the session, there was evidence that some targets did not align with the sensors. In specific experimental conditions the target was found to be near the edge of the sensing array, but it was not the case throughout the entire protocol. When the target was found to be at the edge of the sensor, the solved position of the target was affected by the sensor error, and that was taken into consideration.

A contributing factor to poor alignment may have been that this participant had an upper extremity amputation above the elbow on their right side. One handed liner donning may have been difficult to consistently align the liner in the proper position to interact with the socket. Additionally, this participant routinely asks for the liner to be stretched on a positive mold of their residual limb shape, meaning that when the liner was worn by the participant the liner was also stretched. During the fabrication process, the targets are glued to the liner in an unstretched state, so by stretching the liner, the targets also became distorted. As can be seen in Figure 44 the liner is strained to fit around the residual limb and it caused the

targets, primarily the Fibular Head target, to distortion. This dillemna was ultimately solved when perfroming the liner fabrication method where the iron-polymer targets were glued to the outside of the liner. Before gluing the targets down, the liner could be stretched and the circular targets were glued to the streteched-state liners.

Figure 44: *Participant Three's investigational liner fabricated with the punch method. The fibular head target is distorted because the liner is dramatically stretched over the participant's limb.*

The first rotational don to occur in this session was a toe-in rotation, which for a left legged amputee, shows a negative offset along the X-axis (Figure 45). The rotation, as it was observed for the first participants, was also seen globally across all the sensors, but the amplitude of settling is less than what was observed in the prior sessions. During the second walk the limb settling continued but did not seem to reach a stable, consistent position. Furthermore, the participant voiced that the socket "still felt rotated", possibly corroborating the limb position pattern seen in the INTRAY data.

Additionally, the participant remarked that their "fibula felt tighter" while walking on the toe-in configuration. Visually there is a small reduction in movement in the X-, Y-, and Z- axes at the Fibular Head and Distal Lateral sites (intended to track the Fibula's movement) when comparing the two prior walks to the toe-in configuration walk.

The participant also stated that during the second walk (of the first rotational don), "the pin was not as deep". When looking at the Pin Sensor data, we see that there were numerous steps in the first walk that show the pin further into the bottom of the socket when compared against the second walk. About half of the steps in the first walk do this and the other half seem to be suspended higher, similar to the second walk. The data suggests that the participant was still in the same "click"[1], but that the first walk had numerous steps that were about 1mm deeper into the socket.

This finding put into perspective the difficulty a user may have verbalizing changes in socket fit. If the pin sensor data is presented with high accuracy, participants may be able to notice a change in limb-socket interaction of about 1mm. Furthermore, some users may have the sensation to feel the fit of a socket vary from step to step and when asked to verbalize the socket fit a participant may need to average the feeling of what is happening to provide information to their clinician. In the data presented here, the pin was deeper in the lock body for the first half of the one-minute walking bout, and the participant may have tried to communicate this. This poses the question, do user limit the information they verbalize in order to clearly articulate the fit they are perceiving.

[1] A "click" is the 3mm range within one notch of the ratcheting pin lock system. Pins generally have four to seven notches or clicks that engage the lock body.

At times during the data collection, it was noticed that participants can struggle to articulate and communicate the small changes within the socket that they perceive. As a result, it seemed that participants resorted to repeating their description of the socket fit in different manners to describe the feeling. The granularity of this data may offer a visual and numeric representation of the small fit changes that these participants experience throughout their day.

Following the first rotation, the participant performed a toe-out don. A global rotation was reflected in the sensor data (Figure 45). In this instance, the data shows evidence that the Anterior Distal target was poorly aligned with the corresponding INTRAY. Referring to Chapter 2.4.2, the solved position data of the target for the toe-out don suggests that the target is in position (31,-3,1). This means that the target is shifted towards the upper right sensor and at an extreme edge of the sensing region for the INTRAY. In this experimental condition, the limb was purposely rotated so that the target would move to the right side of the INTRAY. In the case of the Anterior Distal sensor, the target was fabricated in the liner such that in a Neutral position, it was already shifted to the right side of the sensor. This is considered to be a fabrication flaw, rather the target should be centered over the INTRAY when the socket is being worn in a Neutral condition.

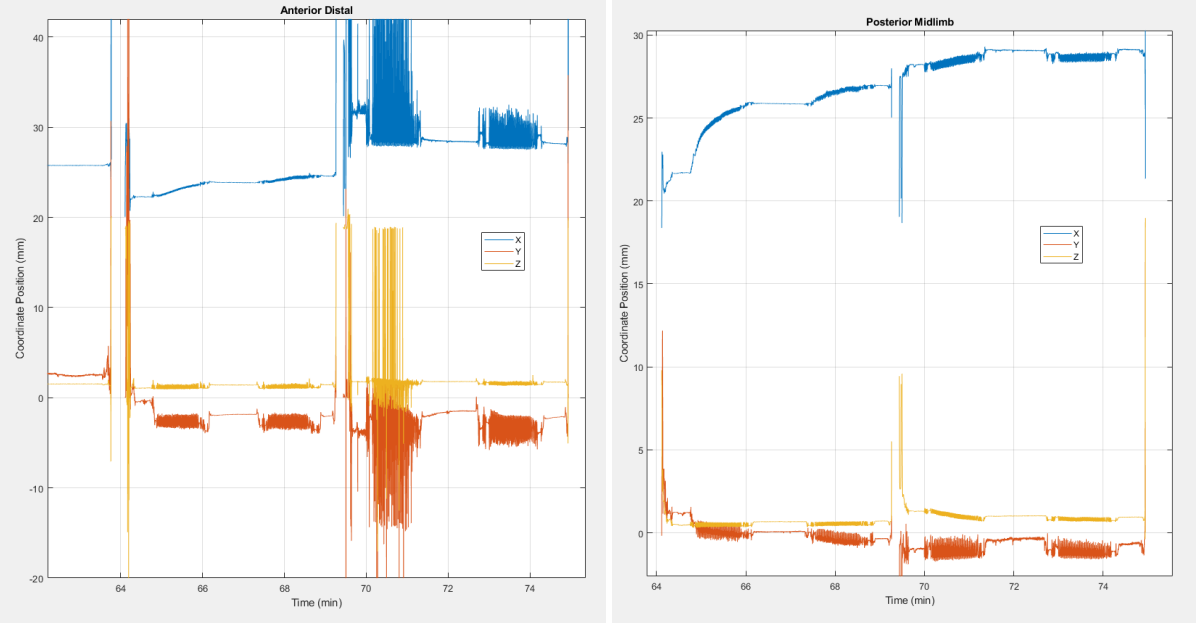

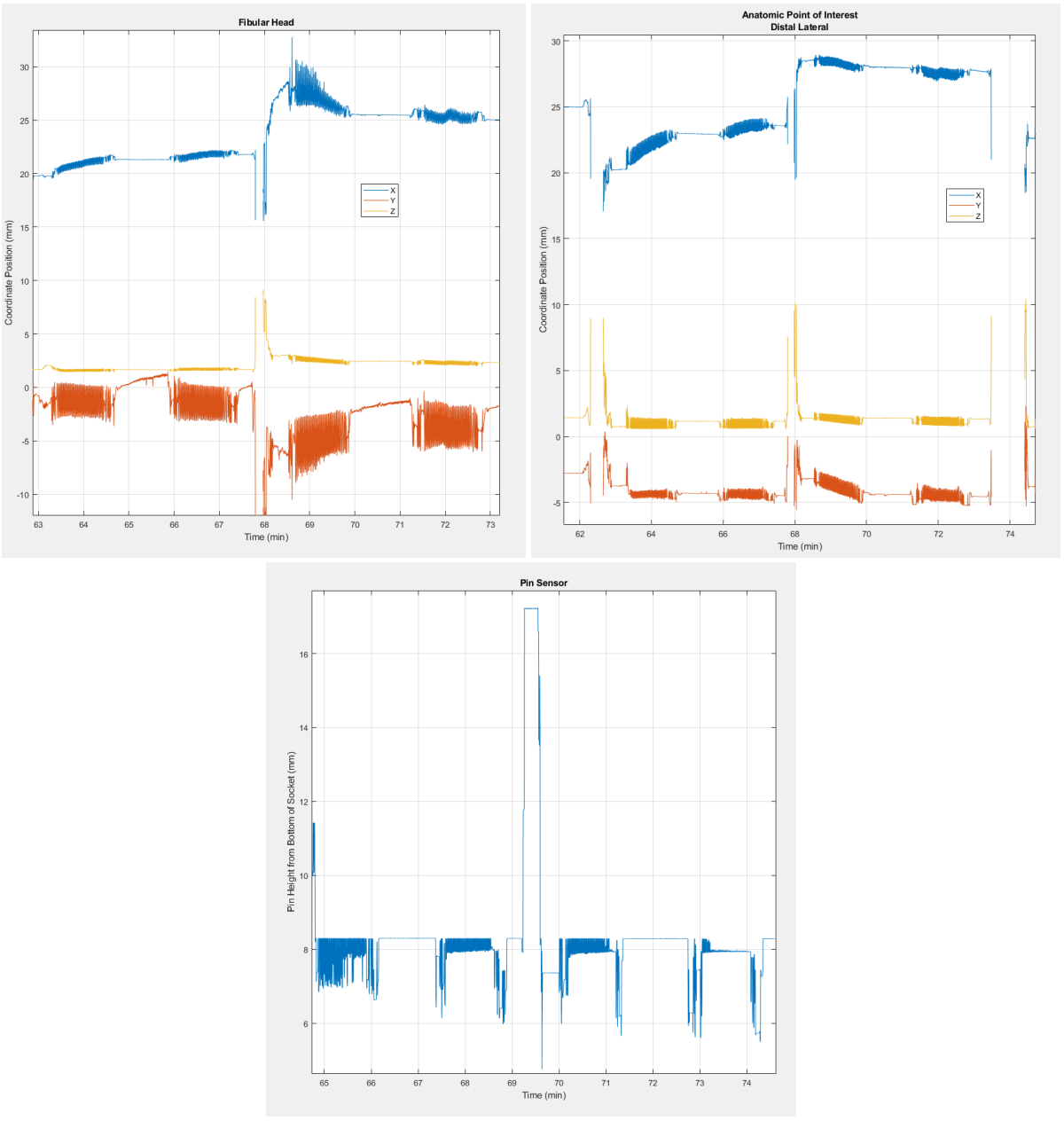

Figure 45: *Rotational experimental conditions for Participant Three. Walk bouts one and two are toe-in, and walk bouts three and four are toe-out rotation. INTRAY sensors are (a) Anterior Distal, (b) Posterior Midlimb, (c) Fibular Head, and (d) Distal Lateral. Panel (e) illustrates data collected from the Pin sensor.*

Briefly described in Chapter 2.6, the sensing region of the INTRAY is approximated by a Reuleaux tetrahedron with a flat base. This is the shape that three overlapping spheres creates, and because the sensor surface restricts the possible location the target can be found, one side of the tetrahedron is flat. The surface area of detection along the base of the sensing region is thus described by a Reuleaux triangle and is calculated by Equation 20 and shown in Figure 46. For this application the side length of the base was chosen to be 28mm because of the 1% signal intensity cutoff (at the 1% signal intensity the radius of the target sensing is 30mm from the center of the inductive sensor), making the sensing area of the base 5.53 cm^2. The centroid of the INTRAY sensor was such that all three sensors would have equal coverage by the target, which in the coordinate system defined in Chapter 2 was (16, -9.23) millimeters.

(20)

$$SA = \frac{1}{2}s^2(\pi - \sqrt{3})$$

In an effort to provide context of the Anterior Distal target offset seen in Participant Three's toe-out rotation condition, the distance from the center of the sensing region to the edge of the sensing region was calculated. Due to the shape of the sensing region, there was a range of distances the target could be offset to lose sensing capabilities. On the short axis the target would need to be offset by 1.15cm, while on the long axis would need to be offset 1.61cm. It is evident that the Neutral position of the Anterior Distal target was around X=27mm, which left little room for the target to travel clockwise within the socket before signal intensity was lost.

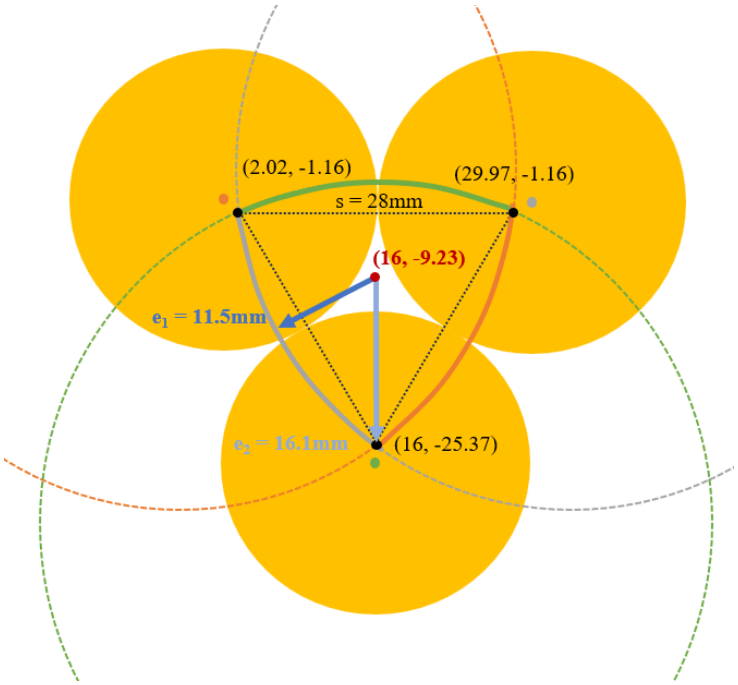

Figure 46: *A diagram describing the sensing region of an INTRAY sensor along the sensor's surface and the tolerance of target-sensor alignment. Thresholding signal intensity at 1.5% yields a radius of observation of 30mm, and the centroid of the sensing region is found at (16, -9.23)mm. Target-sensor alignment tolerance should be less than ±1.15cm.*

Towards the end of the first toe-out walk, the Anterior Distal position sensor seemingly drifted back toward the sensing region of the INTRAY. The same rotation was noticed at both the Fibular Head and Lateral Distal sites, but not the Posterior Midlimb. Rather the Posterior Midlimb site seems to rotate more toward in the clockwise direction, further rotating the toe outward. A complex motion seemingly unfolded at the end of the first toe-out walk and the position was maintained in the second walk.

Over the course of the first walk, the data suggested that the Fibular Head rotated to correct the misalignment (counterclockwise) while simultaneously moving more proximally. The Distal Lateral rotated to correct the misalignment (counterclockwise), yet, it was simultaneously moving distally in the socket (opposite of the Fibular Head). The Posterior Midlimb was observed rotating more toe-out (clockwise),

enhancing the misalignment, while maintaining its depth in the socket. Just prior to the second walk the participant, single-legged jumped on the prosthesis to seemingly force a change of fit. This was unprompted by the research engineer. The participant was recorded as stating that, "[they didn't] think it would naturally self-align," and that the socket was "still rotated" after the second walk. Ultimately the Socket Comfort Scores for the toe-in and toe-out walk were an 8 and a 7 respectively, which was not different from the scores reported throughout the session.

The complex motion observed is challenging to describe, especially with the Anterior Distal sensor not producing viable results. To start, it was clear that the limb was rotated in the socket, as the protocol was designed to do. Participant 3 then had a unique response to the socket misalignment, compared to the first two participants, and the limb began to interact with the socket environment without any external efforts. A hypothesis for what could have happened is that the limb translated in the socket. Because of the non-rigid nature of the limb in the socket, the movement that is observed in the proximal part of the socket (Fibular Head and Posterior Midlimb) may be different that the motion happening in the distal part of the socket (Lateral Distal). Furthermore this type of displacement, may be accentuated by the complexities of the socket shape and where the limb contacts the socket.

During the change of sock ply experiment Participant Three wore, in chronological order, 5-ply, 6-ply, 7-ply, 4-ply, and 5-ply socks. Unlike the first two participants, this participant started the session wearing sock plies to obtain a comfortable fit and this allowed for a decrease in sock ply to be tested.

Like the data collected from the prior two participants, we found that the X-axis data did not respond to changes in sock ply (Figure 47). Rather, this participant had random rotational offsets when the socket was donned and the data reflected the participant's unique limb-socket interaction. The offsets were smaller compared to the rotational don experiment, and the position of the limb persisted throughout each of the three walks. In the rotational experiment, this participant exhibited that the socket would not automatically rotate into alignment like the first two participants and instead the limb would remain in the rotational position it was donned in. This was seen in all of the INTRAY datasets except for the fibular head, which is where the target was significantly distorted along the X-axis, possibly minimizing the global offsets effect on the data.

Similar to the first two participants, the Z-axis data (normal to the socket wall) showed a similar pattern of target separation at varying thicknesses of sock ply that agreed with what was observed before.

The participant made note of only two conditions that were uncomfortable during this protocol. Their Socket Comfort Score was an 8, 8, 6, 7, and 8 in order (5-ply, 6-ply, 7-ply, 4-ply, and 5-ply, respectively). During the 7-ply walk (SCS=6) they mentioned that it was "too tight, [I] can't get deep [in the socket]". It was noticed in the distal INTRAY sensors and the Pin sensor that the participant was marginally (<1mm) higher during the 7-ply walk compared to the prior 5-, and 6-ply walks, while the more proximal sensors showed that the limb was marginally (<1mm) lower. This global offset, in addition to the rotation experienced, may suggest that the point of contact between the limb and the socket wall is occurring at a new location that is likely more distal in the socket.

For instance image that the distal end of the limb (not the inferior aspect) is being constricted because of the additional ply socks added and that becomes a main contact point for the limb remaining suspended from the very bottom of the socket. It may prevent the distal end of the limb from going into the traditional depth of the socket, and now that the upper region of the limb is not being constricted, as it traditionally was, allows it to sink further into the socket. For this case, the participant was concerned about the distal end of the limb because usually that is what's used to drive and control the socket during ambulation.

During the subsequent walk, 4-ply and SCS of 7, they were "moving around too much" and described that immediately after toe off, he felt that his limb hit "three walls". Only the Posterior Midlimb sensors showed a change in overall motion, and it was a marginal increase compared to the previous walks (<1mm). Notably another global shift occurs where the proximal sensors are held up higher (<1mm), while the distal INTRAY sensors drop deeper (<1mm) than the previous walks and the pin drops an additional click deeper into the socket. As sock ply is reduced the opposite constriction could occur, where the traditional contact between the limb and the socket is more proximal, allowing the distal end to drop deeper in the socket. This though is a complex explanation for the data and the non-rigid nature of the limb and liner would need to be further studied.

The variable of limb fluid volume loss during this part of the protocol may confound some of the explanation for the data presented here. Further rigorous experiments would be needed to tease this out.

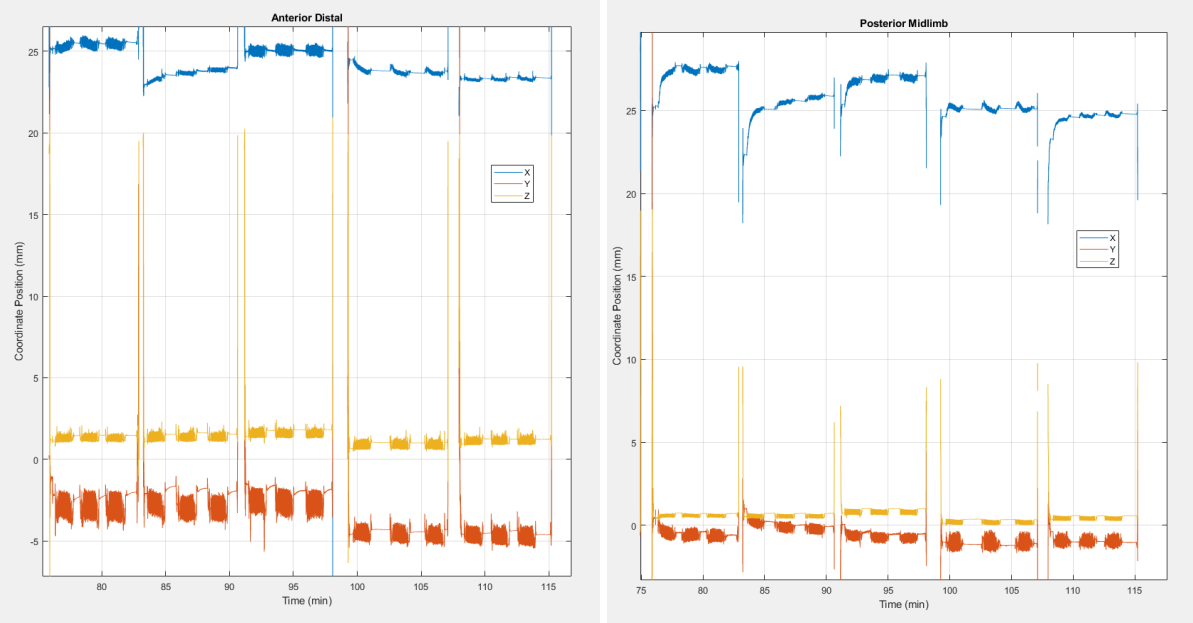

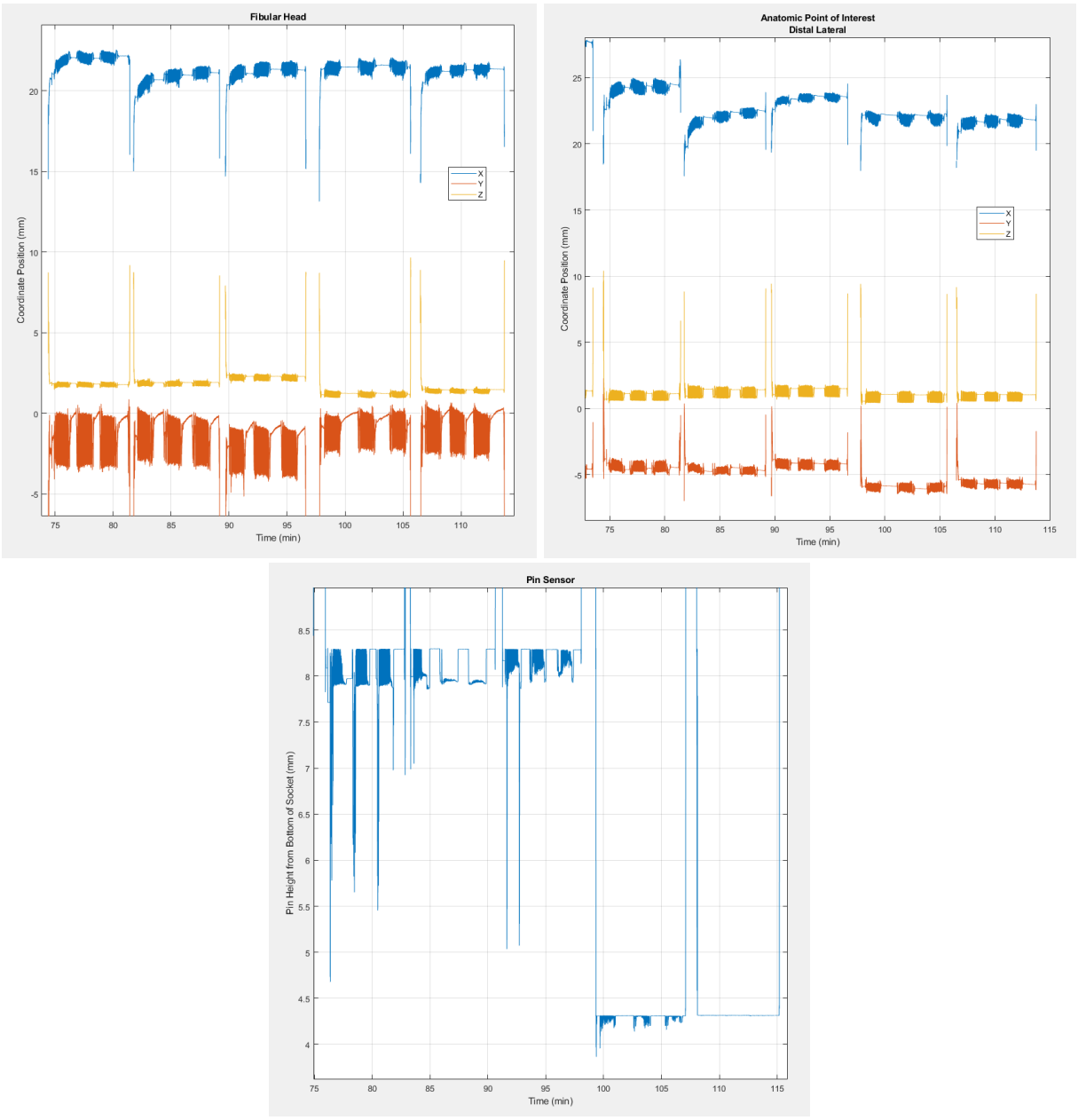

Figure 47: *Sock ply experimental conditions for Participant Three. Walk bouts are in sets of three and correspond to 5-ply, 6-ply, 7-ply, 4-ply, and 5-ply, respectively. INTRAY sensors are (a) Anterior Distal, (b) Posterior Midlimb, (c)Fibular Head, and (d) Distal Lateral. Panel (e) is data collected from the Pin sensor.*

Lastly 1.2g of petroleum jelly was added to the participant's limb. Throughout the entire petroleum jelly and Clean protocol the participant stated they had a Socket Comfort Score of 8, and during the first walk with petroleum jelly they stated that their, "limb is moving in the liner, liner is not moving in socket". A single additional walk was completed just after the three petroleum jelly walks, where extra petroleum jelly was added to the participant's limb to try to get the limb to slide out of liner (Figure 48). The participant had suggested that this was possible.

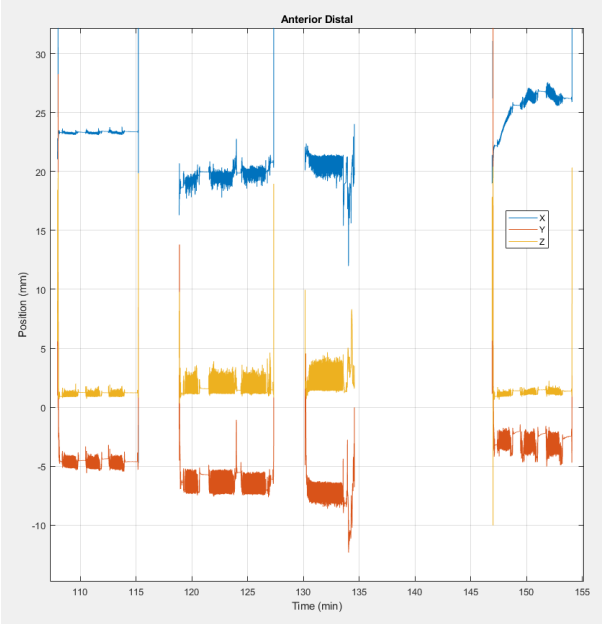
Anterior Distal
Position (mm)
Time (min)
X
Y
Z

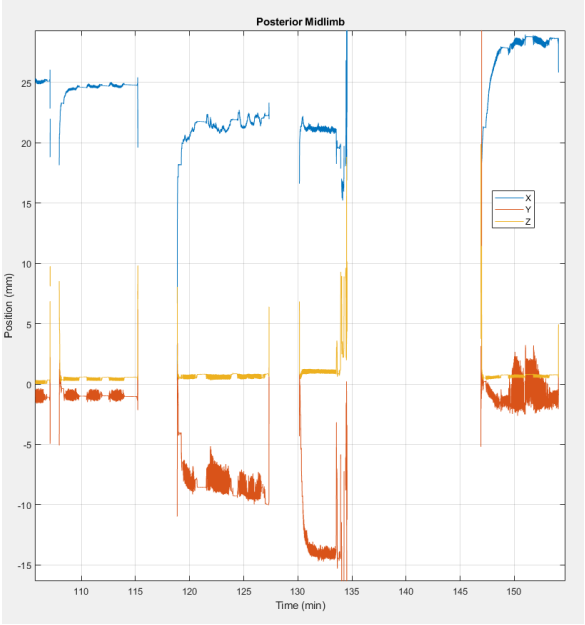
Posterior Midlimb
Position (mm)
Time (min)
X
Y
Z

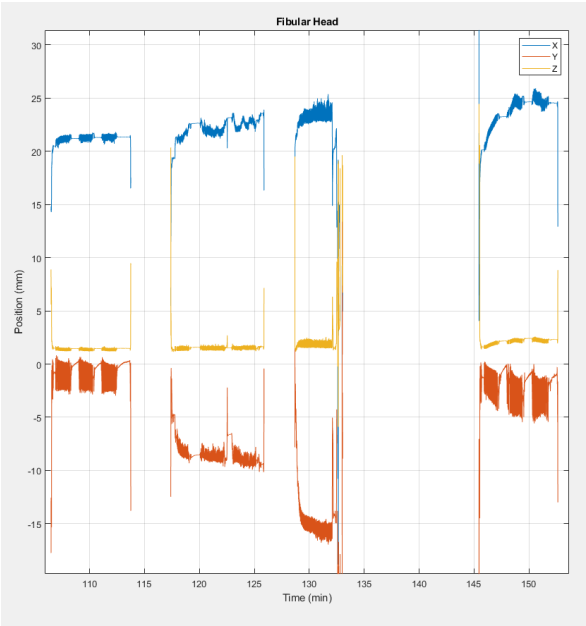
Fibular Head
Position (mm)
Time (min)
X
Y
Z

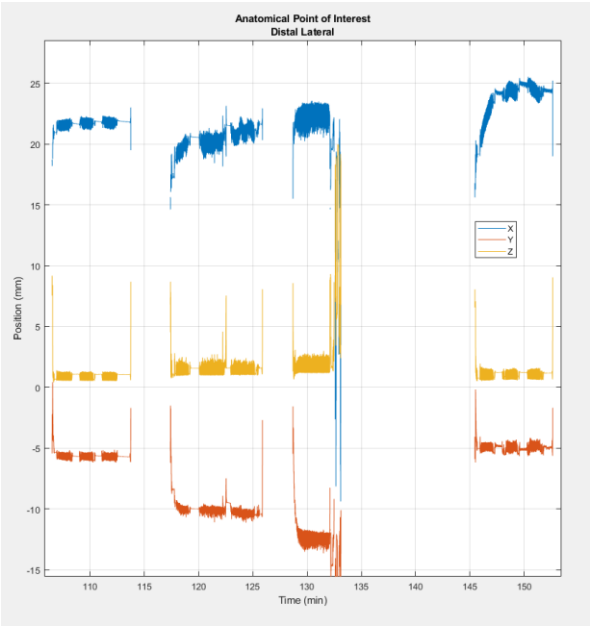
Anatomical Point of Interest
Distal Lateral
Position (mm)
Time (min)
X
Y
Z

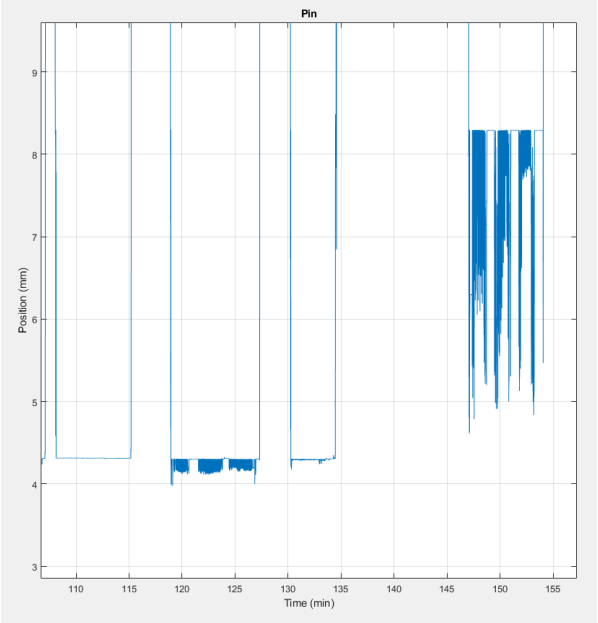

Figure 48: *Petroleum jelly and Cleaned experimental conditions for Participant Three. Walk bouts are in sets of three and correspond to Neutral 3, petroleum jelly, and Cleaned, respectively. Between walk bouts two and three there is an extended walk where additional petroleum jelly was put on the residual limb. INTRAY sensors are (a) Anterior Distal, (b) Posterior Midlimb, (c)Fibular Head, and (d) Distal Lateral. Panel (e) displays Pin sensor data.*

It is thought that the data collected at the INTRAY sensors corroborates the user's feedback, except for the Anterior Distal location. It is evident that the liner-to-socket motion increases at the Anterior Distal site when the limb has petroleum jelly. As for the other locations, the participant adamantly reported that their limb was sliding within the liner and that the liner was not sliding along the socket. The INTRAY data suggests that the liner is sliding along the surface of the socket. There may be some motion between the liner and socket, but rather it is hypothesized that the sensed motion of the INTRAY may actually be primarily noise. The movement displayed is at a similar magnitude to the noise investigated when a socket was walked on with a nude liner. It is believed that there is a small amount of motion, but unlike the previous two participants where larger amounts of motion were observed, this participant has a different interaction with their socket fit.

It was also noticed that once the liner and limb were cleaned, the user immediately had a different interaction with their socket. Firstly, the pin reverted back up one click, and the user had a relatively "dramatic" rotational settling event compared to what was observed in the earlier data of this patient.

This was the first session that was run while recording the depth of the locking pin at the most distal part of the socket. Within the pin sensor data, it was observed that the participant shifts between two depths of pin click. Further, when the pin sensor and Anterior Distal Y-axis data were compared while plotted against time, the waveforms appeared to be out of phase and to have slightly different timing. Figure 49a illustrates that the toe off portion of swing phase and the heel contact of stance phase are the maxima and minima for the Anterior Distal sensor. While the terminal swing phase and terminal stance phase mark the maxima and minima for the pin sensor. Though the maxima and minima were identified during these landmarks, the pin sensor waveform was more square-like than sinusoidal. This is likely due to the physical limits of the lock

body. The pin hits a hard stop when pulling proximally and has slight resistance when pushing deeper into the socket. There were some steps where the pin nearly engaged the next pin click, but it wasn't until the participant wore a 4-ply sock that they reached the lower click. It was also evident that the Anterior Distal motion for initiating heel contact happened prior to the pin sensor motion and the Anterior Distal motion for toe off happened after the pin sensor motion with each step. The timing difference was extremely small, it was about four to six samples apart (125 to 188 milliseconds).

Comparing the Anterior Distal Y-axis INTRAY data to the pin sensor data, it was observed that there may be a correlation (Figure 49b). Time-synced data points, representing pin sensor stance phase minima, between the pin sensor and Anterior Distal sensor were collected from the sock ply experiment was used to create the scatter plot. Again, in the pin sensor data the user was between two clicks. There was more spread seen in the Anterior Distal Y-axis data, but the data seemed to be discretized, matching the discretized pin click data. There are few observations where the pin is transitioning from one click to the next (seen from 5-7.5mm in the pin data), but those points bridge the two clusters of Anterior Distal Y-axis data observed from the two pin clicks. It seems that there may be a threshold for Anterior Distal Y-axis data around -4mm that follows the pin click data. Ultimately it is expected that these two variables would positively correlate because they are sampled from close proximity within the socket and it is believed that the distal limb position may be a driving factor for moving the pin deeper into the socket.

A limitation of the relationship shown in Figure 49b is that the data plotted are time synced. It was noted that the two waveforms were out of phase and had slightly different timing. The data points sampled in Figure 49a, may not aptly show the relationship between Anterior Distal Y-axis movement and pin displacement. For instance, the heel contact minima of the Anterior Distal Y-axis data may more closely correlate with terminal stance phase minima in the pin sensor data. Moreover, causal relationships could be explored with data such as this one. It may turn out that unexpected relationships between two sensed locations emerge. For instance, it could be that the Anterior Distal Y-axis swing phase maxima is most correlated to pin sensor depth, implying that limb position prior to loading predisposes the limb to respond in a certain way once in stance phase. Though exploratory, the INTRAY data could be integral in studying new limb-socket interface mechanic phenomenon.

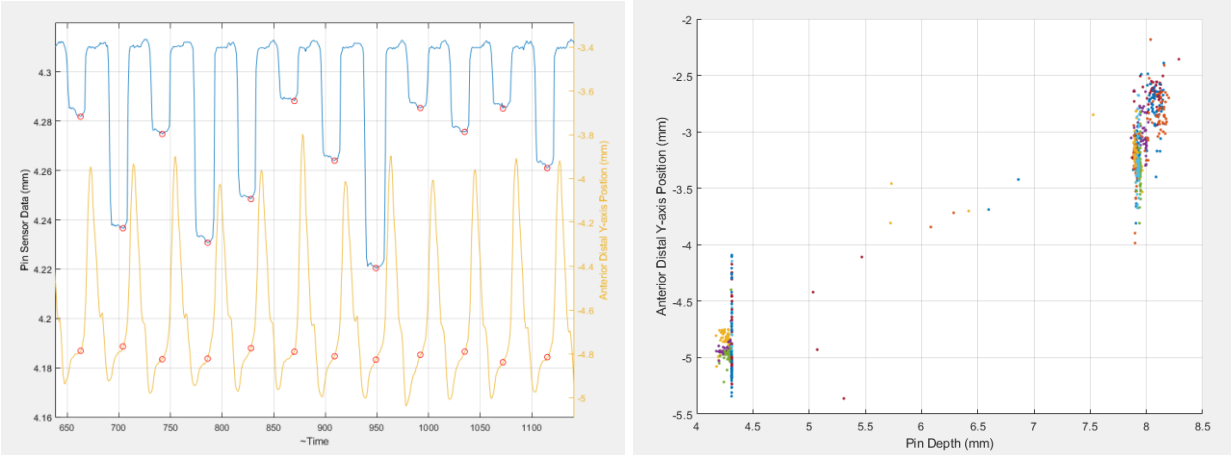

Figure 49: *(a) Time-synced pin sensor data (blue trace) and the pistoning motion (Y-axis) of the Anterior Distal INTRAY (yellow trace). Red circles identify the stance-phase minima in the Pin sensor data and are matched to the Anterior Distal sensor. Early stance-phase the Anterior Distal limb travels deeper into the*

socket, while late stance-phase the limb come out of the socket. (b)Scatter plot of Red Points identified in the Pin data and Anterior Distal time-synced data.

4.1.4 Participant Four

Participant Four is a right legged prosthesis user, male, K3, suction suspension, 1-ply Neutral fit sock usage, 84.0kg, 185cm tall, 65y old, 7y and 10mo since amputation, 15 hrs/day socket usage, TSB socket design, 14cm residual limb, and received an amputation due to a traumatic event. Their limb shape is observed in Figure 50. A liner was fabricated using the punch method. Balloon calibration, thermal calibration, data collection, and data processing were all conducted as described in Chapter 3.

Figure 50: *Participants Four's residual limb*

Participant Four was the first user that wore a pin-less type suspension. This means that the investigation prosthetic socket was made without a lock body in the distal end of the socket and instead a one-way valve was incorporated at the distal end of the socket. The "expulsion" valve allowed air to be forced out of the socket by the mechanical limb-pistoning action, and thus a negative pressure was created within the socket that adhered the prosthetic limb to the residual limb.

This socket suspension type allowed for an Inductive Trilateration Array to be placed along the inferior aspect of the limb, measuring the movement of the very distal end of the limb. This was made possible because the lock body housing assembly was removed from socket fabrication, and the distal liner did not have an umbrella and threading to attach a pin. In fabricating this socket INTRAY sensors were placed at the Anterior Distal, Posterior Midlimb, Fibular Head, and Inferior sites in the socket. Due to the Inferior sensor being on the apex of the distal end, the X-, Y-, and Z-axes described the limbs movement in the medial-lateral axis, anterior-posterior axis, and separation from the bottom of the socket, respectively.

Three of the four rotational don walks were completed, the last was not completed due to the proximal tibia becoming too "aggravated" after the first toe-in rotation. In the Anterior Distal, Posterior Midlimb, and Fibular Head sensors we can see a global shift in the X-axis component corresponding to the toe-out and toe-in rotations, respectively (Figure 51b-d). The limb did not automatically track back into the Neutral line of alignment, and instead seems to maintain its rotation. It is not remarkable that the participant experienced pain on the proximal tibia during a large toe-in socket rotation. What is curious though is that some sockets maintained their misalignment, while for other participants, the socket was able to automatically realign without any external aide. For this participant, it may be advantageous to design a socket that automatically realigns so that the proximal tibia pain does not occur if the socket becomes misaligned.

The inferior sensor, though looking like the other three data traces, presented unique information (Figure 51a). We did not observe the global rotation phenomenon that was seen in nearly all the prior participants' sensors. This is perhaps due to the fact that the limb is rotating about the axis of the distal end, and rather than displacing along the INTRAY sensor, the target is spinning. Furthermore, because the target is circular,

and spinning near the center of the circle, the signal values remain unchanged at each of the individual sensors.

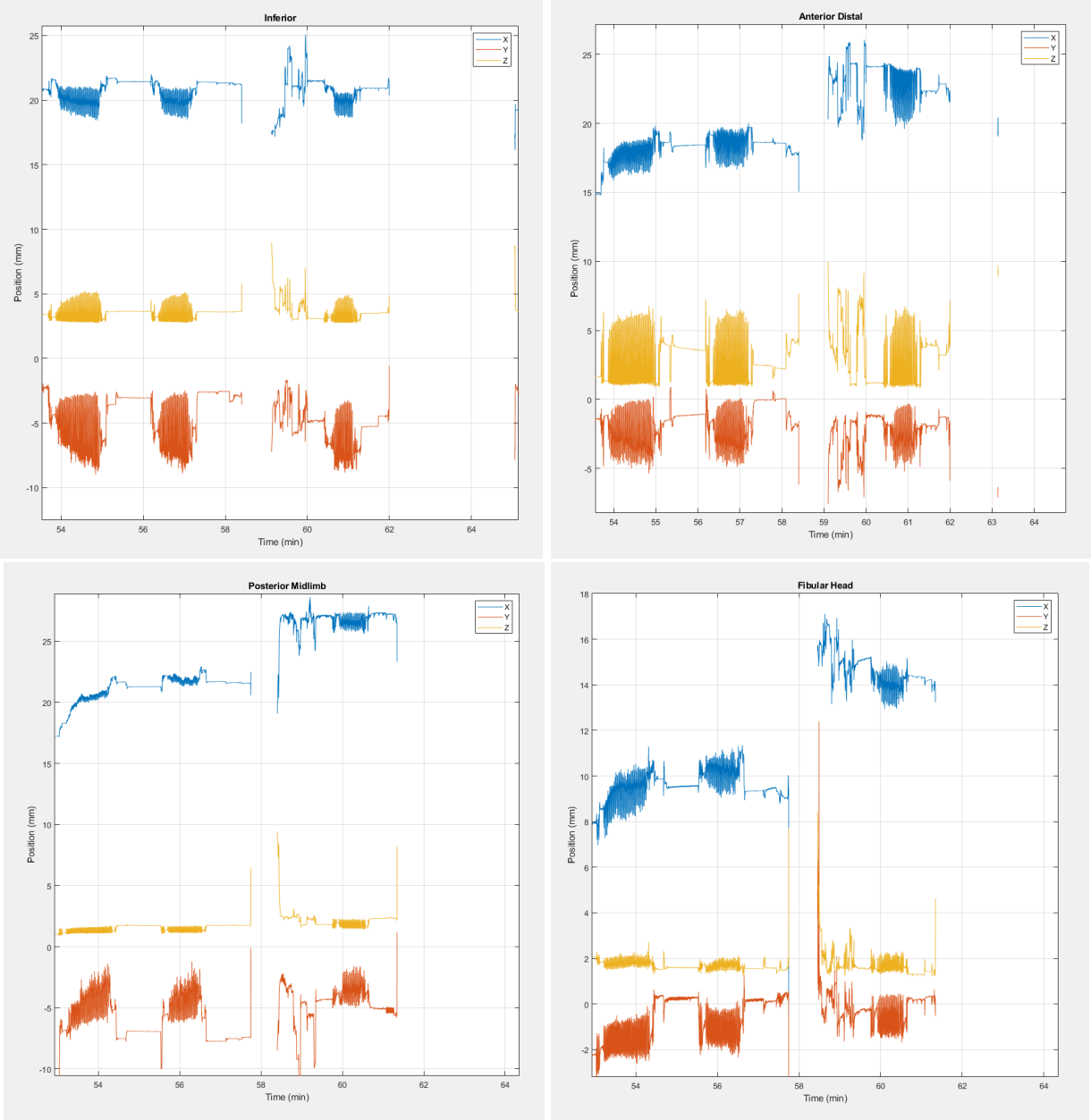

Figure 51: *Rotational experimental conditions for Participant Four. Walk bouts one and two are toe-out, and walk bout three is toe-in rotation. INTRAY sensors are (a) Inferior, (b) Anterior Distal, (c) Posterior Midlimb, and (d) Fibular Head. A second toe-in walk was not completed due to limb discomfort.*

Participant Four had limb discomfort that spanned the rest of the trial and the experimental protocol was, at times, shortened to accommodate the volunteer. Five bouts of walking were performed for the sock ply experiment, which in chronological order were 2-ply, 3-ply, 4-ply, 5-ply, and 4-ply. The third walk of the 2-ply condition was cut short, there was no reduction of sock ply, the order of sock addition was not randomized, instead it was additive, and the final 4-ply condition only had one walking bout due to discomfort. By the end of the sock ply experiment, a Neutral sock ply went from a 2-ply to a 4-ply of socks.

Though verbalizing discomfort and accommodating the discomfit with a change in protocol, the user reported a Socket Comfort Score of 7 throughout the entire sock ply walking experiment.

When the sock ply data was reduced and evaluated the Anterior Distal, Posterior Midlimb, and Fibular Head INTRAY positions showed global rotation along the X-axis, increasing liner-to-socket separation with increasing sock ply along the Z-axis, and some proximal suspension with increasing sock ply along the Y-axis (Figure 52). The Inferior sensor exhibited more consistent limb-socket positioning with some settling early in walks the immediately followed a don.

Most remarkable from this experiment is the dramatic increase in stance to swing phase displacement, in all axes of all INTRAY sensors, while wearing 5-plies of sock configuration. This was thought to be due to the socket's inability to maintain a negative pressure to adhere the prosthetic limb to residual limb.

The investigational socket fabricated was a suction suspension which means that for the socket to adhere to the residuum, a negative pressure is needed within the socket. The generally accepted principle behind suspension sockets is that it takes a few steps to create the negative pressure. The mechanical pistoning action of the residual limb within an airtight chamber, drives air out through the one-way valve installed at the bottom of the socket. Without negative pressure inside the socket, the prosthesis is held on by the knee liner-like knee sleeve (the knee sleeve spans from the outside to the socket, to high up on the thigh, creating an airtight chamber). This is not a secure attachment, and users generally have a poor fit when the socket is only held on by the knee sleeve.

The data collected on the INTRAY sensors was able to observe this phenomenon. At the start of each of the walks directly following a don, the user had large amounts of limb-socket motion that quickly subsided as the negative pressure was reestablished through forcing air out of the one-way expulsion valve. The movement seen at the begging of these walking bout was large, but still less than the movement of the limb during the 5-ply walk.

A plausible explanation for the marked increase in motion of the limb during the 5-ply walk is that the negative pressure within the socket was never able to be established. This was likely because the additional sock ply acted as an air-wick, allowing for pressure equalization between the inside and outside of the socket. This suggests that for this participant, at 5-ply socks, the suspension system no longer functioned properly. The concern with this knowledge is that there can be an upper limit to how much a user may be able to accommodate socket fit with sock ply before rendering the suction suspension useless. Participant Four needed to move from a 2-ply to a 4-ply sock fit within two hours to maintain a comfortable socket fit, and this data suggests that they were at the limit of socket fit accommodation in a very short amount of usage time.

It is known clinically that pinless suspensions can be finicky to implement due to issues such as this. Prosthetists know that a pinless suspension socket requires a very good socket shape and fit so that the user does not need to wear many sockets to accommodate the extra socket volume, and thus some clinicians have unwritten criteria for which users would make good pinless candidates. Data observed in from this participants exemplifies that a tool like the INTRAY sensors could be used to diagnose patient-specific sock ply usage protocols so that a larger population of users can be candidates for pinless suspension types.

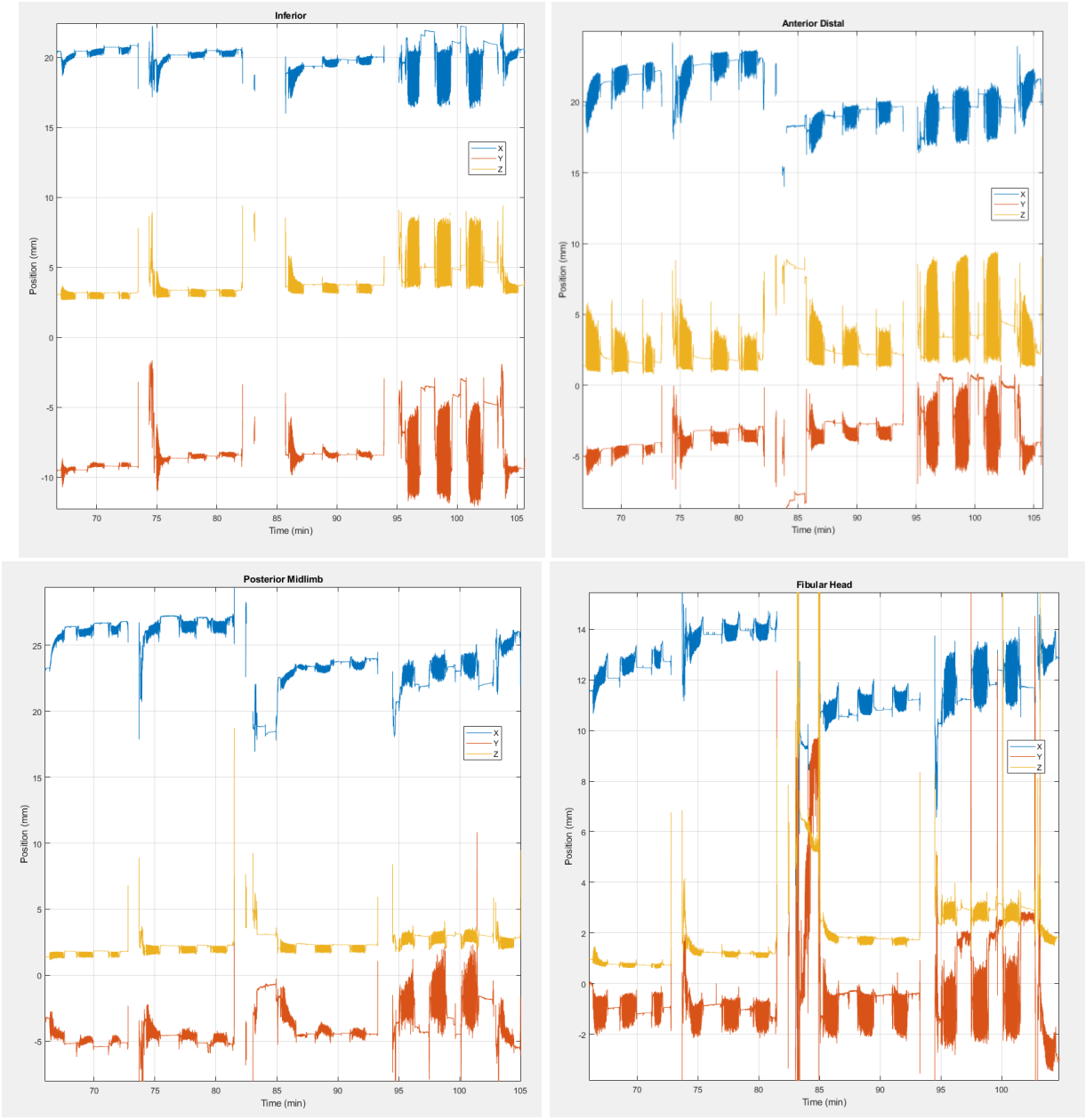

Figure 52: *Sock ply experimental conditions for Participant Four. Walk bouts are in sets of three (except for the last walking bout, which had one) and correspond to 2-ply, 3-ply, 4-ply, 5-ply, and 4-ply, respectively. INTRAY sensors are (a) Inferior, (b) Anterior Distal, (c) Posterior Midlimb, and (d) Fibular Head.*

Following the sock ply conditions the user was wearing 4-ply socks as their new Neutral fit. Also, the volunteer stated that their limb was becoming “angrier” and thus only one one-minute walk was conducted in the remining experimental conditions.1.5g petroleum jelly was added to the limb and then cleaned, and the participant reported a Socket Comfort Score of 7 for both conditions, though the protocol was reduced for the limb being in pain. The participant also suggested that there was “marginally less friction because of petroleum jelly.”

Figure 53 shows the limb motion collected during this protocol. It seemed that the residual limb largely maintained limb-socket motions compared to the Neutral fit, though the Anterior Distal showed slightly more pistoning with petroleum jelly on the limb. The data also suggests that the liner was donned with various rotations along the limb. The Anterior-Posterior pitch can be observed in the Y-axis of the Anterior Distal, Inferior, and Posterior Midlimb sensor. The Y-axis of the Anterior Distal and Inferior showed the same direction of target displacement, while the Posterior Midlimb showed and opposite and equal offset. The rotational yaw can be observed in the X-axes of the Anterior Distal, Posterior Midlimb, and Fibular head, exhibited by the global X- offsets. Lastly the Medial-Lateral roll can be observed in the X-axis of the Inferior sensor, exhibited by the positional offset.

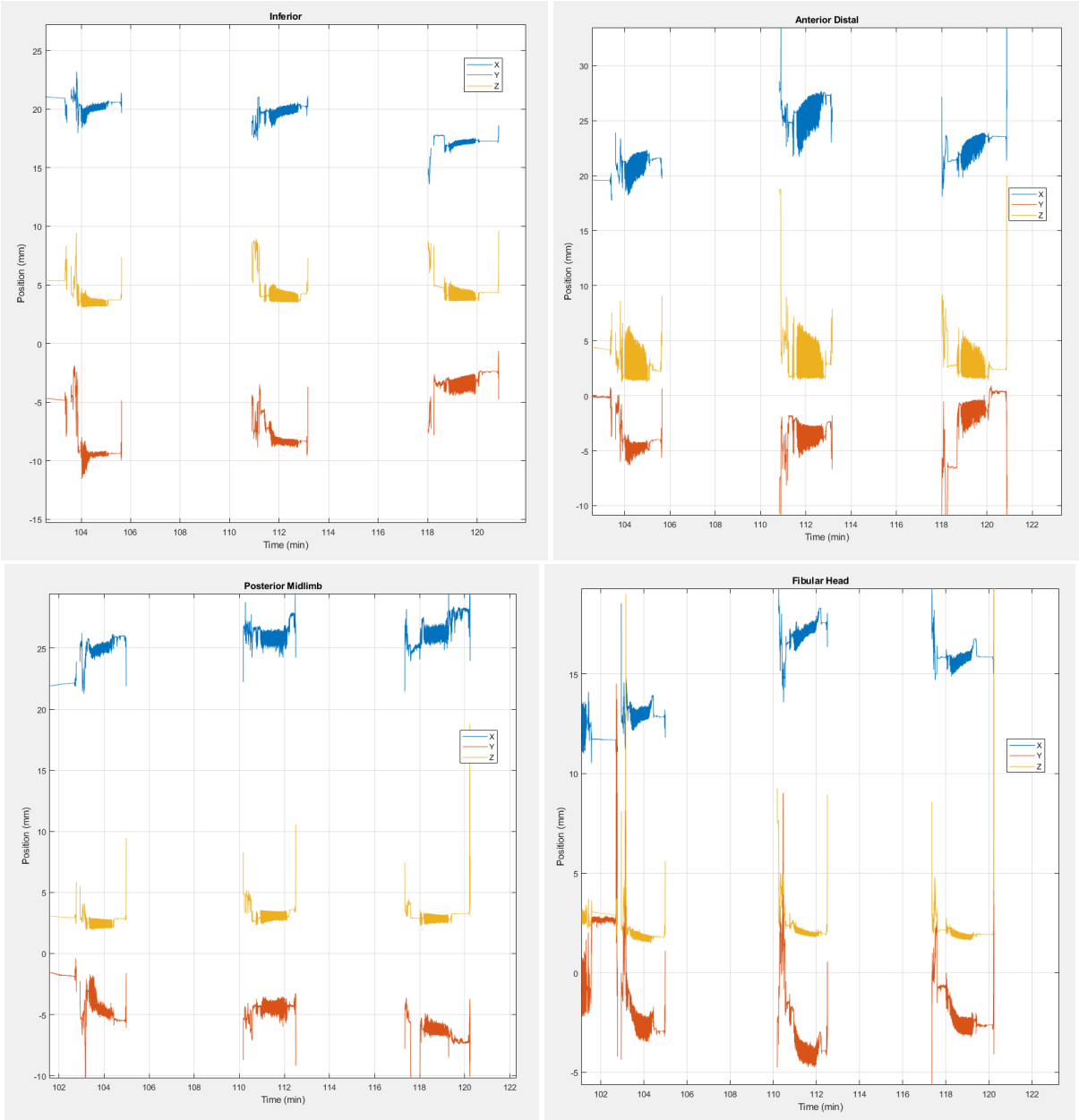

Figure 53: *Petroleum jelly and Cleaned experimental conditions for Participant Four. Walk bouts only have one walk because of socket comfort and correspond to Neutral 3, petroleum jelly, and Cleaned, respectively.*

In each condition a 4-pky sock was worn. INTRAY sensors are (a) Inferior, (b) Anterior Distal, (c) Posterior Midlimb, and (d) Fibular Head.

4.1.5 Participant Five

Participant Five is a right legged prosthesis user, male, K4, suction suspension, 6-ply Neutral fit sock accommodation, 108.0kg, 178cm tall, 62y old, 5y and 7mo since amputation, 10 hrs/day usages, PTB socket design, 16cm residual limb, and received an amputation due to a traumatic event. Figure 54 describes the participants limb shape. A liner was fabricated using the punch method. Balloon calibration, thermal calibration, data collection, and data processing were all conducted as described in Chapter 3.

Figure 54: *Participant Five's residual limb*

Participant Five completed the rotation protocol first by performing a toe-in don, followed by the toe-out don. As observed in Participant Four the inferior sensor a small offset in the X- and Y-axes were observed because the axis of limb-socket rotation was likely closer to the center of the TRAY, but not directly centered. Rather the global rotation was observed along the X-axis of the three other sensors.

Beyond observing the global rotational effect of the experiment, data was used to confirm multi-INTRAY motions. In the steps immediately following both rotational dons, it was seen that the limb settled into its stable position in the same manner. Focusing on the Anterior Distal, Inferior, and Posterior Midlimb sensors there are many orthogonal axes that can be considered together (Figure 55). Particularly, the Y-axis of the Inferior sensor can be related to the Y-axis of the Anterior Distal and Posterior Midlimb sensors assuming that the residual limb is at least a semi-rigid body. The data from the settling shows that the limb moved distally at the Anterior Distal site, posteriorly at the Inferior site, and proximally at the Posterior Midlimb site (Figure 56). This motion has been considered as the Anterior-Posterior pitch when a liner was doffer and re-donned, and had not yet been a limb motion observed in the socket.

Interestingly, when the settling observed in the Y-axis of the Fibular Head sensor was compared to the X-axis of the Inferior sensor, this multi-sensor relationship was not observed. The Fibular Head site suggested that the limb traveled proximally, while the Inferior sensor did not suggest any Medial-Lateral roll, the position remined constant. It is hypothesized that a complex settling limb-socket motion occurs due to the semi-rigid body nature of the limb. It is plausible that soft tissue can be pushed proximally while the distal end of the limb experiences a different effect. It should also be remembered that this was a pinless suspension socket user and the limb-socket motion can be affected by low amounts of negative pressure at the start of a walk immediately following a don. Though it is affected, in this case the limb socket motion seems to accentuated.

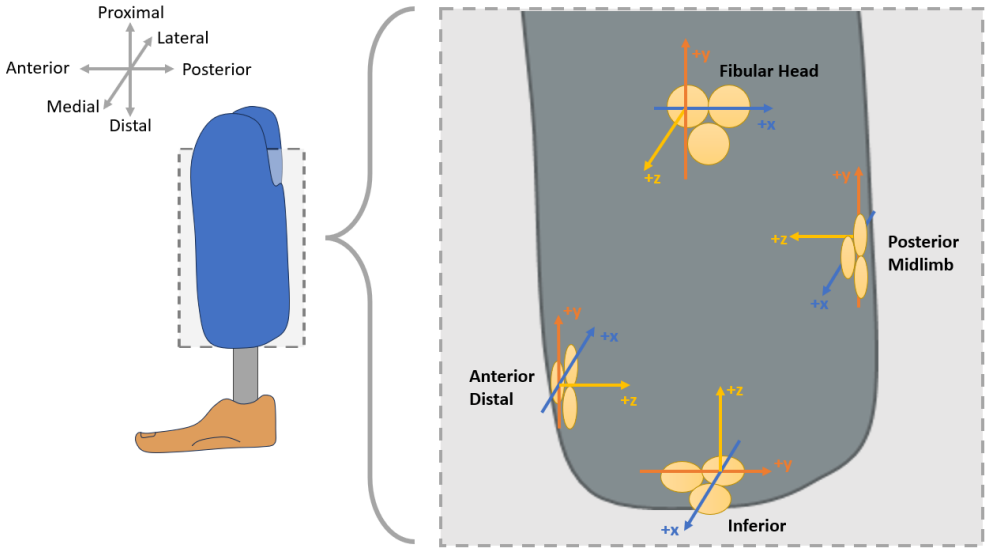

Figure 55: *Diagram illustrating the relative alignment of the INTRAY sensors' axes inside of the socket for a right legged amputee. Blow up image is intended to be a cross-section of the socket, with the common INTRAY sensor placement locations. The origin of each coordinate system is found at the center of the top-left individual sensor.*

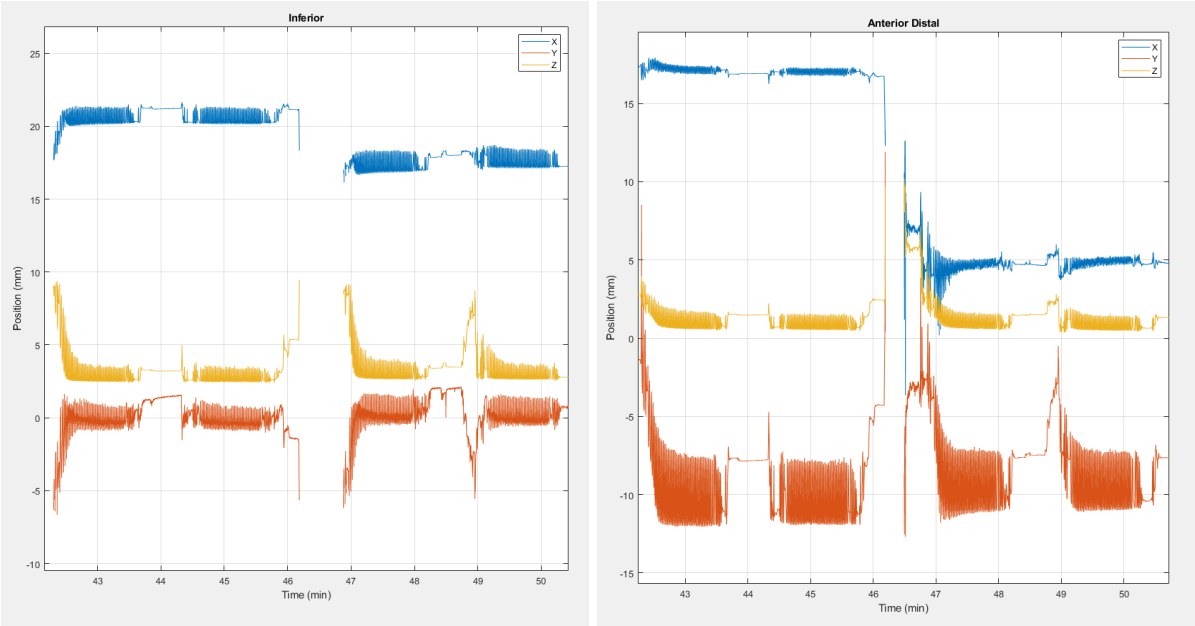

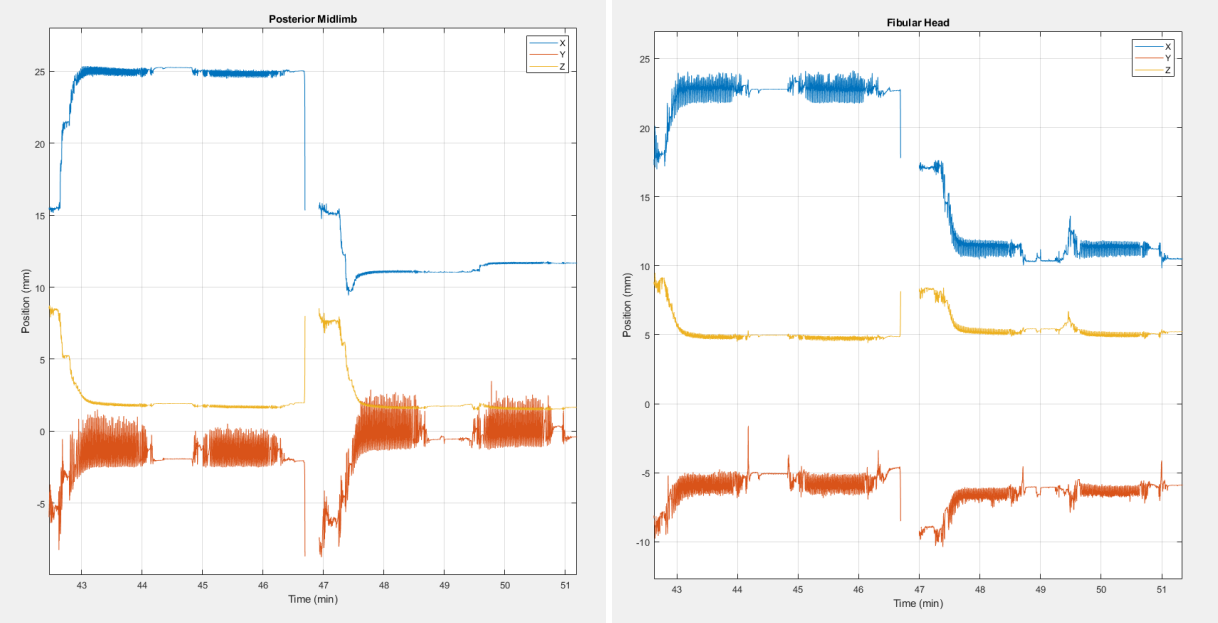

Figure 56: *Rotational experimental conditions for Participant Five. Walk bouts one and two are toe-in, and walk bouts three and four are toe-out rotation. INTRAY sensors are (a) Inferior, (b) Anterior Distal, (c) Posterior Midlimb, and (d) Fibular Head.*

Following the rotational conditions, sock ply was altered in a randomized fashion. The participant wore 3-ply, 4-ply, 2-ply, 5-ply, and 3-ply socks chronologically. As observed for the prior participants, the Z-axis data of all four INTRAY sites suggests that the liner was separated at distances relating to the thickness of sock ply worn (Figure 57).

For this participant it was observed to have less obvious step sizes in separation compared to the pin suspension system. Instinctively, this could be described by the vacuum suspension method, where the vacuum pressure between the socket and liner could remove excess air trapped in the sock weave, and compress the socks more than when being observed with the pin suspension, but this is conjecture. Another factor that could be the case is that the socks were stacked on one another (ie a 2-ply sock is not the same thickness as 2, 1-ply socks), but the granularity of sock usage was unfortunately not recorded.

Over the course of the experiment the user had a Socket Comfort Score of 7 and reported that the 4- and 5-ply condition felt “too snug”, while for the 2-ply condition the limb was “going deeper into the socket”. The INTRAY data was able to corroborate the limb going deeper during the 2-ply walking bouts, but the remaining walking bouts did not show a significant change in limb motion that might describe the limb being too snug or tight.

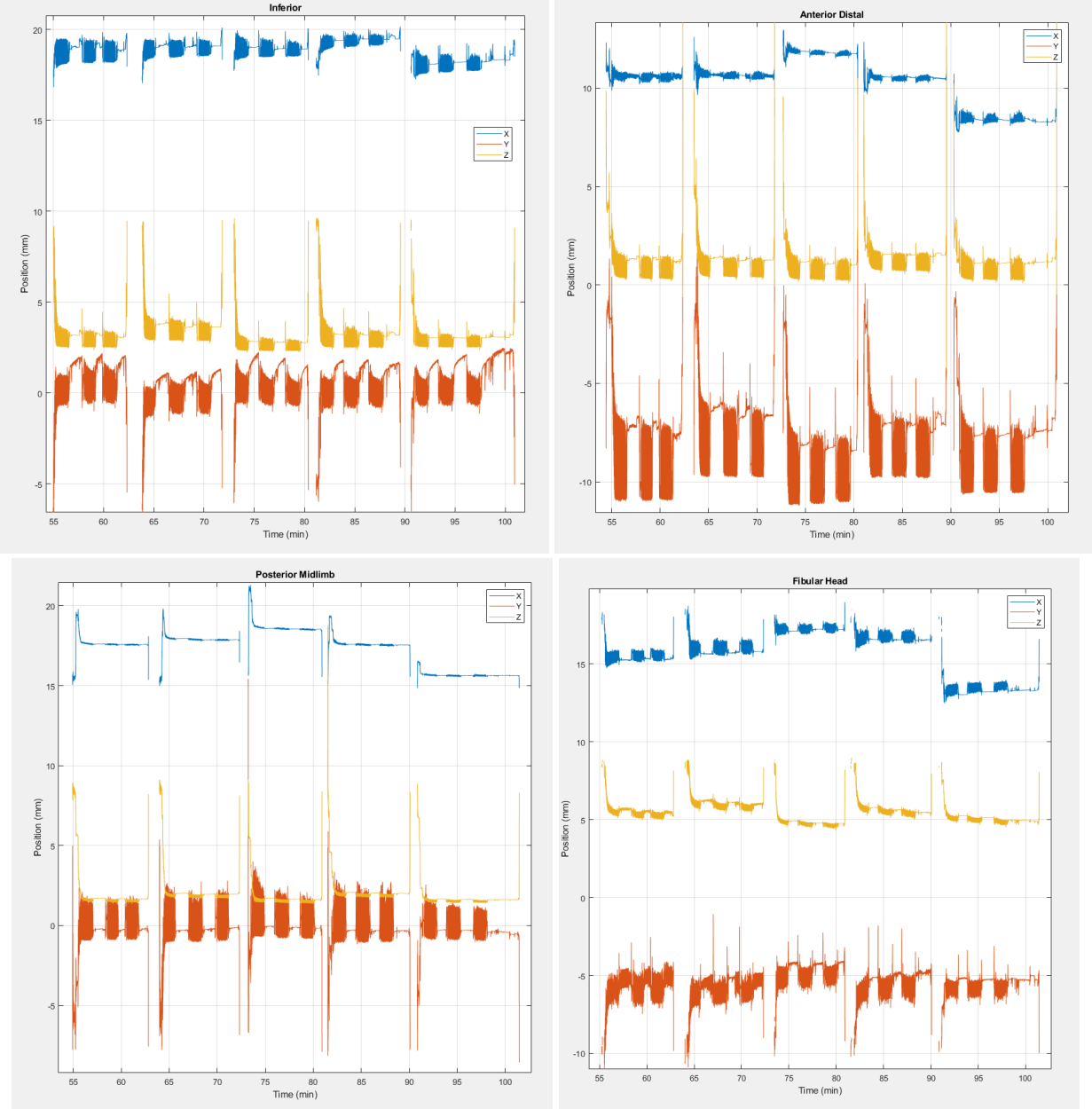

Figure 57: *Sock ply experimental conditions for Participant Five. Walk bouts are in sets of three and correspond to 3-ply, 4-ply, 2-ply, 5-ply, and 3-ply, respectively. INTRAY sensors are (a) Inferior, (b) Anterior Distal, (c) Posterior Midlimb, and (d) Fibular Head.*

Lastly, 1.5g petroleum jelly was added to the participant's residual limb, and clean as done with the prior participants. The recorded Socket Comfort Score was an 8 across the entire petroleum jelly experiment. During the second walk the participant felt their limb moving in the liner, though it was not visually apparent that the limb-socket movement decreased (Figure 58). Global target shifts because of liner misalignment were observed both in a yaw and pitch fashion. Looking along the Coronal Plane (roll), it was seen that there was again poor agreeance between the Inferior and Fibular Head sensor, but still unclear why.

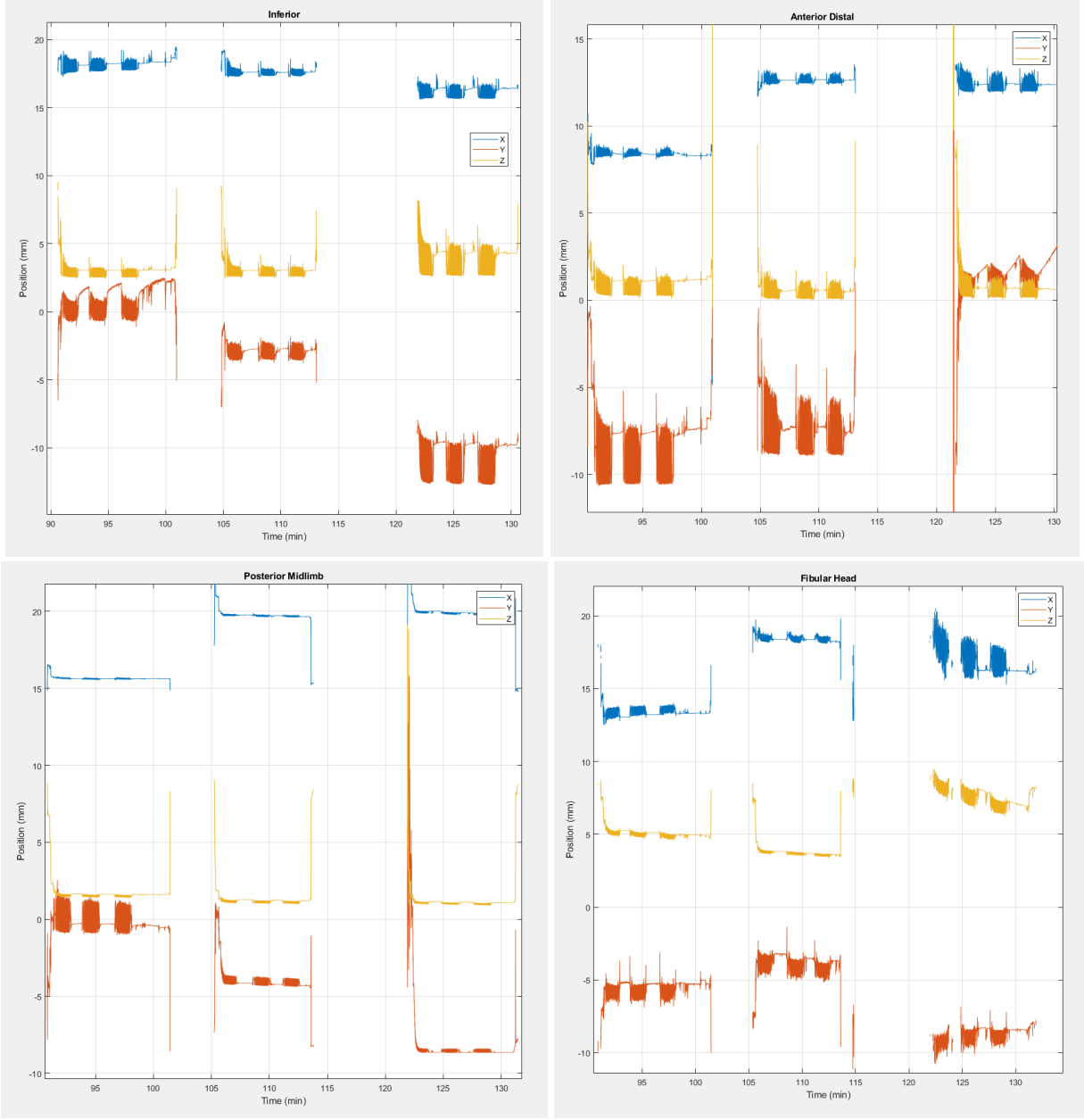

Figure 58: *Petroleum jelly and Cleaned experimental conditions for Participant Five. Walks are in sets of three and correspond to Neutral 3, petroleum jelly, and Cleaned, respectively. INTRAY sensors are (a) Inferior, (b) Anterior Distal, (c) Posterior Midlimb, and (d) Fibular Head.*

4.1.6 Participant Six

Participant Six is a left legged prosthesis user, male, K3, locking pin, 0ply Neutral fit sock usage, 102.9kg, 183cm tall, 59y old, 1y and 0mo since amputation, 13 hrs/day usage, PTB socket design, 16cm residual limb, and received an amputation due to dysvascular and infectious reasons. Figure 59 shows their limb anatomy.

Participant Six was excluded from this investigation because they were not able to wear the research socket comfortably (decided by the research prosthetist). An inclusion criterion of this study was that the participant needed a well-fitting, practitioner-prescribed socket, which though the participant attested his socket to be so, it was not vindicated when observing the participant's interaction with the investigational and practitioner-prescribed sockets. In both visits there was clinical evidence that the investigational socket was poorly fitting – pressure concentrations causing discomfort, excess skin pallor after doffing, and the participant was not able to reliably don the socket so that the pin in the distal end engaged with the lock body so that the socket was safe to walk on. Though there was emphasis to fit the investigational socket, it eventually became clear that the participants practitioner prescribed socket was also poorly fitting.

Figure 59: *Participant Six's residual limb*

An initial consideration was that the investigational socket was not duplicated properly. A process was completed (72) that allowed the shape of the scanned practitioner prescribed socket to be compared the shape of the newly fabricated investigational socket (Table 3).

Table 3: *Participant Six's Practitioner Prescribed versus Investigational Socket Shape Comparison Values*

Sockets Compared	% Volume Difference	% Radii within +/- 1 mm	Min. Radial Error (mm)	Max Radial Error (mm)	St. Dev Radial Error (mm)
Practitioner vs. Investigational	0.269	94.5	-3.68	6.52	0.129

It was seen that there was a 0.269% difference in socket volumes between the practitioner prescribed socket and the newly fabricated investigational socket. It has been considered that a minimum of 1% change in socket volume can be perceptible by the user of the prosthesis, so the difference in volume should have been too small to notice. Additionally, 94.5% of the socket was within 1mm of error, suggesting that the shape of the socket was very similar to the practitioner prescribed. Though the minimum and maximal radial error seemed large, these were generally found at the Brimline, where there was leeway for the fabricator to flare the brimline and trim it appropriately, and at the distal end, where lock body componentry was differing. Overall the mean radial error was less than one millimeter (0.13mm), suggesting that the investigational socket was a proper duplicate of the practitioner prescribed socket (Figure 60).

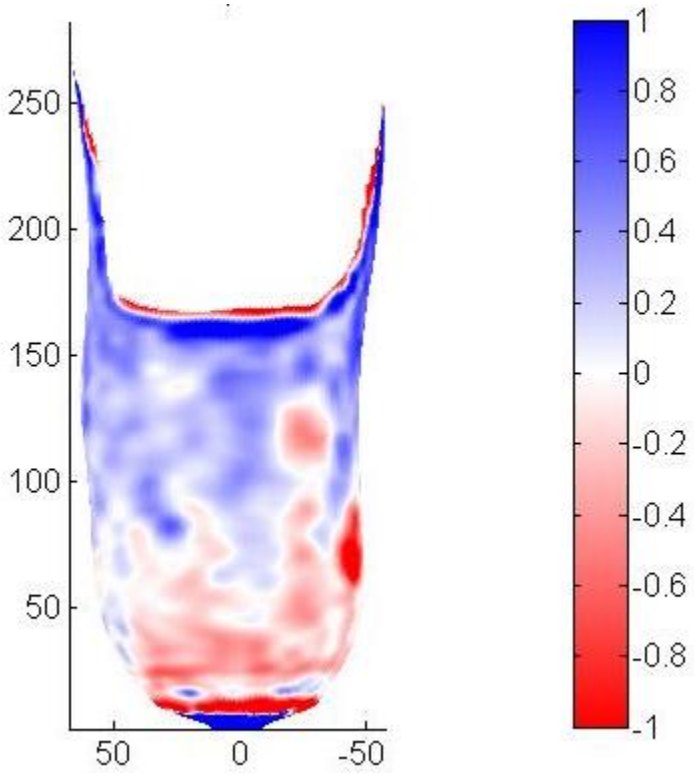

Figure 60: *Heatmap of Participant Six's socket shape differences. Base shape is the practitioner prescribed socket, while investigational socket shape is distinguished by color differences. 94.5% of the sockets were within 1mm of the other.*

Extending on this, and to show a perspective on the intricacies of lower limb prosthetic fit, there were additional modifications made to the investigational prosthesis that may have influenced Participant Six's ability to meet inclusion criteria.

The first change made from the practitioner prescribed socket to the investigational socket is the removal of the flexible inner liner. Figure 61 illustrates the difference between the practitioner prescribed socket and the investigational socket. The brimline of the investigational socket was rigid and modeled after the brimline-profile of the flexible inner liner. Though the socket shape was captured by the investigational socket, the flexibility of the upper brimline was not. On the practitioner prescribed socket the rigid brimline was at times 10mm below the brimline-profile of the flexible inner. As the name suggests, the point of the flexible inner liner is to flex as the user walks on the socket, and it is possible that the limb creates more volume accessible for the proximal regions of the limb making the fit better in the traditional socket versus the investigational.

Furthermore, there was leeway on how the brimline was cut as the fabricator built the socket. As alluded to in the socket shape comparison, the brimlines had larger amounts of shape error than the body of the socket. Visually inspecting the sockets, seen in Figure 61 (though the image perspective may not be consistent), the brimline contours may have been different enough to cause a socket fitting issue. In the method used to duplicate sockets, flexible inner brimlines have been challenging to reproduce and efforts were taken to accurately capture the shape of the traditional socket's brimline.

Figure 61: *(a) Practitioner prescribed socket with flexible inner liner (white). (b) Investigational socket with the Patellar Tendon and Fibular Head INTRAY sensors visible. No flexible inner liner is in the investigational socket, and the brimline differences can be seen visually even though the two images were captures at different angles.*

The second change from the practitioner prescribed socket to the investigational socket was the umbrella size on the distal aspect of the liner. Participant Six's practitioner prescribed liner had an umbrella that was significantly smaller the investigational liner (Figure 62). Wearing a liner with nearly double the diameter of the umbrella may have influenced the interaction of the distal limb with the socket compared to the traditional liner with a smaller sized umbrella. In this investigation, it was presumed that the width of the umbrella may have caused an issue with the limb fitting in the socket and thus a duplicate of the practitioner prescribed liner was ordered. Attempts to perform the punch method liner fabrication were made, but the gel component of the WillowWood Alpha Hybrid did not adhere to the silicone glue used, and thus an investigational liner that duplicated the umbrella size could not be fabricated.

Figure 62: *(left) Punch method investigational liner, (middle) new off the shelf liner that matched the practitioner prescribed liner, and (right) practitioner prescribed liner. Umbrella (plastic casing on the inferior edge) diameters are different between the investigational and practitioner prescribed liners.*

A third aspect that differed between the practitioner prescribed and investigational prosthesis was the liner profile. Participant Six traditionally wore a WillowWood locking liner with Alpha Hybrid elastomer and a uniform 6mm thickness. The investigational liner worn by the user, because the liner duplicate could not be fabricated with the punch method, was a WillowWood locking liner Alpha Silicone elastomer with a progressive shape. Figure 63 was adapted from WillowWood to describe the change in shape and how much volume the two liners occupied in the socket. In short, the investigational liner occupied more volume within the socket than the practitioner prescribed liner because of the progressive shape along the anterior distal portion. At times there was up to 3mm offset between these two liner types, which is significantly larger than the socket duplication shape error. The change in liner profile was considered to have changed the hydrostatic volume of the limb and liner together, making the investigational socket a poor fit.

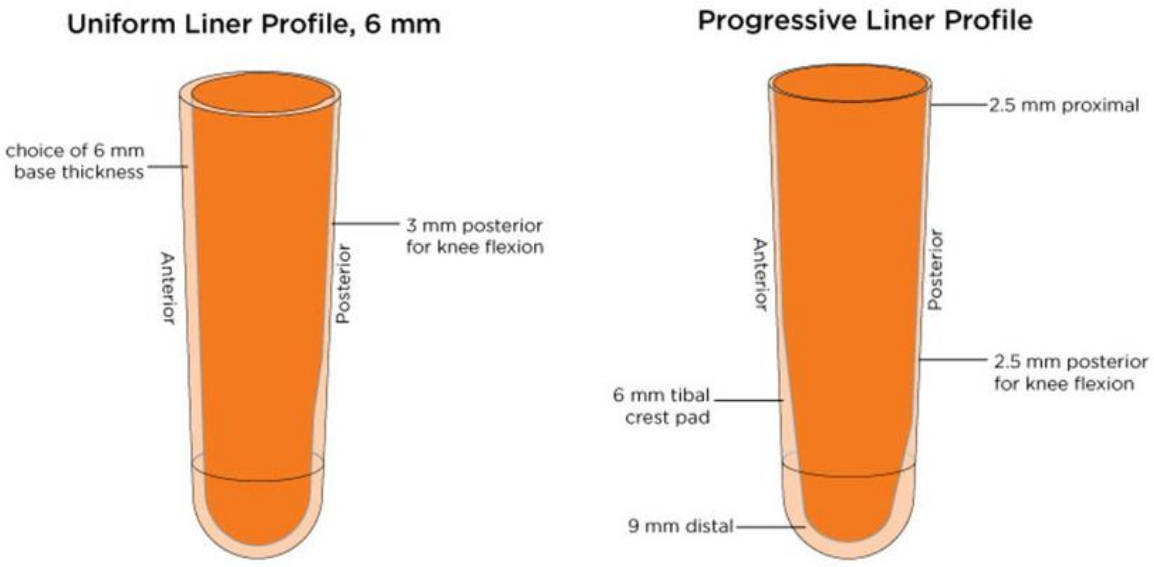

Figure 63: *Liner material profile for (left) a uniform and (right) progressive liner type. Various liner thicknesses change the remaining socket volume available for the residual limb. Adapted from WillowWood (73).*

Another consideration was that this participant was a relatively new user compared to the rest of the cohort in this investigation. It is known that new amputees' residuum will shrink drastically over the first year after surgery. Participant Six was exactly one year post surgery while on this study. It is possible that the practitioner prescribed socket was made so that it could accommodate the atrophy that happens in the first year after amputation, making the socket shape smaller to start with. This suggests that there may have been an element of a poor clinically fitting practitioner prescribed socket, and that the investigational socket was predisposed to be poorly fitting. An additional indication of this was the significant gap from the end of the flexible inner liner to the lock body housing in the distal end of the socket (Figure 64). It was clear that this gap was creating a mark on the user's residual limb and that there were opportunities to improve the fit of the practitioner prescribed socket.

Figure 64: *(a) Participant Six's residual limb showing discoloring on the interior edge that matches the (b) flexible inner liner gap at the distal end of the practitioner prescribed socket.*

Participant Six was a great example of the difficulties with fitting lower-extremity prosthetics within the years after surgery. Likely what happened, and is not uncommon for new users, was that the volunteer did not know they had a poorly fitting socket because they did not have a frame of reference for what a well-fitting socket is like. In the first study visit the user was struggling to don their traditional socket but had associated it to the salty diet they had the prior day. This issue persisted to the second study visit when they tried to wear the investigational socket, and at that point the research clinician was able to better gauge the fit of each socket. The participant remained optimistic that the practitioner prescribed socket was well fitting, but did not have the resources to acknowledge the socket fit could be improved.

Ultimately, there was evidence that the practitioner prescribed socket was not well fitting. This evidence was not abundantly clear when fabricating the investigational socket, but once identified, the participant was excluded from the study.

4.1.7 Participant Seven

Participant Seven is a left legged prosthesis user, male, K3, suction suspension, 0-ply Neutral fit sock usage, 151kg, 185cm tall, 62y old, 11y and 9mo since amputation, 16 hrs/day socket usage, TSB socket design, 20.5cm residual limb, and had their amputation due to a traumatic event. Figure 65 shows Participant Seven's residual limb. A liner was fabricated using the punch method. Balloon calibration, thermal calibration, data collection, and data processing were all conducted as described in Chapter 3. Data from the Fibular Head sensor suggested that the target was misaligned with the sensor and data was not recorded from that sensor.

Figure 65: *Participant Seven's residual limb*

The toe-out and toe-in rotational conditions showed equal and opposite global X-axis offsets in the Anterior Dital and Posterior Midlimb sensors, similar to what was seen in other participants. Neither the Anterior Distal nor Posterior Midlimb sensors rotated back into the Neutral line of alignment (Figure 66). The Inferior sensor did not illustrate a drastic offset. The participant was readily able to dictate that the socket seemed "stuck" in both of the rotated positions and that it felt like "the limb wants to rotate back but cannot," which was established in the INTRAY data. Furthermore, during the second experimental condition (toe-in), the participant felt that the socket was "tighter proximally, by the knee," "tighter in the distal tibia", and their limb was "deeper in the bottom" of his socket.

Visually in the X- and Z- axes of the Anterior Distal site it was seen that the maxima to minimum oscillations are diminished in the second experimental condition (toe-in), possibly suggesting that the limb had restriction motion compared to the previous experimental condition, corroborating the feedback that the participant's limb felt "tighter in the socket". In the Y-axis Anterior Distal data it was seen that the limb was more distal in the socket during the second experimental condition (toe-in) by about 1mm, possibly also corroborating the sensation the participant was "in the bottom" of the socket.

This observation can be made more complex when the Posterior Midlimb site data is considered. During the second condition (toe-in), the Posterior Midlimb site has more X- and Y-axes maximum-to-minimum movement, suggesting that the limb was less restricted. Simultaneously, the Y-axis showed that the Posterior Midlimb was raised proximally. This suggests that the limb may have angled slightly in the Anterior-Posterior plane (pitch), while concurrently restricting Anterior Distal motion and allowing more Posterior Midlimb motion. It is plausible that the data correctly illustrated the limb-socket interaction, but the participant simplified the sensation so that they could clearly articulate the problem with the new fit in the socket. Further studies, correlating these fit perturbations would dramatically improve the efficacy of translating the INTRAY sensor data into the clinic.

Moreover, the volunteer stated that their Socket Comfort Scores were worsening from Neutral, to toe-out, to toe-in, 7 to 6 to 5, respectively. This is a large shift in socket comfort, and it is reassuring that the INTRAY data can corroborate participant feedback as socket comfort is changing. Again, studies relating socket comfort perturbations to the INTRAY data are imperative to translate this tool into the clinic.

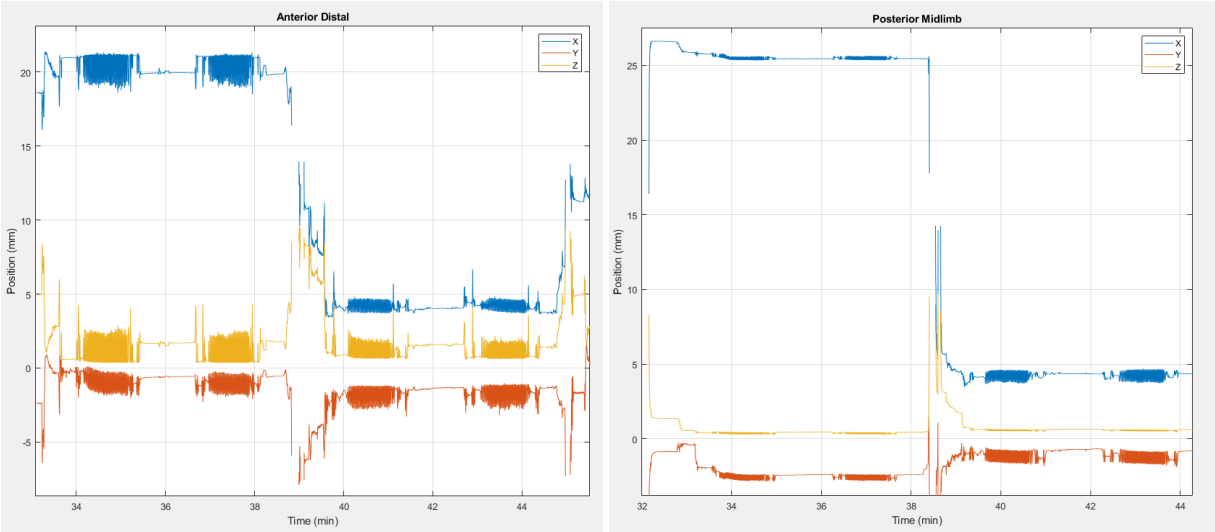

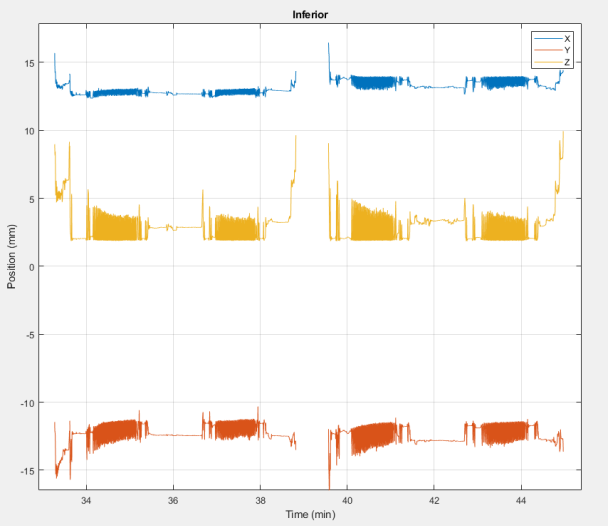

Figure 66: *Rotational experimental conditions for Participant Seven. Walk bouts one and two are toe-out, and walk bouts three and four are toe-in rotation. INTRAY sensors are (a) Anterior Distal, (b) Posterior Midlimb, and (c) Inferior.*

The sock ply experimental conditions for Participant Seven resulted in data that upheld prior study participants observations. The Z-axis channel of all sensors recorded changes that corresponded with adding and removing sock ply (Figure 67).

While performing the sock ply experimental conditions, it was apparent that the fabrication of the liner was not sufficient for prolonged wear. The inferior target-punch was causing indentations on the residual limb and as a result, the protocol was shortened to reduce the chances of causing a stress injury. Upon noticing that the liner was problematic for the participant, the liner was doffed and donned with some rotation on the limb following the first Neutral sock ply walk. As a result of this, the data exemplified a global shift in the position data as described before. The protocol was then truncated, and the volunteer was asked to perform only one walk in each of the remaining experimental conditions.

A notable observation was that the participant felt that their limb was “on the bottom of the socket” during the +1-ply walk. It is conceivable that the limb was deeper along the Y-axis of the Anterior Distal sensor, but that analysis is confounded by the liner misalignment on the limb. Anterior-Posterior angulation (pitch) is observed in the data due to the liner-limb misalignment, but the magnitude of the distal offset in the Anterior Distal site is larger than in the Posterior Midlimb, possibly suggesting that there was downward limb displacement at the Anterior Distal site in addition to the limb-liner misalignment. Contrary to the participant’s attestations, the Z-axis of the Inferior sensor displayed that the limb was not at its global minimum throughout the session.

A second notable observation was that the participant “felt very stuffed in the socket, with more pressure proximally and laterally, and less pressure distally” during the +2-ply condition. It was not visually apparent that any of the INTRAY data supported this sensation.

It is also reasonable that with the limb-liner misalignment the targets became misaligned with the sensors and the data observed had increased error.

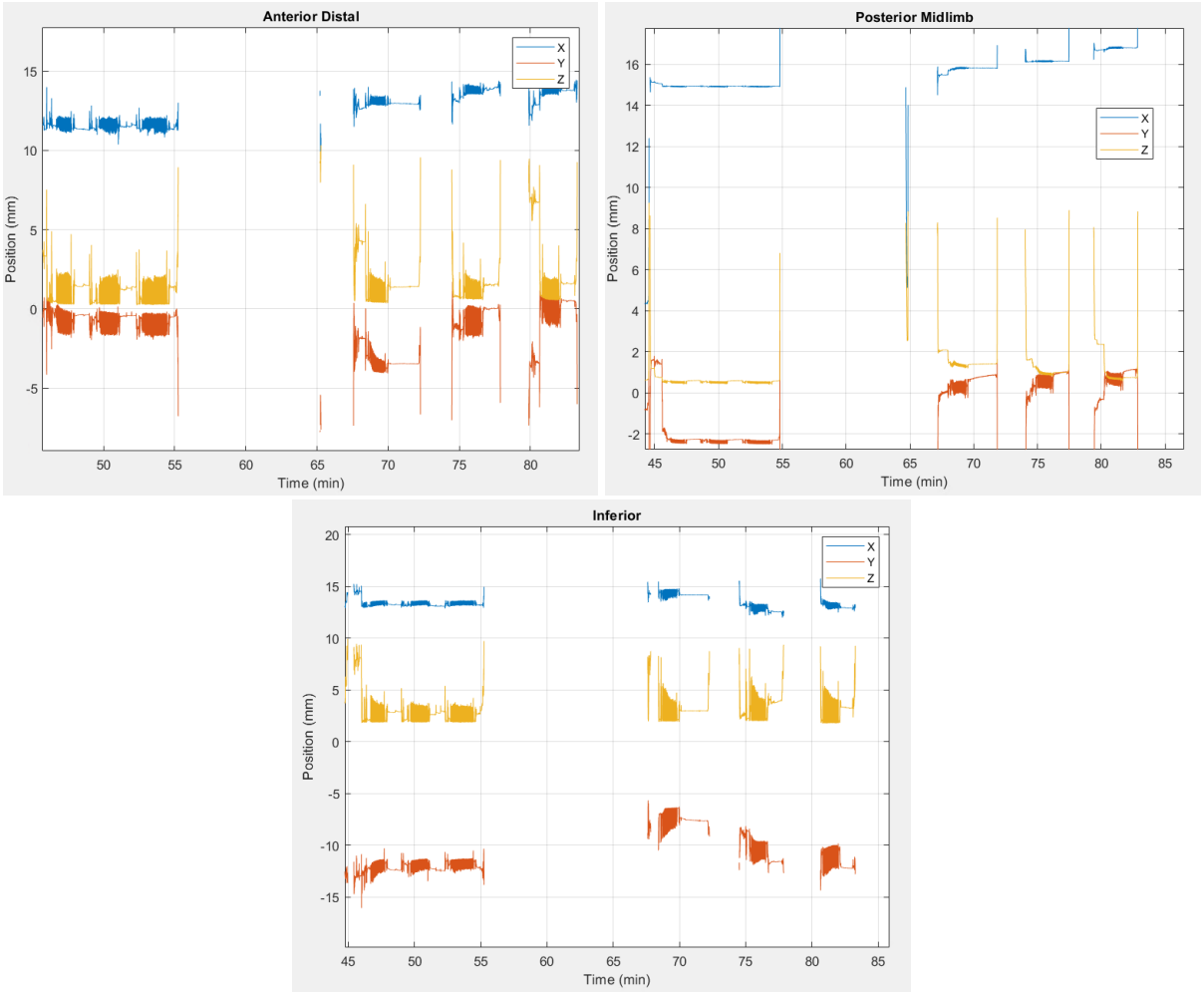

Figure 67: *Sock ply experimental conditions for Participant Seven. The first walk bout is in a set of three, while the other three only have one set of walking and correspond to 0-ply, 1-ply, 2-ply, and 0-ply, respectively. Between the first set of walks and second the liner was removed to check the participants skin integrity. INTRAY sensors (a) Anterior Distal, (b) Posterior Midlimb, and (c) Inferior.*

Lastly 1.8g of petroleum jelly was added directly to the participant's residual limb and later cleaned with soap and water. The participant did not suggest a change in SCS during the three conditions (it remained at 7), but did notice "pistoning more during heel loading," and that it felt like, "the limb was too sweaty" during the petroleum jelly condition walk.

The position data at the distal sites in the socket suggested that during the first half of walking with petroleum jelly on the limb there was a drastic amount of "settling" happening (Figure 68). In the Anterior Distal site it can be seen that the limb was traveling deeper into the socket, while the inferior site simultaneously suggested that the limb was moving posteriorly (positive in the Y-axis for the inferior sensor is the posterior direction). Two plausible phenomena could be happening. Firstly, the limb and liner could be settling in the socket due to a complex interaction of Petroleum jelly, limb fluid volume, and orientation of socket donning. Or secondly, this could be an artifact of the liner slipping on the residual limb due to the reduced friction between the silicone liner and skin. This would mean that the orientation of the limb

anatomy may be in the same position relative to the prosthesis, but the interface to the limb and prosthesis is moving, and the data observed is the drift of the liner about the limb.

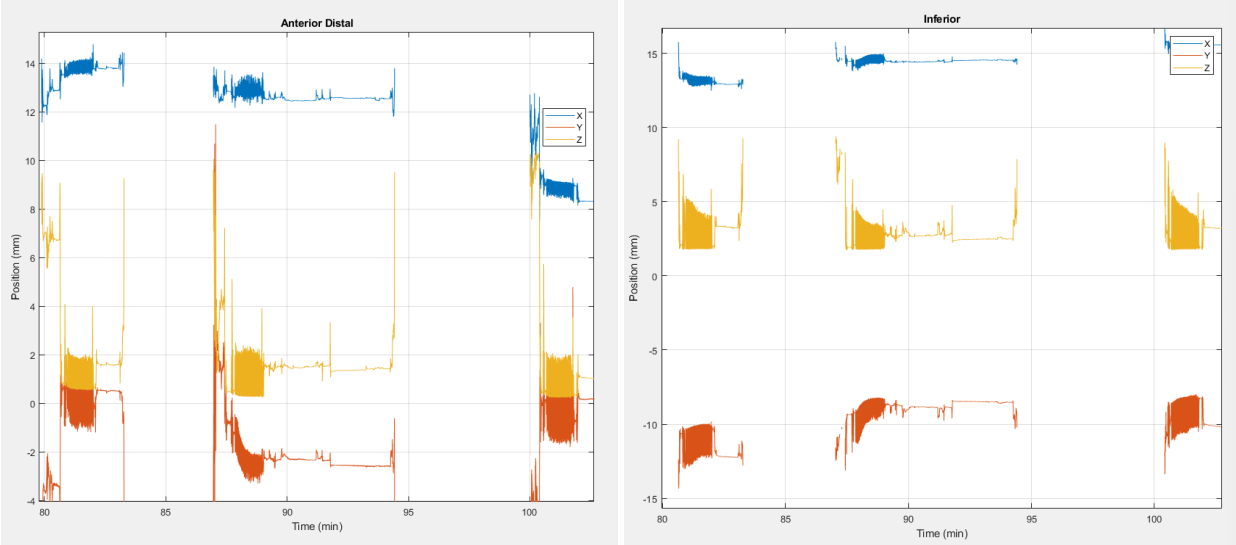

Figure 68: *Petroleum jelly and Cleaned experimental conditions for Participant Seven. Walks are in sets of one in order to not aggravate the distal end of the participant's residual limb and correspond to Neutral 3, petroleum jelly, and Cleaned, respectively. INTRAY sensors are (a) Anterior Distal, and (b) Inferior.*

4.1.8 Participant Eight

Participant Eight is a right legged prosthesis user, male, K3, locking pin suspension, 5-ply Neutral fit sock usage, 78kg, 176cm tall, 49y old, 11y and 0mo since amputation, 16 hrs/day socket usage, TSB socket design, 12.5cm residual limb, and had their amputation due to infection. Figure 69 shows Participant Eight's residual limb. A liner was fabricated using the glue-on method. Balloon calibration, thermal calibration, data collection, and data processing were all conducted as described in Chapter 3. Data from the Medial Femoral Condyle sensor suggested that the target was misaligned with the sensor and data was not recorded from that sensor.

Figure 69: *Participant Eight's residual limb*

As seen with the previous participants' rotational donned conditions, the laterality and orientation of rotation aligns with the positional displacement observed in the X-axis. Socket Comfort Score went from 8 to 6 to 7, for Neutral, toe-out, toe-in respectively. The participant was acutely aware that the socket was not aligned properly and felt pressure on the lateral knee and lateral tibia. They also noted that the "socket wanted to go to its normal spot with each step" but that it couldn't get there on its own, and that the newly created pressure points were "not letting the limb sink all the way" into the socket.

The position data supported the observation that the limb wanted to readjust within the socket with each step but couldn't fully realign. Global shifts in the X-axis with slow settling during each walk can be seen, but the limb never seemed to regain the Neutral position. Contrary to the participant stating that they were not sinking distally in the socket, we found that the sensors were not obviously shifted in the proximal direction. In fact, the participant remained at a constant pin click depth for the majority of the protocol.

As seen with previous participants' sock ply data, it was noticed that the Z-axis position data varied proportionally as sock ply varied. The X-axis channel did not exhibit any remarkable trends beyond slight changes in global limb rotation and proximal-distal position, while the Y-axis channel showed slight global changes in the limb height within the socket with different sock ply. Socket Comfort Scores were 8, 6, 7, 7 and 8, for the Neutral (5-ply), 7-ply, 6-ply, 4-ply, and Neutral conditions respectively. Notes recorded from the participants perception suggested that the primary change in socket fit was tighter with more ply of socks and looser with fewer.

2.2g of petroleum jelly was then applied to this participant's residual limb. A first walk was conducted where the participant didn't feel as if the liner was donned all the way, so it was then removed and put back on properly. Prior to the liner being corrected, the participant turned their head while walking on the treadmill and mis-stepped, almost causing them to fall. While catching their balance there was a single step where the prosthesis internally rotated as the toe was stationary on the rail of the treadmill and the heel continued travelling on the treadmill belt.

The data collected exhibited a spike for that individual step and was primarily observed during the swing phase directly following the weighted misstep. In the X-axis of the Anterior Distal and Fibular Head sites, the residual limb moved clockwise within the socket (more likely, it was rather that the socket had spun counterclockwise around the limb). In the Y-axis at the posterior midlimb site, the limb was more proximal than the surrounding steps. The fact that this was only a single spike suggests that the user was able to realign the prosthesis within the very next step after almost falling. There was an obvious rotation of the limb in the socket seen during swing phase, but the problem was able to self-correct rapidly.

In the subsequent walks with petroleum jelly, there was considerable X-axis settling at the beginning of each of the petroleum walks directly following a socket don. This was not observed in either the Neutral or Clean walks. Also, the position sensors at the Posterior Midlimb and Fibular Head sites suggested that the deepest the limb got in the socket (Y-axis) was during the walks with the petroleum jelly. This is thought to be an artifact of rolling the liner onto the liner with a different orientation, because the pin sensor data suggested that the deepest the participant got in the socket was during the final bout of walking in the Clean condition. Furthermore, in the pin sensor data, it can be seen that the participant sinks one click deeper into the socket on the 22nd step of the first Clean walk. This was the deepest the pin sinks in the socket and the Y-axis of position sensor sites corroborate the pin sinking one click (Figure 70). The distal movement is seen most drastically in the anterior distal sensor and least drastically in the fibular head sensor, which suggests a nonuniform offset across the sensors, possibly implying that the soft tissue of the limb may have elongated as it was allowed to travel deeper into the socket.

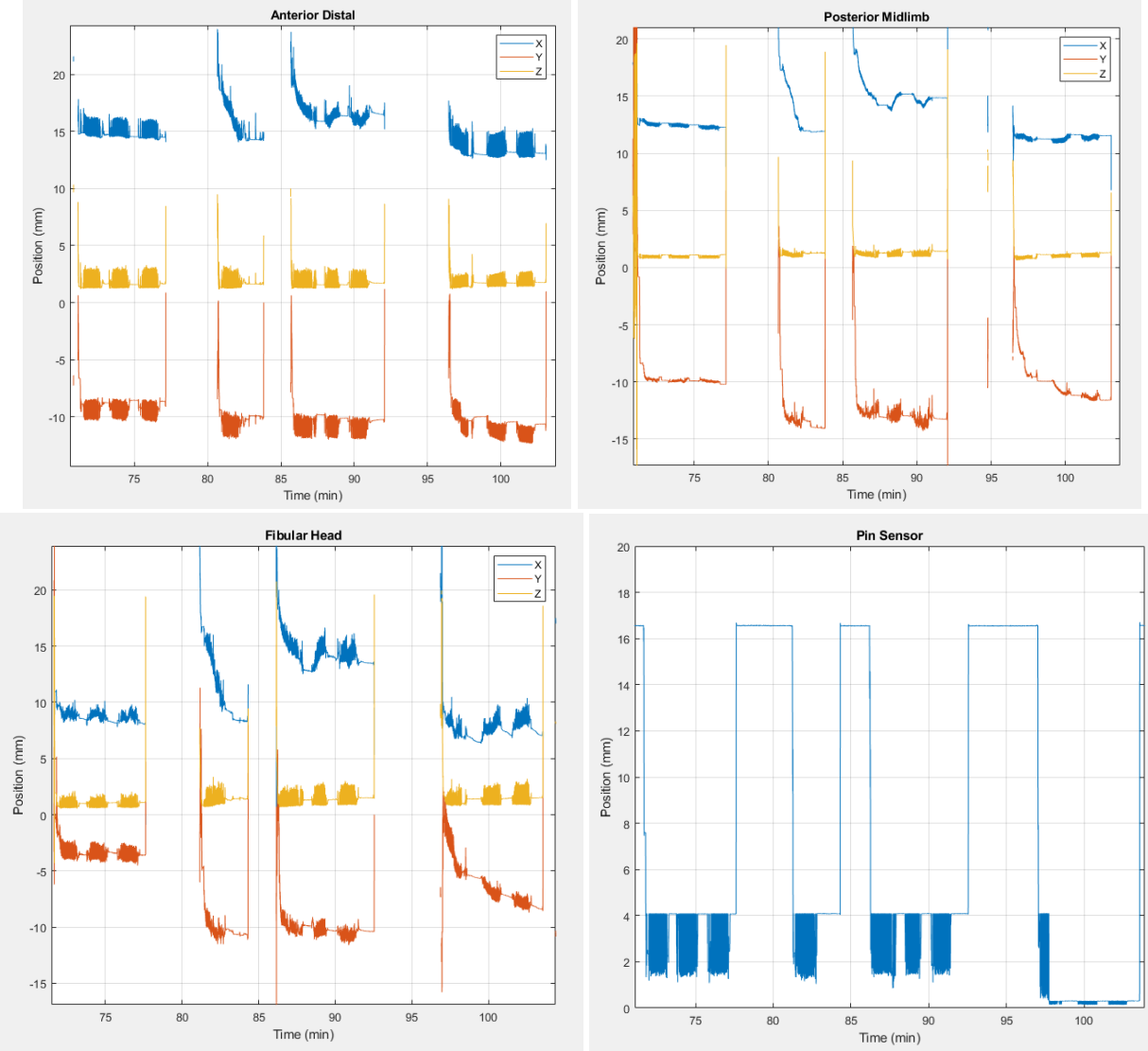

Figure 70: *Petroleum jelly and Cleaned experimental conditions for Participant Eight. Experimental condition walks are in sets of three and correspond to Neutral 3, petroleum jelly, and Cleaned, respectively. The one walking bout of one set was the walk with petroleum jelly where the participant felt as if the liner was not rolled onto the limb sufficiently. INTRAY sensors are (a) Anterior Distal, (b) Posterior Midlimb, and (c) Fibular Head. Data was also collected form the (d) Pin sensing system.*

4.1.9 Participant Nine

Participant Nine is a left legged prosthesis user, male, K3, suction suspension, 3-ply Neutral fit sock usage, 73.5kg, 180cm tall, 65y old, 10y and 3mo since amputation, 12 hrs/day socket usage, PTB socket design, 11.5cm residual limb, and had their amputation due to a traumatic event. Figure 71 shows Participant Nine's residual limb. A liner was fabricated using the glue-on method. Balloon calibration, thermal calibration, data collection, and data processing were all conducted as described in Chapter 3.

Figure 71: *Participant Nine's residual limb*

This volunteer performed a toe-out rotation followed by toe-in and global limb rotations along the X-axis were observed, as it was for the prior cohort (Figure 72). The participant also mentioned that there was no change in Socket Comfort Score across these conditions (remained at 10) and that they did not feel as if the socket was rotated. Interestingly, though the X-axis data showed an offset in the rotation of the limb, it was within the acceptable range of limb rotation on study. Later in the session, the limb was found to be rotated more within the socket, suggesting that the socket could have felt normal to the participant during the rotational conditions. Additionally, there seemed to be more maximum-to-minimum movement in the X- and Y-axes seen in the proximal sensors with the toe-in rotation, but less maximum-to-minimum movement in the distal sensors. Though this limb position maintained a comfortable socket fit, it is possible that the change of limb alignment in the socket created a different interface motion mechanism.

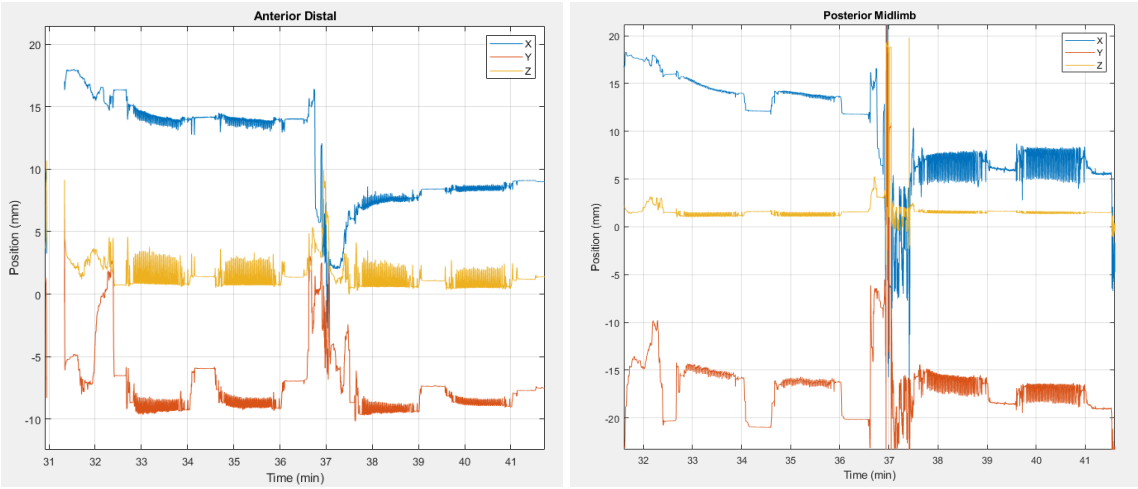

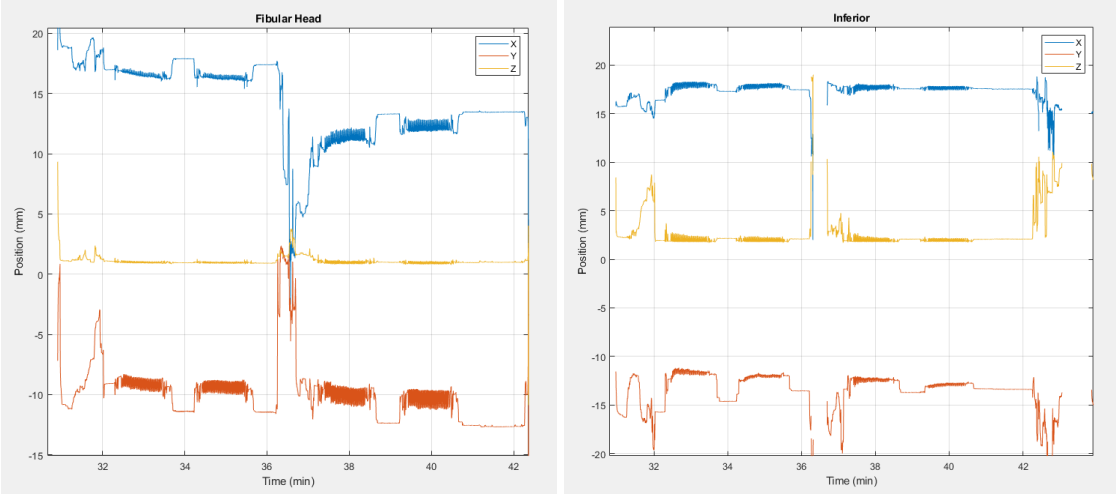

Figure 72: *Rotational experimental conditions for Participant Nine. Walk bouts one and two are toe-out, and walk bouts three and four are toe-in rotation. INTRAY sensors are (a) Anterior Distal, (b) Posterior Midlimb, (c) Fibular Head, and (d) Inferior.*

This participant had a Neutral socket fit with 3-ply worth of sock. The alterations in sock ply were 5-ply, 2-ply, 4-ply, and Neutral, chronologically. As for the other participants in the cohort, the Z-axis data was proportional to the number of socket ply being worn (Figure 73).

All sock ply maintained a Socket Comfort Score of 10, except for the 2-ply, in which the volunteer stated their SCS was a 4 and that they had “less control” of the socket. Midway through the 2-ply walking bout the participant needed to stop and proximally pull the suspension sleeve to fully cover the proximal edge of the liner and socks. Immediately after pulling up the sleeve, the magnitude of motion within the socket reduced. It is plausible that during the start of the 2-ply walk, there was not enough vacuum pressure to maintain a good connection from the limb to the socket, but once this was addressed, the socket began to fit better. Notably the SCS designation and comment about socket control happened prior to the sleeve being readjusted. Once the sleeve adjustment happened, the limb-to-socket motion reduced significantly but follow-up SCS and socket fit perception were not collected to corroborate the data observed.

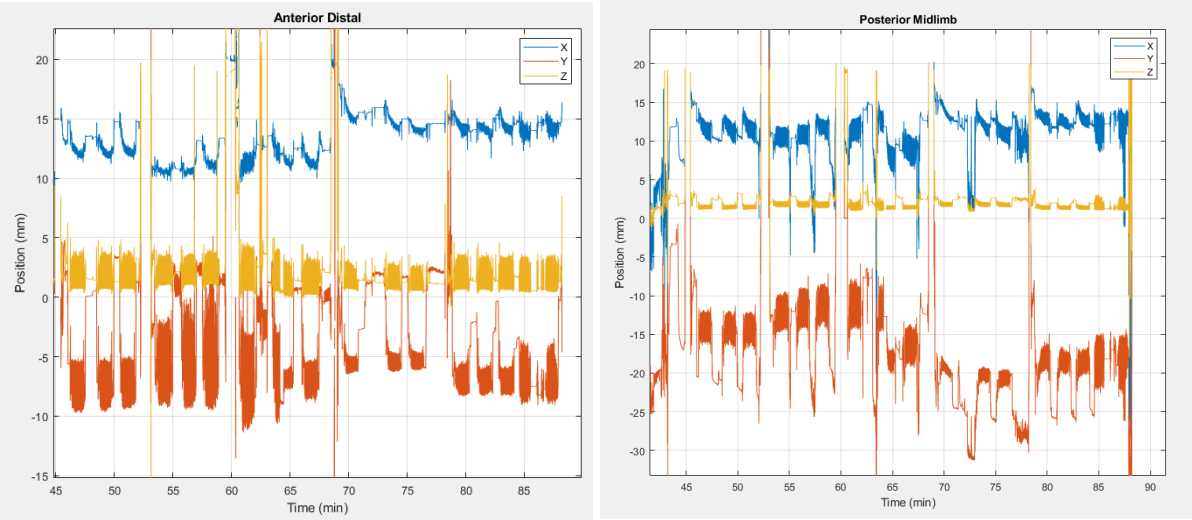

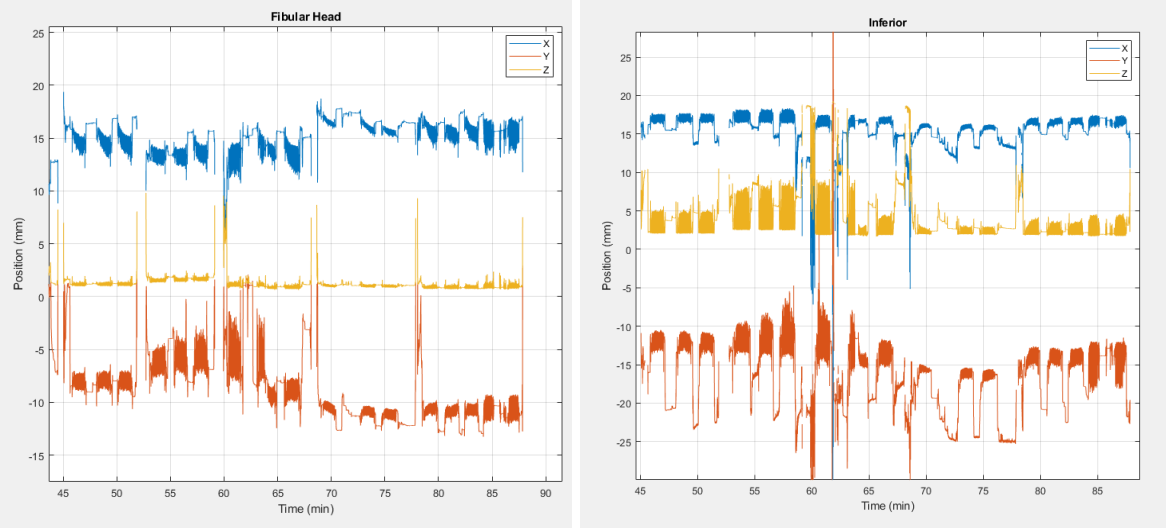

Figure 73: *Sock ply experimental conditions for Participant Nine. All walk bouts are in a set of three and correspond to 3-ply, 5-ply, 2-ply, 4-ply, and 3-ply, respectively. The last two bouts of walking were the uncontrolled bouts as the participant walked down the hallway. INTRAY sensors (a) Anterior Distal, (b) Posterior Midlimb, (c) Fibular Head, and (d) Inferior.*

2.4g of petroleum jelly was brushed onto the residual limb and during the subsequent walks the participant did not change in socket comfort (SCS remained at 10). The participant stated that the limb "felt sweaty" and that he "was using more strength trying to pick up the limb". It was also observed that the toe of the foot began scraping on the treadmill between toe off and mid swing phase. Once the limb and liner were cleaned, the participant stated that he returned to "having control and security" of the residual limb and the foot no longer scraped on the treadmill belt. The data of the distal sensors suggested that there was more motion between the limb and the socket when petroleum jelly was applied to the limb, but was not as apparent for the proximal sensors. In the Z-axis of the Inferior sensor it was seen that there was more limb-socket separation during the petroleum jelly walks, maybe suggesting the limb was further off the limb, causing the toe to drag on the treadmill belt (Figure 74). The Y-axis of the other sensors, do not corroborate this finding, but those results may be confounded by liner misalignment along the limb.

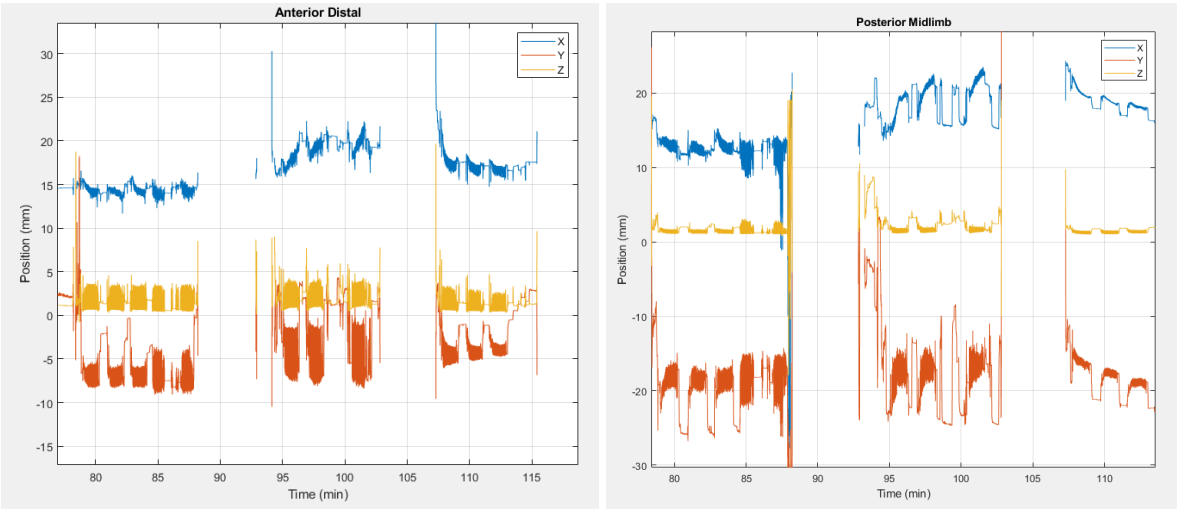

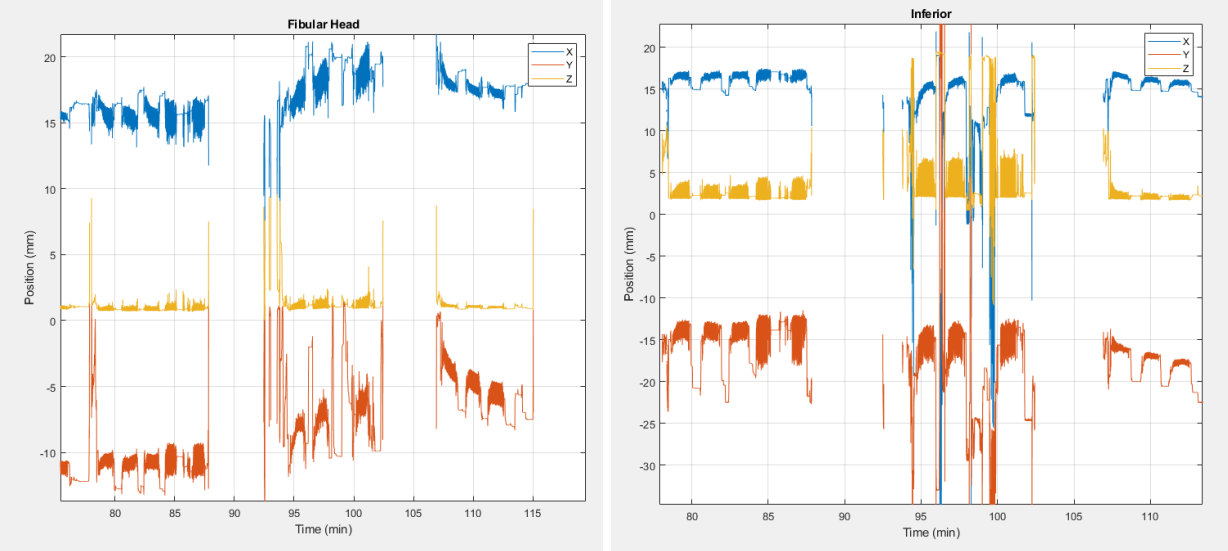

Figure 74: *Petroleum jelly and Cleaned experimental conditions for Participant Nine. Walks are in sets three and correspond to Neutral 3, petroleum jelly, and Cleaned, respectively. Again displayed after the first set of three walks were the two uncontrolled walks in the hallway. INTRAY sensors (a) Anterior Distal, (b) Posterior Midlimb, (c) Fibular Head, and (d) Inferior.*

Just prior to the petroleum jelly walk, the participant visited the restroom. The volunteer wore the investigational socket and walked down the hallway in an unstructured way. In this unconstrained walk, data shows that the participant's cadence changes and there is considerably more variability in the walking waveform (Figure 74). This was thought to not have influenced the data collected for the remainder of the structured protocol but provided a glimpse of how the limb-socket interface changed in the live environment.

4.1.10 Participant Ten

Participant Ten is a right legged prosthesis user, male, K3, suction suspension, 4-ply Neutral fit sock usage, 108kg, 188cm tall, 38y old, 16y and 9mo since amputation, 12+ hrs/day socket usage, TSB socket design, 19.8cm residual limb, and had their amputation due to a traumatic event. Figure 75 shows Participant Ten's residual limb. A liner was fabricated using the glue-on method. Balloon calibration, thermal calibration, data collection, and data processing were all conducted as described in Chapter 3. The Fibular Head site data suggested that the target was misaligned with the sensor, thus data was not analyzed in that channel.

Figure 75: *Participant Ten's residual limb*

The toe-out and toe-in rotation was seen globally within the socket and the limb seemed to be caught in the rotated position (Figure 76). Additionally, an increase in maximum-to-minimum movement was seen in the X-axis of the Anterior Distal and Posterior Midlimb sites during the toe-in rotation.

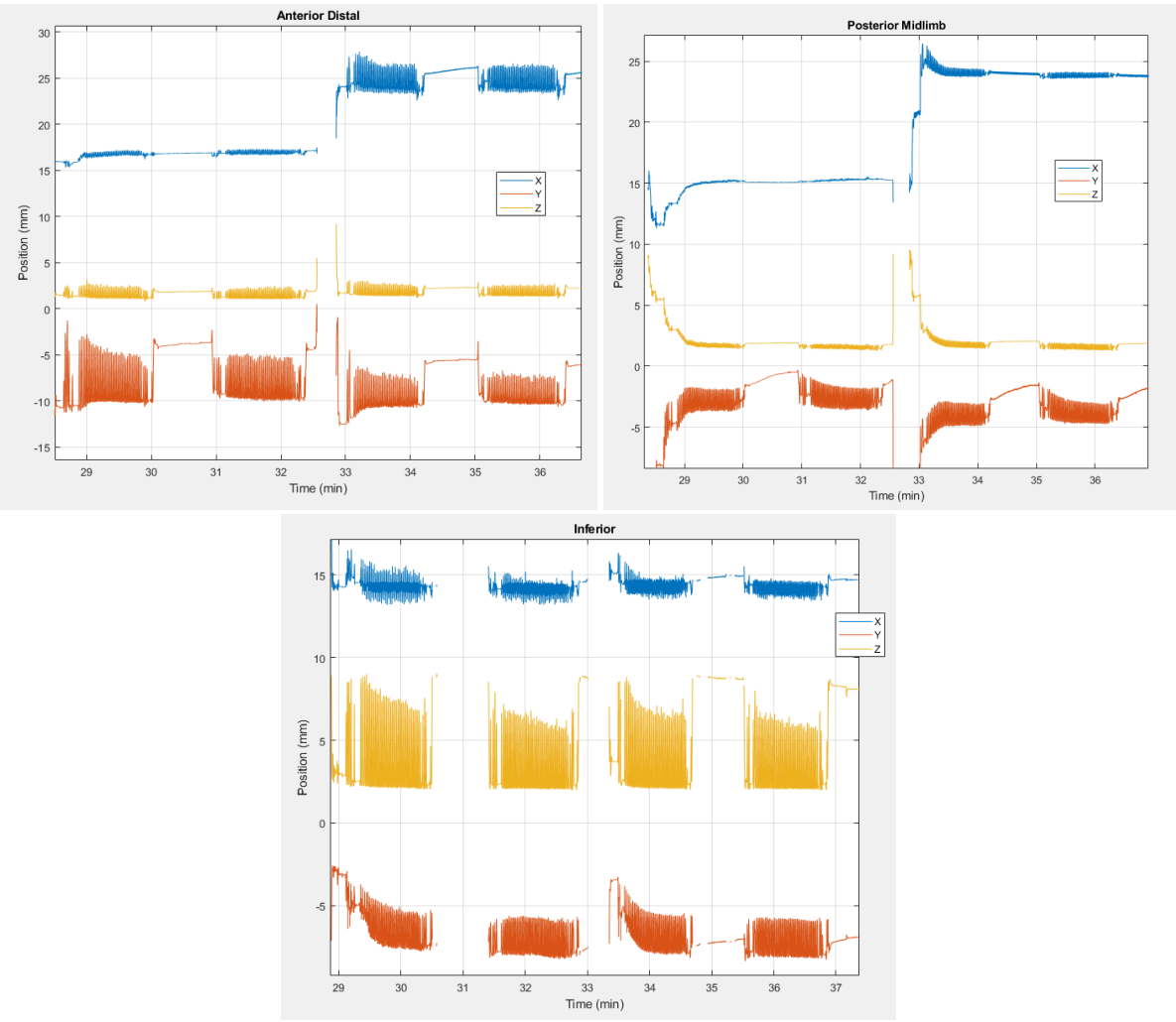

Figure 76: *Rotational experimental conditions for Participant Ten. Walk bouts one and two are toe-out, and walk bouts three and four are toe-in rotation. INTRAY sensors are (a) Anterior Distal, (b) Posterior Midlimb, and (c) Inferior.*

The participant had a Neutral socket fit with a 4-ply sock configuration and then, chronologically, donned a 6-ply, 3-ply, 5-ply, and then returned to Neutral. Z-axis positional data, again, was correlated with sock thickness (Figure 77).

Socket comfort for the 6- and 3-ply configurations were each a little worse compared to the first Neutral walk, which returned to baseline with the 5- and 4-ply configurations. During the 6-ply walk the participant stated that the limb, along the Posterior Distal aspect, was “higher in the socket and had more pistoning”. During the 3-ply walk the participant felt “lower in the socket, even more pistoning, and some pressure of the distal end”, and that it was “most painful on the knee”. During the 5-ply condition they felt that he was “throwing the leg down just before heel contact”, and that they “might feel unstable on uneven ground”. Visually it was not readily apparent that the position data supported or refuted these sensations.

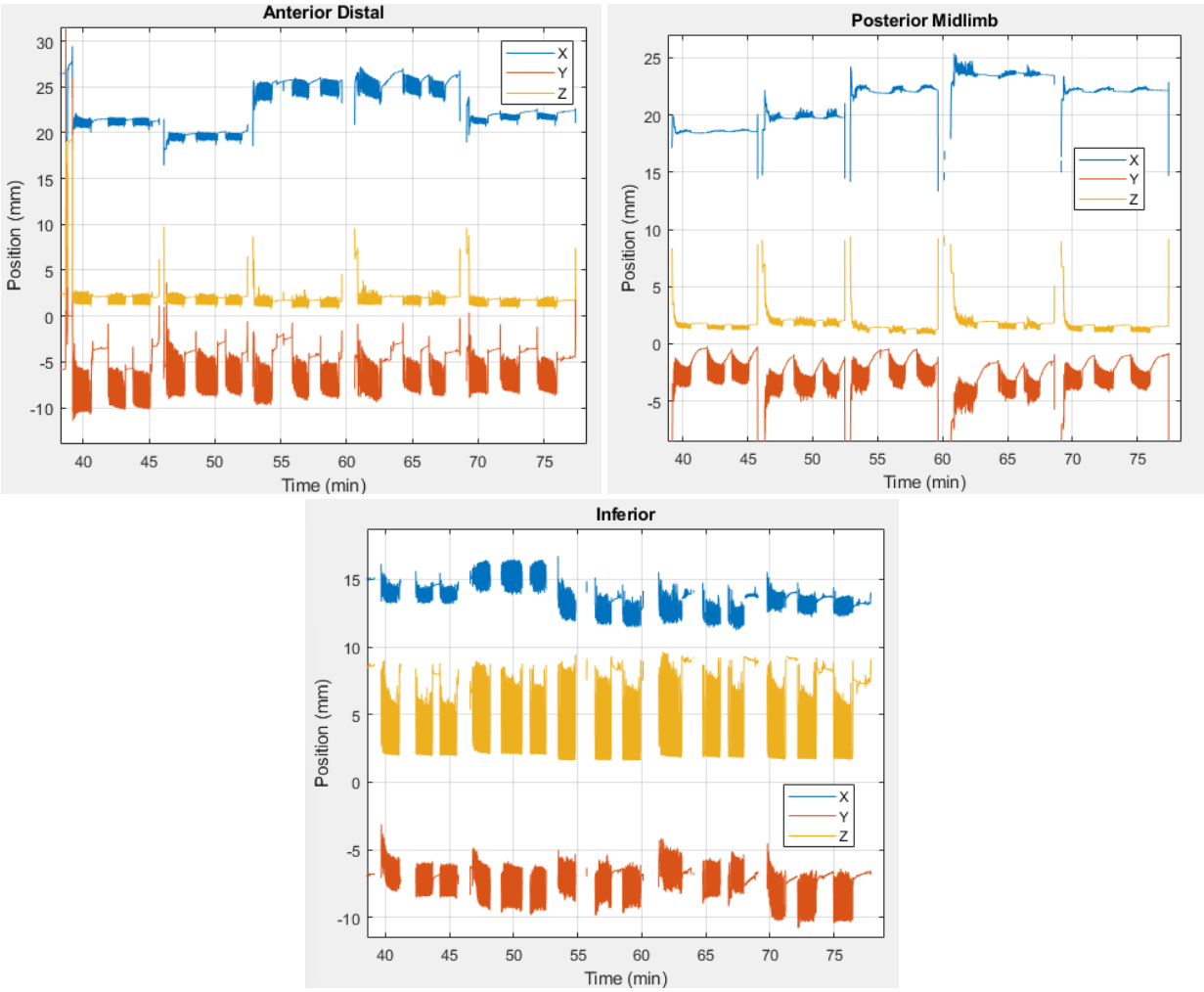

Figure 77: *Sock ply experimental conditions for Participant Nine. All walk bouts are in a set of three and correspond to 4-ply, 6-ply, 3-ply, 5-ply, and 4-ply, respectively. INTRAY sensors (a) Anterior Distal, (b) Posterior Midlimb, and (c) Inferior.*

2.8g of petroleum jelly was placed onto the lower limb (Figure 78). The participant immediately had a worse fit in the socket that was persistent for all of the petroleum jelly walking bouts. Once clean, the participant slowly regained comfort until reaching their initial comfort score. During the petroleum jelly bouts there was a similar sensation that "the prosthesis is being thrown off the limb just prior to heel contact" and that again he was feeling additional pressure at the posterior distal site. Once cleaned, the participant felt that the valve to the suction suspension was not functioning well and that it took upwards of 20-30 seconds before the limb worked itself all the way into the socket. Though dictated at the end of the session, it is likely that this was occurring throughout the entire session, because the participant did not use a suspension sleeve like the other pin-les volunteers had (this participant did not use one because it caused pain behind the knee while seated). Visually, the data did not support or refute this observation.

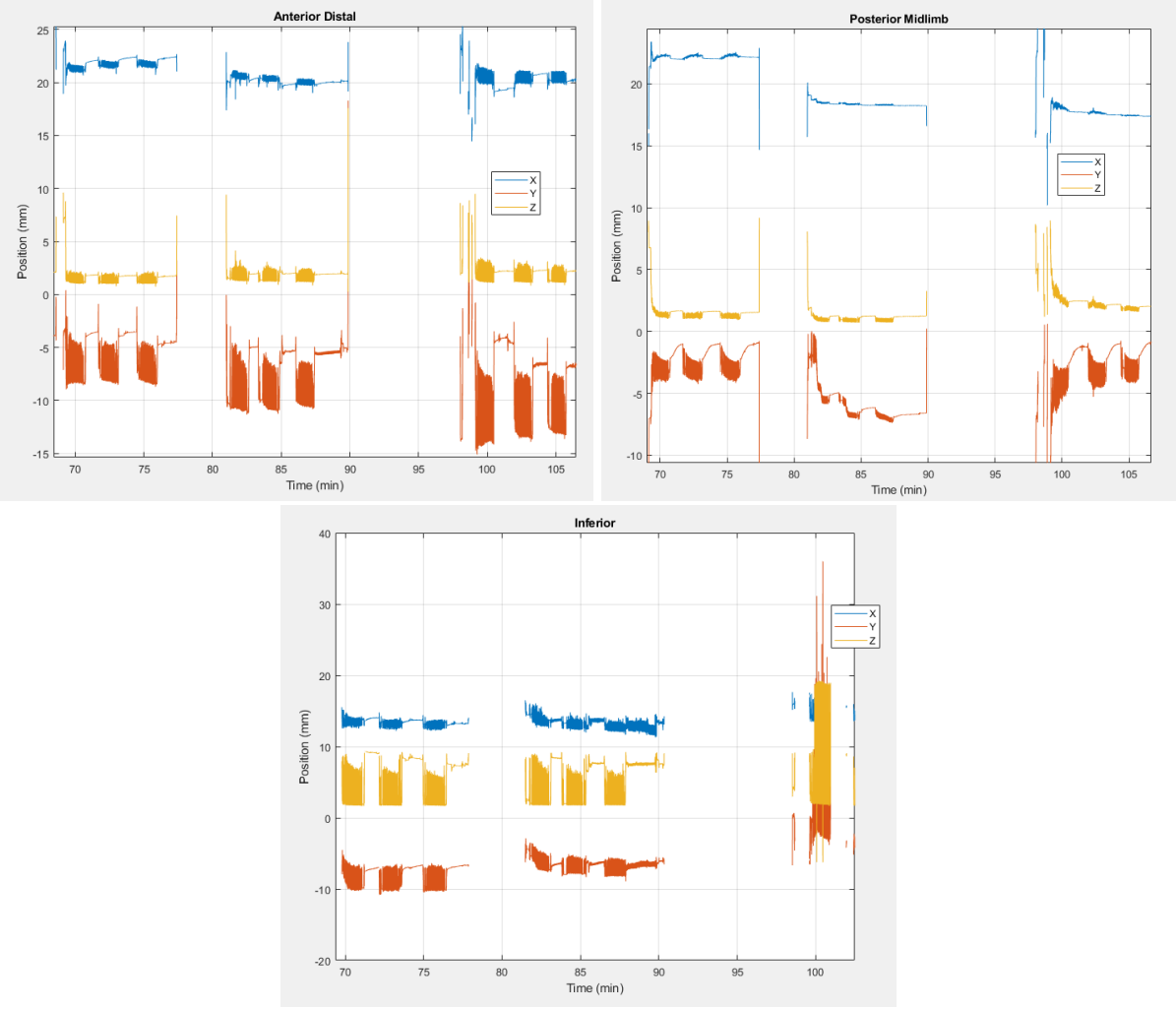

Figure 78: *Petroleum jelly and Cleaned experimental conditions for Participant Nine. Walks are in sets three and correspond to Neutral 3, petroleum jelly, and Cleaned, respectively. Poor target-sensor alignment in the Inferior INTRAY during the Cleaned walk was observed. INTRAY sensors (a) Anterior Distal, (b) Posterior Midlimb, and (c) Inferior.*

In the final portion of the session, the user was asked to walk downstairs, on an uneven surface, and then upstairs. It was recorded that for the first 9 stairs going down, the participant would match their feet on a step before moving to the next step. The remaining steps were taken one over the next, and walking back up the stairs was done one over the next. Figure 79 plots the data collected from this portion and exemplifies the step-to-step movement variability that could be seen at the limb-socket interface when ambulating in a live environment.

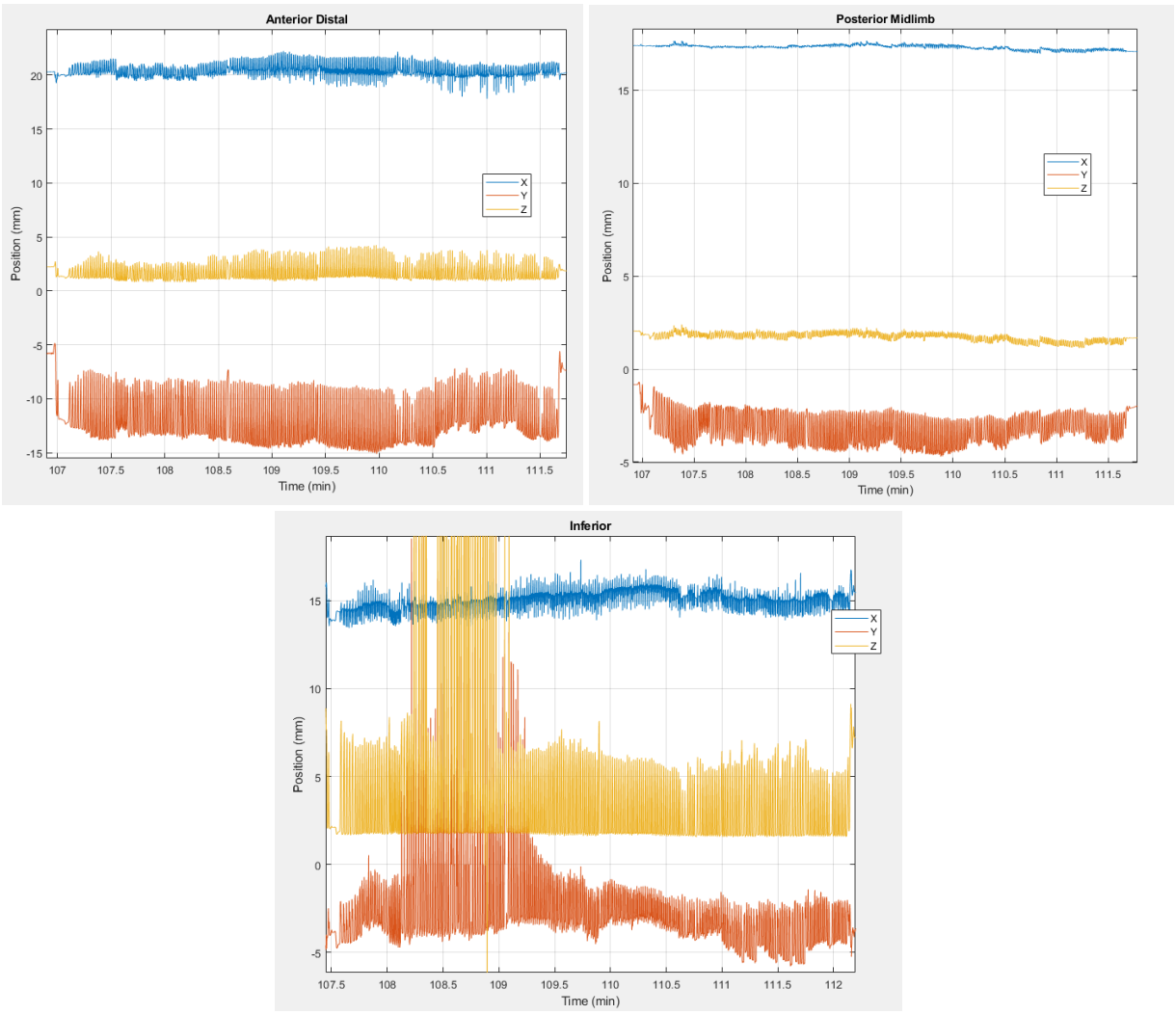

Figure 79: *A brief out-of-laboratory walk where Participant Ten walked downstairs, on uneven grassy terrain, and upstairs. Walking was continuous and there is no clear distinction between stair and uneven terrain walking. Step to step variability is much larger compared to treadmill walking.*

4.2 Cumulative Analysis

4.2.1 Results

Nine participants completed all protocol instructions (n=5 used suction suspension and n=4 used pin suspension). 9526 steps were analyzed across all participants for 10 experimental conditions. Positional data was collected for all participants at the Anterior Distal and Posterior Midlimb sites, and these two sites we used for comparison between experimental conditions. Due to diurnal changes in socket fit, Neutral socket fit conditions were repeatedly tested prior to each experimental condition, leading to three Neutral fit conditions over the course of the protocol. Each investigational condition was compared to the Neutral socket fit data collected immediately before the experimental condition. Socket fit metrics were calculated as described in Chapter 3.5, mean and standard deviation were calculated for the cohort of participants, and

an ANOVA with Bonferroni corrected pairwise comparisons was conducted. Statistical significance was reported for the pairwise comparison of the experimental condition versus the immediately preceding Neutral condition.

The mean Neutral position of the Anterior Distal site relative to the socket's circumferential axis was 0.16±1.3mm. When the limb was rotated clockwise and counterclockwise within the socket, it was 3.6±3.2 (P<0.01) and -3.9±2.8mm (P<0.01), respectively. The Posterior Midlimb site showed similar results, 0.19±1.3, 3.3±3.1 (P<0.01), and -4.2 ±3.6mm (P<0.01), respectively (Figure 80a).

The mean perpendicular distance of the Anterior Distal site from the socket wall during a Neutral fit was -0.025 ±0.20mm. When 1-ply was added, 2-ply was added, and 1-ply was removed from Neutral, it was 0.11±0.18 (P<0.01), 0.39±0.23 (P<0.01), and -0.21 ±0.20mm (P<0.01), respectively. The Posterior Midlimb site showed similar results, -0.031 ±0.16, 0.19±0.24 (P<0.01), 0.40±0.23 (P<0.01), and -0.18±0.26mm (P<0.01), respectively (Figure 80b).

The mean Neutral pistoning of the Anterior Distal site relative to the socket's longitudinal axis was 2.4±0.90mm. When Vaseline was applied to the residual limb, and then cleaned with soap and water, it was 3.2±1.5 (P<0.01), and 1.8±1.4mm (P<0.01), respectively. Posterior results reflected less pistoning and less change across conditions, 1.6±1.0, 1.6±1.2, and 1.5±1.1mm, respectively (Figure 80c).

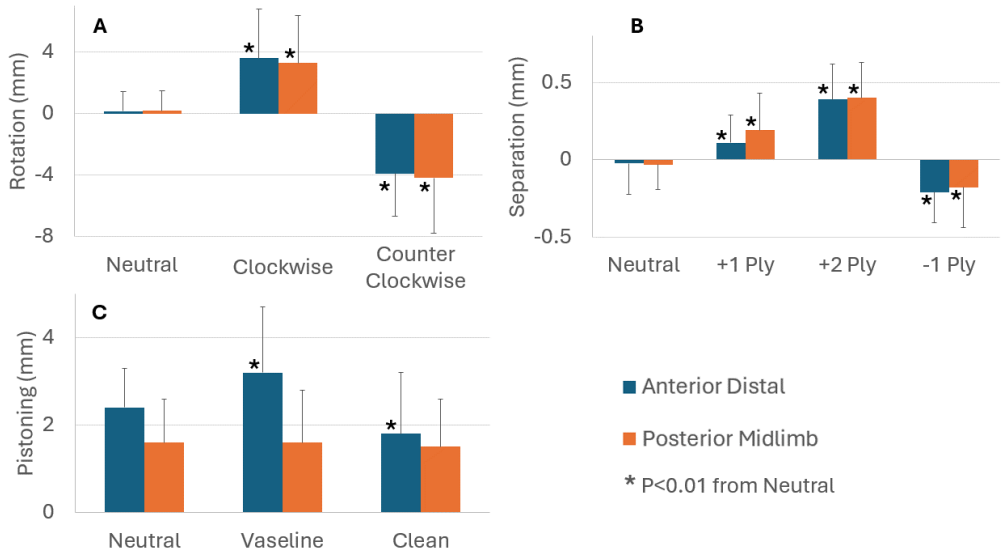

Figure 80: *(a) Limb-socket circumferential position for neutral, clockwise, and counter-clockwise rotation of the limb in the socket. (b) Limb-socket separation for sock ply changes. (c) Limb-socket pistoning for Vaseline application, and cleaning. ANOVA test performed within each INTRAY site location.*

4.2.2 Discussion

The movement sensitivity of the INTRAY sensor provided efficacious three-dimensional data in the context of lower limb prosthetics. As reported in Chapter 2.6 the mean relative displacement error was -0.5mm (range -1.2 to 0.8mm depending where in the sensing region the target was). This implies that the distances

reported were likely underestimated. Furthermore, the error calculations were performed on data collected while the INTRAY sensing unit was in an ideal condition. Data collected from within the socket were not in ideal condition and thus was subject to various forms of noise that was upward of 2.5% signal intensity, discussed in Chapter 3.4. Due to the model used to estimate the target-sensor interaction, 2.5% signal intensity noise could change the accuracy and sensitivity of the INTRAY system, but this was not explored in detail.

Data collected from this experiment is one of few studies that has collected localized movements between the residual limb and the prosthetic socket during socket use. The INTRAY sensor data demonstrated that limb-to-socket movement could be captured in all anatomical planes, simultaneously across numerous locations within the socket, and is sensitive enough to detect changes in socket fit relevant to clinical care.

Intuitively, donning a prosthesis with toe-in and toe-out rotation causes the limb to be rotated within the socket. Due to left-legged and right-legged amputees both being in the study, toe-in and toe-out rotation designations caused the signage reported from the INTRAY sensors to be inconsistent. Instead, “clockwise” and “counterclockwise” limb rotation were used to distinguish the rotation condition experienced. This means that a clockwise limb rotation was toe-in for a right legged amputee and toe-out for a left legged amputee. Counterclockwise rotations were toe-in for a left legged amputee and toe-out for a right legged amputee.

Results from the INTRAY sensors demonstrated that both the Anterior Distal and Posterior Midlimb sites rotated away from the Neutral socket position in directions that agreed with the experimental rotations imposed. Attempts were made by the research engineer to aid the volunteer in rotating the limb 10mm but that was rarely successful because the limb-socket fit prevented the limb from being rotated that much. Furthermore, the rotation was judged based on how the limb interacted with the brimline of the socket, so there was not a reliable measure of how much rotation truly occurred in each event.

The results collected from the second experimental condition suggested that adding and removing sock ply thickness resulted in correlated INTRAY data along the Z-axis. Both the Anterior Distal and Posterior Midlimb sensors showed limb-socket separation of similar magnitude, that was significantly different than the Neutral socket fit. The sock thickness offsets measured by the INTRAY sensors moderately agreed with published studies, but slightly lower magnitude (56,57). The literature suggests that a 1-ply thick sock ranges from 0.4-0.7mm, while our results suggest 0.1-0.2mm (both measured during the stance phase of walking)

A limitation to the data presented is that sock ply thickness has been shown to be non-linear, meaning that the thickness of two 1-ply socks may not be the same as one 2-ply sock. Volunteers in this cohort had Neutral socket fits that required different starting sock ply to obtain a comfortable fit, and various socks were used to obtain the +1, +2, and -1 ply offsets. So for example, if a participant on this study went from two 2-ply socks to one 5-ply sock to perform the +1 ply condition, the physical offset of sock thickness may not be the same as a participant who went from no socks to one 1-ply to perform the +1 condition. This confounding variable was not constrained at the onset of the experiment and thus the variance observed in the data may, as a result, be larger.

Adding petroleum jelly to the residual limb was hypothesized to reduce the motion between the limb and socket measured by the INTRAY sensors because of slippage between the liner and limb. The data collected did not support this hypothesis, and instead the data suggested that there was more pistoning between the limb and socket at the Anterior Distal site. Some participant comments corroborated the hypothesis that the limb would slip within the liner, but yet more liner-to-socket motion was still observed. Conversely, when the limb and liner were cleaned, Anterior Distal positioning was reduced compared to the Neutral condition. Meanwhile, the Posterior Midlimb site maintained a similar amount of pistoning across the three conditions.

It has been presented that pistoning reduction improves the fit of the prosthesis for ambulation, but that pistoning reduction does not directly better skin health (48). In general, prosthesis users want to feel "connected" to their artificial leg to have good control over its movement, which means that user wants less motion between the residual limb and artificial limb. To create less slippage between the residual limb and prosthetic a socket may exert increased forces in pressure tolerant areas, which could lead to worsened skin health.

In this investigation, users had a baseline Neutral pistoning that was nonzero. This is likely due to the practitioner prescribed socket being shaped in a way that minimized pistoning but also maximized limb health. The amount of movement within the socket was so that the user felt connected to the artificial limb, but not too tight to cause pressure related skin injuries. When petroleum jelly was added to the limb pistoning at the Anterior Distal site significantly increased and many users had the largest decrease in socket comfort because their limb was able to slide within the socket. The socket was no longer in the "Goldilocks Zone" that allowed some movement to maintain skin health, but little enough motion to make the socket feel connected to the limb. Not all participants experienced a large change in socket comfort, suggesting that the Goldilocks Zone could be different sizes for different participants (which could depend on the unique limb-socket interface movement dues to individualized socket shapes). Though almost all volunteers equated the experience to having "too sweaty of a limb", which is a known issue in the prosthetics field.

The physical mechanism that permits pistoning to increase due to a slippery liner (or sweaty liner) is unknown and it is likely a complex mechanism. It is conceivable that the limb generally displaced more distally with petroleum jelly on the limb, though the data was confounded by the liner misalignment on the residual limb between these walking conditions. Both the Anterior Distal and Posterior Midlimb data suggested that the average limb depth decreased with the petroleum jelly condition. Once in a different location within the socket, the limb is not as well supported by the socket and thus motion increases. Ultimately, depending on the participant and the fit of their socket, a user may feel the change in the socket support and may report a change in socket comfort.

A quick remedy to increased motion would be to clean both the limb and liner. In the walks immediately following the liner being cleaned with soap and water, a statistically significant reduction in pistoning was observed. Not only did it remedy the excess pistoning seen during the petroleum jelly walks, but it even reduced pistoning from the Neutral walk at the Anterior Distal site. In general, socket comfort returned to baseline after the limb and liner were cleaned. This suggests that something as trivial as cleaning the liner and limb prior to use can affect the fit of the socket.

Interestingly, while the Anterior Distal site displayed varying pistoning amounts, the Posterior Midlimb site remained unaffected. At the outset, the pistoning amount along the Posterior Midlimb was less than what was observed in the Anterior Distal site. Though the reasoning for this is not fully understood it may relate to how transtibial sockets are designed to prove support in pressure tolerant zones and build relief for pressure intolerant areas. The Posterior Midlimb site is designed to be load tolerant, while the Anterior Distal site is generally not load tolerant. The relief designed for the Anterior Distal site may allow the limb to move more than it would in a site that was designed to apply pressure and support the limb.

Additional metrics were explored for correlations to the experimental test conditions but were not found to have cohort-wide results. Instead, there were various trends thought to be found within participants that were unique to that individual. This study was not powered to study individualized socket fit perturbations within each user, but instead Socket Comfort Scores and volunteer sensation notes were used to explore the value of the movement data collected. For many cases, participant feedback was easily corroborated by the movement data collected, while for some cases the data did not support nor contradict user feedback, and rarely did the data disagree with user feedback. Though, this deduction may be strongly influenced by hindsight bias.

Clinical scalability for individualized patient fit data is imminent because the sensored-socket fabrication and data processing is largely automated. Future investigations should be aimed at validating the sensor's ability to measure clinically relevant changes in prosthetic fit at the individualized level. Diurnal socket fit perturbations are known obstacles for prosthesis users and are poorly replicated in controlled laboratory environments. With an unobstructive sensor, such as the inductive trilateration array, live-environment investigations can be conducted to better understand how lower extremity prostheses fall short of their users needs.

4.3 Take-home Data

In an effort to realize the practicality of recording live-environment data, three participants were asked to wear sensored-sockets for one week after completing the structure laboratory protocol. Data was recorded for all days the socket was out of the laboratory, though the users were not able to wear the socket for the entirety of the three weeks. All three participants had unrelated medical conditions that prevented them from wearing the socket for prolonged periods.

While the sockets were worn at home, users were asked to document any significant changes in socket fit and comfort that occurred naturally. In addition to this, the volunteers were asked to proactively perform and document minor socket fit perturbations that could be tolerated. The recorded timepoints and fit perturbations were collected by the Research Prosthetist, while the Research Engineers were blinded to the results.

Evidently, one issue with wearing the sensored prosthetic at home, was aligning the targets with the sensors. Each participant had periods of time when a sensor would drift out of the sensing region of the INTRAY, and thus data was lost in those periods. This was a consistent barrier for collecting uninterrupted data, and should be addressed with future iterations of the socket and liner fabrication process.

Chapter 5. Transtibial Amputee Residual Limb Microvasculature

5.1 Introduction

Following amputation, lower extremity prosthesis use introduces a challenge to the skin of the residual limb by requiring it to become load bearing. Initially skin health and integrity is a concern for users because of multiple reasons such as inadequacy for load bearing and liner irritation, thus users progressively increase their interaction with their prosthetic to build a tolerance to the artificial limb (74). Even with ramped usage to condition the residual limb, nearly 75% of prosthesis users will experience skin problems over the course of using their prosthetic leg (36). Depending on the severity of the skin problem users may be required to stop using their prosthetic device, require a higher-level amputation, or the injury may become life threatening, all reducing quality of life (75,76).

Numerous investigations have studied the atypical pressure and shear stresses at the interface between the liner and the socket and have shown complex patterns (16,33,34,38,77). The stresses observed have been hypothesized to have dire effects on the integrity and health of the residual limb skin, but few studies have directly compared skin physiology to interface mechanics seen in the socket (20). A novel sensor was developed to measure the movement between the socket and the prosthetic liner worn by users and the data was used to provide localized limb-to-socket interface dynamics.

Optical coherence tomography (OCT) is an established imaging modality that can be used in biological tissues to obtain higher resolution structural images compared to ultrasound (78). Further, OCT angiography is a technique that uses the movement of red blood cells within the blood vessels to visualize the structure of vasculature. In this study OCT angiography was used to collect high resolution images of the superficial skin blood vessels in lower limb amputees to observe possible physiological adaptations and compared to the data collected on limb-to-socket interface dynamics.

5.2 Materials and Methods

Informed consent was obtained from all subjects involved in the study following University of Washington Institutional Review Board's approval of the study procedures (Study 00006874). Inclusion criteria were participants with a unilateral transtibial amputation at least nine months prior, 18 years of age or older, regularly visited a prosthetist, and use of their prosthesis more than seven hours per week. Exclusion criteria was presence or history of skin breakdown at various locations of interest.

Participants were part of a longitudinal study. The first session completed was a two-hour controlled laboratory setting where participants completed sets of consistent treadmill walking with instrumented prosthetic sockets. An investigational prosthesis was fabricated that duplicated the practitioner-prescribed prosthesis shape of the participant's socket and was instrumented with inductive sensing arrays embedded within the layers of the socket. A prosthetic liner was also modified to have ferrous-polymer targets affixed to the liner, positioned to overlap with the sensor arrays within the socket.

Sensor-target locations were over the anterior distal (defined by the relief in the socket shape) and posterior midlimb (defined by the center of the posterior aspect of the socket shape) sites. During the session, participants completed a series of socket-fit perturbation variables (such as socket rotation, sock ply addition and removal, etc.) that each had a matched-control, "neutral" socket fit. The neutral socket fit was the fit that the participant was most comfortable in and was the way the socket would be worn throughout the day. Data collected for limb-to-socket movement in the neutral socket fit position was aggregated from this laboratory session and used as an approximation for the limb-to-socket movement experienced by their traditional prosthesis.

Limb-to-socket data was processed and evaluated on an individual step basis. The heel-contact and toe-off, double-peak, nature of the walking waveform was identified to evaluate the data during the participant's stance phase of walking. Stance phase limb-to-socket movement data was chosen to be just prior to the peak at heel contact (0.15 sec) to just after the peak at toe off (0.15 sec). This was defined based on the pressure and shear investigations that found pressure and shear ramped immediately prior to and following heel contact and toe off, respectively. Limb-to-socket slippage data was plotted in the circumferential-longitudinal plane and total displacement was calculated.

The second visit was a two-hour imaging session where four anatomical sites were imaged. Two locations were chosen on the amputated limb, distal tibia and posterior midlimb, and matched-control locations on the sound limb were identified. The imaging procedure was repeated from Swanson et al.'s Maximum Dilation OCT Test: Vessel Structure Assessment (40). The anterior distal imaging site was notably *not* in the same location that the anterior distal movement data was collected from. This is because of the curvature of the distal tibia, and instead the imaging site was 1-2cm medial of the anterior distal apex, because it was a flatter region and provided a better area for imaging. The posterior midlimb site was imaged as close to the site that the ferrous-polymer target overlapped with.

Prior to imaging procedures, participant demographic information was recorded and the participant sat with their prosthesis donned for about 10 minutes. Once doffed, a relaxed position for imaging was achieved. To image the anterior side of the limbs, participants sat supine in a hospital gurney with the back of the bed-backing raised for support. To image the posterior side of the limb, participants lay prone in the hospital gurney with pillows supporting the upper torso. In each position the limb being imaged was supported by a vacuum splint (Vac-Lock Cushions, CIVCO Radiotherapy) so that the imaging surface was level and to reduce any large movements by the participant.

Next, a custom warming probe was placed on the skin (79). The warming probe was affixed to the skin with double sided medical tape (3M 2477P-4-10) so that the skin was in a relaxed state and not pulled. Mineral oil was used as the conducting agent within the center opening 1cm radius. The skin was warmed for 10 minutes once the temperature of the ring and oil stabilized at 51.5ºC.

The camera, which was mounted to the side of the gurney, was then placed so that a custom bracing-arm contacted the top of the warming probe. The bracing arm reduced motion artifact and helped maintain focus while imaging. The hole in the center of the bracing arm matched the hole of the warming probe so that OCT image acquisition could happen through the mineral oil medium.

A Swept-Source Optical Coherence Tomography (SS-OCT) system, with a central wavelength of 1300nm, A-line scan rate of 100kHz, and lateral/axial resolution of 20um and 10um respectively (OCS1310V1, Thorlabs Inc), was used to acquire Speckle Variance angiography images of cutaneous microvasculature. A lens with a 2.56cm field of view was used on the SS-OCT probe (OCT-LK4 lens, Thorlabs Inc., Newton, NJ, USA).

Four 7.0 x 2.0 x 8.0mm (750 x 250 x 1431pixels) images were captured, each with five repetitive B-scans in each anatomical location. The rasterization was programmed so that the individual images overlapped by 0.2mm. This was done to reduce image acquisition time and thus reduce the likelihood of motion artifact. Image acquisition time was between 12-15 seconds, and during this time participants were asked to hold their breath to further reduce motion artifact. Once all four images were captured, the OCT camera and warming probe were removed, and the mineral oil was cleaned from the participants' skin. The process was then repeated for the remaining three sites.

Raw spectral data from the imaging session was converted to spatial-intensity data and variance was calculated as described by Choi et al. (42). The highly reflective skin surface (stratum corneum) was identified and the spectral variance data from each of the four images per site were registered based on the identified skin surface. Spectral variance data were arranged so that vessel data at consistent depths beneath the skin surface could be visualized. Bins of 10 pixels in depth (56 μm) were created until the vessel data was no longer observable. An enface image was created and metrics were calculated from the data in each image.

Vessel area density was calculated by creating a binary image of the superimposed layers at each given depth and dividing the number of identified vessel pixels by the total pixels in the image. The papillary plexus was defined as the first two bins (56-167 μm) and the sub-papillary plexus was defined as the last three bins (168-335 μm). Capillary density was calculated by identifying the number of non-connected capillary loops in the first depth layer divided by the area of the image acquired. Vessel orientation plots were created by identifying the centroid of a capillary loop and superimposing the underlying vessel data in the papillary layer around that centroid. All non-connected capillary loops identified had this completed and each of the capillary loops were superimposed on one another. For each plot an ellipse was fit to the shape of the vessel orientation and an aspect ratio was calculated to quantify the non-circular shape and alignment (Figure 81).

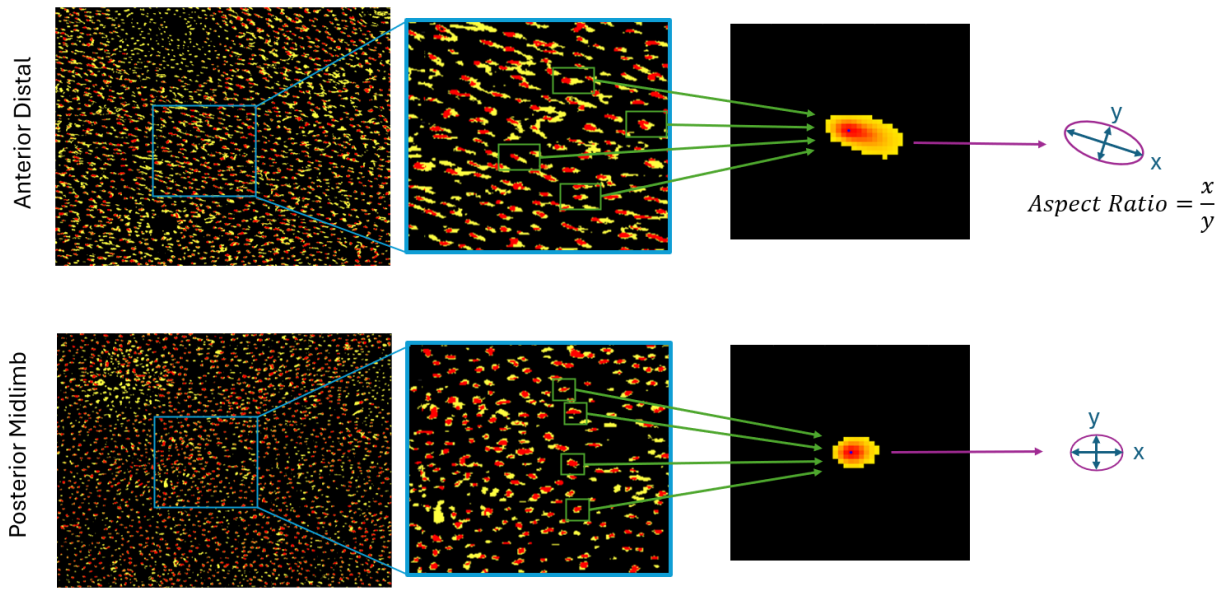

Figure 81: *Methodology for obtaining residual limb vessel alignment within the papillary layer. Centroids of the capillary loop apexes (red) were aligned (blue point). Features of the deeper papillary layer (yellow) for all capillary loops identified in the image were superimposed creating a heatmap describing the average shape of vessel alignment. An aspect ratio was calculated based on the elliptical shape identified from the average vessel alignment heatmap.*

5.3 Results

Four participants with unilateral transtibial amputation were recruited. All participants were male, currently using suction socket suspension, and received an amputation due to a traumatic event. Two of the four participants regularly smoked. The median (range) age of participants was 62 years (38-65), time since amputation 11 years (5.6-16.8), usage per day was 12 hours (10-16), and time between sessions was 86 days (16-116). QNN had significant skin grafting on the posterior aspect of both the residual limb and intact limb.

16 microvasculature images were acquired after 10 minutes of controlled vasodilation, one from the residual limb posterior midlimb, residual limb anterior distal, intact limb posterior midlimb, and intact limb anterior distal for each participant. Grayscale microvasculature images for Participant Five can be seen in Figure 82, and Figure 83 shows the depth-segmentation based on depth from the stratum corneum for those same images. This was conducted for each of the participants and can be seen in Appendix 3.

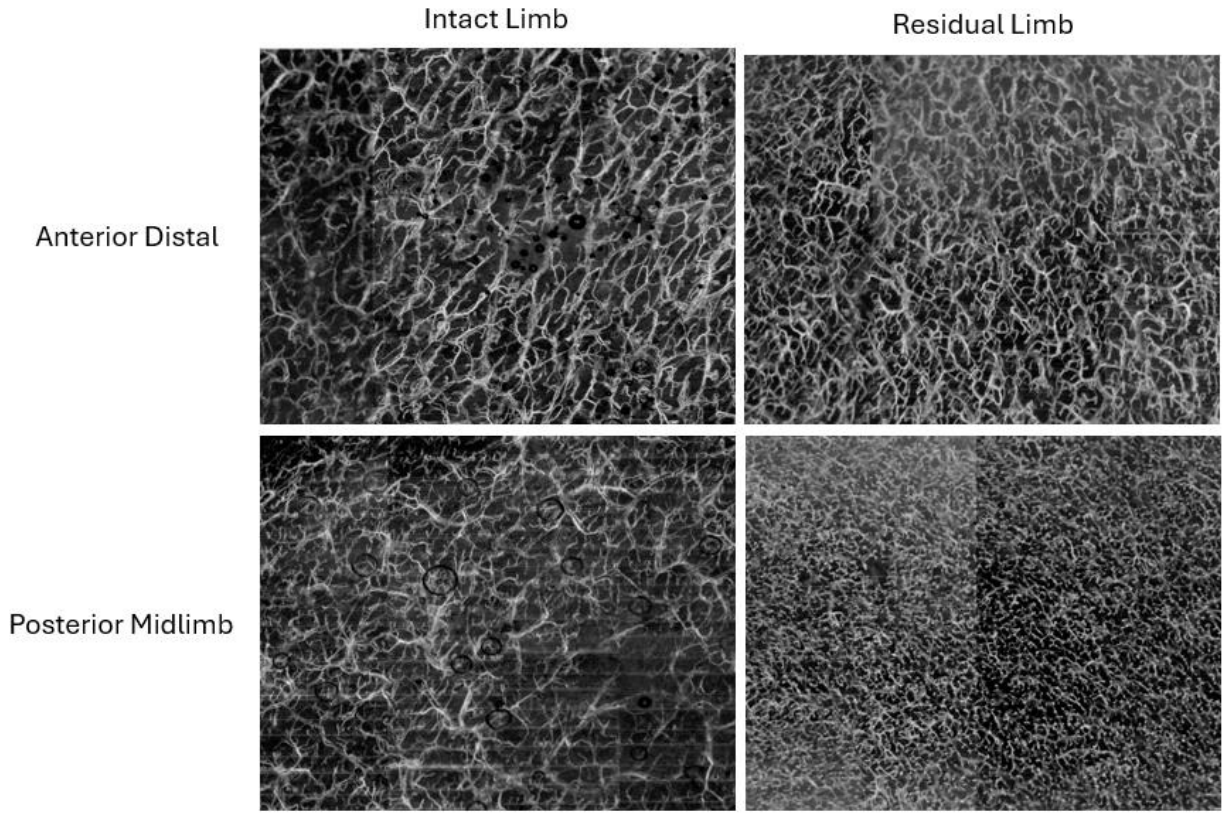

Figure 82: *Optical Coherence Tomography Angiography images collected from Participant Five in the (a) Intact Limb Anterior Distal site, (b) Residual Limb Anterior Distal site, (c) Intact Limb Posterior Midlimb site, and (d) Residual Limb Posterior Midlimb site. All images are an en face projection of the tomography images collected and presented in grayscale.*

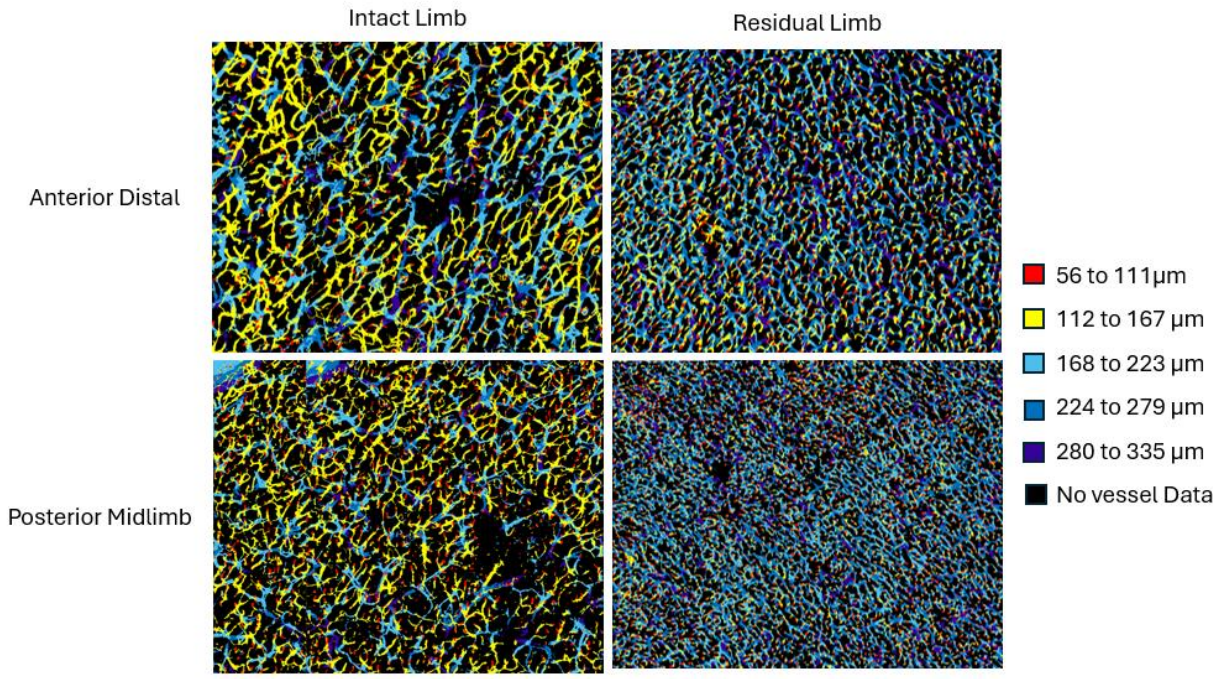

Figure 83: *Optical Coherence Tomography Angiography images with vessel depth identified. Images were collected from Participant Five in the (a) Intact Limb Anterior Distal site, (b) Residual Limb Anterior Distal site, (c) Intact Limb Posterior Midlimb site, and (d) Residual Limb Posterior Midlimb site. Depths are of equal bin sizes (10 pixels or 55µm) and distinguished by the colors shown in the legend.*

In the residual limb, there was greater capillary loop density (Figure 84a) and higher sub-papillary plexus vessel area density (Figure 84c) found for 6 of 8 matched-control images. Participant Seven (noise in the data may have influenced this) and Participant Ten (poor focus) anterior distal were the cases that the capillary density data suggested otherwise. Participant Ten (visually looks like larger vessels) posterior midlimb and Participant Nine (visually looks like larger vessels) anterior distal suggested more density in the sub-papillary layer on the intact limb.

Yet, in 7 of 8 matched-control images the intact limb had higher vessel area density in the papillary plexus (Figure 84b). Participant Nine posterior midlimb was the only instance where the data did not support this and may have been due to the intact limb having significant skin grafting on it.

Of the images acquired from the residual limb, two had papillary vessel aspect ratios greater than two (Participant Five anterior distal, and Participant Seven anterior distal). Papillary vessel aspect ratios were plotted against the average cumulative limb-to-socket slippage during stance phase as measured by the inductive sensor arrays (Figure 85). The INTRAY sensor for Participant Five posterior midlimb was misaligned with the target and the data was not used in this analysis.

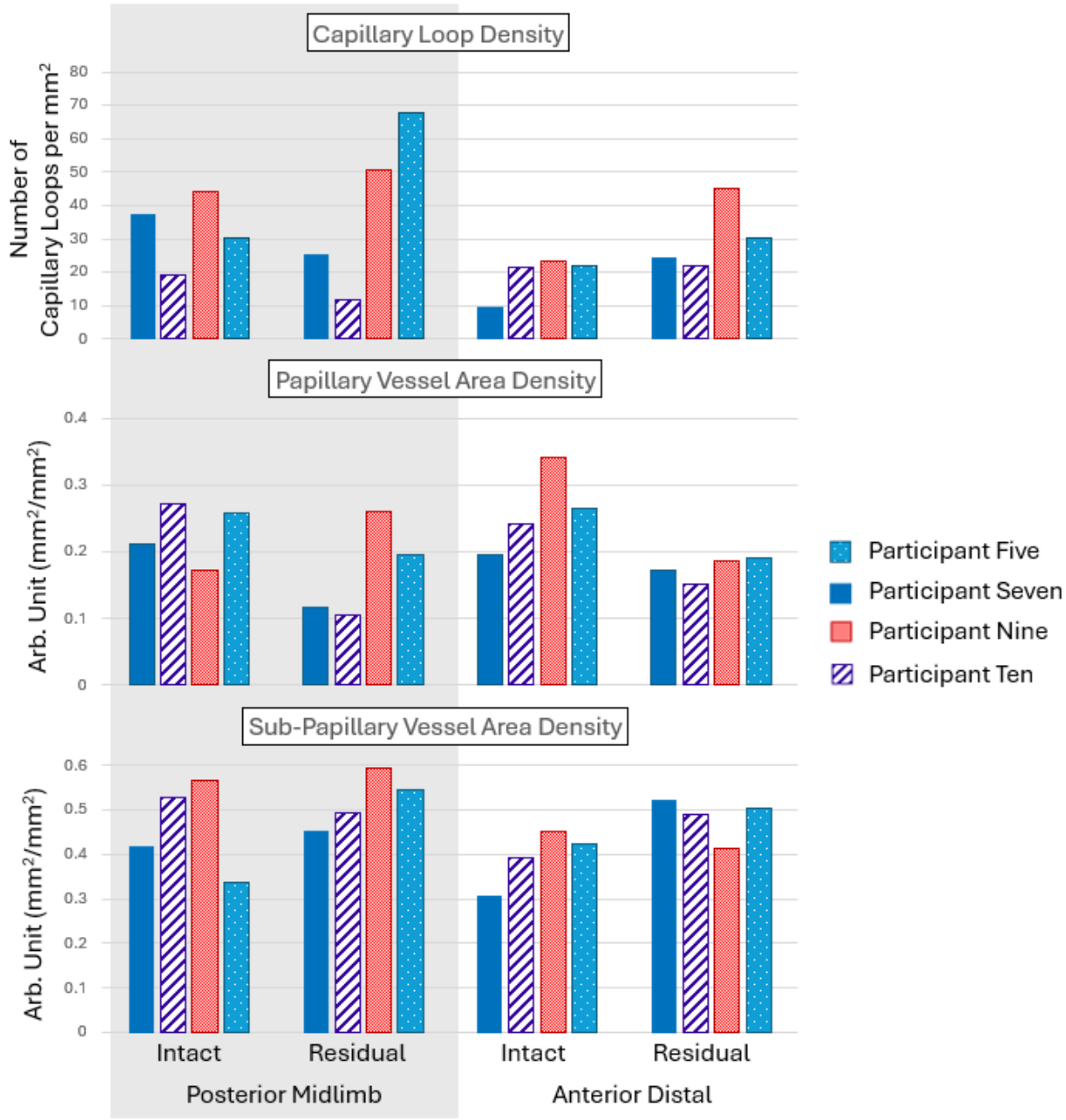

Figure 84: *Quantification of vessel features. (a)Capillary Loop Density is the number of identified capillary loops (defined as individualize vessel features in the first depth bin) per area. (b) Papillary Vessel Area Density is the percent area of vessel features found in the papillary layer (defined as the first two depth bins). (c) Sub-papillary Vessel Area Density is the percent area of vessel features found in the sub-papillary layer (defined as the last three depth bins)*

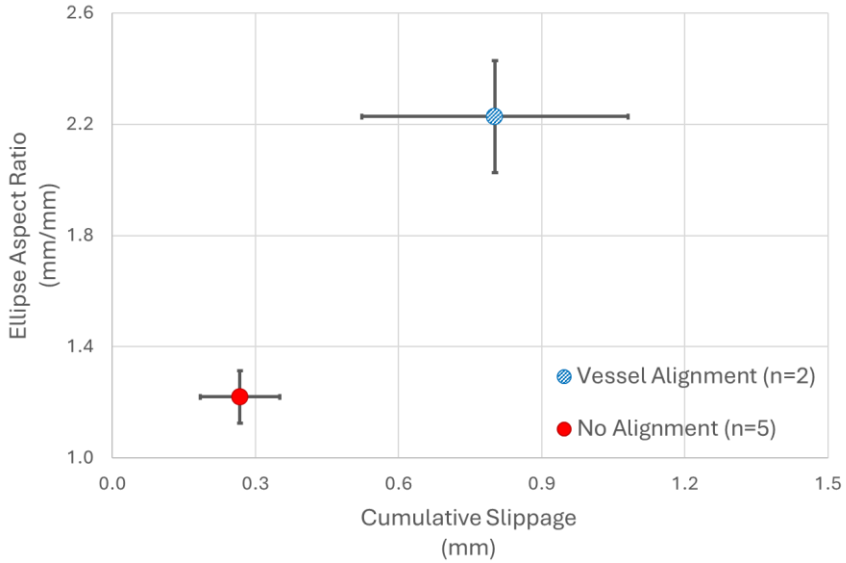

Figure 85: *Relationship between the Ellipse Aspect Ratio and Cumulative Limb-to-Socket slippage during stance phase. Ellipse Aspect Ratio was calculated from the average vessel orientation heatmaps for each of the residual limb imaging sites. Cumulative Limb-to-Socket slippage data was collected from custom movement detection sensors and calculated by totaling the distance the limb travel along the socket in the longitudinal and circumferential plane. Points plotted are the mean and the error bars are the standard error for the two groups. Vessel alignment was observed in two cases, both being anterior distal sites.*

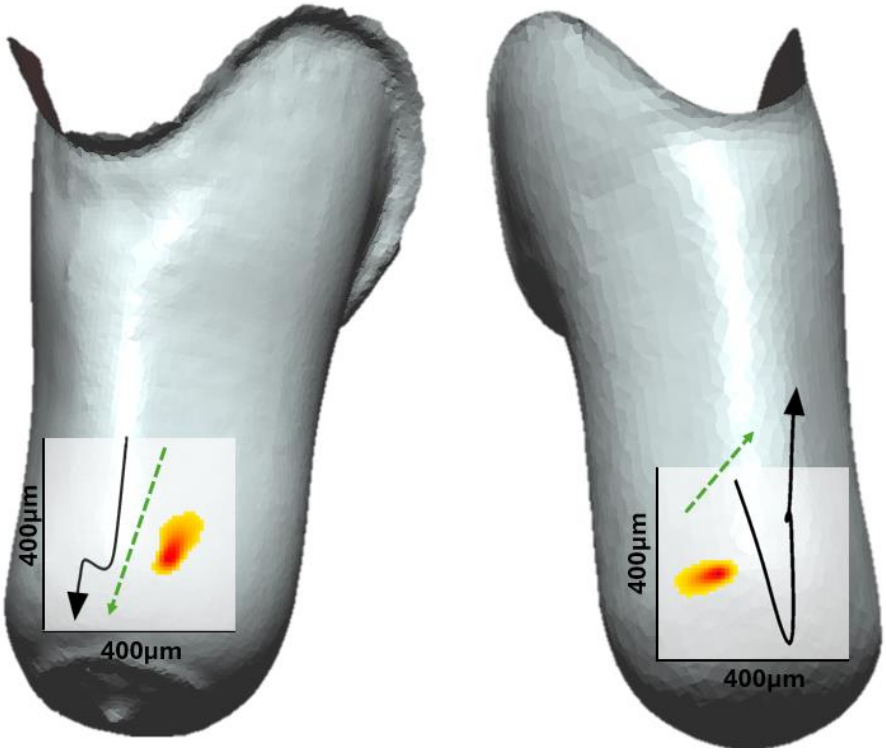

Figure 86: *Comparison of Limb-to-socket slippage during stance phase to Vessel alignment heat maps. Socket shapes for the two participants are shown and overlayed is the movement and vessel heatmap data (Sockets are not to scale with data - white areas are a scale of 400x400µm). Black arrows show the slippage resultant directions throughout the stance phase of walking. Green dashed arrows reflect start and ending points of slippage from the stance phase of walking.*

Slippage and vessel orientation data are presented in Figure 86 for the two instances of papillary vessel arrangement. It can be seen in one case that the papillary plexus capillary loop aligns well in the opposite direction of slippage. In the other case, there are two distinct longitudinal motions that oppose each other. The cumulative displacement (green arrow) though, well aligns so that the capillary loop alignment is opposing the direction of slippage.

5.4 Discussion

It is commonly thought that superficial blood vessels in the skin project loops perpendicular to the skin surface to vascularize the dermis around the papillae structures found at the dermal-epidermal junction. Immediately below the capillary loops, the vascular network is understood to travel transversely, connecting the capillary loops to the deeper vascular network. These two distinct characteristics have been defined as the papillary plexus and reticular (referred to here as sub-papillary) plexus of the dermis, respectively (80,81).

Inherently, the capillary loop projections are in the axis of the Optical Coherence Tomography (OCT) images captured and thus commonly only the apex of the loop can be visualized. Meaning that the projecting vessels that connect the apex of the capillary loop and the transverse network are largely hidden in the imaging-induced-shadow cast by the apex of the loop. This is supported by the OCT images collected in this study because obvious blood vessels were identified superficially (56 to 111 μm) that were not connected to any nearby vessels in both the intact and residual limb photos. These small vessel structures were eventually connected to the vascular network in the deeper layers, and those deeper networks were highly interconnected.

Compared to the intact limb, the residual limb has stark differences in both papillary and sub-papillary structures. In general, the residual limb had a larger capillary loop density and greater sub-papillary vessel area density compared to the intact limb. Yet, in seven of the eight cases, the vessel area density in the papillary plexus was greater for the intact limb compared to the residual limb.

This is believed to be due to taller capillary loop projections in the residual limb. The papillary layer defined in the depth-segmentation process was held constant at a depth of 56 to 167μm below the skin surface. In Figure 83 the (yellow) features, 112 to 167 μm below the skin surface, in the intact limb are more branched and interconnected, while the residual limb shows minimal interconnections. We hypothesize that with shorter capillary projections at the dermal-epidermal junction, the blood vessels are free to move in a more transverse pattern closer to the skin surface (which is the definition of the reticular plexus). While for the residual limb, with taller capillary projections, the blood vessels need to travel deeper into the skin before spreading in a transverse pattern, as can be seen by the (light blue) structures 168 to 223 μm below the skin surface. This hypothesis is described visually in Figure 87.

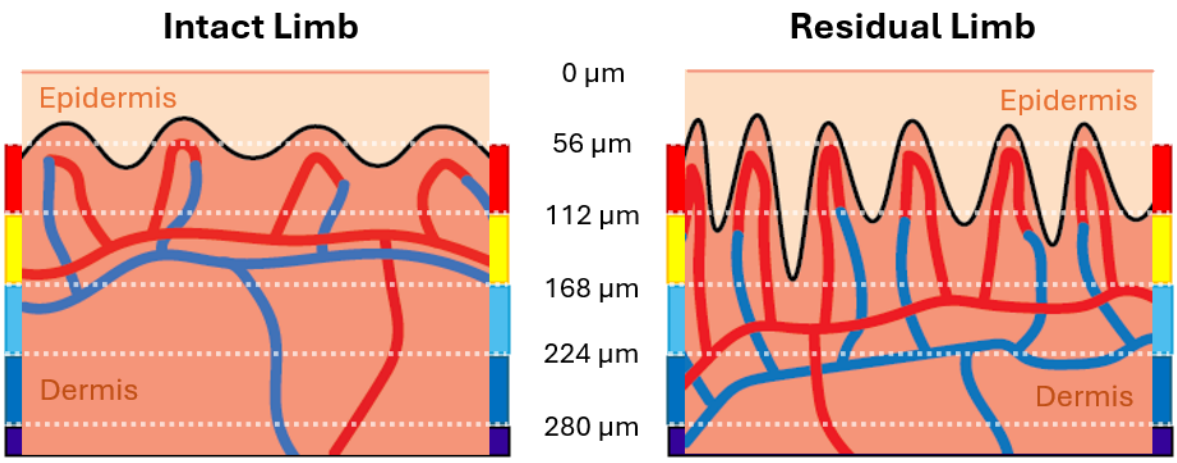

Figure 87: *A schematic representation of the observed vessel features in the (a) intact and (b) residual limb. The intact limb features capillary loop projections that are less numerous and shorter in height, which allows for transverse vessel networks to occur closer to the skin surface (yellow region). The residual limb features higher capillary loop density and taller loop projections, making the transverse sub-papillary vessel network occur deeper from the skin surface (blue region). Reported dermal-epidermal junction papillae structure reflect the observed capillary loop features of the intact limb and it is hypothesized that it is also reflected in the residual limb.*

If this is the case, the reported metric papillary vessel area density may be misleading for the intact limb, but an apt measurement to compare superficial vessels between the intact and residual limbs. This is because the papillary density calculation in the intact limb would be measuring vessels that should be considered part of the sub-papillary plexus due to the vessel characteristics. Still, we can use this metric to compare the interconnectedness at the superficial layers of the skin between the intact and residual limb, which the intact limb predominantly has larger interconnectedness at the (yellow) 112 to 167µm.

The skin's papillae structure are not easily visualized with OCT due to the lack of variation in light-scattering properties of the epidermis and dermal tissue, though other research groups have attempted to process OCT data to show the shape of the dermal-epidermal junction and papillae (82). Thus the skin structure was not evaluated directly in this study, but rather the vasculature characteristics of the intact limb are similar to papillae structure reported in the literature. In an investigation that looked at skin structure versus age, Cucumel et al. reported a papillae density between 10-55 per mm^2 and papillae height between 14-28 µm tall, and that both density and height were negatively correlated with age (83). We report a capillary loop density in the intact limb of 10-44 per mm^2 and capillary loop projection less than 56µm in height. An additional study by Hagisawa et al. took skin samples from postmortem subjects over the sacrum, ischial tuberosity, and center of gluteus maximus and found,

> "The finger-like papillae seemed to have a lot of blood capillaries underneath while flat or trapezoid papillae did not. The loops of blood capillaries found in the dermal papillary ridges were most numerous in the sacral skin. In the ischial skin the dermal papillae consisted of two types of configuration: finger-like papillae possessing the capillary loops and large trapezoid papillae having loose capillary nets. In contrast the gluteal skin had no dermal papillae and blood capillaries appeared to be scattered. Sacral skin was characterized by a dense distribution of blood capillaries, but less elastic fibres in the dermal papillae. In the gluteal skin, blood capillaries were scattered, but a moderate distribution of elastic fibres was observed. Ischial skin had moderate density of blood capillaries and densely distributed thick elastic fibres." (84)

Furthermore, Swanson et al. reported that the epidermis of the residual limb was on average 17μm, thicker compared to the contralateral limb (40). The depth bins created in presented investigation were made from the skin surface, meaning that the depth of the transverse network may be influenced by a thicker epidermis. Though this may influence our results, we don't believe that it detracted from our conclusion because 17μm is less than a third of the range of each segmented section, and because the epidermal thickness measurement can be challenging to reliably make with the image acquisition method.

This suggests strong evidence that the vasculature structure may closely reflect the tissue structure in the skin. If this is found to be true, the residual limb may have taller and more papillae at the dermal-epidermal junction which is illustrated in Figure 87b.

Our limb-to-socket movement data suggested that there were small amounts of slippage at all sites tested. There is a plausible positive correlation between OCT structural vessel arrangement and limb-to-socket slippage, though the sample size from this investigation is too small to perform reliable statistical calculations. This suggests that the more a liner slips along the surface of the socket during stance phase of walking, the more a capillary loop may orientate in the papillary plexus.

This explanation is strengthened with additional factors. Shear, measured at the socket, is a result of the friction that prevents the liner from slipping across the surface of the socket (50,85). For movement to happen between the liner and socket, the frictional forces between the liner and socket wall need to be overcome, meaning that the maximal shear force is also overcome. Ultimately the force that acts on the liner to move it along the socket surface, starts with the residual limb's bone and soft tissue but is delivered to the liner by the residual limb's skin. At the liner-to-skin interface, shear is imparted on the skin due to the frictional forces between the liner and limb. This is how prosthetic liners are designed to work, the shear elasticity of a liner dissipates the shearing force between the residual limb skin and socket wall as reported by Cagel et al. (12). Shear forces can be upwards of 60 kPa at the socket wall, and some of that force is translated to the skin after most of it is dissipated by the liner. In a modeling investigation by Cagel et al. (50), they allowed a slight amount of slippage between the liner and the limb and the results were very strongly correlated to skin irritation.

Simply put, in order to create slippage between the liner and socket, maximal shear forces are incurred at the residual limb's skin to move the liner along the skin surface.

The anterior distal and posterior midlimb sites were chosen as investigational sites in this study due to the difference in empirical evidence about the two environments' pressure and shear. The anterior distal site generally sees more shear than the posterior midlimb, which means that to create slippage at the anterior distal site, there is historically more shear translated to the skin on the residual limb at that anatomical site. Our data shows that all sites had slippage, which suggests that maximal shear forces had been overcome during the stance phase of walking. The two locations that had vessel orientation (papillary vessel aspect ratio greater than 2) were found in the anterior distal site. We suspect that the vessel arrangement may be a result of the increased amount of forces on the limb in the anterior distal site compared to the posterior midlimb site. In one anterior distal site (Participant Nine) we did not observe vessel orientation but a smaller slippage was recorded at that location compared to the anterior distal sites that showed vascular orientation.

This participant also had a uniquely shaped socket compared to the other participants, it had a suprapatellar containment shape, possibly altering the pressure distribution to what was assumed from the literature.

Logically, the direction of vessel arrangement and slippage was considered similar to what was presented by Swanson et al. (40). There was a loose relationship between the direction of slippage (green arrow) and the direction of papillary vessel orientation (Figure 86). If the vessel orientation data is correlative to slippage/shear, and our hypothesis about the vessel structure reflecting papillae structure, we may be observing a directionality in the skin structure. Meaning that the papillae are oriented in the opposite direction of slippage. Furthermore, the direction of the skin structure is such that as the skin is sheared in the liner, the papillae would become aligned perpendicular to the skin surface (Figure 88).

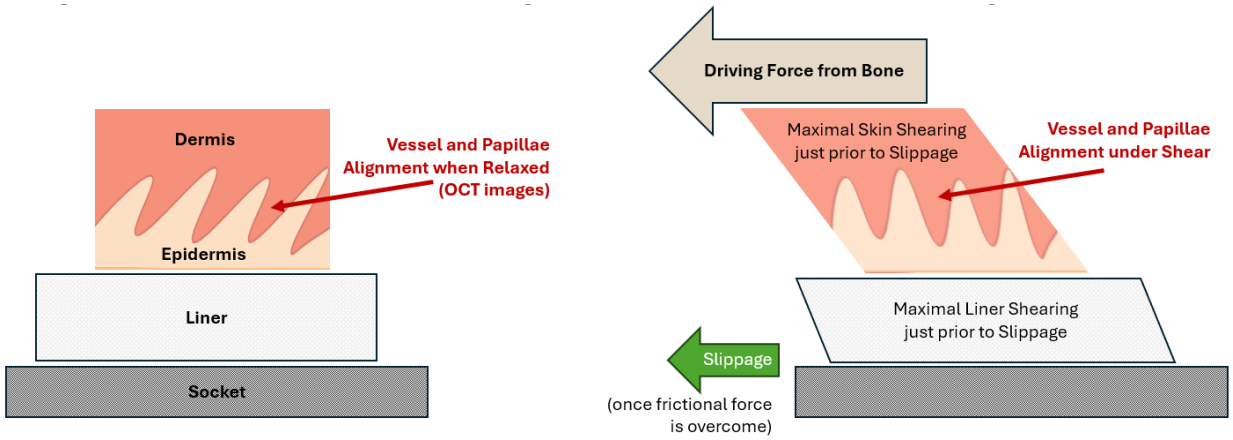

Figure 88: *Hypothesized vessel alignment adaptation due to elevated shear stress. In a relaxed state, left panel, the skin and liner experience no shearing. OCT images were collected at a relaxed state and vessel orientation was observed. When in a sheared state, right panel, force from the bone is transferred to the liner via the skin. Slippage between the liner and socket suggest that maximal liner and skin shearing has occurred. Data loosely suggests that vessel alignment is in the direction of slippage (green arrows Fig. 86) and thus shear. As the skin is sheared, the vessels and papillae orient perpendicular to the skin surface.*

This hypothesis has limitations though. As noted in the methods, the vessel data and movement data may have been sampled in anatomical locations that were close to each other (1-2cm) but not directly over the same spot. The posterior midlimb likely had more overlap between where the OCT imaging and the slippage data was collected, but the anterior distal site was limited by experimental set up. The warming probe could not maintain a seal to hold the mineral oil on the highly curved distal tibia site. Instead, the imaging site was moved medially so that the surface was flatter. From the pressure and shear literature, we know that the microenvironment may be different over the 1-2cm misalignment and the resultant direction of shear may be different in the two locations.

Additionally, there is human error in aligning the axes of the slippage sensor and the axis of the residual limb compared to the OCT camera. Caution was taken to maintain the coordinate system so that motion data and vessel structure data could be compared but it was still subjected to error that may influence the comparison of movement and vessel directionality. It is unknown how much this would affect the interpretation.

The implications from the data analysis in this investigation suggests that there are larger and more papillae that may orient in directions based on the cyclic environment it is exposed to. This adaptation would be

advantageous because it would lengthen the dermal-epidermal junction, increasing the number of cells, anchoring proteins, and surface area at the more superficial layer of skin (86). The study by Cucumel et al. (83) found that there was a negative correlation between age and papilla size and abundance and there data agreed with other papers found in the field. The increase in papillae was associated with increased vascularization and improved nutrient delivery to the epidermis. Another study performed in rats, suggested that by brushing the gums of the rats for one minute, twice-daily, for a month increase the depth of the papilla (87). In another study in pigs, there was no long-term structural adaptation when the greater trochanter of the pig was stressed with a consistent load applicator for multiple weeks (88). The authors do acknowledge the difficulty of trying to perform structural analysis in a 2D plane and this could be a factor in why there was no structural adaptation observed. In studies performed by Arao et al. it was reported that skin vessel and papillae can vary drastically between load tolerant and load intolerant area. For instance, dermal papillae found in the center of gluteus maximus can be scarce and have a height of 380μm, while dermal papillae found over the sacrum are dense and have height of 747μm (89). Furthermore, Arao et al. noticed that there were structural difference in the papillae at different locations, which they described as finger-like or trapezoidal in the sacrum and center of gluteus maximus, respectively. Blood content was positively correlated with epidermal thickness, suggesting that more blood flow was needed to provide support to a thicker epidermis (90). It is interesting that in general the capillary apexes collected in this experiment started at a similar depth below the stratum corneum for all anatomical sites and all participants, but may suggest that the residual limb requires more blood flow and more nutrients to maintain health.

5.5 Conclusions

- Capillary loop density and sub-papillary vessel density is greater in the residual limb compared to match-controls in the contralateral, intact limb.
- Residual limb capillary loop projections are taller and more numerous than the match-controls in the contralateral, intact limb.
- There is strong evidence that vascular characteristics reflect dermal papillae structural characteristics, suggesting that residual limb papillae are taller and more numerous than the match-controls in the contralateral, intact limb.
- Limb-to-socket slippage during stance phase of walking data may positively correlate with papillary plexus capillary arrangement.
- Direction of limb-to-socket slippage may negatively correlate with the direction of papillary plexus capillary arrangement.
- We suggest that residual limb papillae in areas of high shear stress with consistent directionality are arranged such that when put under that shear stress the papillae will become perpendicular to the skin surface.

References

1. Adams CT, Lakra A. Below-Knee Amputation. In: StatPearls. Treasure Island (FL): StatPearls Publishing; 2024 [cited 2024 Sep 16]. Available from: http://www.ncbi.nlm.nih.gov/books/NBK534773/

2. Colombo G, Facoetti G, Rizzi C. Automatic Below-Knee Prosthesis Socket Design: A Preliminary Approach. In: Duffy VG, editor. Digital Human Modeling: Applications in Health, Safety, Ergonomics and Risk Management. Cham: Springer International Publishing; 2016. p. 75–81.

3. Shaikh S. 3D Printing Applications in Lower Limb Prosthetics: Sockets, Knee Joint and Foots. In: Shaikh S, editor. 3D Printing in Prosthetics and Orthotics: Innovations and Opportunities [Internet]. Singapore: Springer Nature; 2024 [cited 2024 Sep 16]. p. 69–80. Available from: https://doi.org/10.1007/978-981-97-4913-3_6

4. Orfit Industries [Internet]. 2024 [cited 2024 Sep 16]. The Art of Moulding a Prosthetic Socket. Available from: https://www.orfit.com/prosthetics-orthotics/blog/moulding-a-prosthetic-socket

5. Socket fabrication | O&P Virtual Library [Internet]. [cited 2024 Sep 16]. Available from: http://www.oandplibrary.org/poi/1979_02_068.asp

6. Kim S, Yalla S, Shetty S, Rosenblatt NJ. 3D printed transtibial prosthetic sockets: A systematic review. PLoS ONE. 2022 Oct 10;17(10):e0275161.

7. Physiopedia [Internet]. [cited 2024 Sep 16]. Lower Limb Prosthetic Sockets and Suspension Systems. Available from: https://www.physio-pedia.com/Lower_Limb_Prosthetic_Sockets_and_Suspension_Systems

8. Hachisuka K, Dozono K, Ogata H, Ohmine S, Shitama H, Shinkoda K. Total surface bearing below-knee prosthesis: Advantages, disadvantages, and clinical implications. Arch Phys Med Rehabil. 1998 Jul 1;79(7):783–9.

9. Selles RW, Janssens PJ, Jongenengel CD, Bussmann JB. A randomized controlled trial comparing functional outcome and cost efficiency of a total surface-bearing socket versus a conventional patellar tendon-bearing socket in transtibial amputees. Arch Phys Med Rehabil. 2005 Jan 1;86(1):154–61.

10. Klute GK, Glaister BC, Berge JS. Prosthetic Liners for Lower Limb Amputees: A Review of the Literature. Prosthet Orthot Int. 2010 Jun 1;34(2):146–53.

11. Cagle JC, Reinhall PG, Hafner BJ, Sanders JE. Development of Standardized Material Testing Protocols for Prosthetic Liners. J Biomech Eng. 2017 Apr 1;139(4):0450011–04500112.

12. Cagle JC, Hafner BJ, Sanders JE. Characterization of Prosthetic Liner Products for People with Transtibial Amputation. J Prosthet Orthot JPO. 2018 Oct;30(4):187–99.

13. Fey NP, Klute GK, Neptune RR. The influence of energy storage and return foot stiffness on walking mechanics and muscle activity in below-knee amputees. Clin Biomech Bristol Avon. 2011 Dec;26(10):1025–32.

14. Fey NP, Klute GK, Neptune RR. Altering prosthetic foot stiffness influences foot and muscle function during below-knee amputee walking: A modeling and simulation analysis. J Biomech. 2013 Feb 22;46(4):637–44.

15. Prosthetic Feet [Internet]. Amputee Coalition. 2016 [cited 2024 Sep 16]. Available from: https://www.amputee-coalition.org/resources/prosthetic-feet/

16. Sanders JE, Zachariah SG, Jacobsen AK, Fergason JR. Changes in interface pressures and shear stresses over time on trans-tibial amputee subjects ambulating with prosthetic limbs: comparison of diurnal and six-month differences. J Biomech. 2005 Aug 1;38(8):1566–73.

17. Sanders JE, Fatone S. Residual limb volume change: Systematic review of measurement and management. Vol. 48, J Rehabil Res Dev. 2011. p. 949–86.

18. Article - Lower Limb Prostheses - Policy Article (A52496) [Internet]. [cited 2024 Sep 16]. Available from: https://www.cms.gov/medicare-

coverage-database/view/article.aspx?articleId=52496

19. Webster JB, Hakimi KN, Williams RM, Turner AP, Norvell DC, Czerniecki JM. Prosthetic fitting, use, and satisfaction following lower-limb amputation: A prospective study. J Rehabil Res Dev. 2012;49(10):1453–504.

20. Baumann M, Price C, Brousseau L, Loftsgaarden M, Powell J, Sanders J, et al. The relationship between residual limb health, motion within the socket, and prosthetic suspension. PM R. 2023 Apr;15(4):510–21.

21. Fajardo-Martos I, Roda O, Zambudio-Periago R, Bueno-Cavanillas A, Hita-Contreras F, Sánchez-Montesinos I. Predicting successful prosthetic rehabilitation in major lower-limb amputation patients: a 15-year retrospective cohort study. Braz J Phys Ther. 2018;22(3):205–14.

22. 27: Management of Pain in the Amputee | O&P Virtual Library [Internet]. [cited 2024 Sep 17]. Available from: http://www.oandplibrary.org/alp/chap27-01.asp

23. Noll V, Whitmore S, Beckerle P, Rinderknecht S. A Sensor Array for the Measurement of Relative Motion in Lower Limb Prosthetic Sockets. Sensors. 2019 Jan;19(12):2658.

24. Henrikson KM, Weathersby EJ, Larsen BG, Cagle JC, McLean JB, Sanders JE. An Inductive Sensing System to Measure In-Socket Residual Limb Displacements for People Using Lower-Limb Prostheses. Sensors. 2018 Nov 9;18(11):3840.

25. An Easy-to-Use Socket-Suspension System Monitor for Lower Limb Amputees | IEEE Journals & Magazine | IEEE Xplore [Internet]. [cited 2024 Sep 17]. Available from: https://ieeexplore.ieee.org/document/9107262

26. Wirta RW, Golbranson FL, Mason R, Calvo K. Analysis of below-knee suspension systems: Effect on gait. J Rehabil Res Dev. 1990;27(4):385.

27. Ferguson J, Voss GO, Fairhurst SR, Hansen A. Devices, Systems, And Methods For Socket Fit Management [Internet]. US20230018447A1, 2023 [cited 2024 Sep 17]. Available from: https://patents.google.com/patent/US20230018447/en

28. Rich TL, Voss G, Fairhurst S, Matsumoto M, Brielmaier S, Koester K, et al. Feasibility testing of a novel prosthetic socket sensor system. Disabil Rehabil. 2022. p. 1–8.

29. Radcliffe CW. The Biomechanics of Below-Knee Prostheses.

30. Zhang M, Turner-Smith AR, Tanner A, Roberts VC. Clinical investigation of the pressure and shear stress on the trans-tibial stump with a prosthesis. Med Eng Phys. 1998 Apr;20(3):188–98.

31. Sanders JE, Lam D, Dralle AJ, Okumura R. Interface pressures and shear stresses at thirteen socket sites on two persons with transtibial amputation. J Rehabil Res Dev. 1997 Jan;34(1):19–43.

32. Dumbleton T, Buis AWP, McFadyen A, McHugh BF, McKay G, Murray KD, et al. Dynamic interface pressure distributions of two transtibial prosthetic socket concepts. J Rehabil Res Dev. 2009;46(3):405–15.

33. Davenport P, Noroozi S, Sewell P, Zahedi S. Systematic Review of Studies Examining Transtibial Prosthetic Socket Pressures with Changes in Device Alignment. J Med Biol Eng. 2017 Feb 1;37(1):1–17.

34. Sanders JE, Fergason JR, Zachariah SG, Jacobsen AK. Case study: Interface pressure and shear stress changes with amputee weight loss: Case studies from two trans-tibial amputee subjects. Prosthet Orthot Int. 2002 Jan 1;26(3):243–50.

35. Pascale BA, Potter BK. Residual Limb Complications and Management Strategies. Curr Phys Med Rehabil Rep. 2014 Dec 1;2(4):241–9.

36. Highsmith MJ, Kahle JT, Klenow TD, Andrews CR, Lewis KL, Bradley RC, et al. Interventions to Manage Residual Limb Ulceration Due To Prosthetic Use in Individuals with Lower Extremity Amputation: A Systematic Review of the Literature. Technol Innov. 2016 Sep 16;18(2–3):115–23.

37. Rink CL, Wernke MM, Powell HM, Tornero M, Gnyawali SC, Schroeder RM, et al. Standardized

Approach to Quantitatively Measure Residual Limb Skin Health in Individuals with Lower Limb Amputation. Adv Wound Care. 2017 Jul 1;6(7):225–32.

38. Pandey B, Arora AS. Detection of Pressure Points on the Residual Limb in Transtibial Amputation Using Thermal Imaging. In: 2021 IEEE 2nd International Conference On Electrical Power and Energy Systems (ICEPES) [Internet]. 2021 [cited 2024 Sep 18]. p. 1–3. Available from: https://ieeexplore.ieee.org/abstract/document/9699646

39. Vinjamuri R. Prosthesis. BoD – Books on Demand; 2020. 142 p.

40. Swanson EC, Friedly JL, Wang RK, Sanders JE. Optical coherence tomography for the investigation of skin adaptation in lower limb prosthesis users. Vol. 33, J Prosthet Orthot. 2021. p. 255–65.

41. Aumann S, Donner S, Fischer J, Müller F. Optical Coherence Tomography (OCT): Principle and Technical Realization. In: Bille JF, editor. High Resolution Imaging in Microscopy and Ophthalmology: New Frontiers in Biomedical Optics [Internet]. Cham (CH): Springer; 2019 [cited 2024 Sep 18]. Available from: http://www.ncbi.nlm.nih.gov/books/NBK554044/

42. Choi WJ, Reif R, Yousefi S, Wang RK. Improved microcirculation imaging of human skin in vivo using optical microangiography with a correlation mapping mask. J Biomed Opt. 2014 Mar;19(3):036010.

43. Meulenbelt HEJ, Geertzen JHB, Dijkstra PU, Jonkman MF. Skin problems in lower limb amputees: an overview by case reports. J Eur Acad Dermatol Venereol JEADV. 2007 Feb;21(2):147–55.

44. R.F. Tuma, W.N. Durán, K. Ley. Handbook of Physiology: Microcirculation. 2008.

45. Weathersby EJ, Vamos AC, Larsen BG, McLean JB, Carter RV, Allyn KJ, et al. Performance of an auto-adjusting prosthetic socket during walking with intermittent socket release. Vol. 9, Journal of Rehabilitation and Assistive Technologies Engineering. 2022. p. 20556683221093271.

46. Weathersby EJ, Gurrey CJ, McLean JB, Sanders BN, Larsen BG, Carter R, et al. Thin Magnetically Permeable Targets for Inductive Sensing: Application to Limb Prosthetics. Sensors. 2019 Sep 19;19(18):4041.

47. Askari P, Barekat F. Trilateration and Bilateration In 3D and 2D Space Using Active Tags. 2017 Oct 18;

48. Eshraghi A, Osman NAA, Gholizadeh H, Karimi M, Ali S. Pistoning assessment in lower limb prosthetic sockets. Prosthet Orthot Int. 2012 Mar 1;36(1):15–24.

49. Darter BJ, Sinitski K, Wilken JM. Axial bone-socket displacement for persons with a traumatic transtibial amputation: The effect of elevated vacuum suspension at progressive body-weight loads. Prosthet Orthot Int. 2016 Oct;40(5):552–7.

50. Cagle JC, Reinhall PG, Allyn KJ, McLean J, Hinrichs P, Hafner BJ, et al. A finite element model to assess transtibial prosthetic sockets with elastomeric liners. Med Biol Eng Comput. 2018 Jul;56(7):1227–40.

51. Söderberg B, Ryd L, Persson BM. Roentgen Stereophotogrammetric Analysis of Motion between the Bone and the Socket in a Transtibial Amputation Prosthesis: A Case Study. JPO J Prosthet Orthot. 2003 Jul;15(3):95.

52. Gholizadeh H, Abu Osman NA, Lúvíksdóttir ÁG, Eshraghi A, Kamyab M, Wan Abas WAB. A new approach for the pistoning measurement in transtibial prosthesis. Prosthet Orthot Int. 2011 Dec 1;35(4):360–4.

53. Childers WL, Siebert S. Marker-based method to measure movement between the residual limb and a transtibial prosthetic socket. Prosthet Orthot Int. 2016 Dec 1;40(6):720–8.

54. Pew CA, Roelker SA, Klute GK, Neptune RR. Analysis of the Relative Motion Between the Socket and Residual Limb in Transtibial Amputees While Wearing a Transverse Rotation Adapter. J Appl Biomech. 2020 Nov 3;37(1):21–9.

55. Sanders JE, Harrison DS, Allyn KJ, Myers TR, Ciol MA, Tsai EC. How do sock ply changes affect residual-limb fluid volume in people with

transtibial amputation? Vol. 49, J Rehabil Res Dev. 2012. p. 241–56.

56. Sanders JE, Cagle JC, Harrison DS, Karchin A. Amputee socks: how does sock ply relate to sock thickness? Prosthet Orthot Int. 2012 Mar;36(1):77–86.

57. Cagle JC, D'Silva KJ, Hafner BJ, Harrison DS, Sanders JE. Amputee socks: Sock thickness changes with normal use. Prosthet Orthot Int. 2016 Jun;40(3):329–35.

58. Lannan FM, Powell J, Kim GM, Hansen CR, Pasquina PF, Smith DG. Hyperhidrosis of the residual limb: a narrative review of the measurement and treatment of excess perspiration affecting individuals with amputation. Prosthet Orthot Int. 2021 Dec 1;45(6):477–86.

59. Lannan FM, Meyerle JH. The Dermatologist's Role in Amputee Skin Care.

60. Lyon CC, Kulkarni J, Zimerson E, Van Ross E, Beck MH. Skin disorders in amputees. J Am Acad Dermatol. 2000 Mar;42(3):501–7.

61. Swanson EC, Friedly JL, Wang RK, Sanders JE. Optical coherence tomography for the investigation of skin adaptation to mechanical stress. Vol. 26, Skin Res Technol. 2020. p. 627–38.

62. Trilateration. In: Wikipedia [Internet]. 2024 [cited 2024 Sep 30]. Available from: https://en.wikipedia.org/w/index.php?title=Trilateration&oldid=1226607139

63. Sanders JE, Redd CB, Larsen BG, Vamos AC, Brzostowski JT, Hafner BJ, et al. A Novel Method for Assessing Prosthesis Use and Accommodation Practices of People with Transtibial Amputation. J Prosthet Orthot JPO. 2018 Oct;30(4):214–30.

64. Weathersby EJ, Cagle JC, Larsen BG, Henrikson KM, Sanders JE. Development of a magnetic composite material for measurement of residual limb displacements in prosthetic sockets. J Rehabil Assist Technol Eng. 2018 Apr 3;5:2055668318763481.

65. X-LSM200A Specifications - Zaber [Internet]. [cited 2024 Sep 18]. Available from: https://www.zaber.com/products/linear-stages/X-LSM/specs?part=X-LSM200A

66. Ballesteros D, Carter RV, Allyn KJ, Lanahan CR, Krout AJ, Hafner BJ, et al. Fabricating sockets with distance sensors for monitoring prosthesis use and socket fit. JPO: Journal of Prosthetics and Orthotics. 2023. p. 10.1097/JPO.0000000000000464.

67. Carter RV, Larsen BG, McLean JB, Garbini JL, Sanders JE. Incorporating a Ferrous Polymer Target into Elastomeric Liners for Socket Fit Sensing in Prosthesis Users. Sensors. 2020 Oct 1;20(19):5620.

68. Hinrichs P, Cagle JC, Sanders JE. A portable bioimpedance instrument for monitoring residual limb fluid volume in people with transtibial limb loss: A technical note. Vol. 68, Med Eng Phys. 2019. p. 101–7.

69. Sanders J, Cagle J, Allyn K, Harrison D, Ciol M. How do activities walking, standing, and resting influence trans-tibial amputee residual limb fluid volume? J Rehabil Res Dev. 2014;51(2):201–12.

70. Sanders JE, Moehring MA, Rothlisberger TM, Phillips RH, Hartley T, Dietrich CR, et al. A bioimpedance analysis platform for amputee residual limb assessment. Vol. 63, IEEE Trans Biomed Eng. 2016. p. 1760–70.

71. Bennett S, Gurrey C, Wang H, Weissinger M, Larsen B, Sanders JE. A sensor to monitor limb depth in transtibial sockets with locking pin suspension: a technical note. Vol. 45, Prosthetics and orthotics international. 2021. p. 362–7.

72. Sanders J, Severance M. An assessment technique for computer-socket manufacturing. J Rehabil Res Dev. 2011;48(7):763–74.

73. WillowWood® [Internet]. [cited 2024 Oct 1]. Alpha® Hybrid | WillowWood. Available from: https://willowwood.com/product/alpha-hybrid-bkc/

74. Esquenazi A, DiGiacomo R. Rehabilitation after amputation. J Am Podiatr Med Assoc. 2001 Jan;91(1):13–22.

75. Brunelli S, Bonanni C, Foti C, Traballesi M. A Literature Review of the Quality of Life, Health Status and Prosthesis Satisfaction in Older

Patients With A Trans-tibial Amputation. Can Prosthet Orthot J. 2(1):33640.

76. Chatterjee S, Majumder S, RoyChowdhury A, Pal S. Review: Problems with Use of Trans-Tibial Prosthesis. J Med Imaging Health Inform. 2016 Apr 1;6(2):269–84.

77. Devin KM, Tang J, Moser D, Jiang L. Assessing Socket Fit Effects on Pressure and Shear at a Transtibial Residuum/Socket Interface. Appl Bionics Biomech. 2023 Aug 16;2023:3257059.

78. Deegan AJ, Wang RK. Microvascular imaging of the skin. Phys Med Biol. 2019 Mar 21;64(7):07TR01.

79. Johnson JM, Kellogg DL. Local thermal control of the human cutaneous circulation. J Appl Physiol. 2010 Oct;109(4):1229–38.

80. Lopez-Ojeda W, Pandey A, Alhajj M, Oakley AM. Anatomy, Skin (Integument). In: StatPearls [Internet]. Treasure Island (FL): StatPearls Publishing; 2024 [cited 2024 Sep 22]. Available from: http://www.ncbi.nlm.nih.gov/books/NBK441980/

81. Aleemardani M, Trikić MZ, Green NH, Claeyssens F. The Importance of Mimicking Dermal-Epidermal Junction for Skin Tissue Engineering: A Review. Bioengineering. 2021 Nov;8(11):148.

82. Israelsen NM, Maria M, Mogensen M, Bojesen S, Jensen M, Haedersdal M, et al. The value of ultrahigh resolution OCT in dermatology - delineating the dermo-epidermal junction, capillaries in the dermal papillae and vellus hairs. Biomed Opt Express. 2018 Apr 19;9(5):2240–65.

83. Cucumel K, Botto JM, Domloge N, Farra CD, Cucumel K, Botto JM, et al. Age-Related Changes in Human Skin by Confocal Laser Scanning Microscope. In: Senescence [Internet]. IntechOpen; 2012 [cited 2024 Sep 18]. Available from: https://www.intechopen.com/chapters/30063

84. Hagisawa S, Shimada T, Arao H, Asada Y. Morphological architecture and distribution of blood capillaries and elastic fibres in the human skin. J Tissue Viability. 2001 Apr 1;11(2):59–63.

85. Sanders JE, Daly CH. Normal and shear stresses on a residual limb in a prosthetic socket during ambulation: comparison of finite element results with experimental measurements. J Rehabil Res Dev. 1993;30(2):191–204.

86. Sanders JE, Goldstein BS, Leotta DF. Skin response to mechanical stress: adaptation rather than breakdown--a review of the literature. J Rehabil Res Dev. 1995 Oct;32(3):214–26.

87. Sb Carter. The masticatory musoca and its response to brushing; findings in the merion rat, meriones libycus, at different ages. Br Dent J. 1956;(101).

88. Goldstein B, Sanders J. Skin response to repetitive mechanical stress: a new experimental model in pig. Arch Phys Med Rehabil. 1998 Mar;79(3):265–72.

89. Arao H, Shimada T, Hagisawa S, Ferguson-Pell M. Morphological characteristics of the human skin over posterior aspect of heel in the context of pressure ulcer development. J Tissue Viability. 2013 May;22(2):42–51.

90. Sandby-Møller J, Poulsen T, Wulf HC. Epidermal thickness at different body sites: relationship to age, gender, pigmentation, blood content, skin type and smoking habits. Acta Derm Venereol. 2003;83(6):410–3.

Appendix 1 – Robotic Three Axis Control Flow Diagram

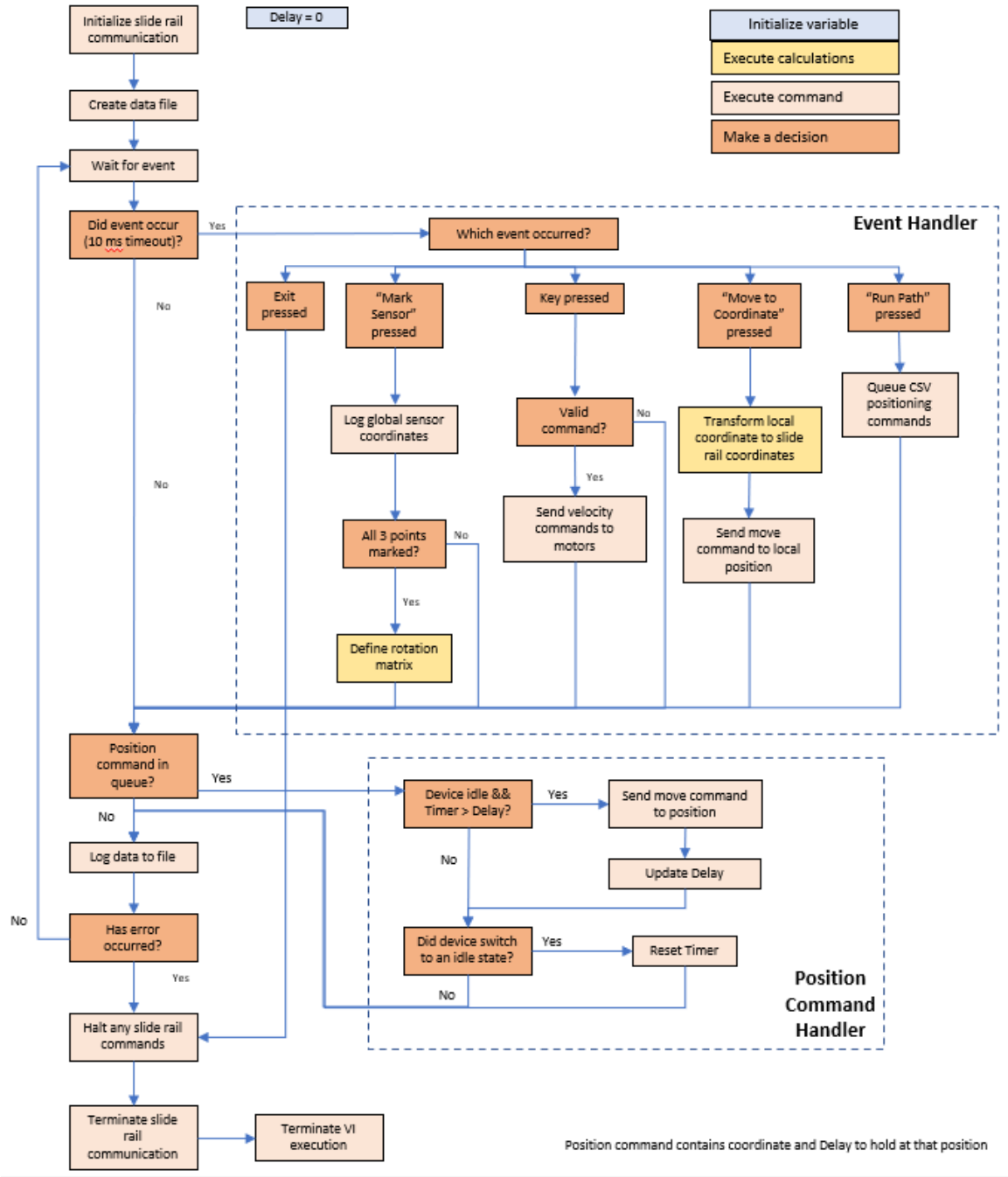

Appendix 2 – Single-Sensor Model Planar Data

Plane 1:

Sig. Value (arb. Unit)		Radial (mm)									
		0	5	10	15	20	25	30	35	40	45
Height (mm)	0	6174800	6250518	6376165	6504054	6646857	6775680	6826780	6830024	6831765	6830485
	1	6388560	6433389	6515732	6602091	6697985	6788194	6826557	6830096	6830485	6830485
	2	6528802	6557018	6613187	6674746	6742049	6801648	6827447	6830263	6830597	6830597
	3	6620610	6638432	6677205	6720889	6768622	6809952	6827837	6830319	6830597	6830597
	4	6683113	6694707	6720944	6752282	6786449	6815236	6828188	6830374	6830597	6830652
	5	6725317	6732808	6751181	6773548	6798242	6818866	6828466	6830374	6830652	6830652
	6	6754744	6759654	6772389	6788581	6806490	6821462	6828633	6830319	6830652	6830652
	7	6775569	6778894	6787696	6799406	6812472	6823407	6828855	6830374	6830652	6830708
	8	6790215	6792402	6798685	6807100	6816735	6824871	6829078	6830374	6830708	6830708
	9	6800761	6802228	6806601	6812772	6819887	6825946	6829245	6830319	6830652	6830764
	10	6808375	6809286	6812472	6817013	6822240	6826780	6829412	6830374	6830652	6830708
	11	6813882	6814492	6816735	6820109	6823982	6827503	6829523	6830374	6830652	6830764
	12	6817922	6818422	6819998	6822462	6825427	6828021	6829690	6830430	6830652	6830708
	13	6820942	6821220	6822407	6824204	6826446	6828522	6829801	6830430	6830652	6830764
	14	6823129	6823407	6824204	6825594	6827336	6828855	6829929	6830430	6830652	6830708
	15	6824871	6825038	6825594	6826669	6827910	6829189	6830024	6830430	6830652	6830708

Plane 2:

Sig. Value (arb. Unit)		Radial (mm)									
		0	5	10	15	20	25	30	35	40	45
Height (mm)	0	6186388	6271468	6409700	6535527	6638108	6750369	6820275	6829078	6829578	6829985
	1	6390695	6448434	6542300	6626092	6699353	6776121	6823296	6829968	6830319	6830485
	2	6529712	6568111	6631438	6689238	6741015	6793177	6824927	6830207	6830597	6830652
	3	6621557	6646532	6690001	6730676	6767593	6804001	6825946	6830263	6830597	6830708
	4	6683657	6700608	6730183	6758844	6785565	6811140	6826724	6830207	6830652	6830708
	5	6725864	6737126	6757797	6778198	6797606	6816013	6827280	6830207	6830652	6830764
	6	6755170	6762832	6777315	6792014	6806133	6819498	6827781	6830263	6830652	6830764
	7	6775900	6781246	6791295	6801951	6812306	6822018	6828243	6830263	6830652	6830708
	8	6790492	6794146	6801426	6809065	6816735	6823926	6828633	6830263	6830708	6830764
	9	6800983	6803558	6808676	6814326	6819998	6825316	6828967	6830319	6830652	6830819
	10	6808621	6810396	6814048	6818200	6822462	6826446	6829245	6830319	6830652	6830819
	11	6814104	6815347	6817978	6821109	6824260	6827280	6829412	6830430	6830708	6830764
	12	6818144	6819033	6820998	6823240	6825668	6827965	6829690	6830430	6830708	6830764
	13	6821164	6821795	6823185	6824927	6826780	6828522	6829857	6830485	6830708	6830764
	14	6823407	6823815	6824927	6826168	6827558	6828911	6830024	6830485	6830708	6830819
	15	6825038	6825372	6826168	6827114	6828243	6829300	6830096	6830541	6830764	6830764

Plane 3:

Sig. Value (arb. Unit)		Radial (mm)									
		0	5	10	15	20	25	30	35	40	45
Height (mm)	0	6172865	6254229	6403192	6523736	6642320	6763862	6823926	6830430	6830819	6830819
	1	6388456	6444480	6538566	6624499	6705912	6785952	6825538	6830485	6830819	6830875
	2	6529872	6565711	6628711	6687923	6744950	6799239	6826446	6830485	6830819	6830875
	3	6620988	6645611	6688202	6729580	6770147	6807876	6827058	6830485	6830819	6830819
	4	6683385	6700062	6729032	6758183	6787143	6813660	6827558	6830430	6830819	6830819
	5	6725590	6737017	6757302	6777867	6798741	6817755	6827965	6830485	6830819	6830819
	6	6754950	6762943	6777094	6791793	6806933	6820664	6828299	6830430	6830819	6830875
	7	6775790	6781357	6791211	6801870	6812861	6822851	6828688	6830430	6830764	6830819
	8	6790381	6794257	6801371	6809009	6817089	6824482	6828911	6830485	6830819	6830875
	9	6800983	6803669	6808732	6814326	6820275	6825723	6829189	6830485	6830819	6830819
	10	6808510	6810507	6814104	6818200	6822629	6826724	6829412	6830541	6830819	6830819
	11	6814048	6815513	6818144	6821109	6824371	6827447	6829578	6830541	6830819	6830875
	12	6818144	6819144	6821053	6823296	6825723	6828077	6829745	6830541	6830764	6830875
	13	6821164	6821906	6823296	6824982	6826780	6828577	6829857	6830541	6830764	6830875
	14	6823351	6823982	6824982	6826224	6827558	6828967	6830040	6830597	6830764	6830819
	15	6825038	6825483	6826224	6827169	6828243	6829300	6830152	6830652	6830819	6830875

Plane 4:

Sig. Value (arb. Unit)		Radial (mm)									
		0	5	10	15	20	25	30	35	40	45
Height (mm)	0	6168894	6240142	6367727	6489696	6619478	6762337	6825260	6830430	6830708	6830819
	1	6388717	6430574	6516698	6602198	6693011	6786007	6826669	6830430	6830764	6830764
	2	6528855	6555686	6612562	6672613	6737017	6799516	6827280	6830485	6830764	6830764
	3	6620880	6638162	6676226	6718922	6764909	6808154	6827725	6830485	6830708	6830819
	4	6683276	6694484	6720451	6750631	6783599	6813937	6828077	6830430	6830708	6830819
	5	6725536	6733082	6750961	6772334	6796277	6817922	6828355	6830430	6830708	6830819
	6	6754950	6760094	6772389	6787807	6805135	6820775	6828577	6830430	6830764	6830764
	7	6775790	6779225	6787807	6798852	6811529	6822851	6828855	6830430	6830764	6830819
	8	6790381	6792789	6798796	6806767	6816069	6824482	6829078	6830430	6830764	6830819
	9	6800928	6802560	6806878	6812639	6819498	6825705	6829245	6830430	6830708	6830764
	10	6808510	6809730	6812750	6816957	6822018	6826669	6829467	6830430	6830764	6830819
	11	6814048	6814826	6817089	6820164	6823926	6827447	6829578	6830485	6830708	6830819
	12	6818144	6818644	6820275	6822518	6825316	6828021	6829745	6830485	6830708	6830764
	13	6821109	6821517	6822684	6824371	6826446	6828522	6829857	6830485	6830708	6830819
	14	6823351	6823648	6824482	6825779	6827336	6828911	6829985	6830485	6830708	6830764
	15	6825038	6825205	6825890	6826780	6828021	6829245	6830152	6830541	6830652	6830764

Plane 5:

Sig. Value (arb. Unit)		Radial (mm)									
		0	5	10	15	20	25	30	35	40	45
Height (mm)	0	6176484	6260082	6389863	6496258	6605139	6758623	6826446	6830263	6830597	6830764
	1	6388873	6438444	6523417	6599994	6680273	6780915	6826891	6830374	6830652	6830764
	2	6529659	6559899	6617614	6672777	6730786	6796942	6827392	6830430	6830708	6830819
	3	6621474	6639862	6679838	6719469	6761676	6806601	6827725	6830430	6830764	6830875
	4	6683549	6695471	6722747	6751346	6781909	6812994	6828077	6830485	6830764	6830875
	5	6725755	6733404	6752502	6773051	6795474	6817311	6828355	6830430	6830764	6830931
	6	6755115	6760094	6773493	6788470	6804802	6820442	6828577	6830430	6830764	6830931
	7	6775845	6779281	6788581	6799516	6811418	6822740	6828855	6830485	6830819	6830931
	8	6790492	6792734	6799406	6807266	6816124	6824426	6829078	6830430	6830764	6830931
	9	6800983	6802505	6807266	6813105	6819609	6825723	6829300	6830430	6830819	6830931
	10	6808565	6809619	6813049	6817311	6822184	6826724	6829523	6830485	6830764	6830986
	11	6814104	6814770	6817256	6820442	6824093	6827558	6829690	6830541	6830764	6830931
	12	6818144	6818644	6820442	6822851	6825538	6828132	6829857	6830541	6830819	6830931
	13	6821164	6821462	6822796	6824593	6826669	6828633	6829968	6830541	6830764	6830931
	14	6823407	6823648	6824649	6825946	6827503	6829022	6830152	6830597	6830819	6830931
	15	6825094	6825205	6826001	6827002	6828188	6829412	6830263	6830652	6830819	6830931

Appendix 3 – OCT Images with Depth Segmentation

Participant Ten

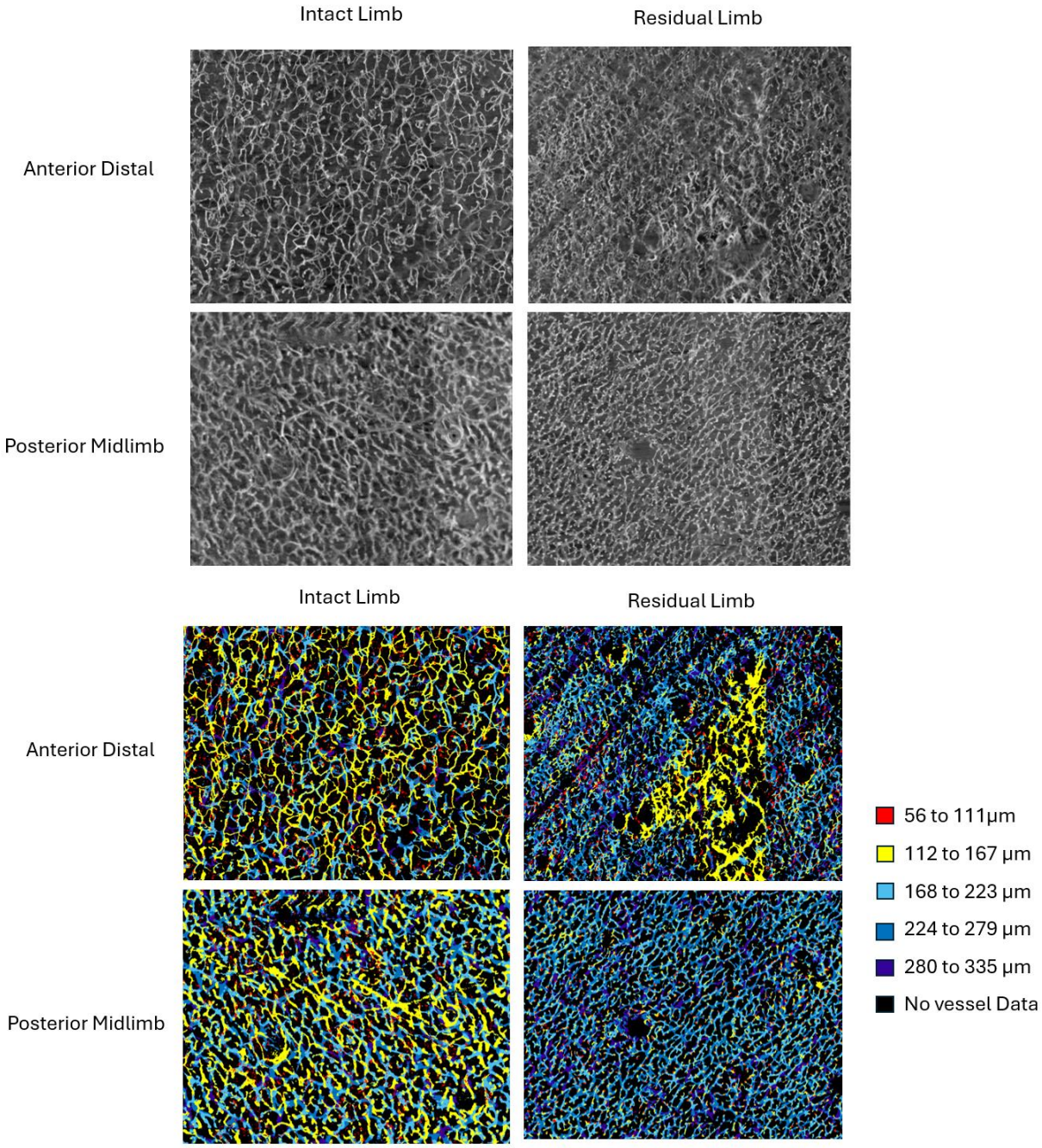

Participant Seven

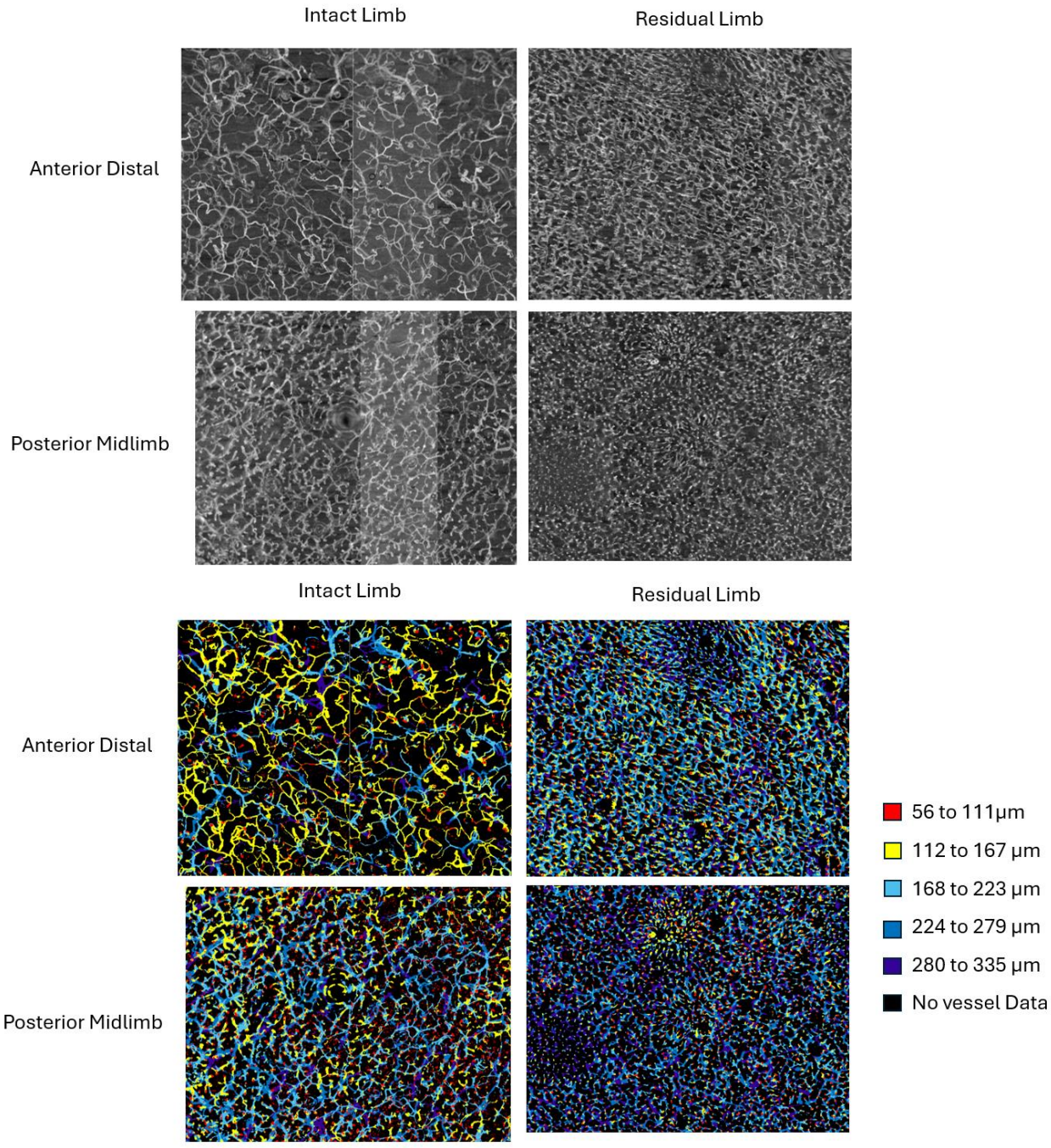

Participant Nine